DEVELOPING A QFD-BASED DESIGN-INTEGRATED STRUCTURAL ANALYSIS METHODOLOGY

A thesis submitted for the degree of Doctor of Philosophy

by

Seyed Omid Mobasseri

School of Engineering & Design

Brunel University

July 2012

ABSTRACT

Design of the mechanical components greatly depends on their expected structural performances. In modern design applications these performances are quantified by computer-based analysis and occasionally confirmed by experimental measurements or theoretical calculations. The dependency of the mechanical product to the structural analysis process is more significant under the product's multi-functionality aspect that requires analyses for a variety of Variable Input Parameters, to obtain various structural responses and against more than one failure or design criterion. Structural analysis is known as the expert field, which requires an upfront investment and facilitation to be implemented in commercial design environment.

On the other hand, the product design process is a systematic and sequential activity that put the designer in the central role of decision making. Lack of mutual understanding between these two disciplines reduces the efficiency of the structural analysis for design.

This research aims to develop an integrated methodology to embed the structural analysis in the design process. The proposed methodology in this research combines the benefits of state-of-the-art approaches, early simulation and Validation and Verification practice, towards the specified aim. Moreover the novelty of the proposed methodology is in creative implication of Quality Function Deployment method to include the product's multi-functionality aspect. The QFD-Based Design Integrated Structural Analysis methodology produces a reliable platform to increase the efficiency of the structural analysis process for product design purpose.

The application of this methodology is examined through an industrial case-study for the telescopic cantilever boom, as it appears in Access platforms, and Cranes products. Findings of the case-study create a reliable account for the structural performance in early stages of the design, and ensure the functionality of the proposed methodology.

ACKNOWLEDGEMENTS

This research would not be possible without the continuous support and assistance of the following people.

Firsts and foremost is Dr Sangarappillai Sivaloganathan, who has not only be an academic supervisor, but a great companion during all the ups and downs of this project. Thank you sincerely Sir for teaching me the life.

The project has been Niftylift's joint research programme with Brunel University. Dr Roger Bowden once again has shown his passion for excellence by his comprehensive and generous support throughout this journey. Thank you Sir for having me on board.

The success of this research is owed to Dr. Martin Cross and Nick Joyce contribution as project's industrial supervisors. Thank you both for taking the worst of the work pressure and sharing your priceless experience with me. Also thank you to Steve Redding and colleagues in Niftylift for their contribution, hospitality and patience.

This research programme was funded by KTP organisation and supported by dedicated effort of Local Management Committee, Lynne Greenstreet, Douglas Irish and Ian Edison. Thank you all for your continuous support and guidance.

Thank you to Dr. Joe Au for his invaluable assistance at the most critical stages, along with School of Engineering and Design, colleagues in Mechanical Lab, Stores, Finance and Accounts. Special thanks to Advanced Design Engineering MSc students of 2010-2011, Risi, Mira, Neha, Mark, Chanachai, George Kutty, Ivan, Ali, Safir and Muthu who contributed to this research in their Design Experience module and Dissertations.

Thanks to my family and friends for their love and support through this long journey.

And finally my greatest gratitude to my lovely Mona who could not do anything better than tolerate me. Your love is my only encouragement during the hard times.

AUTHOR'S DECLARATION

I confirm that this document is my own work except where references are cited. Once again, I would like to thank Dr Sangarappillai Sivaloganathan for his support and guidance during this project, and Dr Roger Bowden and Niftylift for sponsoring this work.

Table Contents

Developing A QFD-Based Design-Integrated Structural Analysis Methodology 1

Abstract 2

1 Introduction 16

1.1 Research aim and objectives 16

1.1.1 Motivations 16
1.1.2 Research question 17
1.1.3 Objectives 17

1.2 Thesis structure 17

2 Principles of Applied Stress Analysis 19

2.1 Structural analysis in application, aims and objectives 19

2.2 Quantifiable parameters and failure criteria 21

2.2.1 Elastic Stress 22
2.2.2 Elastic Strain Analysis 27
2.2.3 Stress-strain relationships 34
2.2.4 Failure criteria 36
2.2.4.1 Combined stress theories 36
2.2.4.2 Buckling failure 40

2.3 Numerical method in structural design 42

2.3.1 FEA Procedure 43
2.3.2 Meshing and element properties 43
2.3.2.1 Continuum elements 46
2.3.2.2 Shell element 48

2.4 Experimental analysis 51

2.4.1 Photoelestic measurement 51
2.4.2 Strain analysis using strain gauge 53

2.5 Chapter summary 55

3 Structural Analysis in Product Development 57

3.1 Product design perspective 57

3.2 Implementing Structural analysis in the design process 60

3.3 Systematic Structural Analysis 61

3.3.1 Early simulation 61
3.3.2 Benchmark 64
3.3.3 Expert System and Knowledge Base Engineering 64
3.3.4 Validation and Verification approach 69
3.3.5 Design of Experiment (DOE) 74
3.3.6 Comparative assessment 76

3.4 Quality Function Deployment (QFD) 78

3.5 Chapter summary 80

4 QFD-Based Design Integrated Structural Analysis Methodology 82

4.1 General Provision 82

4.1.1 The common practice 82
4.1.2 Proposed Methodology in abstract 83

4.2 Methodology process model 84

4.2.1 Process start point 84
4.2.2 Stage 1 QFD process 85
4.2.2.1 Stakeholder's requirement 87
4.2.2.2 Measurable performance characteristics 88
4.2.2.3 Independent Parameters 88
4.2.2.4 QFD Chart 1 89
4.2.2.5 QFD Chart 2 90
4.2.2.6 Plan for integrated studies 90
4.2.3 V&V on the instants of reality 92
4.2.4 Results report and iteration 92

4.3 Methodology framework 93

4.4 Chapter summary 95

5 Case Study- Telescopic Cantilever Boom 96

5.1 Telescopic cantilever boom 96

5.2 Benchmark construction 99

5.3 Stakeholder's requirements 103

5.3.1 Stress at contact region 103

5.3.2 Total displacement 103
5.3.3 Vibration 103
5.3.4 Buckling behaviour 103
5.4 Measurable performance characteristics 104
5.5 Independent parameter 105
5.6 QFD chart 1 105
5.7 QFD Chart 2 106
5.8 Plan for individual studies 107
5.9 V&V on the instant of reality 110
5.10 Chapter summary 111
6 Analysis and Results 112
6.0 Introduction 112
6.1 General condition of the analysis 112
6.2 Stress behaviour at vicinity of contact area 115
6.2.1 Element variation 115
6.2.2 Element performance and verification 115
6.2.3 Element validation 121
6.2.4 Load magnitude variation 125
6.2.5 Load type variation and validation 133
6.2.6 Effect of the overlap length 136
6.2.7 Conclusion on stress behaviour due to contact 139
6.3 Displacement behaviour 140
6.3.1 Effect of the element variation 140
6.3.2 Displacement verification 142
6.3.3 Displacement behaviour validation 143
6.3.4 Effect of the load magnitude 145
6.3.5 Effect of the overlap length 146
6.3.6 Conclusion 147
6.4 Vibration behaviour 147
6.4.1 General linear perturbation analysis set up 148
6.4.2 Verification method 148
6.4.3 The variation of load magnitude 150
6.4.4 The effect of the overlap length 152
6.4.5 Conclusion on natural frequency behaviour 153

6.5 Buckling performance 154

6.5.1 General buckling analysis procedure 154
6.5.2 Load type variation 159
6.5.3 Effect of the overlap length 164
6.5.4 Conclusion on buckling behaviour 165

6.6 Chapter summary 165

7 Discussions and Conclusions 167

7.1 Summary 167

7.2 Contribution to knowledge 168

7.3 Recommendation for future developments 168

7.4 Conclusion 169

Appendix I – Stress invariants 171

Appendix II – Maximum shearing stress 173

Appendix III – Principal strains 175

Appendix IV - List of failure modes 177

Appendix V - Nodal degrees of freedom convention 178

Appendix VI – Principal strain angle in rosette 179

Appendix VII – Benchmark parts drawings 180

Appendix VIII - Size of the FEA Problem with Different Elements 186

Appendix IX- Strain gauge specification 189

Appendix X- Specification NI cDAQ-9172 190

Appendix XI - Specification NI 9236 192

Appendix XII- Specification NI 9234 194

Appendix XIII- Tip Displacement Calculation Flowchart 196

References: 197

List of Figures

Figure 1-1 Thesis structure 18

Figure 2-1 Relationship between specific factors to structural design (Ray, 1985) 21

Figure 2-2 Schematic illustration of structural analysis process (NAFEMS, 1987)..... 22

Figure 2-3 The state of a stress in a body in static equilibrium 23

Figure 2-4 Resultant internal forces acting on an arbitrary element of area..... 24

Figure 2-5 State of stress on a parallelepiped (Timoshenko and Goodier, 1951)..... 25

Figure 2-6 Force equilibrium on an infinitesimal parallelepiped (Singh, 1979)..... 26

Figure 2-7 Planes of maximum shearing stress direction 27

Figure 2-8 Deformation of a continuous medium..... 28

Figure 2-9 Deformation of an infinitesimal line element..... 29

Figure 2-10 Physical interpretation of strain tensor normal component..... 32

Figure 2-11 Physical interpretation of strain tensor shear component..... 33

Figure 2-12 Comparison of failure theories in biaxial state of stress (Collins, 1993) 37

Figure 2-13 Types of load-displacement behaviour (Trahair, 1993) 40

Figure 2-14 General FE model set up in Abaqus..... 44

Figure 2-15 Commonly used elements families (Dassault Systèmes, 2007, b)..... 45

Figure 2-16 (a) Linear elements (b) Quadratic elements (c) Modifies second-order element (Dassault Systèmes, 2007, b)..... 45

Figure 2-17 (a) Hourglass mode shapes of a 4 node-reduced-integration element (b) Hourglass mode propagation (Dassault Systèmes, 2010)..... 47

Figure 2-18 Shear locking (a) second order element that allow for the shear forces by allowing curvature in element edges, (b) first order element that restrict the edges to bend and give raise to shear stress (Dassault Systèmes, 2010) 48

Figure 2-19 Variation in rosettes from left to right: Tee, Rectangular and Delta (Vishay, 2010, a)..... 53

Figure 2-20 Strain transformation from principal to a random direction in Mohr's circle (Vishay, 2010, a) 54

Figure 3-1 Design process work flow (Pahl et al., 2006) 58

Figure 3-2 Position of analysis in the context of systematic design methodology 59

Figure 3-3 The Knowledge gap in product development (Adams, 2006) 60

Figure 3-4 Schematic architecture of ES (Labrie et al, 1994) 65

Figure 3-5 Design and analysis iterative cycle (Novak, Dolsak 2008) 66

Figure 3-6 An architectural view of the strategy for the existing commercial software components (Shephard and Wentorf, 1994) 67

Figure 3-7 Overall architecture of the modelling integration framework (Turkiyyah and Fenves, 1996) 68

Figure 3-8 Intelligent support for the FEA- Based design improvement process 69

Figure 3-9 V&V procedure (ASME, 2006) 71

Figure 3-10 A four point convergence curve (Chillery, 2010, b) 72

Figure 3-11 Process flowchart for computing metric process (Roy, 2011) 73

Figure 3-12 Propagation of input uncertainties to output (Roy, 2011) 74

Figure 3-13 Four-phases process planning by QFD (Chen and Ko, 2009) 79

Figure 4-1 Abstract of the proposed structure analysis methodology 84

Figure 4-2 Function Means Tree of a single analysis 86

Figure 4-3 Testing in an Integrated test plan 86

Figure 4-4 Process model of the methodology 87

Figure 4-5 QFD chart 1 89

Figure 4-6 QFD Chart 2 90

Figure 4-7 Structural analysis proposed methodology 94

Figure 5-1 Multi-staged telescopic sections in industrial off-road vehicles 97

Figure 5-2 Multi-staged telescopic assembly (Niftylift, 2010) 98

Figure 5-3 Sliding sections and arrangement of low-friction components in telescopic assembly (Niftylift, 2010) 98

Figure 5-4 Benchmark model of the telescopic cantilever beam 99

Figure 5-5 Test rig assembly 100

Figure 5-6 Total test rig assembly 101

Figure 5-7 The physical test rig 101

Figure 5-8 (a) The detail components of the inner section (b) The detail components of the outer section 102

Figure 5-9 Reaction forces at wear pads generated by self-weight and pay-load 104

Figure 5-10 QFD Chart 1 for the telescopic cantilever boom structural analysis 106

Figure 5-11 QFD Chart 2 for the telescopic cantilever boom structural analysis 106

Figure 6-1 (a) Beam sections in solid (b) Beam section in 3D planar (c) Telescopic assembly in global coordinate system (d) example of Tie pairs (e) example of Contact pairs (f) Coupling pairs (g) Loading point and Boundary Condition region 113

Figure 6-2 Nominated reading points on the centreline of the outer section 116

Figure 6-3 Von Mises stress along the centreline for element variation 118

Figure 6-4 Element performance vs. Analysis running time 119

Figure 6-5 Stress components directions with respect to the global coordinates system (a) S11 in x direction along the length of the beam, (b) S22 in y direction in the thickness direction (c) S33 in z direction across the width of the cross section (Dassault Systèmes, 2009, a) 120

Figure 6-6 Assembly simulation and validation measurement points 121

Figure 6-7 Test rig assembly 122

Figure 6-8 Strain gauges arrangement 122

Figure 6-9 Strain measurement instruments lay out (NI, 2012) 123

Figure 6-10 Von Mises stress propagation due to incremental loading 127

Figure 6-11 Axis of reading on contact area in one side of the structure 128

Figure 6-12 Stress increase due to load magnitude variation on the contact region..... 129

Figure 6-13 E33 comparison in contact area..... 132

Figure 6-14 E33 comparison near to the fixed end..... 132

Figure 6-15 Asymmetric load application, 300mm offset from centreline..... 133

Figure 6-16 Qualitative comparison of Von Mises stress plot for load type variation, (a) Symmetric load (b) Asymmetric load..... 136

Figure 6-17 Von Mises stress plot with overlap variation across half of the width of the outer section (a) reading axis 1(b) reading axis 2 (c) reading axis 3 (d) reading axis 4 (e) reading axis 5 138

Figure 6-18 Telescope vertical deflection on the centreline along the length 141

Figure 6-19 Structure's tip displacement VS. incremental symmetric load..... 142

Figure 6-20 Tip displacement experimental measurement with dial gauge 143

Figure 6-21 Tip displacement validation between simulation with shell and experimental measurement..... 144

Figure 6-22 Vertical displacement validation across the length of the beam under the maximum payload..... 145

Figure 6-23 Tip displacement plot against variable overlap..... 146

Figure 6-24 Structure’s rigidity variation with overlap length 147

Figure 6-25 Natural frequency analysis general set up..... 148

Figure 6-26 A System with Several Masses 149

Figure 6-27 Natural frequency verification for payload variation..... 150

Figure 6-28 Natural frequency verification for payload validation 151

Figure 6-29 Verification of natural frequency response to overlap variation..... 152

Figure 6-30 Validation of natural frequency response to overlap variation 153

Figure 6-31 Buckling analysis procedure in Abaqus..... 156

Figure 6-32 Newton-Raphson solution convergence (Hinton, 1992). 157

Figure 6-33 Newton-Raphson limitation near the load maximum (Dassault Systèmes, 2011). 158

Figure 6-34 Bilinear material model for post-yield behaviour (Johnson and Mellor, 1973). 158

Figure 6-35 Qualitative comparison for load type variation (a) Symmetric load case (b) Asymmetric load case (c) Stress plot at the buckling vicinity under symmetric load (d) Stress plot at the buckling vicinity under asymmetric load 160

Figure 6-36 Structure deformation due to application of BCL 161

Figure 6-37 Stress plot (a) Asymmetric load case (b) Symmetric load case 162

Figure 6-38 Load-displacement diagram, for the two loading steps 163

Figure 6-39 Load-displacement diagram for payload application step 163

Figure 6-40 Safety index variation with overlap length change 165

List of Tables

Table 2-1 Direction cosine for plane of maximum and minimum shear stress (Timoshenko and Goodier, 1951) 27

Table 2-2 Elastic constants relationship 36

Table 2-3 Failure criteria (Collins, 1993) 38

Table 2-4 Modes of buckling classification (Trahair, 1993) 41

Table 3-1 Stages of integrating simulation in design 62

Table 3-2 Benefits and limitations of early simulation (Adams, 2008) 63

Table 3-3 Comparative assessment of available methods to implement structural analysis in design 77

Table 4-1 Study plan based on MPC 91

Table 5-1 Measurable Performance Characteristics (MPCs) 104

Table 5-2 Plan for individual studies 108

Table 5-3 Plan for procedural integrated analysis 109

Table 5-4 Verification and Validation plan 111

Table 6-1 General simulation set up condition in Abaqus 114

Table 6-2 Stress study condition, dependency on the choice of element 115

Table 6-3 Choice of elements for the telescopic cantilever study (Dassault Systèmes, 2007, b) 115

Table 6-4 Von Mises stress results and analysis running time with variation of elements 117

Table 6-5 FEA problem size using different elements 119

Table 6-6 Stress tensor comparison between shell and solid elements 121

Table 6-7 Element validation and quantitative comparison 124

Table 6-8 Stress study condition, dependency to the load magnitude 125

Table 6-9 Von Mises stress results for incremental loading 126

Table 6-10 Strain and stress tensor propagation in incremental loading 130

Table 6-11 Stress study condition, dependency to the type of load 133

Table 6-12 Von Mises stress validation under the impact of asymmetric loading 134

Table 6-13 Strain and stress tensor validation for asymmetric loading 135

Table 6-14 Stress behaviour study, dependency to the overlap length 137

Table 6-15 element variation study on displacement behaviour 140

Table 6-16 Telescope vertical deflection under the maximum payload on the centreline along the length 141

Table 6-17 Telescopic cantilever tip displacement variation with incremental symmetric load 142

Table 6-18 Tip displacement validation along the length of the beam under the maximum payload 144

Table 6-19 Vertical deflection validation along the length of the beam under the maximum payload 145

Table 6-20 Tip displacement results for variable overlaps 146

Table 6-21 Natural frequency study, dependency to the load magnitude 150

Table 6-22 Natural frequency verification results 150

Table 6-23 Validation of natural frequency, quantitative comparison 151

Table 6-24 Natural frequency study, dependency to the overlap length 152

Table 6-25 Natural frequency verification results 152

Table 6-26 Validation of natural frequency response to overlap variation 153

Table 6-27 Buckling behaviour study, dependency to load type variation 159

Table 6-28 Eigenvalue buckling study results for load type variation 159

Table 6-29 Results for the load control study up to the maximum feasible tip displacement (up to material interference occurrence) 163

Table 6-30 Buckling behaviour study, dependency to overlap length variation 164

Table 6-31 Buckling results for the Eigenvalue buckling study with load type variation 164

List of Abbreviations

AI: Artificial Intelligence

ASME: American Society of Mechanical Engineers

CAD: Computer Aided Design

CAE: Computer Aided Engineering

DCV: Design Commitment Validate

DOE: Design of Experiment

DVC: Design Validate Commitment

ES: Expert System

FEA: Finite Element Analysis

KBE: Knowledge Base Engineering

KBS: Knowledge Base System

MPC: Measurable Performance Characteristics

NAFEMS: National Agency for Finite Element Methods and Standards

PDS: Product Design Specification

QFD: Quality Function Deployment

SME: Small Medium Enterprise

SQR: System Required Quantities

SSB: Strong Sense Benchmark

V&V: Verification and Validation

1 Introduction

1.1 Research aim and objectives

This research aims to develop an integrated methodology to embed the structural analysis in the design process.

Structural analysis is respected as a specialist field of knowledge. An effective communication and common understanding of the practice is not possible without knowing its aims and objectives. The science of applied stress analysis describes these objectives as quantifiable parameters, that provide a common ground between two disciplines to pursue the mutual goal.

On the other hand the design process is recognised as a procedural and systematic approach developed over the last few decades. A successful product design process has to be built bearing this perspective in mind. The design of mechanical parts in particular is highly dependent on the quantification of the mechanical performance for the designated service condition. The role of structural analysis in the design process of a mechanical product can be even more significant considering the multi-functionality of the products, which require more exhaustive multi-objective analysis.

Structural analysis is the central activity to design for mechanical performance, and therefore necessitates a systematic protocol.

1.1.1 Motivations

In the growing competitive business environment, more effective use of the resources is a must. Investment in new technologies and development for enterprise has to be carefully assessed and justified.

Modern structural design practice requires a heavy upfront investment in hardware, software, education, and skills development. However, investment in these components is necessary but not sufficient to make analysis the predominant design tool for structural analysis. An additional component, the systematic integration of analysis within design, is required to make the most of the investment.

The motivation behind this research is to address this underlying issue in the product design environment.

1.1.2 Research question

The following research question is investigated in this research:

> *"How is it possible to increase the effectiveness of structural analysis by its interactive and systematic integration within the product design process?"*

The following objectives are identified to address this question.

1.1.3 Objectives

- Determine the structural analysis aims, objectives, quantifiable parameters, and acceptance criteria.
- Explore available methods to achieve structural analysis goal.
- Understand the product design environment and investigate the state-of-the-art methods to address product design requirements in structural analysis.
- Assess the current state of knowledge with its strengths and weaknesses
- Propose and establish a robust method to integrate structural analysis in the design process and address the identified shortages.
- Validate the proposal by application on a real-case design scenario and collecting the target outcomes.

1.2 Thesis structure

The scope of this research is organised as follow. Chapter 2 describes structural analysis practice with its aims and objectives. The objectives are further elaborated with their corresponding quantifiable parameters. The available methods of achieving these outcomes are introduced with the focus on the most common industrial methods.

Chapter 3 explains the design perspective to develop a mechanical product. The mainstream approach in product design is introduced and the current state-of-the-art practices to accommodate structural analysis in design are further developed. The available methods' strengths and weaknesses are discussed. The identified shortage is planned to be answered by the application of Quality Function Deployment (QFD) method. The fundamentals and the opportunity for QFD to be integrated with structural analysis process is studied

The proposed methodology for design integrated structural analysis process is described in Chapter 4. The methodology, that starts with a multi-functional mechanical product

concept and ends with characterisation of the structural behaviour with variation of the input parameters, is detailed and the intermediate milestones are identified.

Chapter 5 introduces a case-study structure to validate the proposed methodology. The telescopic cantilever boom in the current industrial application is defined as the case-study. The methodology presented in Chapter 4 is used to develop a list of required analyses and corresponding verification and validation scenarios that thoroughly and completely answer the stakeholders' requirements.

The proposed studies of the previous chapter are conducted and the corresponding results to each of the stakeholders' requirements are packaged in chapter 6. This chapter contains the conclusive remarks on each of the required structural performances.

Chapter 7 contains the summary of the research followed with suggestions for future developments and conclusions. The outline of this research is shown in Figure 1-1.

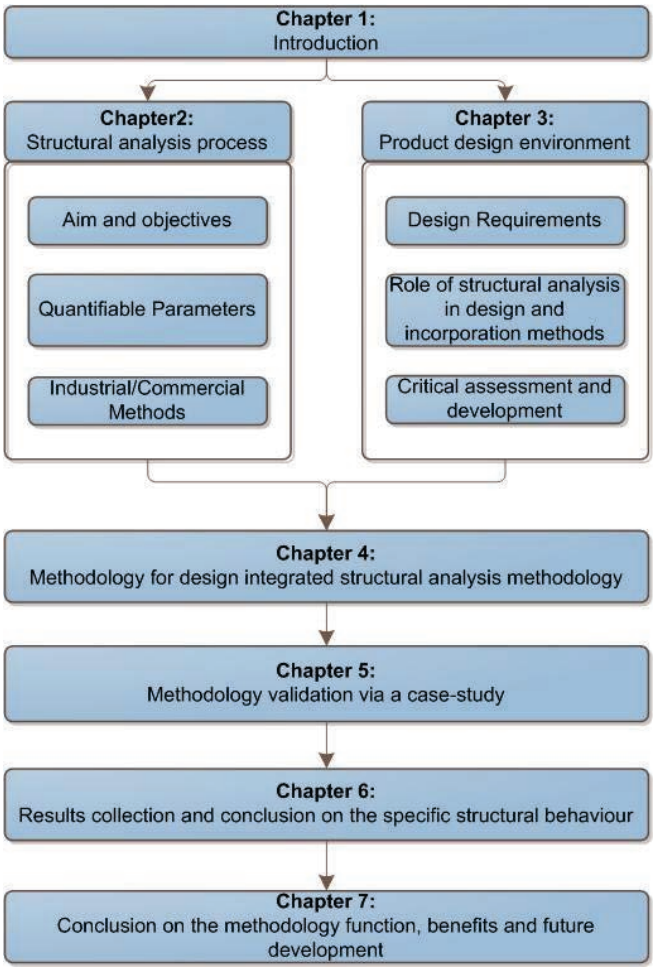

Figure 1-1 Thesis structure

2 Principles of Applied Stress Analysis

This chapter discusses the structural analysis process by identifying its aim and objectives. The process can only be comprehended by its outcomes as quantifiable parameters.

The knowledge of structural analysis in application is the key entry to the subject. Valuable heritage of theoretical material and classic methods has been incorporated in modern structural analysis. This collection of background knowledge, identified as fundamental for analyst-designer communication, is decoded in this chapter.

The modern application of structural analysis for the design of complex structures, hugely benefits from developments in numerical methods. This chapter continues with a brief introduction to the mainstream numerical methods with particular attention to Finite Element Methods (FEM) as the leader in industrial application. General procedural steps to set up a FE model are described in this chapter. Whilst most of the stages for creating a FE model replicate a real-life scenario (e.g. load, boundary condition, interactions etc.) the geometry discretisation is exclusively a modelling approximation that converts a continuous medium into a discrete geometry. The process known as meshing and incorporated by assigning elements is recognised as the key transitional stage between 3D CAD models into FE models. This topic is discussed in more detail in this chapter.

The chapter follows with the application of experimental measurements as the traditional method of analysing the structure. The role of experimental analysis to validate the simulation becomes more significant in the modern application. The practice is broadly classified as whole-field and point-by-point methods. Among the available techniques in each class, the commonly practiced methods of photoelastic measurement and strain gauge measurements are nominated for further discussion.

2.1 Structural analysis in application, aims and objectives

Engineers of all disciplines are often required to design structural components or machine parts which must support loads. The mission of structural design is to ensure structural integrity, defined as "*the capacity of engineering components to withstand service loads, effectively and efficiently, during their service life"* (Samuel and Weir, 1999, p.3). To clarify the practice some basic definitions are provided (Samuel and Weir, 1999):

- The engineering component generally addresses any engineering structure that may be constructed from several interconnected parts into a single entity.
- Service loads are those that the designer considers as credible to be imposed on the component during its service life
- Effectiveness of the structure refers to its capacity to accept service loads without exceeding the specified criteria.
- Efficiency of the structure concerns about the structures mass or cost.

The objectives of structural design are highlighted (Ray, 1985, Sack,1984):

- Determine the general layout and shape of the component.
- Evaluate the component's service load during its expected life.
- Material selection against maximum allowable stress.
- Expression of design criteria e.g. stress, in terms of the loads and dimensions.

Figure 2-1 relates the specific factors that need to be considered in structural design. The shape of the component is decided by the required functions and the effect of applicable loads. The response of the applied load is observed in the form of total stress and displacement which determines unit stresses and strains. The aim of the structural analysis is essentially coupled to the quantification of these two parameters. The variation of stress and strain and their statues in the worst-case operational scenario is the basis for decision on the size of the components (Ray, 1985).

The design of the structure is inherently endangered by failure (Samuel and Weir, 1999). Failure refers to any action resulting in inability of any part of the structure to function in a manner intended (Ugural, 1999). The component must be designed so that failure will not occur as a result of excessive distortion, cracking or rupture of the material etc. The failure criteria are critical information to define the design frame. This information may be set by standards, previous experience or field measurements.

The state of stress and strain and their relationship as well as structural failure criteria are described in section 2.2.

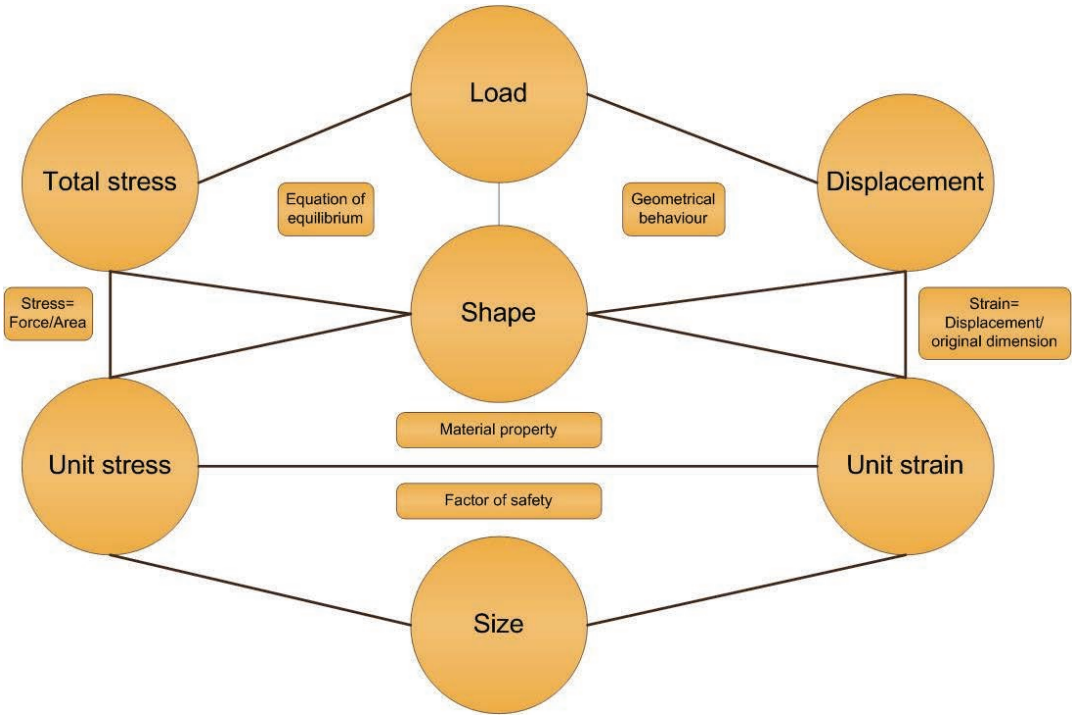

Figure 2-1 Relationship between specific factors to structural design (Ray, 1985)

2.2 Quantifiable parameters and failure criteria

Theory of solid mechanics is one of the analytical methods that inform the structural design. The foundation of the solid mechanics is on the spring-like behaviour of the material that is known as theory of elasticity and described by Hook's law (Rees, 1997).

Mechanics of materials and theory of elasticity deal with the internal behaviour of loaded solid bodies. The differences between these two approaches lie primarily in the extent to which strains are described and in the nature of simplifications used. Formulas of the mechanics of materials normally give average stresses at any section. Concentrated forces and abrupt changes in the cross section initiate irregular stresses (Peterson, 1974). Therefore only at distances close to the depth of the member from such disturbances stresses are in agreement with the mechanics of material theory (Ugural, 1999).

There are three types of argument that can be deployed in solving any structural problems (NAFEMS, 1987):

- Equilibrium: These arguments relate stress (σ) to applied forces, or more often stresses to other stresses. In the case of dynamic excitation, the inertia forces would also be considered.

- Compatibility: These are purely geometrical argument that relates strain (ε) to displacement. The compatibility equation depends on the definition of strain and the type of deformation and geometry of the particular structure.
- Stress-strain law: These constitutive relationships are empirical and depend on experimental evidence. For most materials, within their useful working range, these laws may be taken as linear.

Structural analysis can therefore be schematically summarised as Figure 2-2.

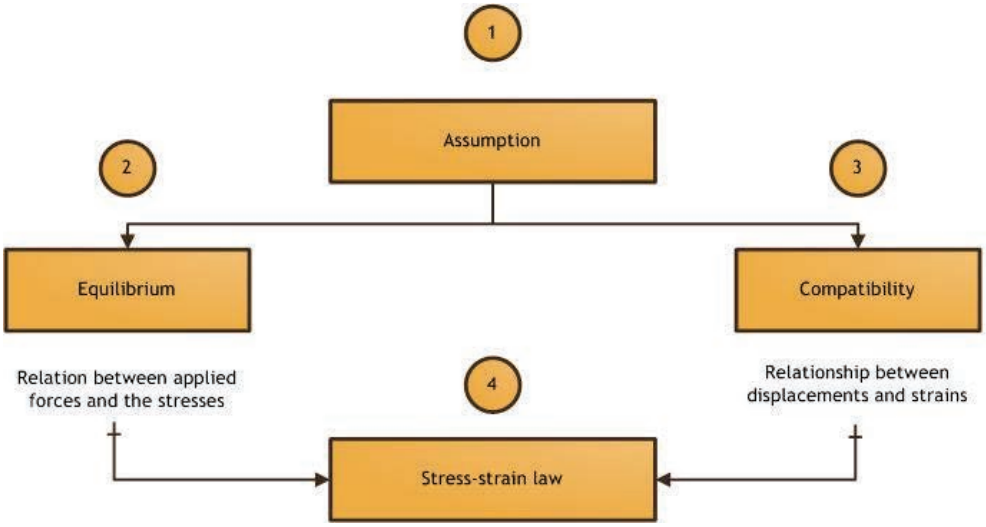

Figure 2-2 Schematic illustration of structural analysis process (NAFEMS, 1987)

While the compatibility and equilibrium arguments are highly interdependent (Gerstle, 1974; Sack, 1984; Rees, 1997), stress-strain law, is an independent argument (NAFEMS, 1987). This argument depends on material property. Four fundamental elastic constants of Modulus of Elasticity (Young's Modulus), Poisson's Ratio, Modulus of Rigidity (Shear Modulus) and Bulk Modulus (Rees, 1997; Rees, 2003) are required to define an isotropic homogenous material.

More rigorous understanding of the state of the stress and strain in three dimensions is required to comprehend the complex shapes and assemblies with considerable number of links and connections (Krishnakumar, n.d.). Sections 2.2.1, 2.2.2 and 2.2.3 expand on the stress and strain relationship in elastic material.

2.2.1 Elastic Stress

Stress definition: The stress definition is valid in a continuum problem that assumes the material contains sufficiently dense substances that every point of the region

occupied by the material. The theory of stress depends on Newton's laws of motion, which are independent from the nature of continuous materials e.g. elastic, plastic etc.

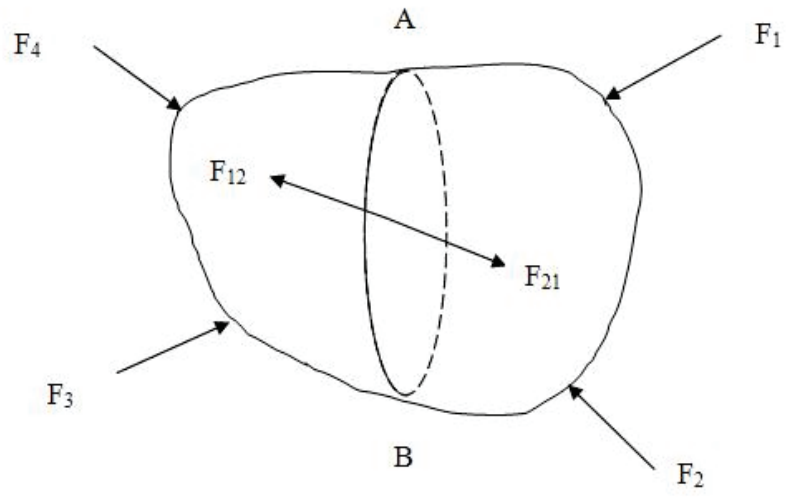

Figure 2-3 The state of a stress in a body in static equilibrium

Figure 2-3 shows the state of stress on a body in static equilibrium under the action of the system of external forces F_1, F_2 ..., F_n. If the body is cut in half by an imaginary plane AB the forces along the particles in that plane tend to hold the body together. The force equilibrium condition on two halves represented by F_{21} and F_{12} retain the body in equilibrium (Singh, 1979).

Eq. 2-1

$$F_{21} = -F_{12}$$

If the resultant internal force, ΔF, acting on an arbitrary element in the area ΔA as shown in Figure 2-4 such that:

Eq. 2-2

$$\Sigma \Delta A \,.\, \Delta F = F_{21}$$

ΔF can be split to its component in normal direction of $\bar{n}$ and the other two perpendiculars in plane direction in a Cartesian coordinate system. The normal component of load, ΔF_n produces the normal component of stress at point O as:

Eq. 2-3

$$\sigma = \lim_{A \to 0} \frac{\Delta F_n}{\Delta A}$$

The other two perpendicular load components in the plane of the section are ΔF_{s1} and ΔF_{s2} which produce the shear components of stress. These are:

Eq. 2-4

$$\tau_{s1} = \lim_{A \to 0} \frac{\Delta F_{s1}}{\Delta A}$$

$$\tau_{s2} = \lim_{A \to 0} \frac{\Delta F_{s2}}{\Delta A}$$

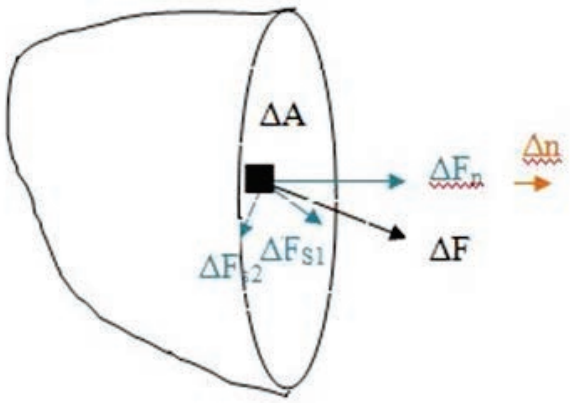

Figure 2-4 Resultant internal forces acting on an arbitrary element of area

The definition above justifies the argument that declares stress as tensor quantity by showing the necessity of direction and a plane of reference in addition to magnitude.

Stress tensor at a point: The state of the stress at a point in the Cartesian system is represented by the following nine components of stress known as the stress tensor (Pilkey, 1994).

Eq. 2-5

$$\tau_{ij} = \begin{bmatrix} \tau_{xx} & \tau_{xy} & \tau_{xz} \\ \tau_{yx} & \tau_{yy} & \tau_{yz} \\ \tau_{zx} & \tau_{zy} & \tau_{zz} \end{bmatrix}$$

All the stress components have been shown on a parallelepiped in Figure 2-5 where the leading diagonal terms are normal stresses and off-diagonal terms are shear stresses (Timoshenko and Goodier, 1951). In the double subscription system used to represent the stress components, the first subscript denotes the plane normal direction, and the second subscript denotes the direction toward which the stress acts. The double subscription of normal stress can be simplified to a single subscription as σ_x, σ_y, σ_z. The shear stresses τ_{xy} and τ_{yx} are shown acting on their face perpendicular to the x and

y axis respectively. The concept of stress tensor symmetry and the reduction in the parameters can be explained by the moment equilibrium condition (Wang, 1953).

Eq. 2-6

$$\tau_{xy} = \tau_{yx}\ ,\quad \tau_{xz} = \tau_{zx}\ ,\quad \tau_{yz} = \tau_{zy}$$

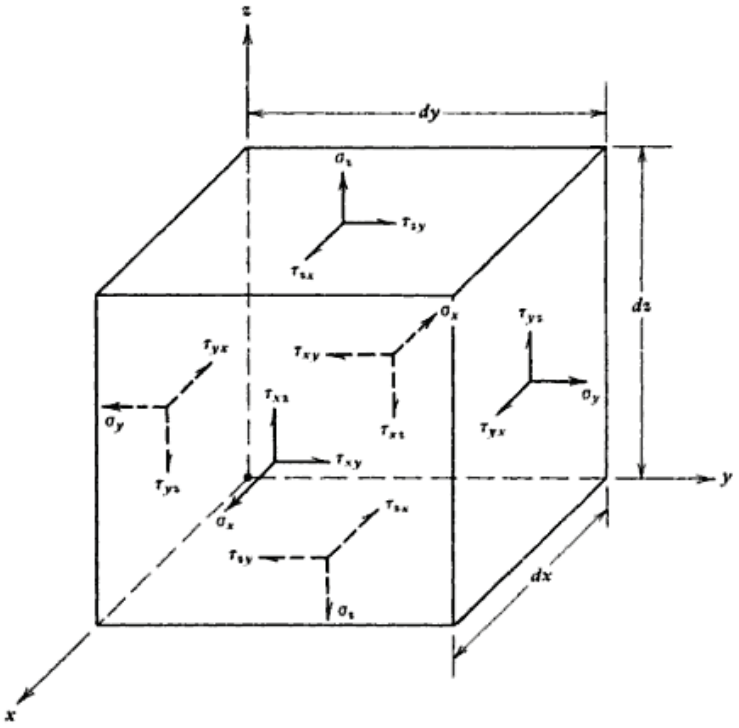

Figure 2-5 State of stress on a parallelepiped (Timoshenko and Goodier, 1951)

Therefore the components of stress tensor in Cartesian coordinates reduce from 9 to 6 independent components which means that the Eq. 2-5 can be rewritten as:

Eq. 2-7

$$\tau_{ij} = \begin{bmatrix} \sigma_x & \tau_{xy} & \tau_{xz} \\ \tau_{xy} & \sigma_y & \tau_{yz} \\ \tau_{xz} & \tau_{yz} & \sigma_z \end{bmatrix}$$

The equilibrium of forces in 3 directions, using Newton second law of motion, on an infinitesimal parallelepiped as shown in Figure 2-6, can be written as:

Eq. 2-8

$$\frac{\partial \sigma_x}{\partial x} + \frac{\partial \tau_{xy}}{\partial y} + \frac{\partial \tau_{xz}}{\partial z} + B_x = \rho \overline{a_x}$$

where B_x is components of the body force in x direction, expressed per unit volume, $\overline{a_x}$ is acceleration in the x direction and ρ is density of material. In the absence of inertia and body force (Chandrupatla and Belegundu, 2002), Eq. 2-8 reduced to:

Eq. 2-9

$$\frac{\partial \sigma_x}{\partial x} + \frac{\partial \tau_{xy}}{\partial y} + \frac{\partial \tau_{xz}}{\partial z} = 0$$

$$\frac{\partial \tau_{xy}}{\partial x} + \frac{\partial \sigma_y}{\partial y} + \frac{\partial \tau_{yz}}{\partial z} = 0$$

$$\frac{\partial \tau_{xz}}{\partial x} + \frac{\partial \tau_{yz}}{\partial y} + \frac{\partial \sigma_z}{\partial z} = 0$$

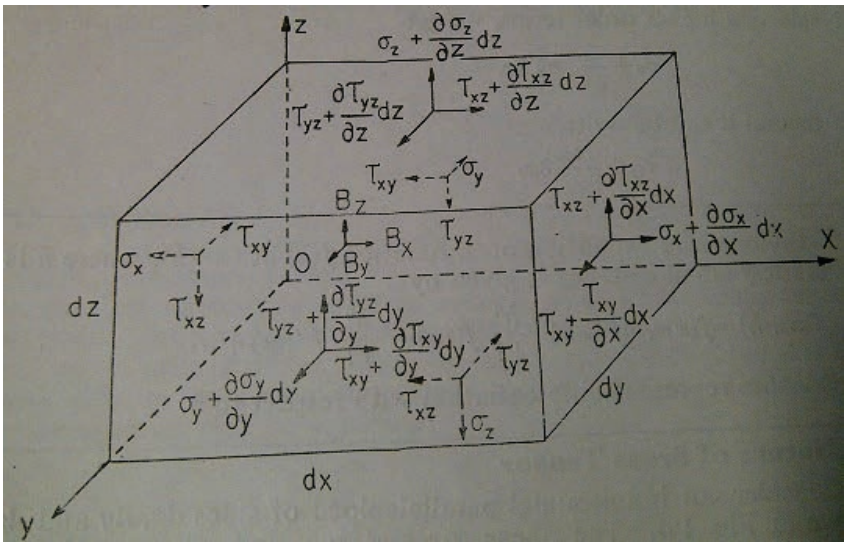

Figure 2-6 Force equilibrium on an infinitesimal parallelepiped (Singh, 1979)

Stress invariants and maximum shearing stress: The combinations of stresses at a point which do not change with the orientation of the coordinate axes are called stress invariants (Pilkey, 1994). This concept, elaborated in Appendix I, leads to:

Eq. 2-10

$$\sigma_x + \sigma_y + \sigma_z = I_1 = \text{First stress invariants}$$

$$\sigma_x\sigma_y + \sigma_y\sigma_z + \sigma_x\sigma_z - \tau_{xy}^2 - \tau_{yz}^2 - \tau_{xz}^2 = I_2 = \text{Second stress invariant}$$

$$\sigma_x\sigma_y\sigma_z - \sigma_x\tau_{yz}^2 - \sigma_y\tau_{xz}^2 - \sigma_z\tau_{xy}^2 + 2\tau_{xy}\tau_{yz}\tau_{xz} = I_3 = \text{Third stress invariant}$$

Maximum shearing stress can be defined as:

Eq. 2-11

$$\tau_{ns}(\max) = \pm\left(\frac{\sigma_1-\sigma_3}{2}\right),\ \ \tau_{ns}(\max) = \pm\left(\frac{\sigma_1-\sigma_2}{2}\right),\ \tau_{ns}(\max) = \pm\left(\frac{\sigma_2-\sigma_3}{2}\right)$$

The direction cosines for planes of $\tau_{ns}(\max)$ and $\tau_{ns}(\min)$ are given in Table 2-1.The planes of maximum shear stress are shown in Figure 2-7. Appendix I and II details the derivation of Eq. 2-10 and Eq. 2-11.

Table 2-1 Direction cosine for plane of maximum and minimum shear stress (Timoshenko and Goodier, 1951)

	$\tau_{ns}(\max)$			$\tau_{ns}(\min)$		
a_{nx}	$\pm\frac{1}{\sqrt{2}}$	0	$\pm\frac{1}{\sqrt{2}}$	0	0	±1
a_{ny}	$\pm\frac{1}{\sqrt{2}}$	$\pm\frac{1}{\sqrt{2}}$	0	0	±1	0
a_{nz}	0	$\pm\frac{1}{\sqrt{2}}$	$\pm\frac{1}{\sqrt{2}}$	±1	0	0

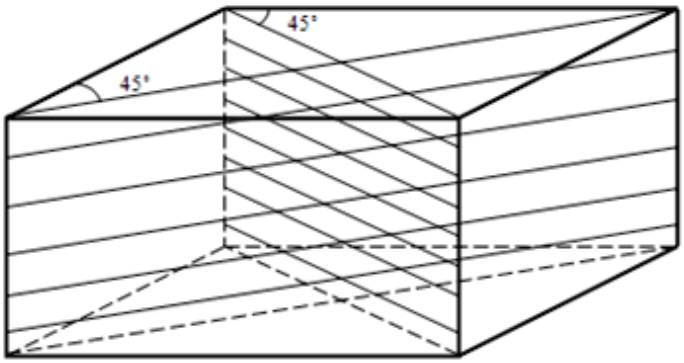

Figure 2-7 Planes of maximum shearing stress direction

2.2.2 Elastic Strain Analysis

Deformation of a continuous medium: The deformation on a continuous medium can be described with a closed region of R that is deformed to be R′, as shown in Figure 2-8 that cause a particle P (x, y, z) moves to the point P′ (x′, y′, z′) in a Cartesian coordinate system. The deformation of the medium is defined by equations:

Eq. 2-12

$$x' = x'(x,y,z)\,,\qquad y' = y'(x,y,z),\qquad z' = z'(x,y,z)$$

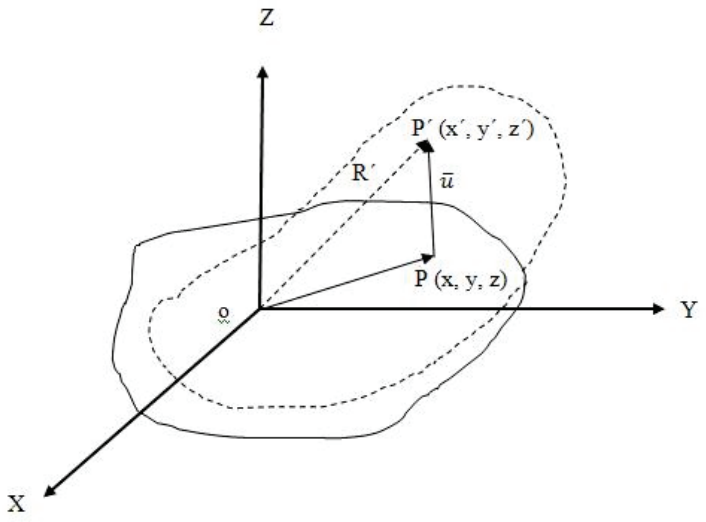

Figure 2-8 Deformation of a continuous medium

Assume that (x´, y´, z´) are continuous and differentiable in the variable (x, y, z) and the points P and P´ are so close to each other that displacement is infinitesimally small. The components of displacement can be written as:

Eq. 2-13

$$u_x = x' - x, \qquad u_y = y' - y, \qquad u_z = z' - z$$

The displacement components can be combined in the form of vector as:

Eq. 2-14

$$\bar{u} = \hat{\imath}u_x + \hat{\jmath}u_y + \hat{k}u_z$$

Where $\hat{\imath}, \hat{\jmath}, \hat{k}$ are unit vectors along positive (x, y, z) axes respectively. The displacement vector will vary continuously from point to point and so it forms a vector field called displacement field. It is a function of coordinates of the unreformed geometry i.e.

Eq. 2-15

$$u_x = f_1(x, y, z), \qquad u_y = f_2(x, y, z), \qquad u_z = f_3(x, y, z) \ldots$$

A necessary condition for a deformation to be physically possible is for Jacobian D to be greater than zero (Chou and Pagano, 1967), where:

Eq. 2-16

$$D = \begin{vmatrix} \frac{\partial x'}{\partial x} & \frac{\partial x'}{\partial y} & \frac{\partial x'}{\partial z} \\ \frac{\partial y'}{\partial x} & \frac{\partial y'}{\partial y} & \frac{\partial y'}{\partial z} \\ \frac{\partial z'}{\partial x} & \frac{\partial z'}{\partial y} & \frac{\partial z'}{\partial z} \end{vmatrix} = \begin{vmatrix} 1+\frac{\partial u_x}{\partial x} & \frac{\partial u_x}{\partial y} & \frac{\partial u_x}{\partial z} \\ \frac{\partial u_y}{\partial x} & 1+\frac{\partial u_y}{\partial y} & \frac{\partial u_y}{\partial z} \\ \frac{\partial u_z}{\partial x} & \frac{\partial u_z}{\partial y} & 1+\frac{\partial u_z}{\partial z} \end{vmatrix}$$

This condition ensures that the displacement possesses a single-valued continuous solution (Singh, 1979). D= 1 indicates the particles of a body are not displaced.

The deformation of the continuous medium can be expanded for an infinitesimal line element PQ passes into the line element P′Q′ under deformation as shown Figure 2-9. In general it is expected that both length and direction of PQ will be changed.

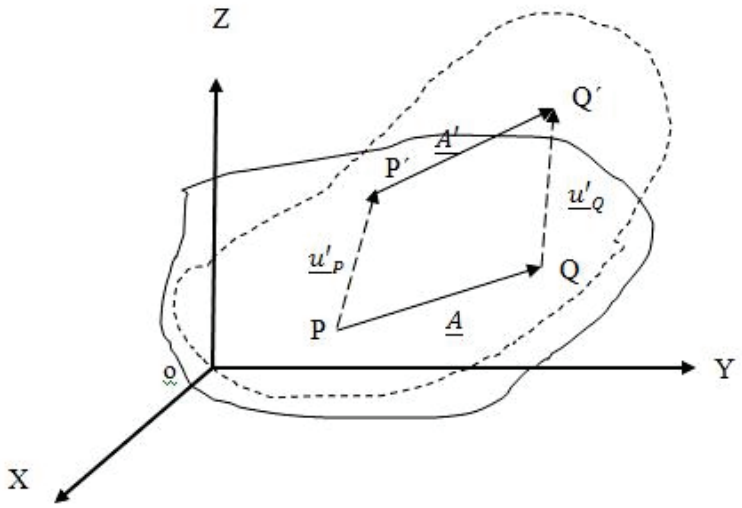

Figure 2-9 Deformation of an infinitesimal line element

However this only concerns the change in the original length of $\underline{A}$ to $\underline{A}'$ given as:

Eq. 2-17

$$\underline{A} = A_x\hat{\imath} + A_y\hat{\jmath} + A_z\hat{k}\,, \qquad \underline{A'} = A_x'\hat{\imath} + A_y'\hat{\jmath} + A_z'\hat{k}$$

Eq. 2-18

$$\overline{\partial A} = \underline{A'} - \underline{A}$$

Or in the matrix format:

Eq. 2-19

$$\begin{Bmatrix}\delta A_x\\ \delta A_y\\ \delta A_z\end{Bmatrix}=\begin{bmatrix}\frac{\partial u_x}{\partial x} & \frac{\partial u_x}{\partial y} & \frac{\partial u_x}{\partial z}\\ \frac{\partial u_y}{\partial x} & \frac{\partial u_y}{\partial y} & \frac{\partial u_y}{\partial z}\\ \frac{\partial u_z}{\partial x} & \frac{\partial u_z}{\partial y} & \frac{\partial u_z}{\partial z}\end{bmatrix}\begin{Bmatrix}A_x\\ A_y\\ A_z\end{Bmatrix}$$

$$\overline{\delta A}=\delta A_x\hat{\imath}+\delta A_y\hat{\jmath}+\ \delta A_z\hat{k}$$

Therefore changed vector is:

Eq. 2-20

$$\underline{A'}=(A_x+\delta A_x)\hat{\imath}+\ \big(A_y+\delta A_y\big)\hat{\jmath}+(A_z+\delta A_z)\hat{k}$$

For two different displacement fields, $\underline{u_i^{(1)}}$ and $\underline{u_i^{(2)}}$, applied one after another the final length of the element A´´ in an arbitrary point can be determined as (Singh, 1979).:

Eq. 2-21

$$A_i''=A_i+\left(\frac{\partial u_i^{(1)}}{\partial x_j}+\frac{\partial u_i^{(2)}}{\partial x_j}\right)A_j$$

Therefore the following rules may be framed for determining successive deformation:

- The total deformation is equal to the sum of the individual deformations, each computed separately from the original geometry.
- The order of the application of the displacement field does not affect the total deformation.

Displacement of a particle: Displacement of a particle is a vector quantity that is determined by its initial and final locations regardless of the path between them.

If the displacements of all particles in a mechanical system are equal the system will undergo translation. A rotation of a mechanical system manifests by all its particles describe a circular arcs of the same angle with their planes perpendicular to that axis. A rotation is a rigid-body displacement. A rigid body would experience a plane displacement, if the displacement vectors of all its particles are parallel to the plane of displacement. Translations and rotations are plane displacement (Singh, 1979).

Rigid body displacement can be classified under translation or rotation of a medium. From displacement components at a single point, it is not possible to tell whether the displacement is due to distortion of the body or to rigid body displacement. Distortion or strain imply a change in displacement from one point to another and can be associated with derivatives of displacements with respect to x_j, i.e., $\frac{\partial u_i}{\partial x_j}$.

In order to eliminate the effect of rigid body rotation the change in displacement is written as:

Eq. 2-22

$$\frac{\partial u_i}{\partial x_i} = \frac{1}{2}\left(\frac{\partial u_i}{\partial x_j} + \frac{\partial u_j}{\partial x_i}\right) + \frac{1}{2}\left(\frac{\partial u_i}{\partial x_j} - \frac{\partial u_j}{\partial x_i}\right) = \epsilon_{ij} + \omega_{ij}$$

Where ϵ_{ij} and $\omega_{ij}$are strain and rotation matrix respectively (Singh, 1979).

Homogeneous deformation: If the final position of the point P (x′,y′,z′) is a linear function of its initial position (x,y,z) the six components of strain will be constant throughout the medium (Chandrupatla and Belegundu, 2002). Components of strain tensor will then become:

Eq. 2-23

$$\epsilon_{xx} = \frac{\partial u_x}{\partial x} = C_{11}, \qquad \epsilon_{yy} = \frac{\partial u_y}{\partial y} = C_{21}, \qquad \epsilon_{zz} = \frac{\partial u_z}{\partial z} = C_{31}$$

$$2\epsilon_{xy} = C_{12} + C_{21}, \qquad 2\epsilon_{yz} = C_{23} + C_{32}, \qquad 2\epsilon_{xz} = C_{13} + C_{31}$$

Where C_{ij}, i=1,2,3 ; j=0, 1, 2, 3 are arbitrary constants .

This type of deformation is called homogenous deformation. Consequently the relative elongation of an infinitesimal line element depends only on its direction; it does not depend on its location in the body. Likewise the change in angle between two infinitesimal line elements does not depend on their location, but only on their initial directions.

Physical interpretation of strain tensor: This section defines the diagonal and off-diagonal terms of the strain matrix. This can be provided by a line element of PQ of length Δx along the x axis that passes to P′Q′ after deformation with the length of Δx′ shown in Figure 2-10. The orthogonal projection of P′Q′ in the x direction is:

Eq. 2-24

$$(\Delta x')_x = \Delta x + (u_x)_Q - (u_x)_p$$

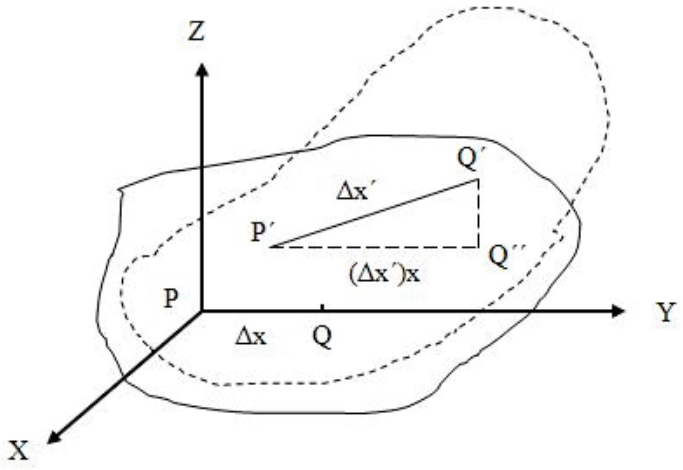

Figure 2-10 Physical interpretation of strain tensor normal component

The strain component ϵ_{xx} can be approximated, by expansion of $(u_x)_Q$ in the neighbourhood of point p, to be the elongation in the x-direction of infinitesimal line segment originally in the x-direction per unit of original length. The same interpretation may be given for the other diagonal terms of strain matrix.

Eq. 2-25

$$(\epsilon_{xx})_P = \left(\frac{\partial u_x}{\partial x}\right)_P$$

If the line element of PQ with the length of Δx along x-direction and PR with the length of Δy along y-direction is considered, deformed state passes PQ to P´Q´ and PR to P´R´ as shown in Figure 2-11 (a).

The change in the right angle of the pair in infinitesimal line segment at P is determined by projections of PQ and PR on the *xy* plane is given in Figure 2-11 (b) (Singh, 1979). The orthogonal projection of P´R´ along the *x* and *y* axis result in:

Eq. 2-26

$$\tan\theta = \theta = \frac{\partial u_x}{\partial y}$$

$$\tan\beta = \beta = \frac{\partial u_y}{\partial x}$$

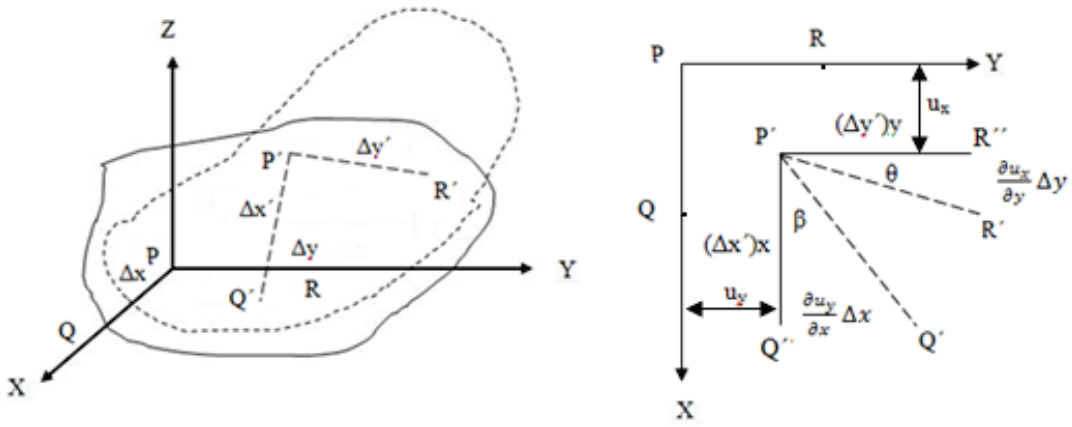

(a) **(b)**

Figure 2-11 Physical interpretation of strain tensor shear component

The subsequent decrease in the right angles at P is formulated as (Timoshenko and Goodier, 1951) :

Eq. 2-27

$$\theta + \beta = \frac{\partial u_x}{\partial y} + \frac{\partial u_y}{\partial x} = \gamma_{xy} = 2\epsilon_{xy}$$

Where γ_{xy} is the shear angle and in general can be determined as $\gamma_{ij} = 2\epsilon_{ij}$. Therefore the shearing angle is the decrease of the right angle between infinitesimal orthogonal line elements at appoint as a result of deformation. These shearing are the off-diagonal terms in the strain tensor.

Principal strains: The determination of the principal strains is critical to computing the directions for which the strains have extreme values. The derivation detailed in Appendix III leads to the strain extreme values as:

Eq. 2-28

$$J_1 = \epsilon_x + \epsilon_y + \epsilon_z = first\ invariant\ of\ strain$$

$$J_2 = \epsilon_x\epsilon_y + \epsilon_y\epsilon_z + \epsilon_z\epsilon_x - \frac{\gamma_{xy}^{\,2}}{4} - \frac{\gamma_{yz}^{\,2}}{4} - \frac{\gamma_{xz}^{\,2}}{4} = second\ invariant\ of\ strain$$

$$J_3 = \begin{vmatrix} \epsilon_x & \frac{\gamma_{xy}}{2} & \frac{\gamma_{xz}}{2} \\ \frac{\gamma_{xy}}{2} & \epsilon_y & \frac{\gamma_{yz}}{2} \\ \frac{\gamma_{xz}}{2} & \frac{\gamma_{yz}}{2} & \epsilon_z \end{vmatrix} = third\ invariant\ of\ strain$$

2.2.3 Stress-strain relationships

Hook's law relates stress and strain in an elastic portion of the material behaviour:

Eq. 2-29

$$\sigma = E\epsilon$$

Similarly, linear elasticity can be measured in a member subjected to shear loading:

Eq. 2-30

$$\tau = G\gamma$$

where τ is a shear stress, γ is shear strain and G is the Shear Modulus. In the elastic range the relation of the lateral strain to the axial strain specified by Poisson's ratio states (Pilkey, 1994):

Eq. 2-31

$$\nu = \left|\frac{\text{Lateral strain}}{\text{Axial strain}}\right|$$

The most general linear relationship which connects stresses to strains is known as the generalised Hook's law that can be expressed as:

Eq. 2-32

$$\epsilon_{ij} = c_{ijkl}\tau_{kl}$$

Solving for stress:

Eq. 2-33

$$\tau_{kl} = \left[c_{ijkl}\right]^{-1}\epsilon_{ij}\,, \tau_{kl} = C_{ijkl}\epsilon_{ij}$$

where C_{ijkl} is modulus of elasticity or elastic constants. These are 81 elastic constants for the most general cases. It can be proven that last two indices are interchangeable when the only non-zero strain components are $\epsilon_{12}\ and\ \epsilon_{21}$ (Wang, 1953). Elasticity tensor is also interchangeable for the first two indices when the state of strain indicates that the only non-zero strain component is ϵ_{11}. These symmetric properties of elastic constants reduce the number of independent elastic constants by 27 and 18 respectively, to a total of 36. Thus stress-strain relationship can be written as:

Eq. 2-34

$$\begin{Bmatrix}\tau_{11}\\ \tau_{22}\\ \tau_{33}\\ \tau_{12}\\ \tau_{23}\\ \tau_{13}\end{Bmatrix}=\begin{bmatrix}C_{11} & C_{12} & C_{13} & C_{14} & C_{15} & C_{16}\\ C_{21} & C_{22} & C_{23} & C_{24} & C_{25} & C_{26}\\ C_{31} & C_{32} & C_{33} & C_{34} & C_{35} & C_{36}\\ C_{41} & C_{42} & C_{43} & C_{44} & C_{45} & C_{46}\\ C_{51} & C_{52} & C_{53} & C_{54} & C_{55} & C_{56}\\ C_{61} & C_{62} & C_{63} & C_{64} & C_{65} & C_{66}\end{bmatrix}\begin{Bmatrix}\epsilon_{11}\\ \epsilon_{22}\\ \epsilon_{33}\\ \gamma_{12}\\ \gamma_{23}\\ \gamma_{13}\end{Bmatrix}$$

The elasticity matrix shows another degree of symmetry under anisotropy condition when the variation of the body under deformation occurs isothermally or adiabatically. This reduces the number of independent constants to 21. In the isotropic materials that possess elastic properties independent of the orientation of the axis the matrix of elasticity reduces to:

Eq. 2-35

$$\begin{bmatrix}2G+\lambda & \lambda & \lambda & 0 & 0 & 0\\ & 2G+\lambda & \lambda & 0 & 0 & 0\\ & & 2G+\lambda & 0 & 0 & 0\\ & & & G & 0 & 0\\ & & & & G & 0\\ Symmetric & & & & & G\end{bmatrix}$$

Therefore there are only two independent constants that determine the stress-strain relationship which are shear modulus of elasticity, G, and Lam's constant. Relationships between various elastic constants are shown in Table 2-2. Using these relations the strain components can be written as (Chandrupatla and Belegundu, 2002):

Eq. 2-36

$$\epsilon_x=\frac{1}{E}\left[\sigma_x-\nu(\sigma_y+\sigma_z)\right],\quad \epsilon_y=\frac{1}{E}\left[\sigma_y-\nu(\sigma_x+\sigma_z)\right],\quad \epsilon_z=\frac{1}{E}\left[\sigma_z-\nu(\sigma_y+\sigma_x)\right]$$

$$\gamma_{xy}=\frac{\tau_{xy}}{G},\qquad \gamma_{yz}=\frac{\tau_{yz}}{G},\qquad \gamma_{xz}=\frac{\tau_{xz}}{G}$$

Table 2-2 Elastic constants relationship

	λ, G	K, G	G, ν	E, ν	E, G
λ= Lam's modulus	λ	$K - \frac{2G}{E}$	$\frac{2G\nu}{1-2\nu}$	$\frac{\nu E}{(1+\nu)(1-2\nu)}$	$\frac{G(E-2G)}{(3G-E)}$
G= Shear Modulus	G	G	G	$\frac{E}{2(1+\nu)}$	G
K= Bulk modulus	$\lambda - \frac{2G}{3}$	K	$\frac{2G(1+\nu)}{3(1-2\nu)}$	$\frac{E}{3(1-2\nu)}$	$\frac{EG}{3(3G-E)}$
E= Young's modulus	$\frac{G(3\lambda+2G)}{(\lambda+G)}$	$\frac{9KG}{3K+G}$	$2G(1+\nu)$	E	E
ν= Poisson's Ratio	$\frac{\lambda}{2(\lambda+G)}$	$\frac{3K-2G}{GK+2G}$	ν	ν	$\frac{E}{2G} - 1$

2.2.4 Failure criteria

Quantification of the stress and strain parameters is only comprehensible by clarification of failure criteria. Mechanical failure is defined as any change in the size, shape or material properties of a structure or component that renders it incapable of performing its intended functions satisfactorily (Collins, 1993). The list of possible failure modes is presented in Appendix IV. There are two types of excessive elastic deformation which could result in structural failure (Pilkey, 1994):

- Deformation satisfying the usual conditions of equilibrium, such as deflection of the beam or angle of twist of a shaft. The ability to resists such deformation is referred to as the stiffness of a member.
- Inordinately large displacement under conditions of unstable equilibrium that may occur in a thin-plate when the in-plane forces exceed the critical load. This form of instability is referred to as buckling.

This section elaborates on these two failure phenomena.

2.2.4.1 Combined stress theories

Predicting failure and establishing a geometry that will avert failure is a relatively simple matter in the case of static uniaxial stress. A few simple tension and compression experiments can produce a simple stress-strain relationship for a material of interest. Failure is normally predicted to occur when the maximum normal stress reaches the yield point that is determined from the experimental stress-strain relationship (Collins, 1993).

In reality when the component is subject to a biaxial or a triaxial state of stress, the procedure above is unable to predict failure. There is an attempt to solve this problem by developing a theory that relates the behaviour of the complex situation to simpler behaviour which can be evaluated through tests of a number of characteristic moduli. The predominant theories are shortlisted in

Table 2-3 along with mathematical expressions and their shortages (Pilkey, 1994; Collins, 1993). The principal stresses are denoted as $\sigma_1 > \sigma_2 > \sigma_3$ and yield stress in tension or compression as σ_f .

Figure 2-12 shows comparative graphical representation of the failure theories in biaxial stress scenario. It is accepted that Von-Mises and Tresca are the most representative criteria of initial yield behaviour in metallic materials (Rees, 2003). The regions represent the boundary of incipient failure. All state of stress that lies outside the regions would be predicted to result in failure. If the tensile strength σ_t , is equal to compressive strength, σ_c , the regions are symmetrical about the coordinate origin. If the tensile and compressive failure strength differs, the failure boundaries are displaced so that the centre of the region no longer coincides with the $\sigma_1 - \sigma_2$ coordinate origin.

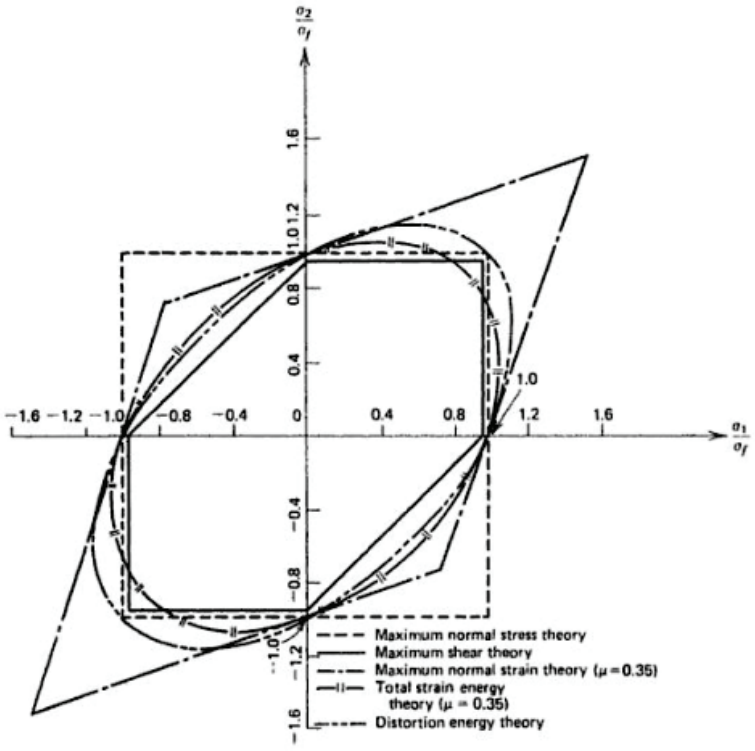

Figure 2-12 Comparison of failure theories in biaxial state of stress (Collins, 1993)

Table 2-3 Failure criteria (Collins, 1993)

Failure theory	Criterion	Theory statement	Mathematical expression	Application	Weakness
Rankine	Normal stresses theory	Yield occurs when one of the principal stresses at a point in the structure subjected to the combined stresses reaches the yield strength in simple tension or compression of the material.	$\sigma_1 = \sigma_f$ $\lvert\sigma_3\rvert = \sigma_f$	For brittle materials the maximum normal stress theory is the best available failure theory, though it may yield conservative results for some states of the stress.	Predict failure in the case of hydrostatic stress (compression or tension) when the magnitude of the principal stress $\sigma = \sigma_1 = \sigma_2 = \sigma_3$ becomes equal to the simple tensile yield point that is experimentally invalid. Poor to predict onset of yielding and should not be used for ductile materials.
Tresca-Guest	Maximum shearing stress	Failure is predicted to occur in the multiaxial state of stress when the maximum shearing stress magnitude becomes equal to or exceeds the maximum shearing stress magnitude at the time of failure in a simple uniaxial stress test using a specimen of the same material.	$\lvert\tau_1\rvert \geq \lvert\tau_f\rvert$ $\lvert\tau_2\rvert \geq \lvert\tau_f\rvert$ $\lvert\tau_3\rvert \geq \lvert\tau_f\rvert$ or $\lvert\sigma_1 - \sigma_2 \geq \lvert\sigma_f\rvert\rvert$ $\lvert\sigma_2 - \sigma_3 \geq \lvert\sigma_f\rvert\rvert$ $\lvert\sigma_3 - \sigma_1 \geq \lvert\sigma_f\rvert\rvert$	Predicting the hydrostatic stress as failure is eliminated in this theorem.	It has been observed that only one other theory, the distortion energy theory, gives better agreement with experimental data for ductile behaviour under multiaxial states of stress.

Failure theory	Criterion	Theory statement	Mathematical expression	Application	Weakness
St. Venant	Maximum normal strain	"Failure is predicted to occur in the multiaxial state of stress when the maximum principal normal strain become equal to or exceeds the maximum normal strain at the time of failure in a simple uniaxial stress test using a specimen of the same material."	$\sigma_1 - \nu(\sigma_2 + \sigma_3) \geq \sigma_f$ $\sigma_2 - \nu(\sigma_1 + \sigma_3) \geq \sigma_f$ $\sigma_3 - \nu(\sigma_1 + \sigma_2) \geq \sigma_f$ $\sigma_1 - \nu(\sigma_2 + \sigma_3) \geq -\sigma_f$ $\sigma_2 - \nu(\sigma_1 + \sigma_3) \geq -\sigma_f$ $\sigma_3 - \nu(\sigma_1 + \sigma_2) \geq -\sigma_f$		The same shortage as Rankin's theorem to predict failure in the case of hydrostatic stress is also applicable to St. Venant theory. Further the theory is been found inadequate for brittle material failure as well.
Von Mises	Maximum distortion energy theory	Failure is predicted to occur in the multiaxial state of stress when the distortion energy per unit volume becomes equal to or exceeds the distortion energy per unit volume at the time of failure in a simple uniaxial stress test using a specimen of the same material	$\frac{1}{2}\begin{bmatrix}(\sigma_1 - \sigma_2)^2 \\ +(\sigma_2 - \sigma_3)^2 \\ +(\sigma_1 - \sigma_3)^2\end{bmatrix} \geq \sigma_f$	Widely accepted as the comprehensive failure criteria in structural design	

2.2.4.2 Buckling failure

The simplest model of the structural behaviour under static loads, assumes that the equilibrium path is linear so all deformations are proportional to the magnitude of the load set acting on the structure. This model, known as inelastic behaviour, requires the material to have a linear relationship between stress and strain.

The stability of this model determines a risk of form failure, as the structure may not be able to maintain its original geometry due to the applied load (Iyengar,1988). The failure in the inelastic stability is expressed as geometrical non-linear behaviour and characterise by the divergence in the equilibrium curve as shown in Figure 2-13. A critical point in the state of equilibrium where the two paths intersect is known as the Bifurcation Point and is associated with classical buckling (Falzon, Hitchings, 2006). This is regarded as the limit of the elastic non-linear behaviour. In elastic buckling, the primary or pre-buckling response is in a different direction to the buckling response. Thus the buckling response remains zero until the buckling load is reached. Buckling therefore is described as the behaviour in which a structure suddenly deforms in a plane different to the original plane of loading and response. The buckling phenomenon can be classified in terms of the buckling mode as shown in Table 2-4 (Trahair, 1993).

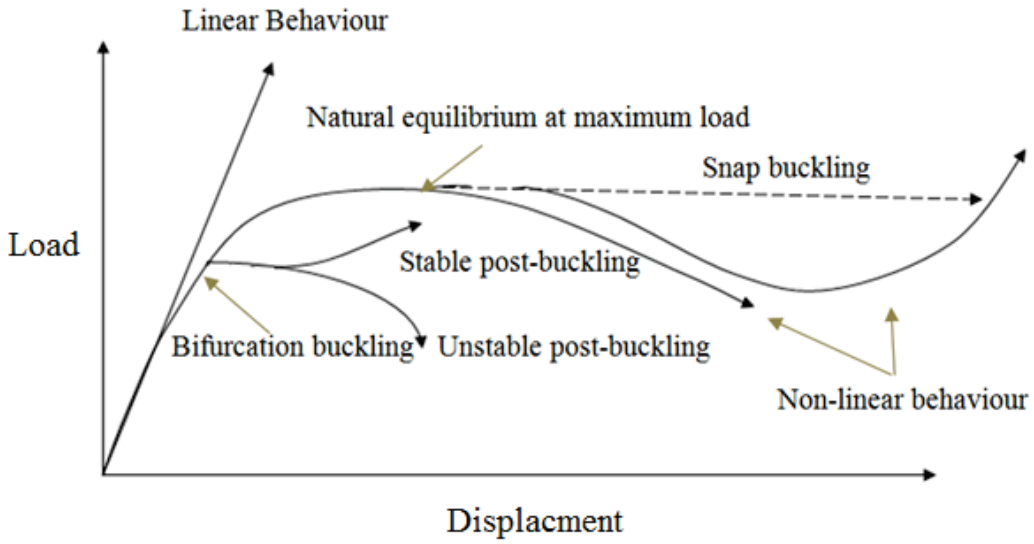

Figure 2-13 Types of load-displacement behaviour (Trahair, 1993)

Table 2-4 Modes of buckling classification (Trahair, 1993)

Mode	Description	Visualisation
Flexural	It may involve transverse displacement of the member cross-section and is resisted by the flexural rigidity of the member. It occurs when the second-order moment caused by the product of the axial compression forces with the displacements are equal to the internal bending resistance at any point in the structure.	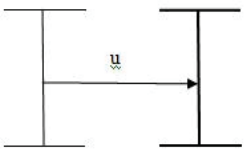
Torsional	This involves twist of the member cross-section, and is resisted by the tensional rigidity and the warping rigidity. It occurs when second-order torque caused by the axial compression force and the twist are equal to the sum of the internal torsion resistances at any point in the structure.	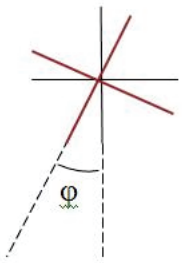
Flexural-torsional	This involves the mixture of two above phenomena and therefore resisted by the combination of the bending resistance and the torsional resistance.	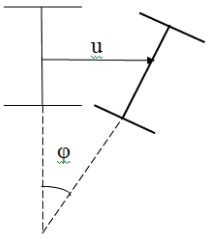
Local	This mode involves deflection of a thin plate out of its original plane. This mode occurs when the second-order actions caused by the in-plane compressions and the out of plane deflections are equal to the internal resistances of the plate elements to bend and twist at any point in the structure.	
Distortional	This is an intermediate mode between local and member buckling. It often involves web flexure and corresponding rotations of the flanges which vary slowly along the member length.	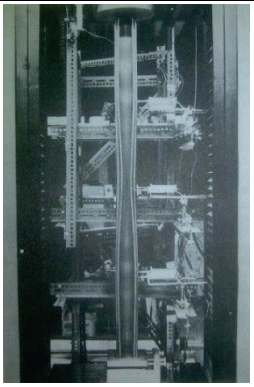

After the buckling load is reached, the post-buckling load-displacement curve may remain constant, or may rise or fall due to the changes in the member stiffness that occur during buckling, which may lead to redistribution of the actions through the structure. The types of load deflection behaviours discussed above are shown in Figure 2-13.

2.3 Numerical method in structural design

Section 2.2 described the objectives of the structural analysis process in terms of its quantifiable parameters and the assessment criteria. In this section the most predominant methods in industry to achieve these objectives are explained.

For simple components with no critical pre-condition, the structural analysis would be simply satisfied with ready-to-use handbook formulae and relationships. The actual stress- strain relationship in a machine component is invariably complex and not always agreeable with straight forward mathematical solutions (Parameswaran, 2004). In this case the numerical methods are employed to solve complex mathematical models (Kurowski, 2004).

The use of numerical methods to overcome complexities and arbitrariness in analysis has been significantly improved by the advent of the computers in engineering. Development of softwares that assist designers to model and analyse complicated geometries and assemblies leads to yet the most exact prediction of stress and strain distribution in the components (Parameswaran, 2004).

In brief, the mainstreams of numerical methods to solve partial differential equations throughout a three dimensional domain (Mottram, 1996) are:

- The Finite Element Method (FEM)
- The Finite Difference Method (FDM)
- The Boundary Element Method (BEM)

FEM has become the most commercially available when solving structure problems in both industry and academia (Mottram, 1996).

National Agency for Finite Element Methods and Standards (NAFEMS) defines Finite Element Method as *"an approximate method for calculating the behaviour of a real structure by performing an algebraic solution of a set of equations describing an ideal model structure with a finite number of variables"* (Mair, 1984, Section 0.2-1).

FEM representes the real structure by a set of elements bounded by a mesh or grid of lines and surfaces. Each element is defined by its boundary geometry, its material property and a few basic parameters such as thickness and cross section area. The loads and displacements that are nominally defined at the nodes of the geometrical mesh (or any other convenient points in the boundary) describe the elements behaviour in relation to adjoining elements. The behaviour of the complete structure is the aggregate behaviour of its elements. Any FEA is only as good as:

- the model of the structure (geometry mesh and elements)
- the assumptions embedded in the properties used for each element
- the representation of the external loads and constraints in terms of the discrete boundary variables.

2.3.1 FEA Procedure

In summary the steps to Finite Element Method are (Huebner et al., 2001):

- Discretise the continuum
- Select interpolation function
- Find the element properties
- Assemble the element properties to obtain the system equation
- Impose the boundary condition
- Solve the system equation
- Make additional computations if desired

The general procedure to set up a computational model in Abaqus software is laid out in Figure 2-14 (Dassault Systèmes, 2009, a). Among these stages special attention is paid to the choice of element.

2.3.2 Meshing and element properties

FEA offers a way to solve a complex continuum problem by subdividing it into a series of simpler interrelated problems. The complex problem is in the form of assemblage of discrete parts or finite element. The degree to which the assemblage represents the whole depends on the number, size and type of elements. There are only special cases that this assemblage leads to an exact representation, and most often the choice of element is a matter of engineering judgement based on the industry's accumulated experience (Huebner et al., 2001).

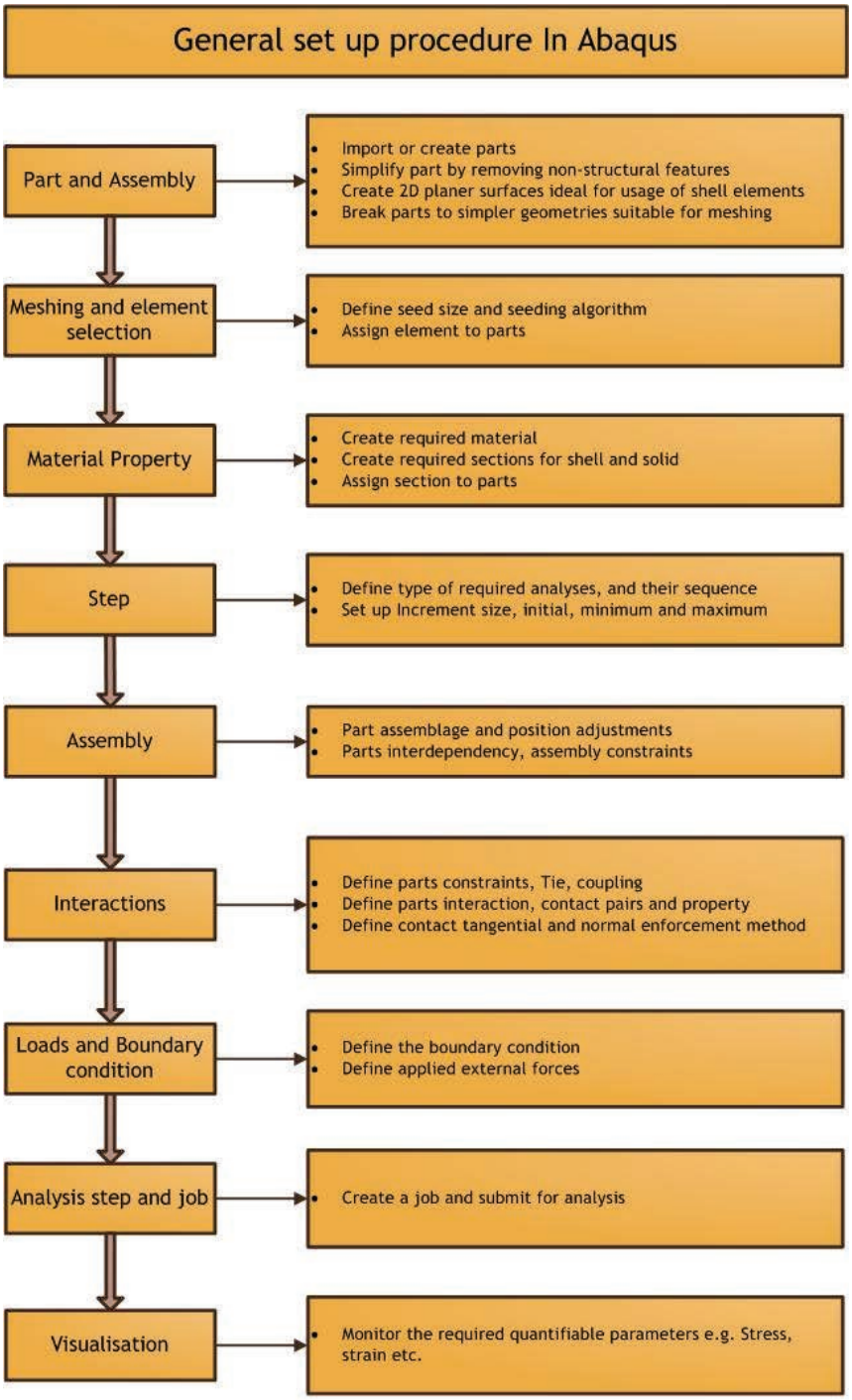

Figure 2-14 General FE model set up in Abaqus

In order to choose an effective combination of assembly, element characteristics have to be identified. Elements can be characterised with their five aspects (Dassault Systèmes, 2007, b):

- Family: This is the geometry type as shown in Figure 2-15. In general terms the elements family can be categorised as Continuum or Structural type.

- Degree of freedom: This is the fundamental variable calculated during the analysis. For a stress/displacement simulation the degrees of freedom are the translations and for structural elements, these are the rotations at each node. The conventions on the nodal degrees of freedom is described in Appendix V (Dassault Systèmes, 2007, b).
- Number of nodes: The degrees of freedom are calculated at the node of the element, the examples are shown in Figure 2-16. The calculated displacement is then interpolated from the nodal displacement.
- Formulation: This describes the mathematical theory used to define the element's behaviour.
- Integration: FEA software uses numerical techniques to integrate various quantities over the volume of each element, thus allowing complete generality in material behaviour.

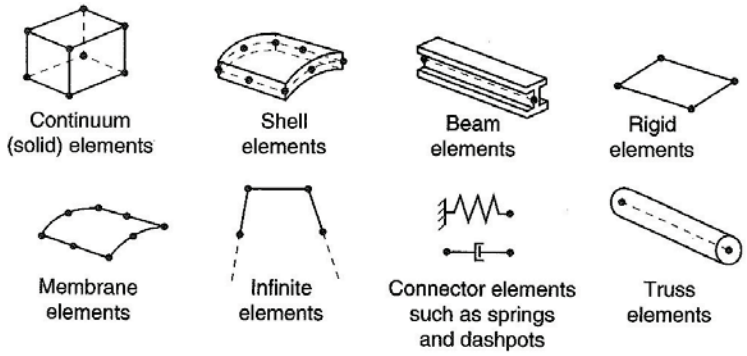

Figure 2-15 Commonly used elements families (Dassault Systèmes, 2007, b)

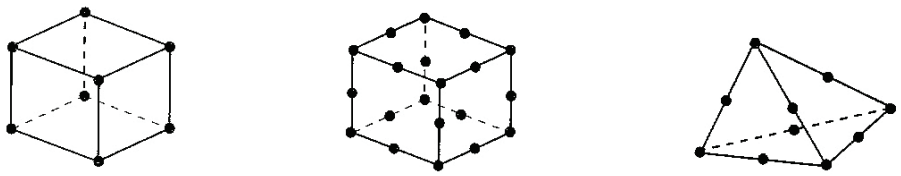

(a) **(b)** **(c)**

Figure 2-16 (a) Linear elements (b) Quadratic elements (c) Modifies second-order element (Dassault Systèmes, 2007, b)

From the modelling perspective the element family, that determines the type of geometry, is the fundamental decision to make. The other element characteristics are available under each type of element family and therefore can follow when the family is

determined. Sections 2.3.2.1and 2.3.2.2 elaborates on the element family with the focus on the elements' geometrical aspects.

2.3.2.1 Continuum elements

Continuum or Solid elements are used for a range of linear and nonlinear analysis containing contact, plasticity, and large deformation (Bathe, 1996). The solid elements are available in different shapes e.g. triangular/tetrahedral and bricks/quadrilaterals. Triangular elements are geometrically versatile and are used in many automatic meshing algorithms. It is very convenient to mesh a complex shape with triangles and second order and modified triangular are suitable for general usage.

However the good mesh of hexahedral elements usually provides a solution of equivalent accuracy. Quadrilaterals and hexahedral have a better rate of convergence than triangles and tetrahedral. Furthermore, sensitivity to mesh orientation in regular meshes is not an issue. First order triangles and tetrahedrals are usually overly stiff which means that extremely fine meshes are required to obtain accurate results (Dassault Systèmes, 2010).

First order triangular and tetrahedral elements should be avoided as much as possible in stress analysis problems as they are overly stiff and exhibit slow convergence with mesh refinement. Second-order elements provide higher accuracy than first order elements, in smooth problems that do not involve complex contact conditions, impact, or severe element distortions. They capture stress concentrations more effectively and can produce a curved geometry with fewer elements. Finally they are very effective in bending dominated problems.

Reduced integration that uses a lower-order integration to form the element stiffness, are also available in Solid genre. Reduced integration reduces running time, especially in three dimensions. Combination of second-order and reduced-integration elements generally yields more accurate results than the corresponding fully integration elements. However for the first-order elements the accuracy with reduced integration is largely dependent on the nature of the problem.

This combination is also subjected to the risk of Hourglassing. In cases where element contains only one integration point, it is possible that a mode of distortion with zero strain occurs within an element. This in turn leads to uncontrolled distortion of the

mesh, shown in Figure 2-17. The hourglass control option in first-order elements can be used only with a fine mesh (Dassault Systèmes, 2010).

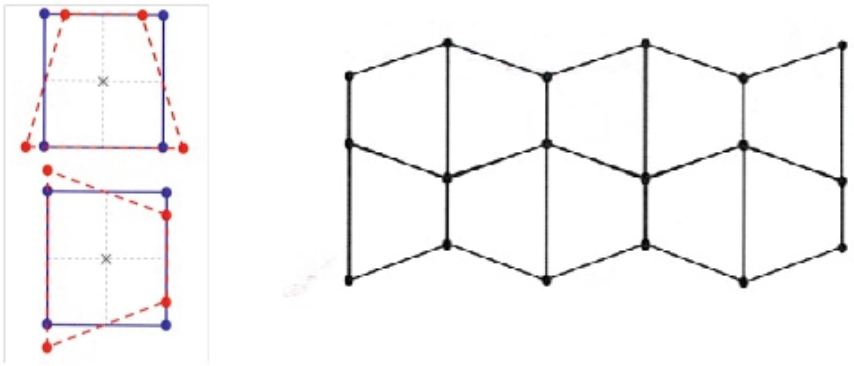

(a) **(b)**

Figure 2-17 (a) Hourglass mode shapes of a 4 node-reduced-integration element (b) Hourglass mode propagation (Dassault Systèmes, 2010)

Fully integrated elements are not subject to hourglass but may suffer from 'Locking' behaviour in the form of shear or volumetric locking. Shear locking is a type of malfunction in first-order fully integrated elements that are subject to bending. The numerical formulation gives rise to so-called parasitic shear strain , a type of shear strain that does not exist, and causes over stiffness performance by the element. As it is shown in Figure 2-18 (a), the second order elements edges can assume a curved shape that maintain the angle between isoperimetric lines as 90°. In contrast the first order element, Figure 2-18 (b), requires the element edges remain straight and therefore impose a artificial change in the isoperimetric lines angle. The element formulation make them inadequate for application in the presence of shear forces.

Volumetric locking is more likely to happen in the case of incompressible material. Spurious pressure stresses develop at the integration point, causing an element to behave stiffly for deformation that should cause no volume changes. If materials are almost incompressible second order fully integrated will start developing volumetric locking when the plastic strains are on the order of the elastic strain. Volumetric locking in this scenario happens after a significant strain, and is often accompanied by a mode that looks like Hourglassing. Frequently this problem can be avoided by refining the mesh in regions of large plastic strain.

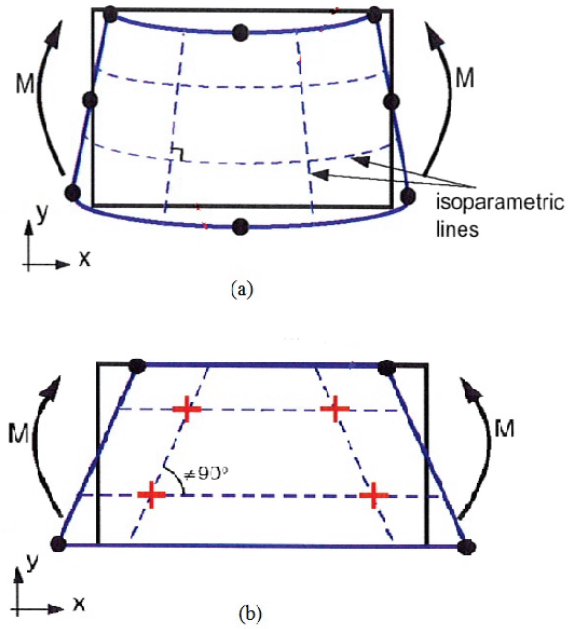

Figure 2-18 Shear locking (a) second order element that allow for the shear forces by allowing curvature in element edges, (b) first order element that restrict the edges to bend and give raise to shear stress (Dassault Systèmes, 2010)

Incompatible mode elements are first-order elements that are enhanced by incompatible modes to improve their bending behaviour. In addition to the standard displacement degree of freedom, incompatible deformation modes are added internally to the elements. In addition, these degrees of freedom eliminate artificial stiffening due to Poisson's effect in bending. In regular displacement elements the linear variation of the axial stress due to bending is accompanied by a linear variation of the stress perpendicular to the bending direction, which leads to incorrect stresses and an overestimation of the stiffness. The incompatible modes prevent such a stress from occurring. The incompatible mode elements perform almost as well as second order elements in many situations if the elements have an approximately rectangular shape. The performance reduced considerably if the elements have an approximately rectangular or a parallelogram shape.

2.3.2.2 Shell element

Shell elements, part of the Structural Family of elements, are another form of 3D geometrical discretisation methods.

For three dimensional thin structures, shell elements are capable to model in topologically two dimensions. The reduction in dimensionality is achieved by

incorporating thin plate-bending theorem that is normally applicable to the thickness no greater than one-tenth of the other two in-plane dimensions (Reddy, 2006).

Geometrically, plate problem is similar to plane stress problems, except that plates are also subject to transverse loads that cause bending about axes in the plane of the plate (Reddy, 2006). The general rules of classical plate bending theory (Huebner et al, 2001), also known as Kirchhoff hypotheses, are applicable only if:

- The deflection of the centre plane is small compared to the thickness.
- The centre plane has no strain during bending.
- The stress components normal to the centre plane σ_z is small.
- Normal to the centre plane remains normal during bending.

According to the above assumptions:

Eq. 2-37

$$\epsilon_z = \gamma_{xz} = \gamma_{yz} = \sigma_z = 0$$

And the in-plane displacements are related to the deflection:

Eq. 2-38

$$u_x = -z\frac{\partial w}{\partial x}\,, \qquad u_y = -z\frac{\partial w}{\partial y}$$

The Kirchhoff hypotheses result in decreasing the complexity of a three dimensional plate problem to two dimensions and in effect reduce the problem to finding only w(x,y) (Ugural, 1999). Conventional strain-displacement relations for non-zero strain parameters are identified by Eq. 2-23. Substitution Eq. 2-38 into the conventional relationship results in:

Eq. 2-39

$$\epsilon_x = -z\frac{\partial^2 w}{\partial x^2}\,, \qquad \epsilon_y = -z\frac{\partial^2 w}{\partial y^2}\,, \qquad \gamma_{xy} = -2z\frac{\partial^2 w}{\partial y \partial x}$$

Eq. 2-39 provides the strains at any point in the plate. Considering the Kirchhoff assumptions stated in Eq. 2-37, the three dimensional Hook's stress strain relation is reduced to:

Eq. 2-40

$$\sigma_x = \frac{E}{1-\upsilon^2}(\epsilon_x + \upsilon\epsilon_y), \qquad \sigma_y = \frac{E}{1-\upsilon^2}(\epsilon_y + \upsilon\epsilon_x), \qquad \tau_{xy} = G\gamma_{xy}$$

Substitution with Eq. 2-39 and expressing G with respect to E and ν Gives:

Eq. 2-41

$$\sigma_x = \frac{-zE}{1-\upsilon^2}\left(\frac{\partial^2 w}{\partial x^2} + \upsilon\frac{\partial^2 w}{\partial y^2}\right), \sigma_y = \frac{-zE}{1-\upsilon^2}\left(\frac{\partial^2 w}{\partial y^2} + \upsilon\frac{\partial^2 w}{\partial x^2}\right), \tau_{xy} = -\frac{zE}{1+\upsilon}\frac{\partial^2 w}{\partial y \partial x}$$

From Eq. 2-41 it is observed that the stress is vanished in mid-surface, where z=0 and vary linearly over the thickness of the plate. This variation over the thickness causes bending moments, twisting moments, and vertical shear forces.

Eq. 2-42

$$\begin{Bmatrix} M_x \\ M_y \\ M_{xy} \end{Bmatrix} = \int_{-\frac{t}{2}}^{\frac{t}{2}} \begin{Bmatrix} \sigma_x \\ \sigma_y \\ \sigma_{xy} \end{Bmatrix} z dz$$

Where M_{xy}=M_{yx} $M_{xy} = M_{yx}$ and:

Eq. 2-43

$$\begin{Bmatrix} Q_x \\ Q_y \end{Bmatrix} = \int_{-\frac{t}{2}}^{\frac{t}{2}} \begin{Bmatrix} \tau_{xz} \\ \tau_{yz} \end{Bmatrix} dz$$

Eq. 2-43 shows despite neglecting effects of shear strain components of γ_{xz} and γ_{yz} , vertical forces Q_x and Q_y are not negligible.

Using shell elements, when applicable, provides a more economical solution than solid elements. In stress/displacement problems containing contact surfaces there are two types of shell elements:

- Conventional shell elements, that discretise a reference surface by defining the element's planar dimensions, its surface normal, and its initial curvature
- Continuum shell elements, resemble three-dimensional solid elements in that they discretise an entire three-dimensional body

Conventional shell element's behaviour satisfies Kirchhoff-Love constraints formulations. Like Solid elements the reduced integration for the stiffness matrix is

possible in conventional shell elements. Reduced integration typically provides more accurate results with more efficient time frame in three dimensional problems. In first order elements it is required to check the likelihood of hourglassing, and mitigating the risk with hourglass control.

The initial geometry of the conventional shell can be defined by creating a planar geometry of the body. This reference surface is typically coincident with the shell's mid-surface. However, many situations arise in which it is more convenient to define the reference surface as offset from the shell's mid-surface.

Continuum shell elements are similar to continuum solids from a modelling point of view. However they should be correctly oriented, since these elements contain thickness direction information. In comparison continuum elements provides a more accurate solution for contact type of problem, since they employ two sided contact which consider thickness variation. However it is important to note that a conventional shell provides superior performance.

2.4 Experimental analysis

Section 2.3 discussed the numerical solution of FEM and its considerations to obtain the structural analysis objectives. Another mainstream method of obtaining these objectives in application is known as experimental stress analysis. Experimental methods for stress analysis can be classified as (Singh 1979):

- Whole-field methods: those which give information about stress or strain distribution in the whole-field e.g. photoelasticity, photoelastic coating, brittle lacquers, grid method, Moire method, holography and interferometers etc.
- Point-by point methods: those which provide information at selected points only e.g. electrical resistance strain gauges, mechanical extensometers, optical extensometers and variable capacitance transducers etc.

These methods may be further classified as static or dynamic methods and destructive and non-destructive methods (Singh 1979). The most implicational candidates of each class are shortlisted for further discussion in sections 2.4.1 and 2.4.2 .

2.4.1 Photoelestic measurement

The photoelastic method depends on the property of certain transparent solids by which they become doubly refractive under the action of stress, magnitude of the optical effect

bearing a definite relation to that of the stress (Singh, 2011). In applying this method to analyse the stresses in any body subjected to given loads, a scale model of the body is first made out of a stress- optically sensitive or more commonly known as photoelastic material. The model is subjected to loads similar to those applied to the prototype, and the optical effects are measured. The material of model having been calibrated, these observations lead directly to numerical values of stress-differences and with the help of theory of elasticity produce the complete determination of the state of stress at all points of the model (Singh, 1997).

Stress-optic law in a transparent isotropic model in which the stresses are two dimensional and within the elastic limit states that the angular phase difference between the two rectangular wave components travelling through the model is directly proportional to the difference of principal stresses.

Eq. 2-44

$$\alpha \propto (\sigma_1 - \sigma_2)$$

$$\sigma_1 - \sigma_2 = \left(\frac{\lambda}{C}\right).\left(\frac{\alpha}{2\pi}\right).\frac{1}{h} = \frac{f_\sigma n}{h}$$

where f_σ equal to $\left(\frac{\lambda}{C}\right)$ is material fringe value in terms of stress and has the unit kg/cm^2/fringe/cm and n equal to $\left(\frac{\alpha}{2\pi}\right)$ $is\ the$ relative retardation in terms of a complete cycle of retardation and is called the fringe order. h is model thickness in cm , and $F = \frac{f_\sigma}{h}$ is model fringe value. Rearranging Eq. 2-40 Gives:

Eq. 2-45

$$\varepsilon_1 - \varepsilon_2 = \frac{(1+\nu)}{E}(\sigma_1 - \sigma_2) = f_\varepsilon \frac{n}{h}$$

$f_\varepsilon = \left[\frac{(1+\nu)}{E}\right] f_\sigma$= material fringe value in terms of strain and has the units cm/fringe.

Thus photoelastic effect law can be summarised as:

- The light on passing through the stressed model becomes polarised in the direction of the principal stress axis and is transmitted only on the planes of principal stress.

- The velocity of transmission in each principal plane is dependent on the intensity of the principal stress in these planes.

The points of equal phase difference due to temporary double refraction is called fringe. These are also the points of equal brightness or darkness.

2.4.2 Strain analysis using strain gauge

Strain gauge method is one of the oldest and currently the most commonly used method. Wide range of technologies is deployed in the strain gauge design field, e.g. mechanical, optical electrical gauges to name but a few (Singh,1997). Amongst the available techniques the electrical resistance strain gauges are the most important one that will be discussed in this section (Vishay, 2010, b).

"A strain gauge rosette is an arrangement of two or more closely positioned gauge grids, separately oriented to measure the normal strains along different directions in the underlying surface of the test part." (Vishay, 2010, a, pp151). Three basic types of strain gage rosettes are shown in Figure 2-19:

- Tee: two mutually perpendicular grids.
- 45°-Rectangular: three grids, with the second and third grids angularly displaced from the first grid by 45° and 90°, respectively.
- 60°-Delta: three grids, with the second and third grids 60° and 120° away, respectively, from the first grid.

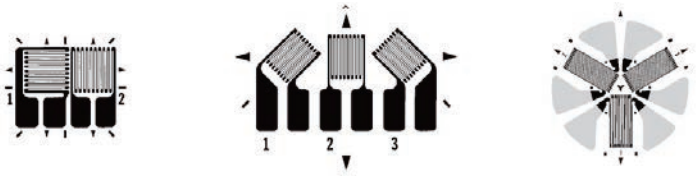

Figure 2-19 Variation in rosettes from left to right: Tee, Rectangular and Delta (Vishay, 2010, a)

The tee rosette is only appropriate for the predictable principal strain directions. Where the directions of the principal strains are unknown, a three-element rectangular or delta rosette is appropriate; In this case the rosette can be installed in any required orientation (Potma, 1967). In order to develop the conversion equations, a consistent sequential numbering system is required to identify the rosette elements. The convention for rectangular rosette numbering is to assign grid numbers 1 and 3 to two perpendicular

grids therefore the axis of Grid 2 is 45° away. The principal strains can be derived from three directional measurements from Mohr's circle, as shown in Figure 2-20. The normal strain at any angle θ from the major principal axis is (Vishay, 2010, a):

Eq. 2-46

$$\varepsilon_\theta = \frac{\varepsilon_p + \varepsilon_q}{2} + \frac{\varepsilon_p - \varepsilon_q}{2}\cos 2\theta$$

Assuming a rectangular rosette mounted on a surface in an arbitrary angle of θ the three directional measurements yield to the principal strains using the Mohr's circle as it is shown in Figure 2-20 and Eq. 2-46is re-written as (Vishay, 2010, a):

Eq. 2-47

$$\varepsilon_{P,Q} = \frac{\varepsilon_1 + \varepsilon_3}{2} \pm \frac{1}{\sqrt{2}}\sqrt{(\varepsilon_1 - \varepsilon_2)^2 + (\varepsilon_2 - \varepsilon_3)^2}$$

Eq. 2-48

$$\theta = \frac{1}{2}\tan^{-1}\left(\frac{\varepsilon_1 - 2\varepsilon_2 + \varepsilon_3}{\varepsilon_1 - \varepsilon_3}\right)$$

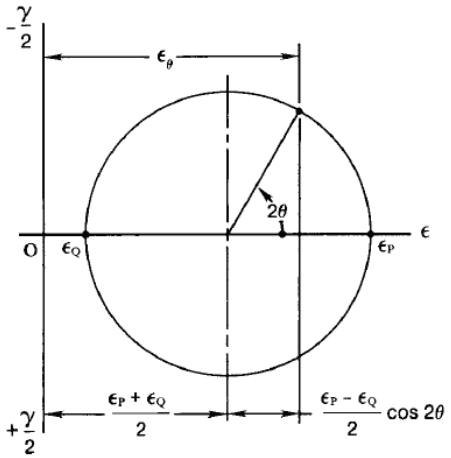

Figure 2-20 Strain transformation from principal to a random direction in Mohr's circle (Vishay, 2010, a)

Eq. 2-47 can readily identify the value for principal strains. Eq. 2-48 gives the angle θ represents the acute angle from the principal axis to the reference grid of the rosette. For the purpose of experimental measurement it is more convenient to translate from reference grid to principal axis as detailed in Appendix VI.

To calculate the stress for a homogeneous isotropic elastic material, Hook's law can be used as described in section 2.2.3 and formulised in Eq. 2-40. The principal stresses can be calculated directly from grid measurement as (Vishay, 2010, a):

Eq. 2-49

$$\sigma_{P,Q} = \frac{E}{2}\left[\frac{\varepsilon_1 + \varepsilon_3}{1-\nu} \pm \frac{\sqrt{2}}{1+\nu}\sqrt{(\varepsilon_1 - \varepsilon_2)^2 + (\varepsilon_2 - \varepsilon_3)^2}\right]$$

Consequently von-mises stress can be calculated as (Vishay, 2010, a):

Eq. 2-50

$$\sigma_v = \sqrt{\frac{\left(\sigma_P - \sigma_Q\right)^2 + \sigma_P^2 + \sigma_Q^2}{2}}$$

2.5 Chapter summary

The mission of structural analysis, the structural integrity, is described with the objectives of the general layout and shape determination, service load and expected life determination, material selection and design criteria expression.

The structural integrity is achieved by determining the capability of the part to perform the required structural functions during its service life. These functions are explained by a number of parameters quantifiable via three types of argument, namely equilibrium, compatibility and stress-strain relationship.

- Stress: The equilibrium conditions used to define the state of the stress in a point. The stress tensor and its components are defined. The conversion of the stress components to the stress invariants, the one independent of directions is also identified.
- Strain: The compatibility condition is used to define the strain on the continuous medium that undergoes deformation. The strain definition in a point in the form of strain tensor is described in the same fashion as stress. The strain invariants on the isotropic homogeneous body.
- Stress-strain relationship: The governing equations to relate stress and strain components are defined using the generalised hook law in three dimensions. The Stiffness matrix and its symmetric nature is described and elaborated using

material elastic constants. The material constants relationship is summarised for further use during the study.

The quantifiable parameters are only comprehensible with knowing the Failure criteria. In order to quantify the product safety the structural performance e.g. stress and displacement have to be compared against failure criteria. Two forms of elastic failure, material yield and geometrical instability are elaborated.

The most applicable industrial methods to achieve these objectives are also explained in this chapter. Numerical methods in particular FEM are one of the industrial and commercial predominant CAE methods. The practice is developed based on the procedural steps to convert a 3D CAD model to FE model. Among the steps within FEM procedure, the element selection is identified as the key transformation point. This stage includes a degree of approximation that has to be carefully understood and selected to avoid discrepancy in the results. Elements vary in terms of the family type, degrees of freedom, number of integration points, number of nodes and formulations. The most distinguishable family types, structural and solid elements are discussed along with the criteria to choose and their application and their common type of malfunctions.

Experimental methods of structural analysis are perhaps the oldest method of the performance quantification. These methods have a significant role in modern analysis as simulation validation method. The techniques are broadly classified as the whole field and point-to-point methods.

- Photoelastic measurement: The most common whole-field method works based on the stress- optically sensitive or more commonly known as photoelastic material.
- Strain gauge analysis: electrical resistance strain gauges are discussed as one the industry leader point-to-point measurement method. The gauges variations are demonstrated with a particular attention to the formulation of rosette gauges.

In conclusion for a successful structural analysis project it is fundamental to identify:

- What is the performance that has to be analysed?
- What are the corresponding quantifiable parameters?
- What are the assessment criteria?
- How can one quantify the required parameters?

3 Structural Analysis in Product Development

In Chapter 2 structural analysis practice and modern practical methods to perform it were discussed. These fundamentals provide the background knowledge for the engineer to generate a successful simulation study and interpret the outcomes. However the efficiency of the practice relies heavily on the integration of the structural analysis in the product design process. This chapter aims to clarify the necessity of systematic approach for engineering product design in view of the influential design methodology developers.

The importance of developing a systematic analysis synthesis is understandable within the context of the new mechanical product design environment. The turning point from a successful single analysis project to an embedded- progressive method is in the implementation approach within the design process. This chapter elaborates on the product design requirements, and focuses on the state-of-the-art systematic practices to implement structural analysis within the design process. The comparative assessment of the current practices is provided in this section. This section concludes with the shortage of product multi-functionality perspective in the discussed methods and requirement for a more design oriented method to produce a descriptive form of reality of interest in product design.

According to a previous study of comprehensive assessment of the design tools by Cross and Sivaloganathan (2005), Quality Function Deployment (QFD) method is identified as a potential candidate to establish the reality of interest with respect to product's multi-functionality aspect. The capabilities and possibilities of QFD are further described in this chapter.

3.1 Product design perspective

The product design process, in general, is widely accepted as a systematic sequence of activities that are formulated to encompass a product from market needs to sale (Ostrofsky, 1977). The need for a systematic approach is raised by the complexity in the process that involves number of disciplinary and interdisciplinary specialities. Almost all products are heavily dependent on the inputs from a number of engineering and non-engineering fields, in a mix that is unique to the product specifications. In order to

conceive such a product, it is essential to coordinate the inputs in a systematic manner (Pugh, 1991).

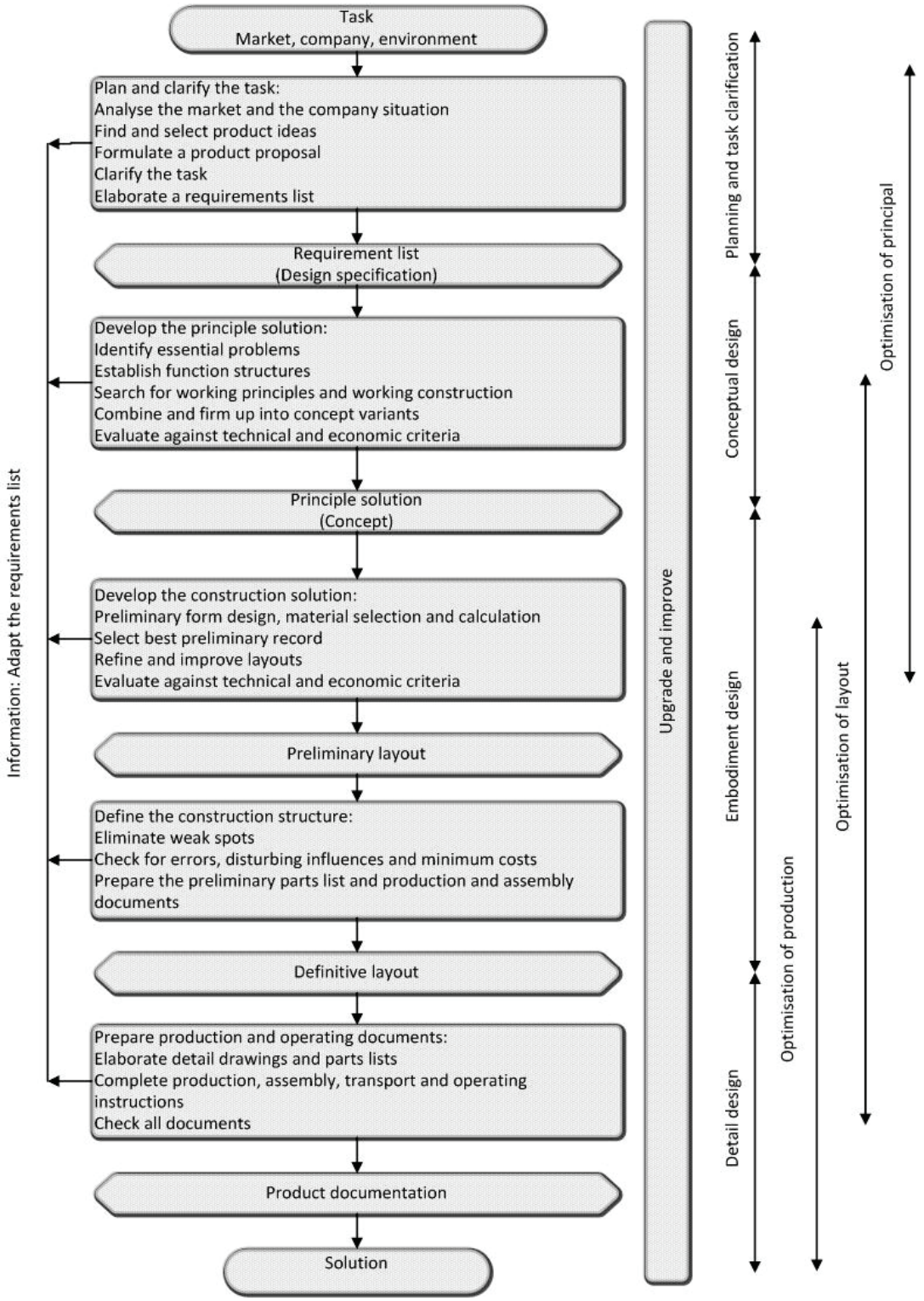

Figure 3-1 Design process work flow (Pahl et al., 2006)

The classic systematic design approaches were established to create visible operational structure to enhance the integration of technological and non-technological subject materials in an effective and efficient manner (Pugh, 1991). Most mainstream design methodologies agree on granting the central responsibility for the technical and economical properties of the product to the designer. More engineering oriented approaches, as shown in Figure 3-1, view the design methodology as a *"concrete course of action for the design of the technical system that derives its knowledge from design science and cognitive psychology, and from practical experience in different domains"* (Pahl et al. 2006, p.9).

The term design science is more elaborated with its elements as scientific methods to analyse the technical systems and their relationship with the environment (Pahl et al. 2006). The body of product specific design methodology in technical terms, consists of a combination of scientific methods that are arranged in a particular order to suite a particular products. These scientific methods can be classified briefly as shown in Figure 3-2.

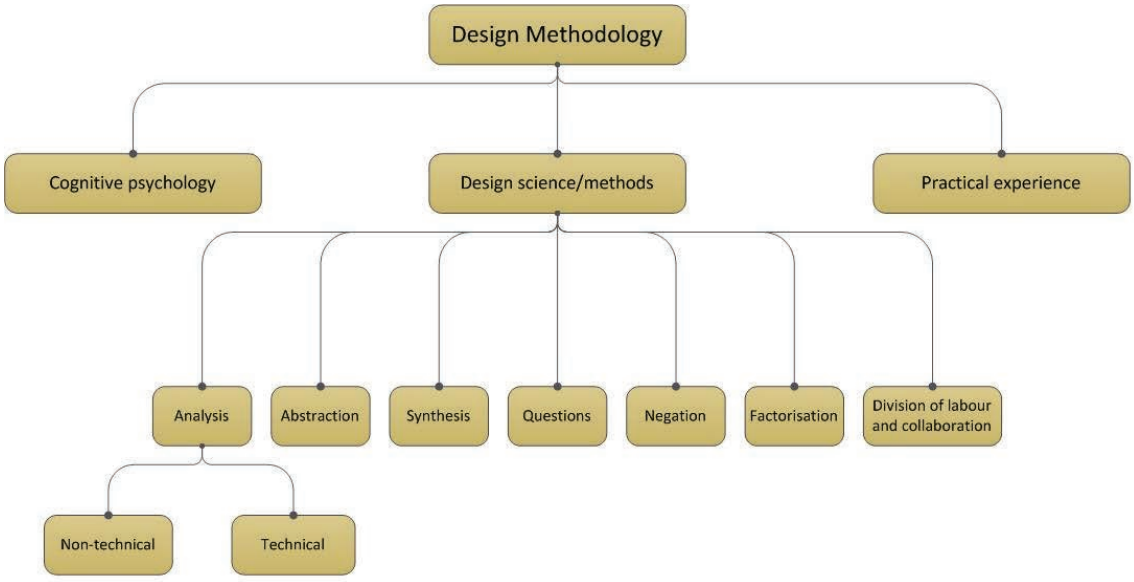

Figure 3-2 Position of analysis in the context of systematic design methodology

In most traditional commercial environments, the dominant approach to implement a systematic design process is known as Decide-Commit-Validate (DCV). In this approach most design decisions, are accepted and implemented before final validation of the collection of decisions that comprise the ultimate design (Adams, 2006). Despite its high take-up among traditionally established organisations, the risk of propagating

mistakes, made in early stages and their consequences are high. The risk is more visible in light of the identified gap between product understanding and resource commitments schematically shown in Figure 3-3. The greater the gap between product understanding and the resource committed, the greater the risk delay and expenditure due to negative variance between actual and anticipated performance (Adams, 2006). This potential shortage of the risk associated with DCV approach is mitigated with the allocated time at the end of the project schedule called "rework" or "redesign".

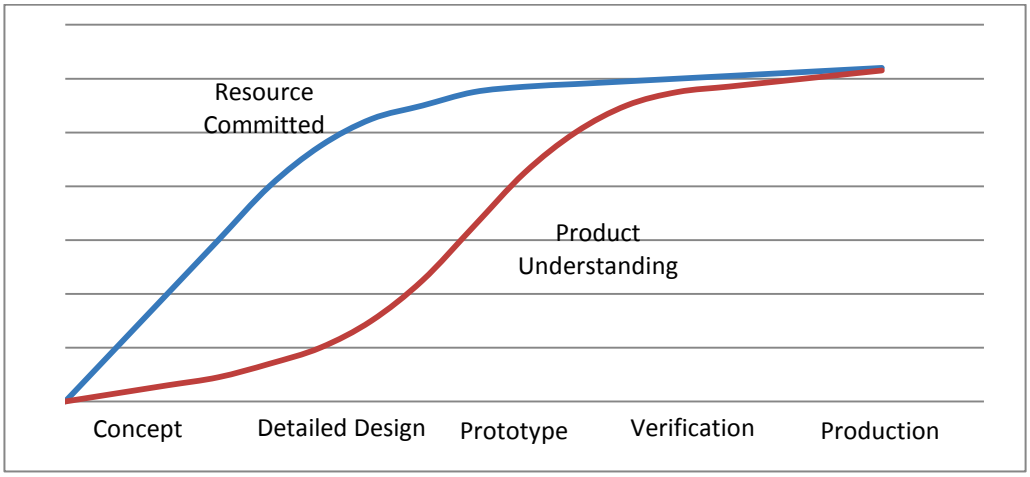

Figure 3-3 The Knowledge gap in product development (Adams, 2006)

3.2 Implementing Structural analysis in the design process

Although structural analysis has been used for several decades, its impact is becoming increasingly important, as SMEs are migrating from experimental testing to simulation-based design. The influence of structural analysis in design is more significant where the primary purpose of design is to carry a load. For most components, design evaluation and improvements based on the results of structural analysis, are integrated parts of the design process (Dolsak and Novak, 2011).

The technological portion of the needs determines the types of analyses required to adequately model product's parts or systems. Understanding the requirements and limitation of each type of analysis is critical when evaluating tools and the engineer's ability to use them (Adam, 2006).

As highlighted in Chapter 2, among the available methods for structural analysis the application of simulation with Computer Aided Engineering (CAE) softwares have been more widely used in academic research due to its extensive application in design process. The position of CAE within the design process has been previously mapped

broadly into Conceptual, Embodiment and Detailed Design (Cross and Sivaloganathan, 2004).

However the systematic nature of design process requires an integrated structural analysis methodology to complement the technology and gain competitive advantage for the enterprise. The implementation plan needs a clear understanding of expected benefits and goals which address stakeholder's needs both economic and technological (Adam, 2006).

As a standard technique for evaluating the mechanical performance of structural system (Turkiyyah and Fenves, 1996), FEA has been used by many researchers in many different disciplines to be systematically implemented within a design process. These studies are mostly inspired by shortages in specific industries and therefore are domain specific. The common trends, repeatedly addressed in recent researches, are discussed in section 3.3.

3.3 Systematic Structural Analysis

3.3.1 Early simulation

Table 3-1 shows the stages in which simulation is typically integrated into the design process. Among the different level of simulation integrity into design process the Conceptual Verification is considered as complimentary action by taking the final step of inserting simulation into decision making process. In most cases the design error that causes failure occurs not just prior to testing, but also in the initial steps. This risk has been addressed by pointing out the importance of analytical support for the design process in early phases of design since the early developments of simulation and FEA in design research in the 1980's and has been a point of concern until now (Sadd and Rolph, 1987). The Conceptual Verification aims to point out the cause of the problem in the conceptual stage, before it propagates through various design commitments (Adams, 2008).

Table 3-1 Stages of integrating simulation in design

Design stage	Application	Impact on design process
Failure Verification	A forensic action to realise the reason for part failure, observed in practice and find out the solution.	Low
Design Verification	Concerns about predictability of the structures behaviour during service in a virtual environment and decides on corrections if necessary.	An additional task between the design and prototype stage. The design has progressed using the same tools, techniques and insights as it would have prior to the availability of simulation.
Concept Verification	This supports any decision before committing to subsequent decisions.	This level of integrity of simulation within the design process leads to a significant re-arrangement in the design process.

The DCV approach, mentioned earlier as the dominant design approach in conventional environments, has been altered to validation before commitment, and transformed to Design-Validate-Commitment, DVC (Adams, 2008). This is essentially a cultural shift in the design process that prompt the designer to consider structural integrity through the wider range of design process. DVC approach enhances the position of simulation from design tool to an ongoing process within the design. In most cases this subtle change will help avoid significant cost and delay when the starting geometry proves to be a problem. Table 3-2 shows the benefits and limitations of early simulation in the design process.

Table 3-2 Benefits and limitations of early simulation (Adams, 2008)

Benefits	Limitations
Reduced product development time: Simulation as concept tends to converge to a working solution considerably quicker due to less complexity in the CAD model. The decisions also can be made before cascading dependencies are implemented, thus they improve the rework time later on in the project.	**Problem solving capabilities:** Once the extent of the problem exceed the problem solving capability of the system, whether it would be knowledge, experience or available tools, the risk begins to accumulate. This is in contradiction with the mission of simulation as a risk mitigating tool.
Increased innovation: Simulation is given a chance to investigate new materials, manufacturing methods or components interactions that challenge accepted design practices in conceptual level.	**Garbage in – Garbage out:** The simulation tools doesn't have any additional insight to the problem other than the one supplied by the user. They simply process the input data to provide solutions with the premise that the user knows what they are doing.
Reduced product cost: Using simulation in early stages of decision making in the Concept Verification mode, provides the best opportunity for the technology to impact final product cost.	**Precise answer to imprecise questions:** The exact answer supplied by simulation is a product of the users' best estimation of the inputs. Variations and inaccuracy in the loads, geometry etc. can lead into misleading design solutions
Reduced development cost: Reduction in the cost of prototyping and test has always been an inspiration for virtual modelling and simulation. Simulation in Conceptual Verification can narrow down the number of alternatives that might have otherwise required testing to explore.	**Discretization error:** The nature of FEA is to break continuum into sub-parts called elements, to provide the solution. Improper use of element may end in far off the mark solution
Improved product quality: The design and failure verification may address inherent quality deficiencies but they don't necessarily improve quality on their own. Decisions that most affect the final product performance and quality are made in earliest stages of design and therefore the value of concept verification simulation is more appreciated for this purpose.	

3.3.2 Benchmark

Benchmark analysis attempts to assess the appropriateness, accuracy and efficiency of proposed simulation procedures. In this sense, software developers use a number of standard, well-established problems, e.g. the NAFEMS benchmark criteria, to verify their solver codes (Abaqus, 2011; NAFEMS, 1990).

However the application of benchmark is not limited to software developers and standard practices. Benchmark has been extensively used for verification of specific simulation techniques and analysis methodologies. This development in the use of benchmark put the practice in pivotal position for developing a product or industry specific simulation methodology. These types of benchmarks represent simplified version of the structural system, of interest, by retaining its salient features. Therefore the typical benchmark experiments' results not only provide an assessment of the method but also characterise the initial performance of the system under study.

The contribution of benchmark in procedural structural modelling and simulation is very well established in the analytical domain; however benchmark role in-line with the design requirement for early simulation has been conveniently overlooked.

Oberkampf et al. (2004) introduced the Strong Sense Benchmarks (SSBs) with the following four characteristics:

- the purpose of the benchmark
- the definition and description of the benchmark
- specific requirements for results comparisons and
- acceptance criteria

The application of the benchmark in structural analysis can be related to the conceptual design part of the process and contribute towards the early stage simulation concept that was discussed in Section 3.3.1.

3.3.3 Expert System and Knowledge Base Engineering

Artificial Intelligence (AI) methods have been applied to FEA for over 20 years to support the decision making process. In principle AI is a sub-section of computer science concerned with developing programs that in some way imitate human intelligent behaviour (Beerel, 1987). The ultimate goal of developing such systems in engineering

design is to introduce an automated procedure to support the iterative cycle of decision making, required by structural analysis for design verification.

Expert System (ES) is a sub-branch of AI and refers to a particular computer programme that encapsulates facts, expert knowledge and reasoning techniques, and simulate the reasoning process to provide expertise (Labrie et al, 1994). The knowledge used by the expert systems is made up of either rules or experiences on the behaviour of the elements of a particular subject domain. The architecture of the typical ES is shown is Figure 3-4 (Martin and Oxman, 1988):

Among the components of ES, Knowledge-base is the fundamental element as the system starts with experts' Knowledge acquisition. The Knowledge-base holds the expert knowledge about the domain. This knowledge is obtained from human experts and is stored in a knowledge-representational form that is inherent to the expert system design. The process of building ES is known as Knowledge Base Engineering (KBE) (Forsyth, 1989). The focus of KBE is to provide an informationally complete description or representation of a design as well as access to external databases. The knowledge based engineering environment is therefore a framework for capturing and defining the process of design creation.

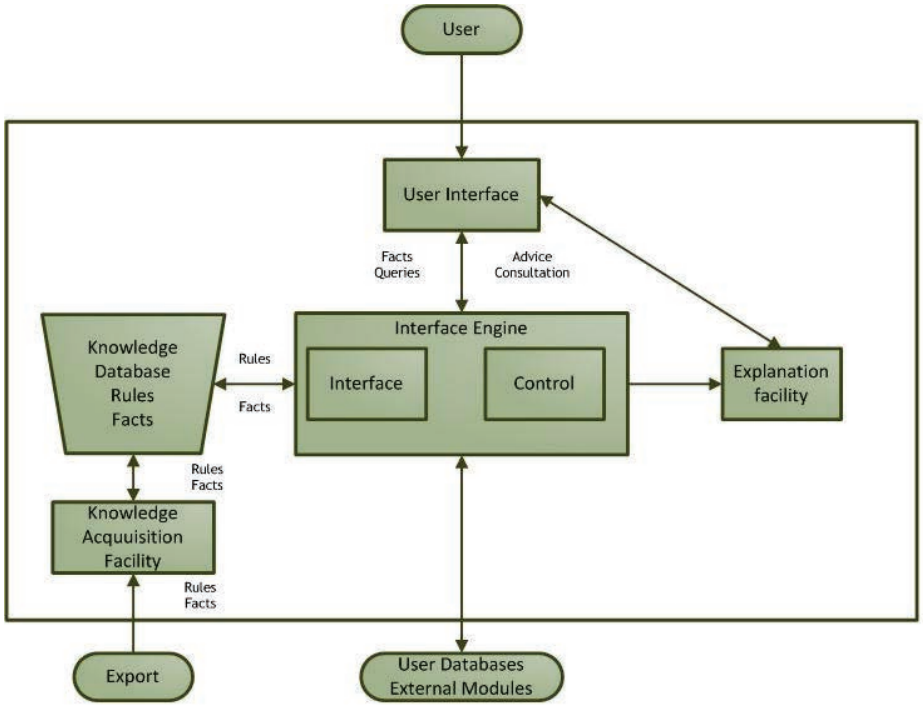

Figure 3-4 Schematic architecture of ES (Labrie et al, 1994)

The position of intelligent support is magnified considering actual structural analysis cycle practice. From a practical standpoint, FEA follows an step-by-step process which, from user perspective, is translated into three basic steps of pre-processing, computational analysis and post-processing. As shown in Figure 3-5, it is a familiar practice for FEA-based design iteration loop to be performed over several cycles, in which the appropriateness of the design candidate is evaluated (Novak and Dolsak, 2008).

In current applications, ES either partially facilitates the various steps of analysis or supports the overall process in more holistic approach. Dolsak and Novak (2011) identified the shortages of FEA in pre-processing and post-processing. This is because they hold a significant role in the quality of performance and still mostly depends on the user's knowledge, experience and even rule of thumbs.

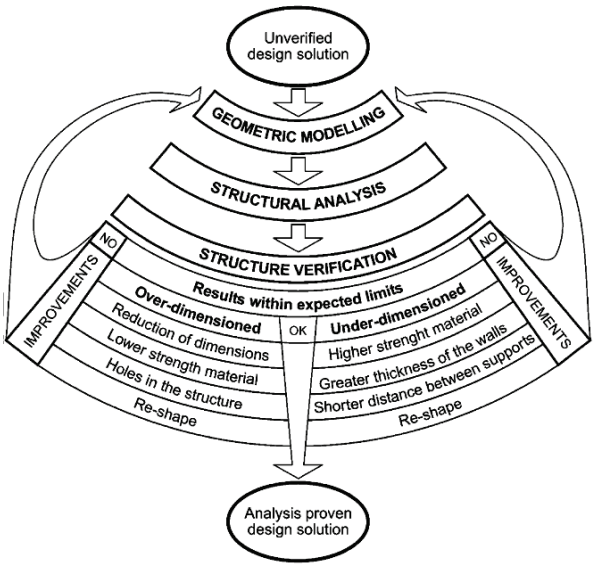

Figure 3-5 Design and analysis iterative cycle (Novak, Dolsak 2008)

The initial motivation of implementing ES on FEA was to support the pre-processing phase, and reduce the amount of repetition due to design iterations (Novak and Dolsak, 2008). These advancements were proposed due to the complexity of mathematical models associated with practical problems in the mechanical design process, which limited the number of models that can be analyzed via closed-form analytical techniques. The inputs to the KBE model contain geometric and non-geometric attributes which can include design specifications, design practices, engineers' expertise, material properties and the boundary conditions. When given a set of inputs, the KBE model can use the knowledge and rules to create an instance of a design which

provides a significant increase in engineering productivity (Pinfold and Chapman, 2001).

In generating KB modules a major effort has been attracted to automate the mesh generation. Kang and Haghighi (1995) proposed a knowledge-based, automatic finite element mesh generator for two-dimensional linear elasticity problems. This involves the decomposition of the original structure into substructures. Dolsak (2002) presents a consultative ruled-base expert system for mesh design aiming to propose the appropriate type of mesh and resolution.

In a recent development, a framework for controlled cost and quality of assumptions in FEA in the field of consultative KB is presented. This framework, assisting users in performing physical modelling and control mesh discretization error, is based on the use of the design of experiments (DOE) method (Bellenger et al., 2009).

Although advancements in pre-processing procedures improve the efficiency of the analysis process and provide reliable control over its specific steps, they do not ensure reliability of the entire analysis. Shephard and Wentorf (1994) attempted to introduce a thorough framework to support the use of existing software as well as the introduction of new techniques without requiring extensive reprogramming efforts. This study presents a framework, shown in Figure 3-6 for analysis idealization control by all possible techniques within a general feedback structure. The framework also supports continual expansion for new analysis goals and strategies.

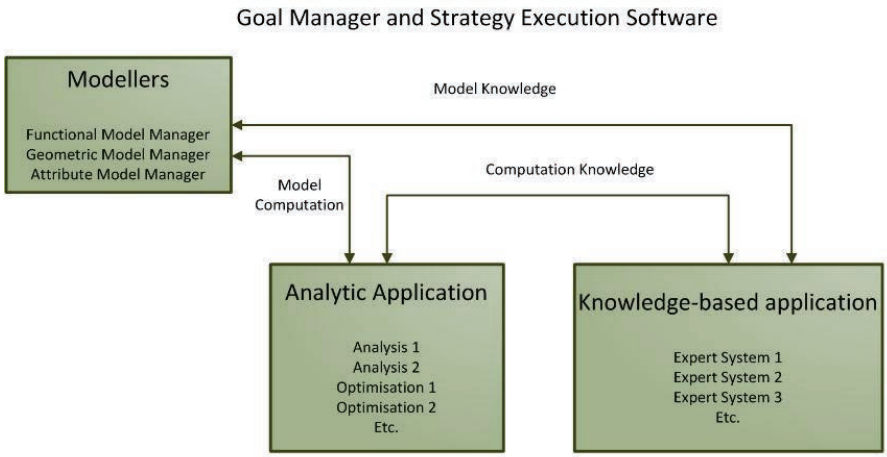

Figure 3-6 An architectural view of the strategy for the existing commercial software components (Shephard and Wentorf, 1994)

Turkiyyah and Fenves (1996) argued this aim as improving the FEM from a low level that is limited to numerical techniques, to a high level that integrates tighter with physical model and CAD model. The proposed framework, illustrated in Figure 3-7 consist of main features of the explicit representation and use of functional descriptions, the explicit representation and use of modelling assumptions, and a hierarchical planning paradigm for driving the modelling task.

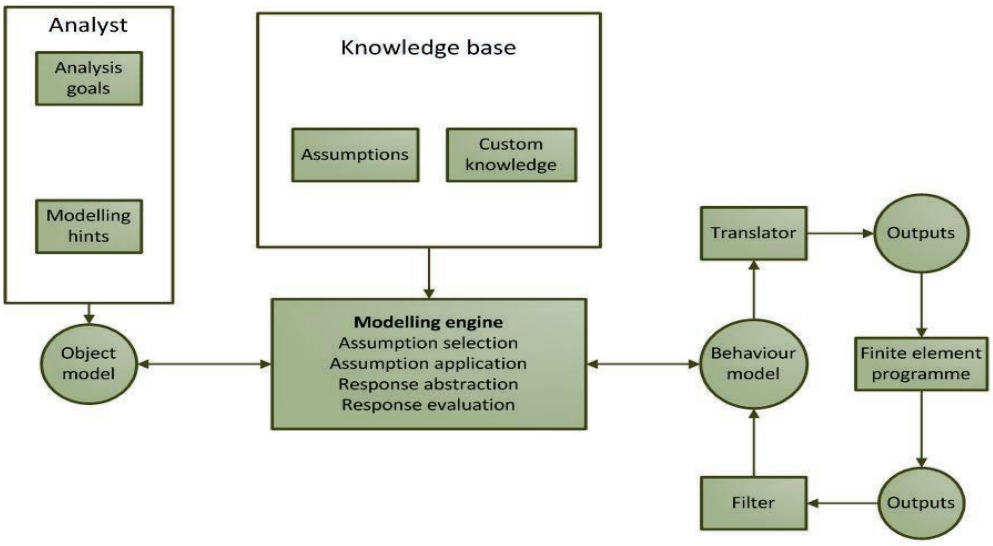

Figure 3-7 Overall architecture of the modelling integration framework (Turkiyyah and Fenves, 1996)

Application of KBE techniques for the automation of the FE model creation was investigated by Pinfold and Chapman (2001). Their proposed method increases the productivity of FEA practice by reducing the repetitions from the process of modelling structure geometry, model simplification and mesh generation.

Dolšak and Novak (2011) present an intelligent environment to address the identified bottlenecks within FEA as

- selection of the most suitable simulation tools,
- selection of the most appropriate, effective, and accurate finite elements,
- determination of a mesh model that will produce acceptable results
- selection of the most effective and accurate solver,
- correct interpretation of the analyses results,
- selection of consequent design actions to improve the structure being analysed,
- coordination, communication, and data exchange.

The proposed intelligent environment consists of four knowledge-based modules, one to support the initial decisions before analysis, two to support the development of a correct and efficient idealised model and the last one for results' interpretation after the analysis process. Figure 3-8 shows the idea on how intelligent analytical KB modules should be integrated into the FEA-based design cycle in order to fill those gaps between the FEA package and geometric modeller to support the designer in decision-making process.

There are also a large number of the focused AI applications that are related to a specific problem (Abbod et al., 2004; Lin and Lo, 2005; Li et al., 2006; Abd El-Ghany and Farag, 2000; Ratchev, 2007).

Figure 3-8 Intelligent support for the FEA- Based design improvement process

3.3.4 Validation and Verification approach

In the product design process the outcomes of numerical solution is not considered as an end on itself but rather an aid to design and manufacturing (Reddy, 2005). When strategic planning and decision making process in a design environment grants a more central role for computer simulation, the credibility of the computational results becomes critical. The standard practices require the simulation process to be extended

beyond the virtual modelling into two major routs of Verification and Validation (V&V) (MacLeod, 2005; Mair, 1984).

V&V approach, as it is advocated by American Society of Mechanical Engineers (ASME) and National Agency for Finite Element Methods and Standards (NAFEMS), is motivated by a managerial perspective which seeks to assure that a sound procedure is followed in developing the model and documenting the numerous physical and numerical parameters required for a structural analysis project. The V&V process also assists on how evidences are collected, and documented which will help establish confidence in the results of complex numerical simulations (ASME, 2006).

Figure 3-9 demonstrates the steps through V&V process (NAFEMS, 2006). This process begins with a Reality of Interest i.e. what is the physical system to be analysed. The modelling logic flows in three stages, from the most general Conceptual, to Mathematical, and more specific Computational Model (ASME, 2006).

The conceptual model is defined with material behaviour, loading and constraints, etc. Analytical description of physical phenomena and processes are called mathematical models (Reddy, 2005). This is created using the conceptual model information, and following the FE model set up procedure in Figure 2-14.

The final model in the sequence, the Computational Model, incorporates the means of achieving a solution (MacLeod, 2005) and consists of the numerical implementation of the mathematical model, in the form of numerical discretization, solution algorithm, and convergence criteria. This stage of modelling contains the particulars of the model that software (code) interprets as the input file (ASME, 2006).

Once the analysis is executed the results should be treated as suspect and the errors should be monitored (MacLeod, 2005). Verification is the process of determining that a computational model accurately represents the underlying mathematical model. Verification process can be conducted in two stages of Code Verification and Calculation Verification, as specified in Figure 3-9 .

Code Verification ensures the mathematical model and solution algorithms are working correctly. Despite the practice is being conducted by software developers mostly, software users would also share the responsibility for Code Verification. Among the available techniques, the most popular method is to compare code outputs with an analytical solution. However, the complexity of most available analytical solutions is a

prohibitive factor towards their implication even in a rather routine application of most commercial software. The Code Verification method with the potential to expand the number and complexity of analytical solutions is termed as a manufactured solution (NAFEMS, 2006).

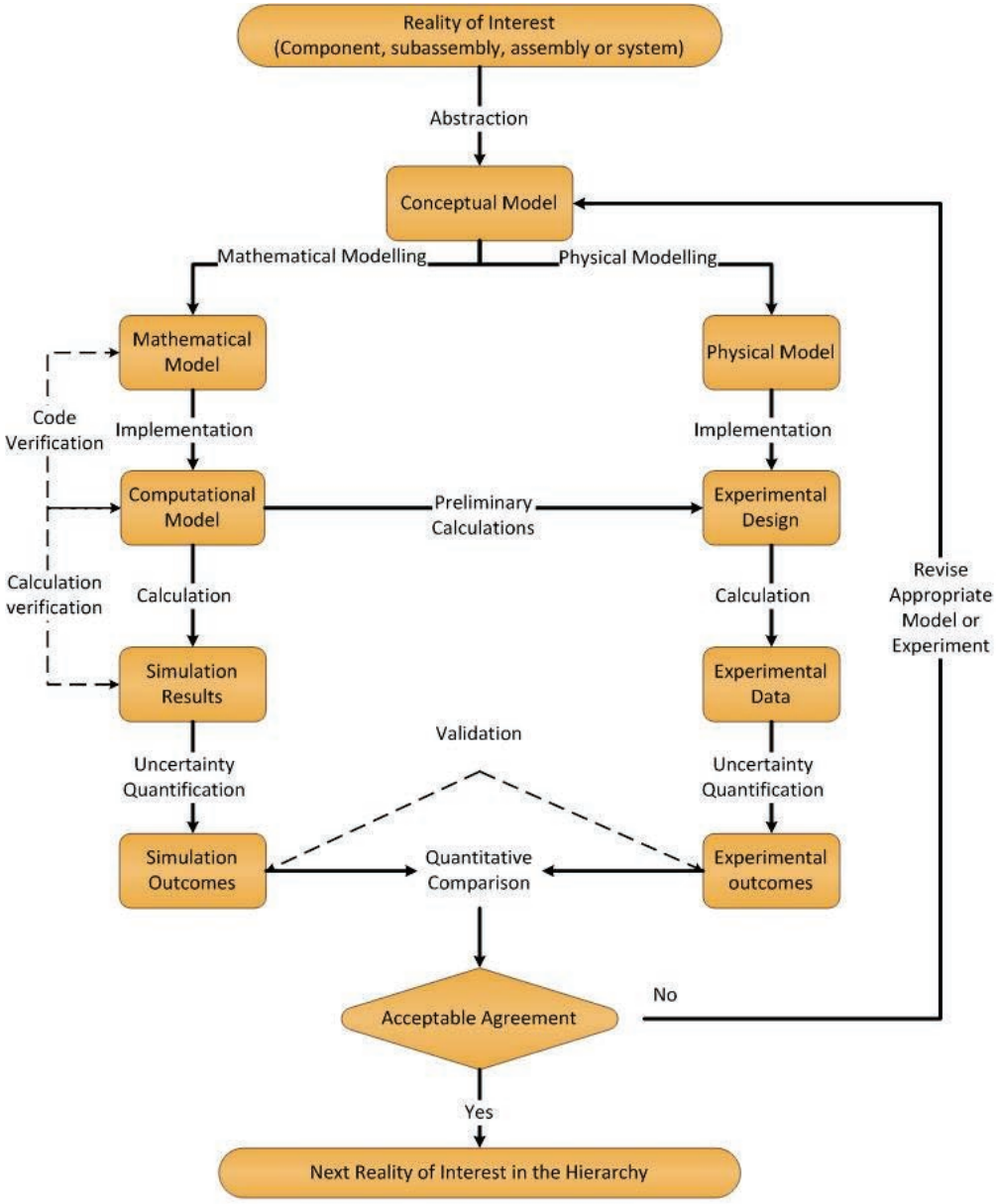

Figure 3-9 V&V procedure (ASME, 2006)

The Calculation Verification, is focused on the accuracy of the discrete solution. Discretisation error is most often estimated by variation of mesh resolution and output comparison. The process that is also known as, mesh convergence, requires a curve of a critical result parameter in a specific location, to be plotted against a measure of mesh density, shown in Figure 3-10. At least three convergence runs are required to establish

convergence with optimised mesh density. However if two runs of different mesh density give the same results, convergence has been most likely achieved (Chillery, 2010, b).

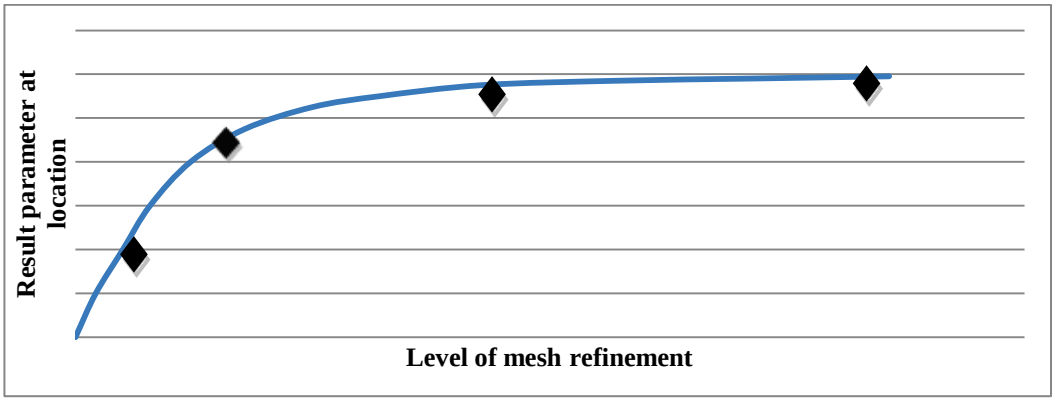

Figure 3-10 A four point convergence curve (Chillery, 2010, b)

The ultimate intention for developing a computational model is to predict the structural behaviour in the absence of experimental data. Neither parts of the above process can address the question of adequacy of the selected models for representing the reality of interest. If the model could adequately predict some related, and simpler instances of the intended use where experimental data would be obtained then the model would be validated to make predictions beyond experimental data (ASME, 2006).

The key components of the Validation process are the:

- Validation experiments that is performed to validate the model.
- Accuracy assessment that ensures adequacy of outcomes.

A comparable set of data can only be achieved if the experimental and mathematical models are in close agreement. This includes features such as geometry, loading and its distributions, supports and constraints conditions, adjoining structure/rig, material properties, environmental condition and measurement/ calculation points (Mair, 1984).

Once the experimental and simulation outcomes are obtained, the accuracy assessment phase begins. Validation metric describes the comparison of Validation experiment and simulation outcomes. A Validation metric is a mathematical operator that requires two inputs: the experimental measurements of the System Required Quantities (SRQs) of interest and the corresponding values from analysis. Figure 2.9 illustrates a flowchart for computing a Validation metric (Roy, 2011).

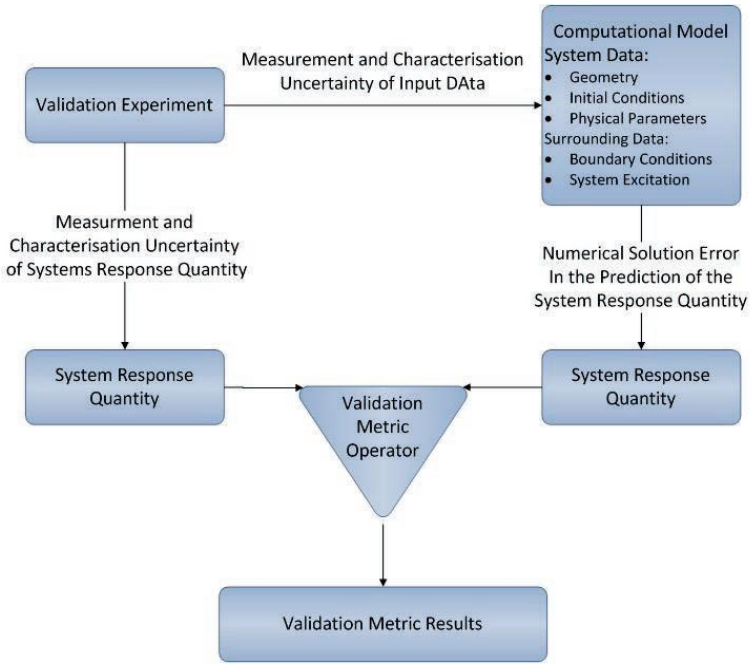

Figure 3-11 Process flowchart for computing metric process (Roy, 2011)

Among recent researchers in application of V&V, the field specific Validation and Verification benchmarks attracted major attention. The code developers such as Abaqus have over 270 formal Verification test cases that focus on engineering accuracy of the code and quantifying the numerical error in the solution (Dassault Systèmes, 2010).

Oberkampf et al. (2004) applied their previously described strong sense benchmarks (SSBs), section 3.3.2, in V&V. Oberkampf also discussed recommendations for constructing and using V&V benchmarks and results comparison. Particular attention has also been paid to the field related computation of nondeterministic results to determine the uncertainty of System Response Quantities (SRQs). Uncertainty can occur due to uncertainties in input quantities, the computation of Validation metrics to quantitatively measure the difference between experimental and computational results, the minimization of model calibration in comparisons with Validation benchmarks, and the constructive role of global sensitivity analyses in Validation experiments (Oberkampf, 2008).

Oberkampf and Barone developed Validation metric features based on the concept of statistical confidence intervals in accordance with ASME Standards (2006).

Understanding of the sources of the uncertainty provides a guidance on how to manage it in the simulation in the most efficient and cost-effective manner. This inspired a

recent study for a higher level of accuracy by classification and quantification of the uncertainties that can propagate into physical and mathematical model and distract output quantities. Figure 3-12 shows the outlines of this approach (Roy and Oberkampf, 2011).

The necessity of integration between V&V and ES was stated by Culbert and Riley (1989). Their proposed methodology can provide the requirements for continual verification aiming for an effective use of V&V in a traceable and testable format.

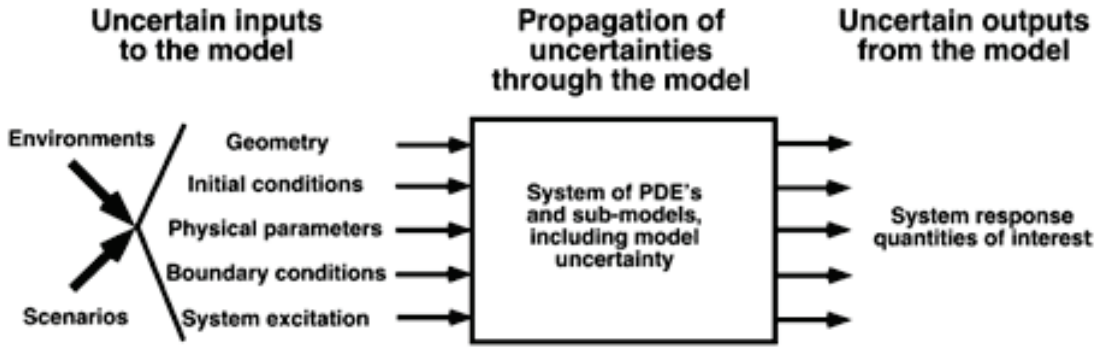

Figure 3-12 Propagation of input uncertainties to output (Roy, 2011)

3.3.5 Design of Experiment (DOE)

As discussed in section 2.2 FEA achieves its aims by quantification of the structures variable responses, such as maximum Von-Mises stress, minimum nodal displacement etc. These responses are expected to vary with respect to input parameters which could be classified as:

- Design parameters e.g. geometry, material, load set etc.
- Modelling and analysis parameters e.g. simplifications, choice of element, meshing, loading and boundary conditions
- Uncertainty parameters e.g. ambient conditions, variation between physical and mathematical model etc.

Design of Experiment addresses analysis of parameters in a systematic manner aiming for an optimal combination. DOE is a series of steps which must follow a certain sequence for the experiment to yield an improved understanding of performance. In general, DOE consists of three phases of planning, conducting and analysis. The purpose of experimentation is to understand the effect of parameters variation on product's performance. The loss function quantifies which input parameter influences

the average and variation of performance characteristics of the product. The approach is based on the use of orthogonal arrays (Taguchi) to conduct small highly fractional factorial experiments up to larger full-factorial experiments. Orthogonal array is only one way of planning for DOE, yet the most flexible to conduct and easy for non-statistically oriented engineers to execute in practice (Ross, 1996).

The Taguchi method incorporates the effect of input parameters as assigned discrete values, called levels that divide each factor to equal increments. The Taguchi approach is not restricted to continuous response variables but can also be used on categorical variables. By choosing a simple factorial design, e.g. one with just two levels or limited interactions, it is possible to filter out the less significant parameters. The shortlisted parameters can be investigated in more complex factorial designs to explore non-linear effects and interactions between parameters (Dar et al. , 2002).

The combined use of FEA and the Taguchi method identifies the relative contributions of design input factors to structural analysis quantifiable parameters. Lin et al. (2009) used this combination to determine the relative contribution of design factors in various performance responses of the biomechanical response of a premolar adhesive (Lin, et all, 2009). A new method of designing quartz crystal microbalance by FEM software is developed by employing Taguchi method (Wu et al. , 2003). The effects of quartz crystal microbalance's resonant frequency influenced by the variation of the deposited mass is investigated in this research using Taguchi method to create the signal to noise ratio to quantify the present variation. The best combination of design parameters is also decided by incorporating Analysis of Mean (ANOM) (Wu et al., 2003). Carino (2006) used orthogonal array (OA) based simulation to assess the effect of uncontrollable factors on complex structural systems. The proposed methodology attempts to produce the maximum information from a predetermined and limited number of numerical simulations, in view of structural layout definition as well as the sensitivity analysis and the consequent optimal layout selection (Carino**,**2006).

In the field of biomechanics Taguchi's parameter design is used to determine how to vary the parameters in a series of FE models, and provides information on the sensitivity of a model to input parameters (Dar et al. , 2002). Taguchi methods are also incorporated to develop the procedural KB Framework, to control cost and quality of assumptions in FEA (Bellengar et al. , 2011):

3.3.6 Comparative assessment

Table 3-3 lists the key strengths and weaknesses of the discussed methods in view of their potential to integrate with design process.

Expert system and knowledge-base engineering main concerns are to assist structural analysis by improving the process bottlenecks as well as reusability of the information. The proposed methods in this field are mostly focused on either fully or partially automate numerical methods, using the accumulated analysis knowledge that is boosted by experts input. Although the topic of process automation is beyond the scope of this research, the concept of reusability of the knowledge can be related to the design process requirement for iteration (Costa and Sobek, 2003). The reusability of the structural analysis data assists the design activity to progresses through conceptual levels towards the desired final state (Adams and Atman, 1999), more effectively.

V&V as the most design oriented approach starts with the reality of interest that can be related to each structural performance. Furthermore V&V is committed to create a fully representative account for the structural analysis for the specific function. The verified and validated analysis method should be adequate for further use with variation of the input parameters.

Benchmark practice is a method to incorporate the values of early simulation in design. The structural performance can be effectively characterised in early stages of the design through the use of salient benchmark. The amount of information obtained with benchmark practice besides its time and cost efficiency makes it viable for the use in design integrated structural analysis methodology.

Finally the application of the Design of Experiment method produces an economic solution for analysis when an excessive number of design input variations are considered to affect the structural performance. DOE can accurately screen the parameters impact for specific objective.

The first observation from the comparative study is that the available methods consider the process mostly from structural analysis perspective. The fact that almost every product requires to satisfy more than one type of structural performance, product multi-functionality aspect, is not attended in the proceeding methods.

Table 3-3 Comparative assessment of available methods to implement structural analysis in design

Method	Strength	Weakness
Early simulation	• Time effective • Prevent error propagation • Suitable for design based on Structural performance	• Concentrate on computer simulation • The benefit is not apparent for enterprise • No methodical approach is available
Benchmark	• Early understanding of performance • Produce production solution for understudy structure and performance • Produce specialist knowledge for structural analysis • Time and cost effective practice	• Concentrate on computer simulation as the main medium of structural analysis • Can be theoretical and not be useful for industry • The amount of effort maybe beyond commercial time constraints • Product multi-functionality has not been observed
Knowledge base	• Make structural analysis available for designers • Provide repeatability and functionality for commercial environment • The most comprehensive method available	• Use significant resources to produce production solution • The current practices are only computer simulation oriented • The proposed methods are oriented around the specific type of analysis and product's multi functionality is not observed •
V&V	• Provides reliability and credibility for analysis results • Merge all three components of structural analysis • Produce a solid knowledge ground	• Resource hungry • Exhaustive practice to close the loop • Requires heavy involvement from expert knowledge • Verification may not be always possible for complex problem • Validation may not be always possible for high consequence products, e.g. nuclear reactor • Products multi functionality has not been observed • The process is subject to error in correlation that needs to be quantified and evaluated
DOE	• Produce a structured method of investigation on the most effective parameters in design of the structure • Can be useful both in computer simulation and experimental practice • Easy to understand and implement in design	• Specific to a type of analysis and not considering product's multi-functionality • Reduce the impact of structural simulation as design optimisation tool and not consider its central role in product development

V&V is the only practice that starts the process with the reality of interest. However further clarification on the reality of interest is required to complete the scope and objectives of the structural analysis practice with respect to product multi-functionality.

A summary of the available design tools and methods along with their opportunities and threats are shortlisted in an comprehensive investigation on developing the company-specific design process model (Cross, Sivaloganathan, 2005). Among the hundred design methods, Quality Function Deployment is capable of adding the missing multi-functionality consideration by mapping the design and stakeholder requirements thoroughly and rating product features accordingly (Cohen, 1995). Capabilities and opportunities of incorporating the QFD into the structural analysis integrated methodology is further discussed in section 3.4.

3.4 Quality Function Deployment (QFD)

QFD is a customer-driven methodology for product design and development that underpins quality systems and has found extensive applications in industry via the development of a multiplicity of tools and systems that aid an enterprise in understanding the voice of the customer (Ramanathan and Yunfeng, 2009). The QFD by definition is *"the converting of the customers' demands into 'Quality Characteristics' and developing a design quality for the finished product by systematically deploying the relationships between the demands and characteristics, starting with the quality of each functional component and extending the deployment to the quality of each part and process"* (Akao, 1990, p.5).

As shown in Figure 3-13 a generic QFD process consists of four phases; relating the voice of the customer to product design requirements (phase 1), translating these into parts characteristics (phase 2), manufacturing operations (phase 3), and production requirements (phase 4). During early design, the first and second phases of the four QFD phases are implemented and part characteristics are defined (Chen and Ko, 2009).

An early review of QFD (Sivaloganathan and Evbuomwan, 1995) concludes that QFD is a powerful tool in the hands of designers to ensure that a specific product is designed to meet the customers' requirements and the principle of deployment used in QFD is a powerful way of ensuring the delivery of the ultimate product characteristics through the design of subsystems, parts and manufacturing. Prasad (1998) identifies several trials of the deployment technique in various areas such as, Total Quality Management,

concept for product alternative selection, multi attribute design optimization etc. This trend of using the principle of deployment continued to expand with time. Chan and Wu (2002) in their review identify this in addition to product development, quality management and customer need analysis as the principal functional domains at the beginning and expand the list to include design, planning, decision making, engineering, management, team work, timing and costing. They also provide a nine step methodology to build the traditional 'House of Quality' together with an illustrative example (Chan and Wu, 2005).

In a conclusive remark of a QFD literature survey, Carnevalli and Miguel (2008) stated the opportunity for QFD adaptation for specific application in conjunction with other techniques such as design of experiments. Jeang et.al (2009) following along these observations report how a hot-bar's soldering process parameters were used to optimize quality characteristics identified using QFD. Lo, Tseng and Chu (2010) describe a QFD based morphological charts to generate concepts for variant or next generation designs. Thus the general trend is to expand on the deployment process for different applications.

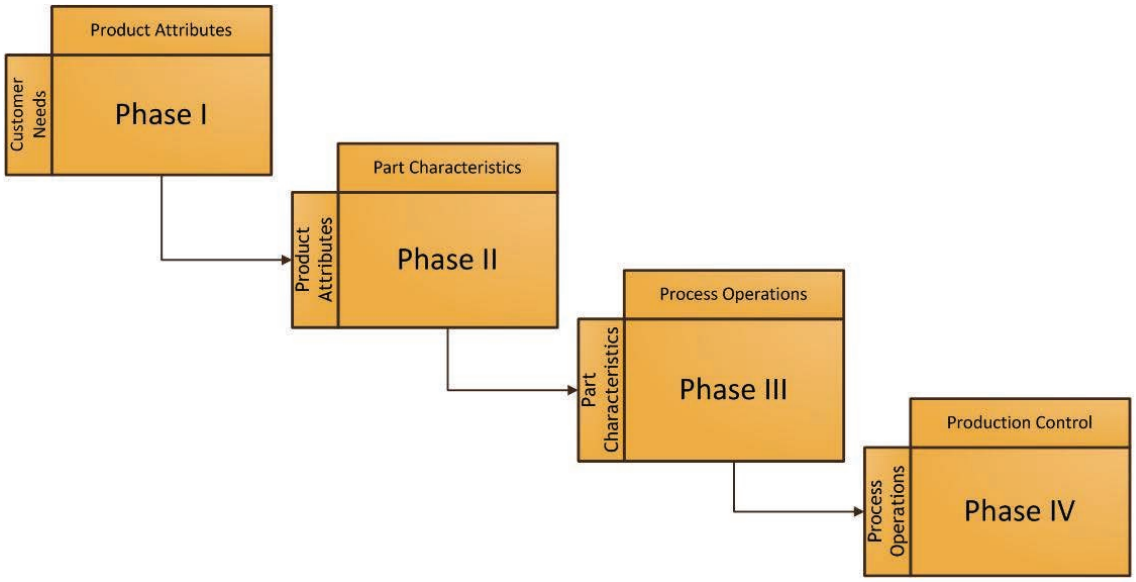

Figure 3-13 Four-phases process planning by QFD (Chen and Ko, 2009).

Products are inherently designed and developed to solve the need of its potential customers. Griffin and Page (1993) identified that the success of a new product should be measured by how well the product is accepted by its customers. Spreng et al (1996) concluded that the customer evaluation of product performance contributes to their

evaluations of satisfaction. Likewise, Cooper and Kleinschmidt (1987) demonstrated that product superiority in terms of product performance, features, and innovativeness was a key factor in differentiating product winners from losers. It is thus evident that product performance measurement is a vital component within the design and development process of a product and furthermore, that these measures should be related to the requirements of its customers/stakeholders. Craig and Hart (2003) stated that measuring product performance has been problematic. They identified that one of the major problems for this was due to the multidimensionality of product development outcomes and whether or not single or multiple metrics were required to measure the performance of the product. If multiple metrics were required, it was further unclear how these metrics could be related to each other.

In summary, QFD function is to collect customer requirements and deploy them during the product realisation process. This function is critical for design validation as in effect, it translates customer needs into part characteristics and production controls that can then be used for design verification, by forming the set of criteria against which product and process compliance can be assessed. This prioritisation of customer needs creates a set of criteria that is used for validating the final product (Maropoulos and Ceglarek, 2010).

3.5 Chapter summary

Chapter 3 is focused on the systematic implication of structural analysis in the design process.

Perspectives of product design in accordance to the mainstream schools of thinking indicate the process as a systematic procedure that develops a product from an abstract to the desired final state. The position of structural analysis within the process of mechanical component design is discussed in view of its function in different stages of mechanical product design. The traditional commercial practice of Design Commitment Validation (DCV) is assessed against a more modern and logical way of product development process, Design Validation Commitment (DVC).

Systematic nature of the design plus time consuming nature of structural analysis requires a structured approach to make the most advantage of the integration practice.

A collection of most practiced approaches throughout academia and industry has been introduced and assessed by their implication. The potentials of outlined methods for

implementation in the design integrated structural analysis methodology are highlighted. However the common lack of product multi-functionality perspective is identified as the key missing component of the available methods.

From a recent comprehensive research and assessment on design tool, Quality Function Deployment is identified as the potential to descriptively develop the reality of interest for the multi-functional product. The customer-driven tool for product design and development is introduced and discussed with the focus on the opportunity to address its expected function.

Chapter 4 will proposed a design integrated structural analysis methodology based on the creative combination of discussed methods in this chapter enhanced by the application of QFD tool.

4 QFD-Based Design Integrated Structural Analysis Methodology

This chapter proposes a methodology for integration of structural analysis in the product design process. The aim of this methodology is to define and plan a required number of analyses and outputs to answer a set of pre-defined stakeholders' structure related requirements. The function of the proposed methodology is to:

- Embed in the product design process progressively from early concept to the finalised state
- Completely satisfy stakeholders' requirements by systematically designing their needs into the analysis
- Cover the multi-functionality aspect of the product and explores their possible overlaps
- Ensure the reliability of the process by adding the benefits of verification and validation

The introduction to this chapter presents an abstract diagram of the methodology. Each stage of the diagram is then explained in subsequent sections. The complete picture of the methodology is presented at the end of this chapter showing the relationships between the parts of the proposed methodology and contributing sections of this document.

4.1 General Provision

4.1.1 The common practice

The structural analysis is a part of a product qualification process within the product design as described in Chapter 3. The multi-functionality aspect requires an uncertain number of structural analyses with number of parameter variations. An unorganised approach leads to a random number of case studies based on the previous design experiences and engineering knowledge. Despite its convenience and flexibility, the efficiency of the process is low because:

- Undefined scenarios lead to the negligence of a certain structural functions and over-analysis of some other functions

- Variations in product input design parameters lead to the exhausting analysis process
- Unstructured analysis process makes the design progress hard to visualise

4.1.2 Proposed Methodology in abstract

The layout and key components of the proposed structural analysis process model is presented in Figure 4-1.

The values of early simulation and the benefits of understanding the structure's performance, before commitment to a finalised solution, are discussed in Chapter 3. This concept is incorporated in the proposed methodology via a conceptual representation of the actual structure of interest.

As discussed in Chapter 3, QFD is a design tool to collect stakeholder's requirements and deploy them during the product realisation process. In the context of the proposed methodology, the product of interest is structural analysis performance and the customers are the internal stakeholders of the analysis results i.e. product designer, project manager etc. In this application, stakeholders' requirements are translated into Measurable Performance Characteristics (MPCs) using the knowledge of structural analysis in the form of its quantifiable objectives and failure criteria, detailed in Chapter 2. The influential design parameters are also identified at the beginning of the practice, as the Design Input Variables. QFD binds this information to establish relationship matrices, that leads to the exact number of required analyses. This extent of application of QFD assists the analyst to identify the reality of interest in a descriptive format as well as understand their overlaps and further expansions. This procedure produces the required predecessors, as a descriptive reality of interest for the V&V process.

The V&V framework, Figure 3-9, is also enhanced by introduction of the instant of reality. The proposed studies are only verified and validated on an instant of reality that can represent the other analyses within the study. In this context the instant of reality replaces the verification and validation of full range of analysis of interests, determined by QFD procedure. Once the simulation results are confirmed, the process continues with conducting the list of required studies. The results and outcomes are arranged in to the stakeholders' initial requirements format to facilitate the communication. The abstract methodology, Figure 4-1, is elaborated in the following sections.

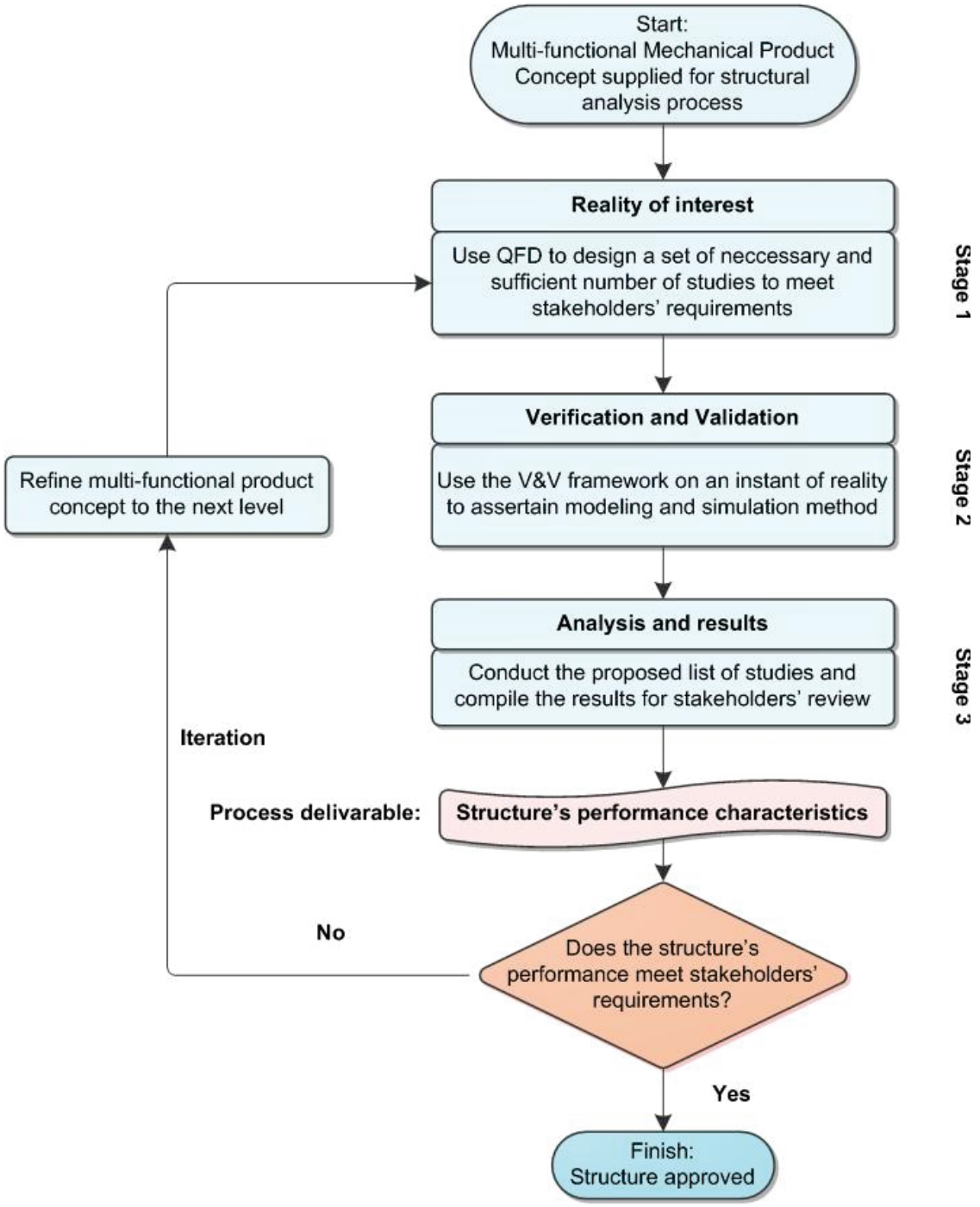

Figure 4-1 Abstract of the proposed structure analysis methodology

4.2 Methodology process model

4.2.1 Process start point

The process starts with a multi-functional mechanical product in the conceptual stage. The fixed input information about the structure such as assembly layout, key components and choice of material, nature of interaction, the boundary conditions and the nature of the applied load is required in order to define the structure. The nature of

the input parameter as constant or variable with their values and range of variation should be defined in this stage.

Based on this information, the proposed concept can be embodied in a 3D model followed by a physical prototype. The techniques to design a salient benchmark, discussed in Table 3-3, facilitate to capture the structure in a simplistic form and reduce the complexity of the full-scale product.

After creating the representative benchmark the reality of interest has to be established with application of the QFD method.

4.2.2 Stage 1 QFD process

The QFD method in principles relates:

a) the requirements by stakeholders

b) the Measurable Performance Characteristics (MPCS) that truly and completely represent and satisfy the requirements

c) the Independent Variable Parameters that have effects on Measurable Performance Characteristics (MPCs) and

d) the effects of varying an Independent Parameter on the relevant MPCs. In this context the MPCs are considered as variables response.

In an individual analysis scenario the stakeholders' requirement is deployed by a Measurable Performance Characteristic, *y*. It is known that the characteristic, *y*, depends on Independent Variable Parameter, *x*:

Eq. 4-1

$$y=F(x)$$

The analysis is designed with provisions to vary parameter, *x*, over a given range and record the MPC response, *y*. The concept for a single analysis can be described by Function Means Tree as shown in Figure 4-2 (Andreassen, 1998).

The multi-functionality of a product adds another dimension to function means tree by taking each of the requirements separately, schematically shown in Figure 4-3. A

considerable amount of overlap between these Function Means Trees encourages the construction of an integrated analysis plan to combines individual analysis.

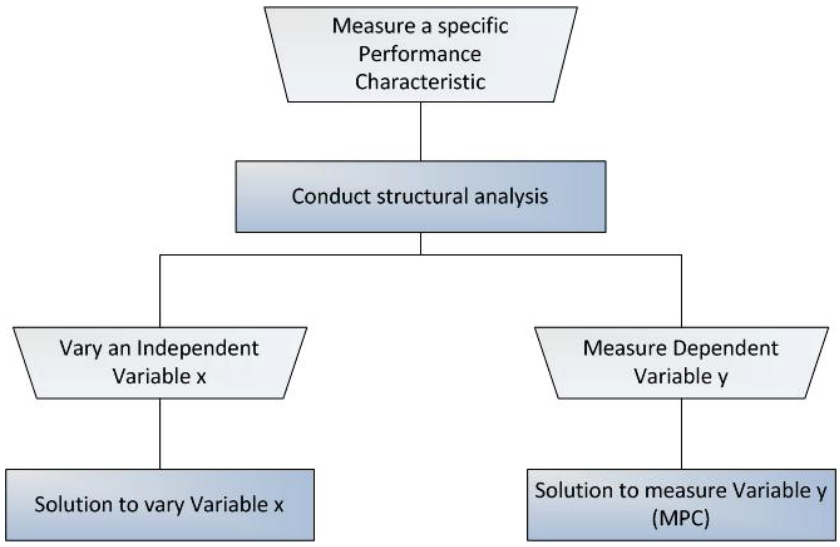

Figure 4-2 Function Means Tree of a single analysis

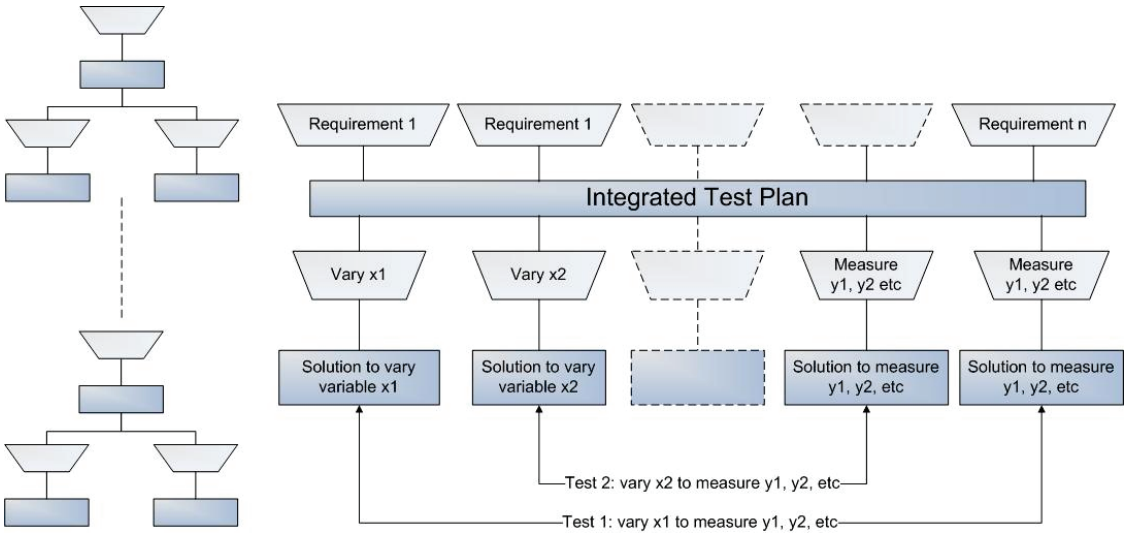

Figure 4-3 Testing in an Integrated test plan

In order to achieve the objective of integrated test plan for structural analysis, QFD procedure can be best described by the process model shown in Figure 4-4. The following sections elaborate the block diagram.

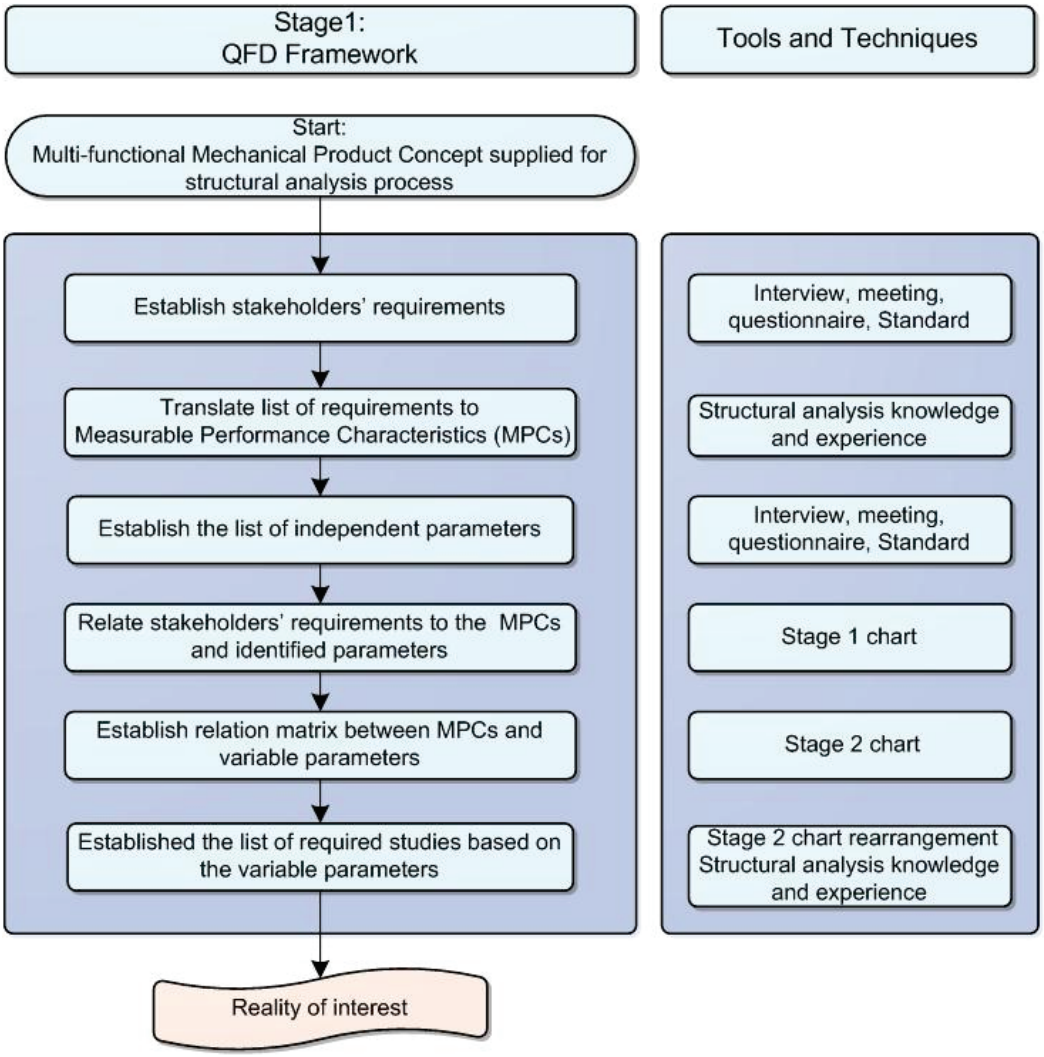

Figure 4-4 Process model of the methodology

4.2.2.1 Stakeholder's requirement

QFD as a customer oriented method starts with collecting stakeholder requirements. By definition, the stakeholder is anyone who is affected by the product or service (Cohen, 1995). The list of stakeholders may include individuals, departments, organisations or groups of the general population. Each stakeholder will normally desire particular performances of the design and their requirements will reflect them. This is a completely product related information and can be collected by meeting, interviewing or from Product Design Specification (PDS) and standard or approval criteria.

In the context of structural analysis, similar to other technical aspects of the product, it is rare that the customers or end users are being actively involved or have a particular interest. However it is customary that the technical performance and safety of the product controlled and accredited by the industry related standard body and against the

industry specific code of conduct. Therefore in this context, it is an accepted argument to consider the product standard, as the customer requirement.

Similar to the external stakeholders' requirement, there are a wide range of internal stakeholders whose requirements have to be satisfied. It is expected that Product Design Specification (PDS) document encapsulate the requirements of internal stakeholders. However considering the PDS as a progressive working document, the internal requirements can be a drifting goal post, and require more direct communications with product's stakeholders.

At the end of this stage a common ground of the engineering knowledge and experience regarding the structural performance of the specified structure is collated.

4.2.2.2 Measurable performance characteristics

The list of MPCs are established based on the stakeholders requirements. This stage is the key transitional stage from abstract statements of needs, to a quantifiable parameter. This task needs an intense knowledge of mechanical and structural analysis as well as the simulation and experimental analysis expertise, discussed in Chapter 2. The accuracy and clarity in MPCs is crucial to ensure the process capability of addressing the outstanding requirements.

The example of MPCs in the field of structural analysis can be Von Mises stress, displacement, natural frequency and buckling critical load. This stage determines the required type of analysis and the expected type of output as well.

4.2.2.3 Independent Parameters

Independent Variable Parameters refer to the ones that have not been defined as the constant in the structure's conceptual definition, at the start point, but considered as effective on the MPCs response. The Independent Variable Parameters in this context refer to those that are of interest for stakeholders and have to be collected according to their knowledge and expertise in the field as well as standard criteria and PDS. The Independent Variable Parameters should be defined with their:

- *Variables value*: This includes the range of variations, the number of increments and value at each increment.

- *Assigned value*: Whether the variable parameter is required to be fixed for a certain MPC or throughout the experiment and its constant value has to be specified.

4.2.2.4 QFD Chart 1

QFD chart 1 is effectively a preliminary step to link stakeholders' requirements to the MPCs and selected Independent Variable Parameters in a relationship matrix.

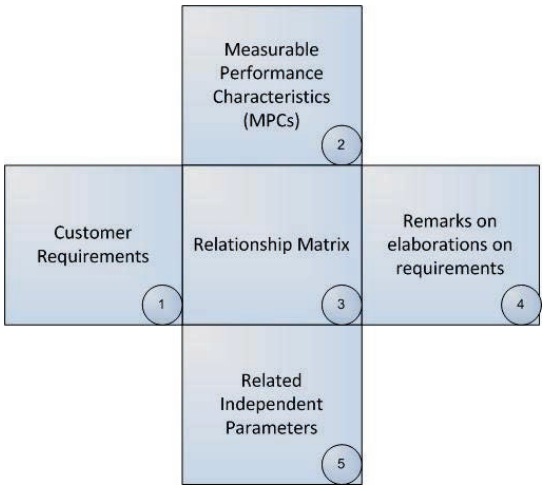

Figure 4-5 QFD chart 1

QFD Chart 1, illustrated in Figure 4-5, typically consists of five blocks of information:

- *Block 1 – Stakeholders' requirements*: As described in Section 4.2.2.1. They have to be structured so that all requirements are similar in content.
- *Block 2 – Measurable Performance Characteristics*: As defined in Section 4.2.2.2.
- *Block 3 – Relationship Matrix*: The relationships between the requirements and the MPCs are determined here. This only aims to show whether a relationship exists or not.
- *Block 4 – Remarks on Requirements*: This is an optional window to elaborate on the requirements.
- *Block 5 –Independent Parameters*: As described in Section 4.2.2.3. Each MPC can be responsive to one or more Independent Parameters. This is the compilation of a list of Independent Parameters that have to be considered during the design of the programme.

4.2.2.5 QFD Chart 2

The QFD chart 2 accommodates Independent Variable Parameters in the columns and MPCs in the rows. The relationship matrix identifies links between MPCs and Independent Variable Parameter. Each cell will then show a MPC related to an experiment based on varying the corresponding variable. Figure 4-6 illustrates a schematic QFD chart 2. The five blocks of information are arranged as:

- *Block 1* – List of MPCs transferred from the Stage 1 Chart
- *Block 2* – Independent Parameters from Stage 1 Chart
- *Block 3* – Relationship matrix: The link between MPCs and Variable Parameter are identified by star and Fixed Parameters by the empty cells.
- *Block 4* – Ranges of the Independent Parameters: These are the ranges which analyses have to be conducted for
- *Block 5* – Remarks on the MPCs: This provides more details of the MPCs.

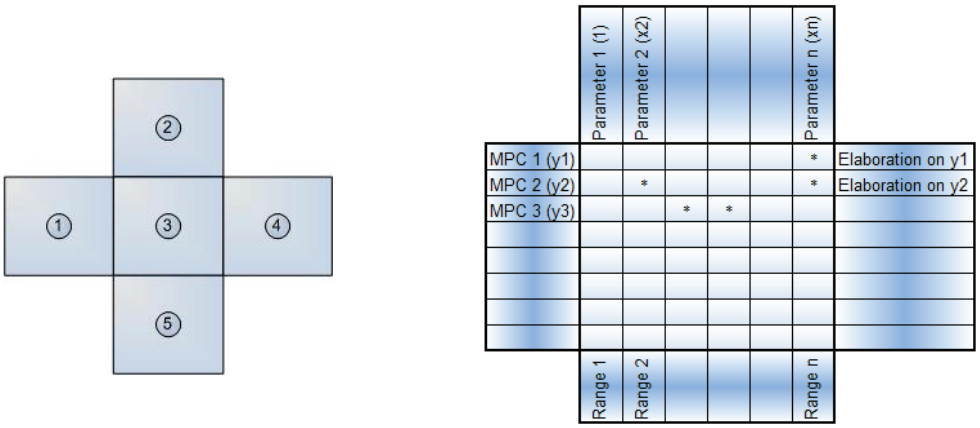

Figure 4-6 QFD Chart 2

As a result, each row entry of the relationship matrix defines analyses that completely address each MPC. By completing the studies for all the designated Independent Variable Parameters a complete picture of required MPC's is expected to achieve. This procedure provides a built-in guarantee that the tests carried out will capture the stakeholder requirements.

4.2.2.6 Plan for integrated studies

The rows of QFD Chart 2 show the list of expected studies with respect to the Independent Variable Parameters. Table 4-1 illustrates transition from QFD Chart 2 to a list of required studies. Each study of Table 4-1 aims for a certain MPC under the

variation of several parameters of interest, whilst the rest of the input variables are remained at their fixed values.

Table 4-1 Study plan based on MPC

Analysis condition					
Study No	MPC	Variable parameter	Range of variation	Increments value	Assigned Parameters
1	y_1	x_1	$a_1<x_1<a_5$	a_1,a_2,a_3,a_4,a_5	$x_2 = b$, $x_3 = c$, $x_4 = e$, $x_5=e$
		x_4	$d_1<x_4<d_3$	d_1, d_2, d_3	$x_1 = a$, $x_2 = b$, $x_3 = c$, $x_5=e$
2	y_2	x_2	$b_1<x_2<b_4$	b_1, b_2, b_3, b_4	$x_1 = a$, $x_3 =c$, $x_4 =d$, $x_5=e$
		x_3	$c_1<x_3<c_4$	c_1, c_2, c_3, c_4	$x_1 = a$, $x_2 =b$, $x_4 =d$, $x_5=e$
3	y_3	x_5	$e_1<x_5<e_2$	e_1, e_2	$x_1 = a$, $x_2 =b$, $x_3 =b$, $x_4 =d$
4	y_4	x_1	$a_1<x_1<a_5$	a_1,a_2,a_3,a_4,a_5	$x_2 = b$, $x_3 = c$, $x_4 = e$, $x_5=e$
		x_5	$e_1<x_5<e_2$	e_1, e_2	$x_1 = a$, $x_2 =b$, $x_3 =b$, $x_4 =d$

Possibility of integration: The nature of the MPC whether it is a stress or natural frequency etc. determines the type of the required analysis. The possibility of study integration emerges when a few MPCs are achievable with one analysis and the variable parameters of interest are in common. For instance the values of stress and strain tensor under similar load magnitude variations are possible to obtain with only one static analysis.

Another possibility of integration emerges when an excessive number of Independent Variable Parameters are of interest of a certain MPC(s). In this case it is possible to plan for a set of design of experiment practice using Taguchi's orthogonal array concept to reduce the number of analysis cases.

Possibility of expansion: On the other hand due to the nature of the Independent Variable Parameters one analysis may not be able to accommodate the range variation and produce to the set of required results. The variation in geometry is typically requires remodelling. In this occasion further expansion within the proposed study is required

It should be noted that the objective of this stage is not to reduce the number of analysis, but to propose the necessary and sufficient number of analysis that completely satisfy

stakeholders' requirements as they initially identified. The practice will be more elaborated through its application on the case-study in Chapters 5 and 6.

4.2.3 V&V on the instants of reality

Following the further developments of Table 4-1 and clarification on the actual reality of interest, the required V&V cases can be determined.

The V&V process, in principle, follows exactly as the frameworks proposed by NAFEMS, shown in Figure 3-9. However it is sensible to conduct V&V only on the select number of analysis that can represent the others within the studies. These cases are termed as instants of reality and referred to the analysis conditions that can be calculated or experimentally measured.

Following understanding the instants of realities each line of study is independently verified and validated. The ascertained simulation is taken forward to conduct the rest of the analysis in the list. The successful performance of this stage solely depends on the analyst knowledge and expertise in quantifiable parameters (MPCs), FEA procedural step and experimental measurement practice all detailed in Chapter 2.

4.2.4 Results report and iteration

The results collection and report follows the same order as the studies. The related MPCs to each stakeholder's requirement are packaged to create a complete account for the area of interests.

From the design perspective, as an iterative process, it is expected that the delivery of the first outputs, follows by the next round of structural analysis to assist the next level of product development. Base on the findings of the previous round, the iteration process is planned by adjustment to the stakeholders' requirements and the design input variable, towards a more targetful process. The iteration allows the methodology to support the design process all the way toward the product finalisation. The use of benchmark may be limited only to the first iteration; however more verification and validation may be expected in the iteration process. The engineering justification along with the analysis expertise is required to ascertain the existing solutions or specify further V&V process.

4.3 Methodology framework

The procedural framework demonstrated in abstract in Figure 4-1 is developed in Figure 4-7. The iterative nature of the methodology enhances the position of the structural analysis in design process, by supporting it from conceptual to the finalisation level.

The efficiency of the model comes from early understanding of the structural behavioural pattern that improves the design understanding of the parameters influence, sensitivities and errors.

The product's multi-functionality impact on structural performance is captured by incorporating the QFD procedure in the methodology. The verified and validated benchmark increase the level of confidence to the simulation outputs in a timely manner, and conclude many of the basic features in simulation in early iterations.

Therefore the structural design frame is expected to be established earlier in the design process and lead to a more definitive answer by considering the combination of structural functions.

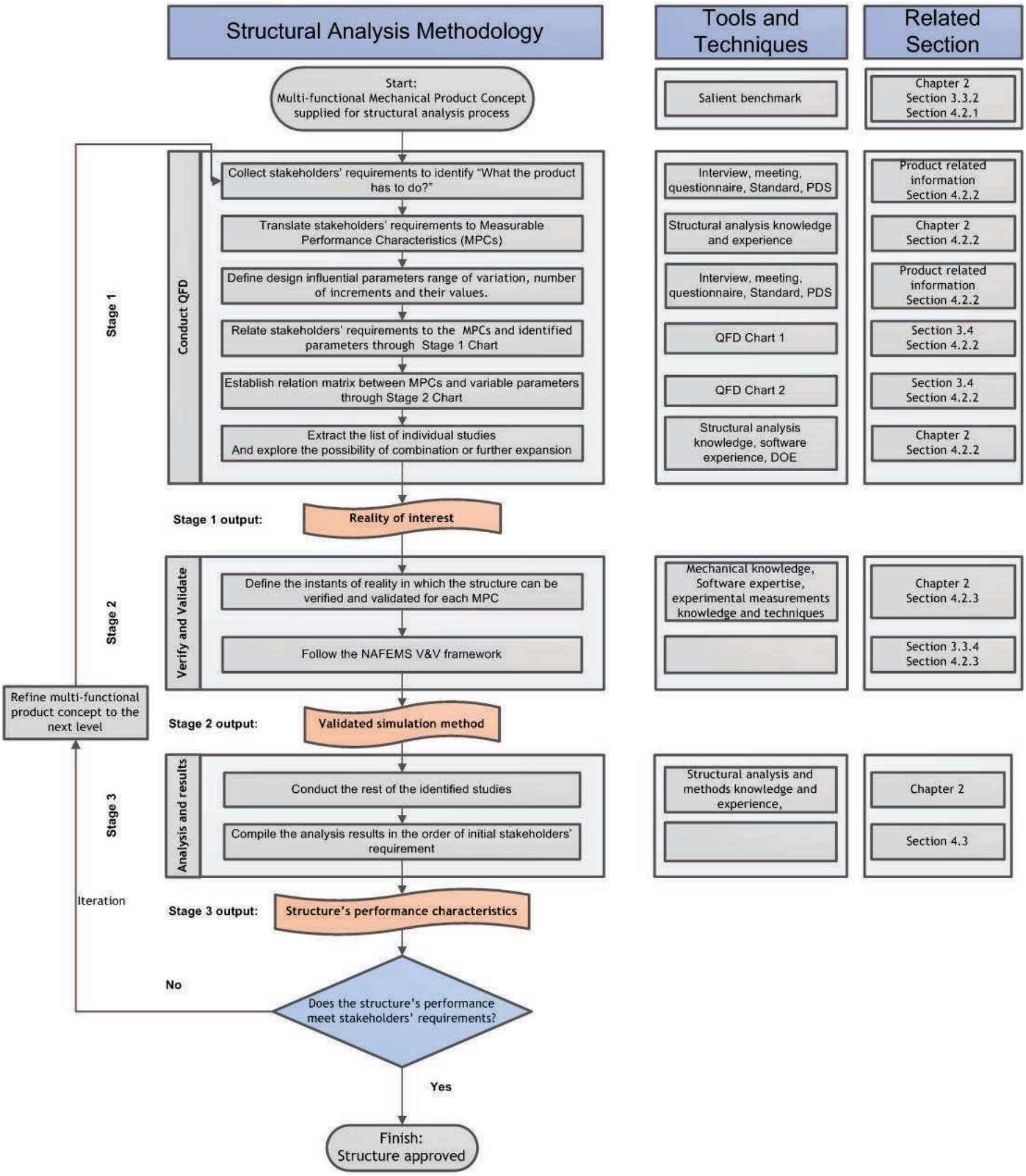

Figure 4-7 Structural analysis proposed methodology

4.4 Chapter summary

The proposed methodology for structural design synthesis and integration in design process is elaborated in this chapter. The proposed methodology starts with salient benchmark to integrate with design in conceptual stage.

The reality of interest as the start point of verification and validation process is descriptively defined by the adaptation of the QFD method. During the QFD process the initial requirements and influential design parameters are obtained through stakeholders' statement of requirements product design specifications and standard criteria. These informations are translated to the structural analysis quantifiable objectives and the relationship between them and the input variable parameters are established. The list of required studies are then extracted and the possibilites of further expansion or integration is identified.

The process is followed with the standrad method of V&V as proposed by NAFEMS. The only note on this method is to select a nominated instants of reality to be verified and validated.

The results collection are followed the same order as the studies. The relevant MPCs are packaged together to satisfy each one of stakeholders' requirements. The methodology can be regarded as an iterative process if the next level of design is planned as a result of structural analysis.

5 Case Study- Telescopic Cantilever Boom

In Chapter 4 the integrated structural analysis methodology is described. This chapter focuses on the application of the proposed methodology on a nominated structure. The purpose of this case study is to validate the proposed methodology on a real-life industrial structure design scenario.

The subject structure is reduced to a concept in order to take advantage of the use of salient benchmark. The following sections introduce the structure and its industrial application that leads to its multi-functional structural aspect. The application of the proposed methodology leads to the list of required analysis, and corresponding V&V cases that satisfy stakeholders' requirements.

The proposed methodology is only applied to the conceptual structure, expecting that the iteration route develop the concept into a later product design stage.

5.1 Telescopic cantilever boom

This case study is inspired by the application of the multi-staged telescopic booms as appear in industrial off-road vehicles e.g. Cranes, Access Platforms, and Tele-Handlers, Figure 5-1. The light weight and compact nature of the telescopic structure besides its adjustable range of working envelope put it among the popular design concepts in the application of load handling in elevation. The commercial products are designed in various shapes, sizes and number of nested sections. Despite the variation in appearance the commonality in the function creates a similar key components and general structural layout.

Figure 5-2 shows typical telescopic sub-assembly in isolation subject to carry a load on its free end (Niftylift, 2010). The telescopic function is created by the means of hydraulic cylinder to extend the assembly to its full working length. The structure is also subject to a rotational function around the fixed end, via a hydraulic cylinder arrangement.

Figure 5-1 Multi-staged telescopic sections in industrial off-road vehicles

The sub-assembly consists of a few internal sliding sections that interacts through a low-friction wear pads components. The wear pads always remain in the overlap region of the sections. The load and stress from consecutive sections are transferred to the fixed end through these interacting surfaces. The adjustable length between the wear pads, known as the overlap zone, supports the reaction from overhanging weights and applied loads. The structure is subject to symmetric as well as asymmetric load due to a rotational function at the free end.

Providing the safe reliable load handling solution is the ultimate design aim for this product. The stakeholders' requirements are collected based on the design review meetings, product design specification, and industry related engineering standards.

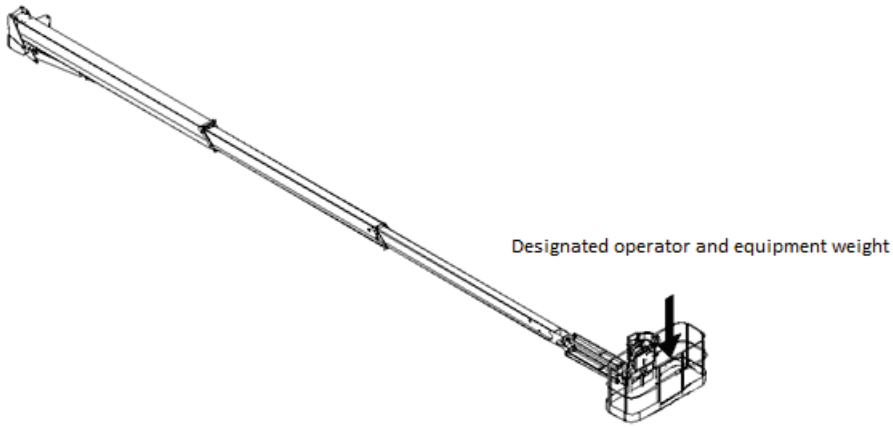

Figure 5-2 Multi-staged telescopic assembly (Niftylift, 2010)

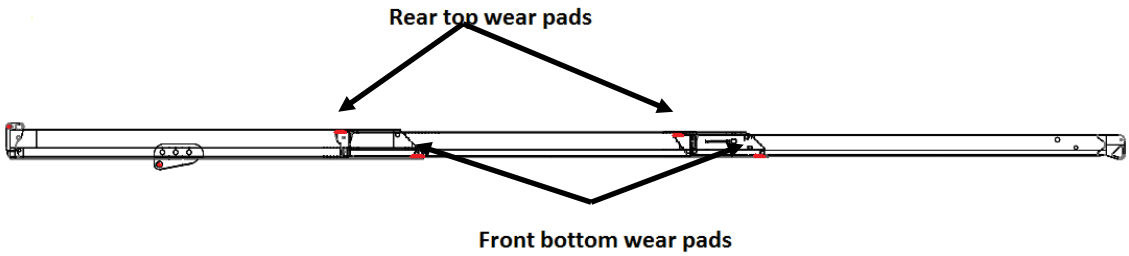

(a)

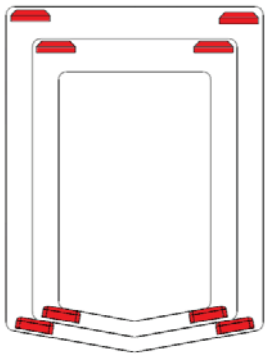

(b)

Figure 5-3 Sliding sections and arrangement of low-friction components in telescopic assembly (Niftylift, 2010)

5.2 Benchmark construction

The benchmark of the full-scale structure including the key components of the assembly is produced. The benchmark model consists of two nested rectangular beams as laid out as Figure 5-4 (a). The beams are interacting through four low-friction wear pads located in the front bottom and rear top of the overlapped area as shown in Figure 5-4 (b). Another two pairs of wear pads on the front and rear side-walls are mounted to control unintended side way movements.

The understudy components are assembled on a rigid test rig as shown in Figure 5-5.

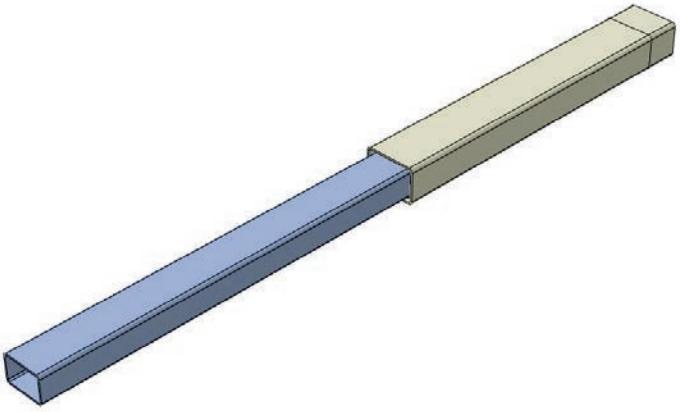

(a)

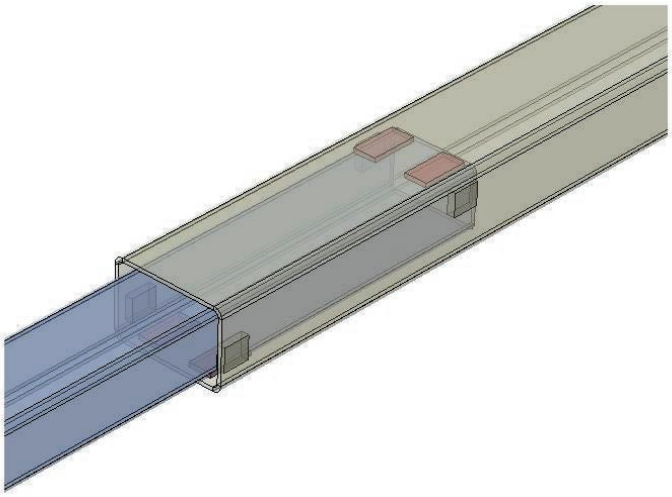

(b)

Figure 5-4 Benchmark model of the telescopic cantilever beam

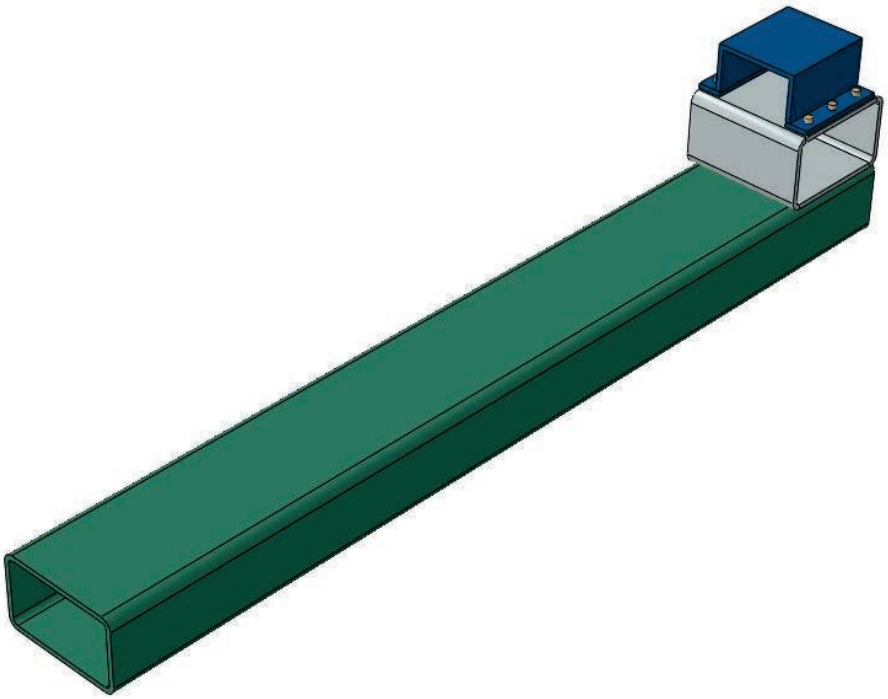

(a)

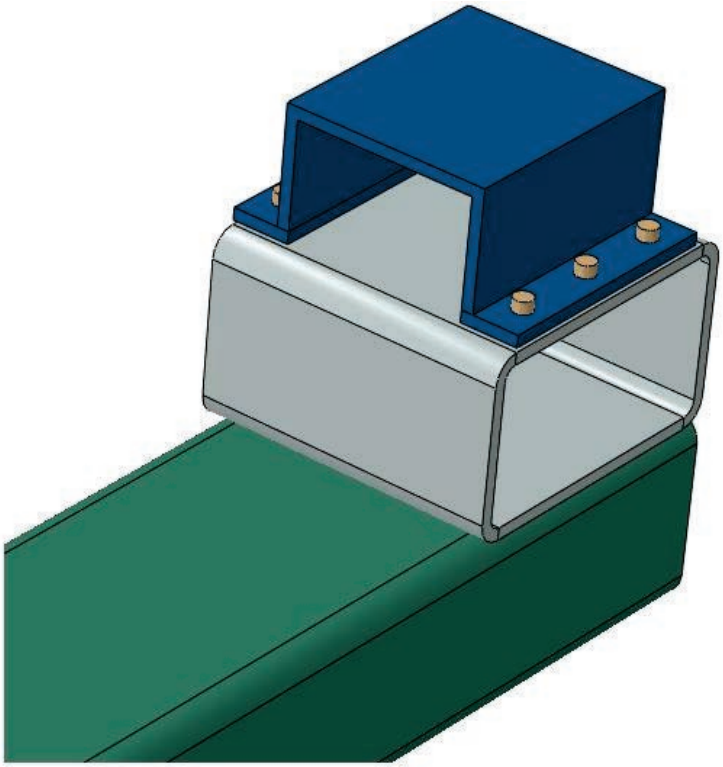

(b)

Figure 5-5 Test rig assembly

Total benchmark prototype is completed by assembling the telescope and test rig and the load hanger pieces as shown in Figure 5-6. The detail dimensions of the components are available in Appendix VII.

The physical prototype is produced accordingly as shown in Figure 5-7 and detailed in Figure 5-8 (a) and (b).

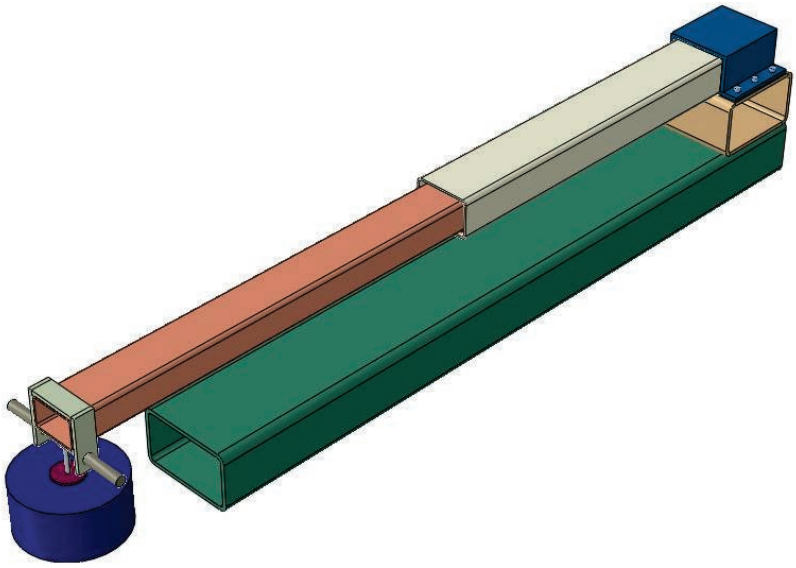

Figure 5-6 Total test rig assembly

Figure 5-7 The physical test rig

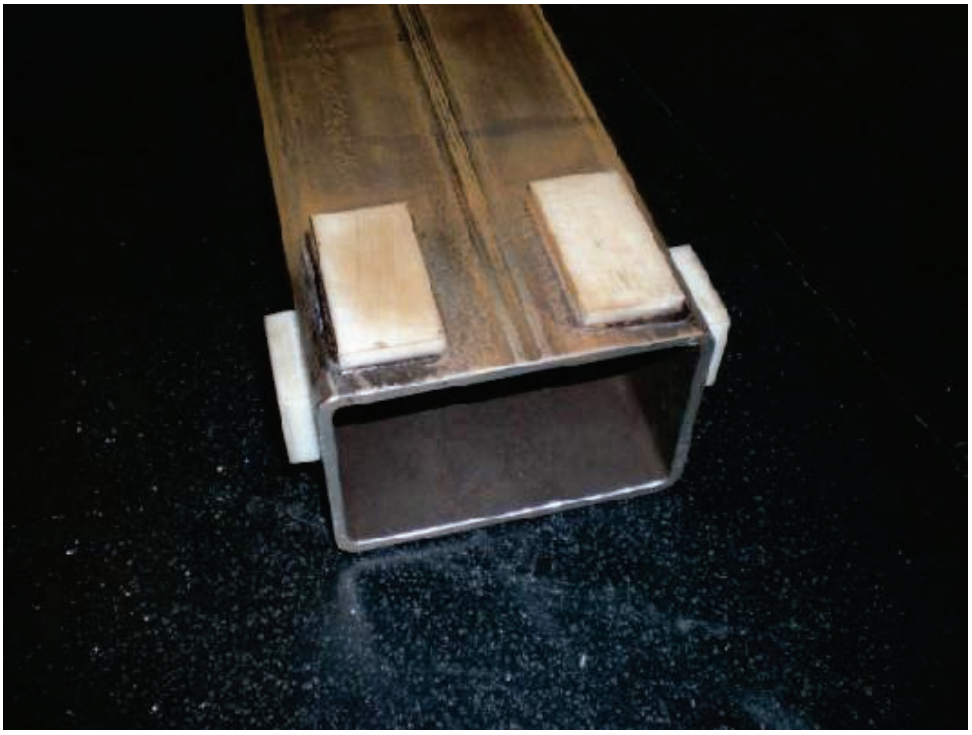

(a)

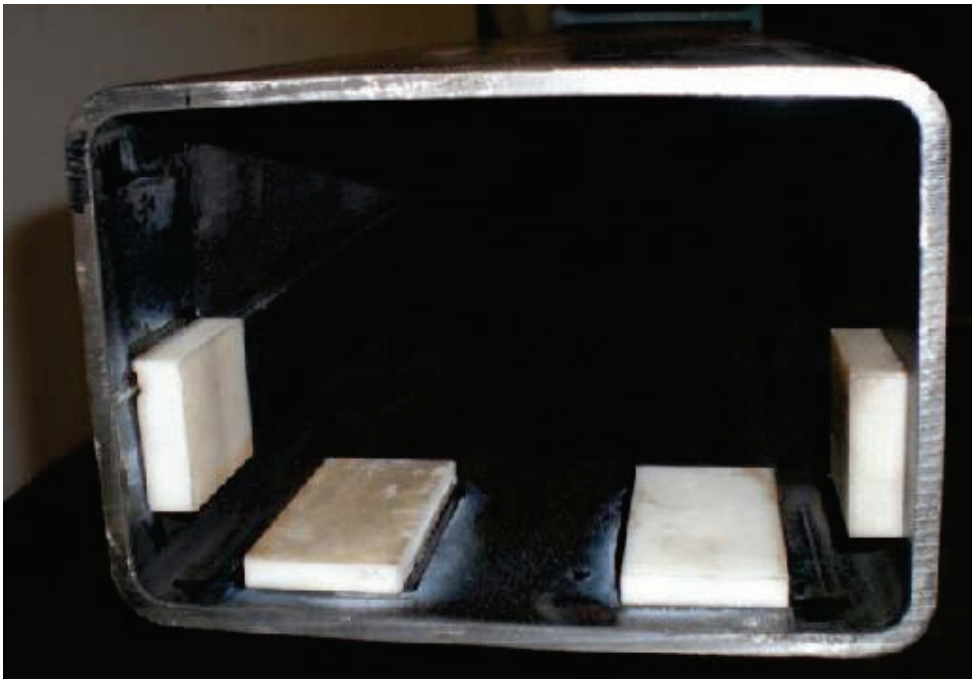

(b)

Figure 5-8 (a) The detail components of the inner section (b) The detail components of the outer section

5.3 Stakeholder's requirements

5.3.1 Stress at contact region

The product standard defines a safe level of stress both locally and globally (BSI, 2001). As it is shown in free body diagram of Figure 5-9 the applied load is reacted at wear-pads and transferred to the next external sections. The assembly at its maximum outreach is expected to experience the highest reaction forces at the wear-pads interacting surfaces. Apart from the stress quantification, its pattern helps to characterise the nature of the structure behaviour.

5.3.2 Total displacement

The assembly experience a total displacement due to self-weight and pay load at the free end. The displacement of the compound cantilever in a constant overlap length behaves linearly with the applied tip load similar to a simple cantilever (Abraham and Sivaloganathan, 2011). The gradient of the load-displacement graph known as structure's rigidity is a characteristic of the structure that is specified by the stakeholders. This information is useful to control the full-scale products displacement range with respect to Product Design Specification (PDS).

5.3.3 Vibration

The interruption in the function due to sudden stop of operation or drive over potholes etc. induces a factor of vibration to sub-assembly. The importance of this factor, specifically in the access platform products, comes from user comfort. Within a range of vibration on overall body, the user can experience a motion-sickness type of uncomforting. In response to these phenomenon designers need to study and quantify the natural frequencies behaviour of the structure.

5.3.4 Buckling behaviour

As it is shown in the cross sectional view of Figure 5-3 (b), the construction of each individual sections are out of thin steel sheets. Design of the long slender components that experience compression inherently associated with buckling failure (Vinson, 1989). As it is described in Chapter 2, this mode of failure acts independently from material failure criteria and governed by geometry. The design of the commercial product

requires analyses to quantify the likelihood of this mode of failure and comply with standard criteria.

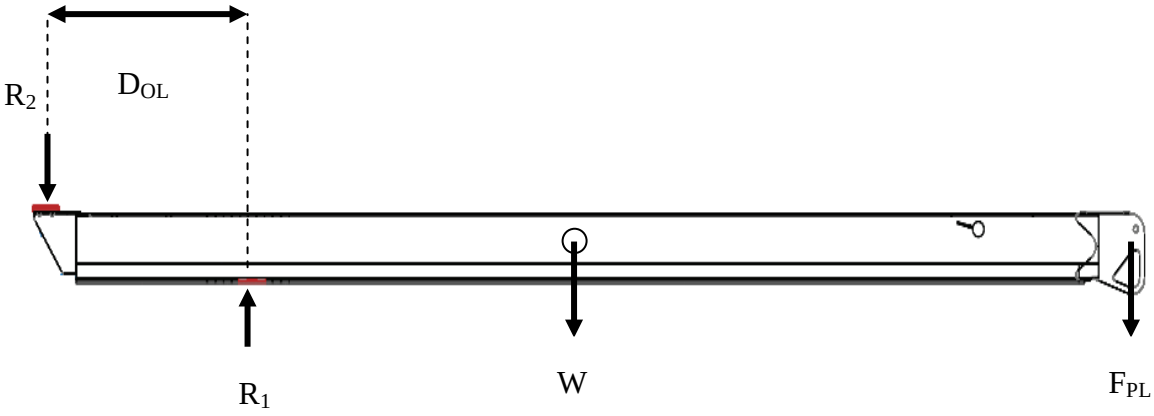

Figure 5-9 Reaction forces at wear pads generated by self-weight and pay-load

5.4 Measurable performance characteristics

The required measurable performance characteristics are derived from stakeholders' requirements. Nevertheless some of stakeholders' requirements e.g. stress and displacement are measurable on their own right, more accuracy is needed to characterise them in mechanical terms. Definitions of stress and strain, discussed in Chapter 2, are incorporated to clarify these parameters. Table 5-1 summarise this part of the process.

Table 5-1 Measurable Performance Characteristics (MPCs)

Stakeholders' requirement	MPC	Notations	Reference
Stress at contact region	Maximum von-mises stress	σ_{vm}	Section 2.2.2
	Directional stress components	σ_{xx} σ_{zz} τ_{xz}	Section 2.2.3
	Directional strain components	ε_{xx} ε_{zz} γ_{xz}	Section 2.2.6
Displacement	Total vertical displacement	$(U_y)_{tot}$	Section 2.2.3
	Local vertical displacement	$(U_y)_n$	
Vibration	Natural frequency	$(f_n)_{tot}$	
Buckling performance	Buckling load factor	BLF	Section 2.2.6
	Buckling mode and location	Qualitative parameter	

5.5 Independent parameter

The influential parameters on the listed MPCs are extracted from the PDS and product application as well as stakeholders' interest, are presented in this section.

Element selection (P1): Chapter 2 indicates the discretisation method as an effective variable on the accuracy of simulation. The stress-displacement simulation can be distracted by the inadequate choice of element. On the other hand there might be more than one solution to provide adequate simulation results. For instance in the case of thin-walled structure both shell and solid element predict the stress-displacement performance accurately (Dassault Systèmes, 2010), however the shell element produces more time efficient solution in three dimensional application and therefore be a preferable option. Despite this is neither specified by stakeholders, PDS nor standard, the element verification is an inevitable part of achieving realistic analysis.

Load magnitude (P2): The load case can be split to two classes of self-weight and payload. Self-weight is the fixed portion of the load which is the function of gravity and structure mass. The applied load is decided by stakeholders in PDS and indicates the products load handling specification. The variation in the load magnitude changes the structures stress displacement performance which in turn influences the buckling probability in the compressive regions.

Load type (P3): Type of applied load is a direct input from the PDS (Niftylift, 2010) that is subject to symmetric as well as asymmetric loads. These will indicate the payload is applied either as concentrated force only, or a combination of concentrated force and moment. The variation affects structure's stress-displacement performance.

Overlap (P4): The integrity of the structure is maintained by the reserved length of nested sections. Ideally the minimum overlap length is desirable in order to achieve a maximum benefit of working length. However reduction in the overlap length significantly increases the reaction forces at wear pad regions which in turn affect the stress- displacement and buckling performance. Also the change in the overlap length will influence the overall length of the assembly which affect the vibration behaviour.

5.6 QFD chart 1

Referring to Figure 4-6 the QFD chart 1 is constructed as shown in Figure 5-10. The corresponding MPCs to each stakeholder's requirement and the list of influential Input Variable Parameters are represented in the matrix format.

	σ_{vm}	σ_{xx} σzz τxz	ε_{xx} ε_{zz} γ_{xz}	$(U_y)_{tot}$	$(U_y)_n$	$(f_n)_{tot}$	BLF	Qualitative	
	Von-mises stress	Stress tensor components	Strain tensor component	Tip displacement	Local vertical deflection	Natural Frequency	Buckling load factor	Buckling mode and location	
Stress at contact region	*	*	*						To approve the stress within the safe design limit
Total displacement				*	*				To approve the dispacement within the safe design limit
Vibration performance						*			To approve the vibration within the human comfort limit
Buckling performance							*	*	To approve the buckling possibility outside safe design limit
	P1, P2, P3, P4	P1, P2, P3	P1, P2, P3	P1, P2, P4	P1, P2, P4	P2, P4	P3, P4	P3, P4	

Figure 5-10 QFD Chart 1 for the telescopic cantilever boom structural analysis

5.7 QFD Chart 2

The QFD Chart 2 is a developed version of Chart 1 that establishes relationship matrix between MPCs and Variable Input Parameters, as shown in Figure 5-11. The matrix not only considers the mechanical relation between MPC and variable parameter but also stakeholders interests in a response due to an input variation i.e. despite type of load can affect natural frequency performance it is not indicated by stakeholders as a concern.

		P1	P2	P3	P4	
		Element selection	Load magnitude	Load type	Overlap length	
R1	Von-mises stress	*	*	*	*	Measured at predefined points at contact region
R2	Stress tensor components	*	*	*		Measured at predefined points at contact region
R3	Strain tensor components	*	*	*		Measured at predefined points at contact region
R4	Total vertical displacement	*	*		*	Measured at tip end
R5	Vertical deflection along the length	*	*			Measured at predefined locations along the length of the assembly
R6	Natural frequency		*		*	Measured at any other point along the length
R7	Buckling load factor			*	*	Predicted as a force-displacement graph
R8	Buckling mode and location			*	*	Observed as deformed shape
		Shell, Solid	Min<(Increments)n<Max	Symmetric, Asymmetric	Min<(Increments)n<Max	

Figure 5-11 QFD Chart 2 for the telescopic cantilever boom structural analysis

5.8 Plan for individual studies

In compliance with Section 4.2.2.6 the list of individual studies are proposed in Figure 5-11. The proposed list, based on the MPCs, specifies the required type of analysis.

The concept of analysis integration and expansion is introduced in section 4.2.2.6 is applied in Table 5-2. The stakeholder requirement for the stress at contact region and displacement behaviour is already combined in one study because of the commonality of required type of analysis and Input Variable Parameters. For instance, the variation in the type of element can produce both corresponding MPCs to displacement and stress behaviour at contact vicinity.

Another opportunity for combination is available within the first study. Since the analysis is inherently conducted under the incremental loading, it is possible to conduct the element variation study with the fixed load increment as specified for load magnitude variation experiment in Table 5-2. Therefore the results of the most satisfying elements can be used for the load magnitude variation experiment toward stress and displacement characterisation. The same set of results also can satisfy the load type variation experiment in the case of symmetric loading, and overlap variation experiment for the maximum overlap length.

In the case of more time consuming analysis condition it is possible to consider the reusability of analysis as the base-state of the other analysis. For instance it is possible to reuse the static results of the overlap variation as the base state of the linear perturbation for the vibration study or buckling procedure when the variation of the same parameter is of interest. The technique known as restart modelling, is worth considering in detailed design stage or when the excessive number of parameters variation is required. In the case that the analysis results obtained quickly there is still a chance to only reuse the model for other MPCs toward various stakeholders' requirements.

The requirement for expansion of the studies is apparent from the type of Input Variable Parameters. All the experiments concerning the type of elements, load type and overlap variation required to be remodelled and reanalysed to accommodate these variation.

The application of this discussion translates Table 5-2 to Table 5-3, the plan for integrated analysis.

Table 5-2 Plan for individual studies

Study	Stakeholders' requirement	Corresponding MPC	Type of analysis	Fixed Parameter	Variable Parameter	Variation
1	Stress behaviour at vicinity of contact area	Von Mises stress	Quasi Static	P2= Symmetric, P3= Max, P4= Max	Element (P1)	Shell/Solid
		Stress tensor		P1=Verified option, P3= Symmetric, P4= Max	Load Magnitude (P2)	Min<(Increments)$_n$< Max
		Strain tensor		P1=Verified option, P2= Max, P4= Max	Load Type (P3)	Symmetric/Asymmetric
	Displacement behaviour	Total displacement		P1=Verified option, P2= Max , P3= Symmetric	Overlap Length (P4)	Min<(Increments)$_n$< Max
		Local deflection				
2	Vibration performance	Natural frequency	Quasi Static followed by linear perturbation (frequency)	P1=Verified option, P2= Max, P4= Max	Load Magnitude (P2)	Min<(Increments)$_n$< Max
				P1=Verified option, P2= Max, P4= Max	Overlap Length (P4)	Min<(Increments)$_n$< Max
3	Buckling behaviour	Buckling load factor	Buckling analysis procedure	P1=Verified option, P2= Max, P4= Max	Load Type (P3)	Symmetric/Asymmetric
		Buckling mode		P1=Verified option, P2= Max, P4= Max	Overlap Length (P4)	Min<(Increments)n< Max

Table 5-3 Plan for procedural integrated analysis

No	Type of analysis	Study condition	Stakeholders requirement	MPC
1	Quasi static	FEA with **Solid elements**, with fixed incremental symmetric load until maximum pay load in maximum overlap condition	Stress behaviour near contact area Displacement behaviour	Von Mises stress Stress tensor Strain tensor Total displacement Local deflection
2	Quasi static	FEA with **Shell elements**, with fixed incremental symmetric load until maximum pay load in maximum overlap condition	Stress behaviour near contact area Displacement behaviour	Von Mises stress Stress tensor Strain tensor Total displacement Local deflection
3	Quasi static	Study with verified element from Study 1 and 2, with fixed incremental **asymmetric** load until maximum pay load in maximum overlap condition	Stress behaviour near contact area	Von Mises stress Stress tensor Strain tensor Total displacement Local deflection
4-8	Quasi static	Study with verified mesh under the maximum symmetric load for **variation of overlap**	Stress behaviour near contact area	Von Mises stress Stress tensor Strain tensor
9-13	Quasi static followed by linear perturbation frequency	Study with verified mesh and max overlap, **for each number of load increments**	Stress behaviour near contact area Displacement behaviour Vibration performance	Von Mises stress Stress tensor Strain tensor Total displacement Natural frequency
14-18	Quasi static followed by linear perturbation frequency	Study with verified mesh under the maximum symmetric load for **variation of overlap**	Vibration performance	Natural frequency
19	Buckling procedure	Study with verified mesh and **max symmetric load**, for max overlap	Buckling behaviour	Buckling Load Factor Buckling mode
20	Buckling procedure	Study with verified mesh and **max asymmetric load**, for max overlap	Buckling behaviour	Buckling Load Factor Buckling mode
21-24	Buckling procedure	Study with verified mesh and max symmetric load, **for variation of overlap**	Buckling behaviour	Buckling Load Factor Buckling mode

5.9 V&V on the instant of reality

Using the outlines of the required analysis from Table 5-3, the plan for verification and validation is drafted. Since the element variation in the first two analyses only has simulation implication they both can be verified and validated with one set of experimental measurement. The instant of reality for this case can be similar as the analysis condition; variation of the load magnitude with all other parameters to be fixed.

The third set of analysis, for the application of the asymmetric load is verified and validated independently since the variation in the load type is expected to induce shear stress/strain components and vary the corresponding MPCs in an unknown fashion. These two V&V cases are assessed as sufficient for the variation of the overlap length since by this stage the stress-displacement performance of the simulation is approved.

The stress response in vicinity of contact area, to variation of the overlap length, analysis 4-8, are not different in nature from the ones that has already been planned for and therefore the behaviour characterisation only relies on the simulation outcomes.

Natural frequency performance of the structure is planned through analysis 9-13 and 14-18. These two sets of analysis are verified and validated independently. The instant of reality is chosen similar to the prescribed analysis condition.

The last three rows of studies, 19, 20 and 21-24 are focused on the buckling performance under various parameters variation. The buckling performance is a probabilistic analysis and there is a likelihood that it does not occur on a proposed prototype. Also in the instance of occurrence, the test is associated with a failure mode that may lead to a structure collapse. Due to these reasons it is not possible to propose a validation test within the capacity of this research. The above discussion is summarised in Table 5-4.

Table 5-4 Verification and Validation plan

No	Stakeholders' requirement	MPCs	Variable parameters	Proposed instant of reality
1	Stress behaviour near contact area Displacement behaviour	Von Mises stress Stress tensor Strain tensor Total displacement Local deflection	Load magnitude	A telescopic cantilever in the horizontal configuration capable to accommodate incremental loading applied in-line with the axis of symmetry
2	Stress behaviour near contact area	Von Mises stress Stress tensor Strain tensor	Load type	A telescopic cantilever in the horizontal configuration capable to accommodate incremental loading applied offset from the axis of symmetry
3	Vibration response	Natural frequency	Load magnitude	A telescopic cantilever in the horizontal configuration capable to accommodate incremental loading applied in line with the axis of symmetry
4	Vibration response	Natural frequency	Overlap length	A telescopic cantilever in the horizontal configuration loaded in line with the axis of symmetry capable to be extended to cover overlap length variation

5.10 Chapter summary

This chapter discussed the application of proposed structural analysis methodology on a nominated structure of telescopic cantilever boom. A simplified representation of the full-scale structure is designed as the benchmark. The areas of stakeholders' interests are summarised and the influential Input Variable Parameters are identified.

Following the methodology flowchart of Figure 4-7 plan for individual analyses is drafted. Using the structural analysis knowledge and software expertise further possibilities for integration and expansions are explored. A total number of 24 analyses are specified to completely satisfy the predefined requirements in conceptual level. Total numbers of four V&V cases are specified to complement the structural analysis practice.

6 Analysis and Results

6.0 Introduction

In Chapter 5 a list of required analysis, Table 5-3, that has to be accompanied with nominated instants of realities, Table 5-4, are produced in accordance to stakeholders' requirements. In this chapter the stakeholders' requirements are answered by conducting the relevant analysis and V&V cases. The report for each stakeholder's requirements is organised as parameter variation analyses along with corresponding instant of realities for verification and validation. Each section is concluded with the behavioural characterisation remarks for further consideration toward the product design process.

6.1 General condition of the analysis

The numerical analyses are conducted in Abaqus 6.10EF, using the procedural steps of Table 6-1. More details of surfaces interactions, boundary conditions and point of load application are shown in Figure 6-1.

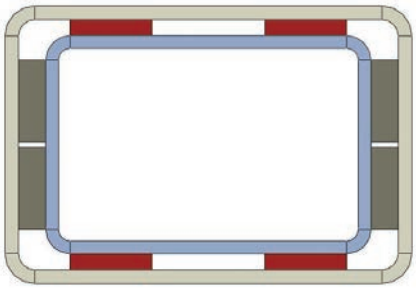

(a)

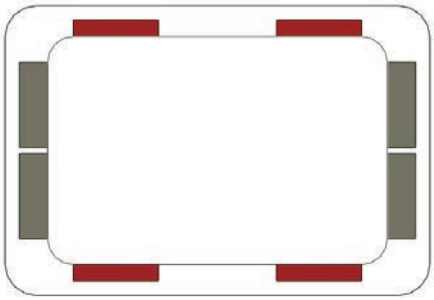

(b)

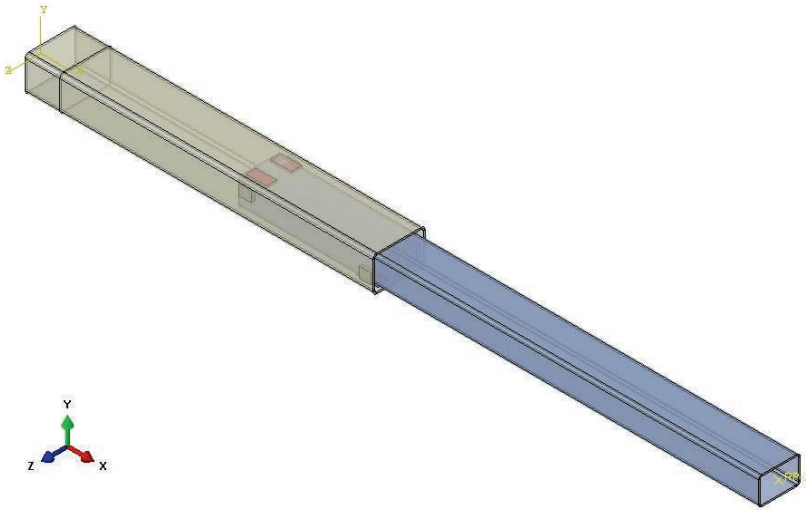

(c)

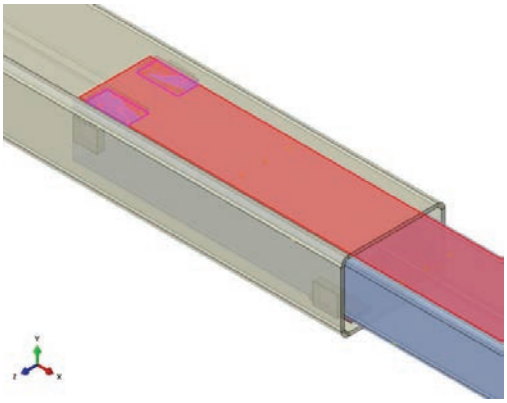

(d)

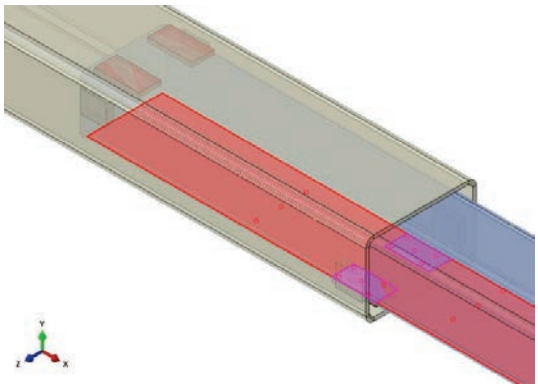

(e)

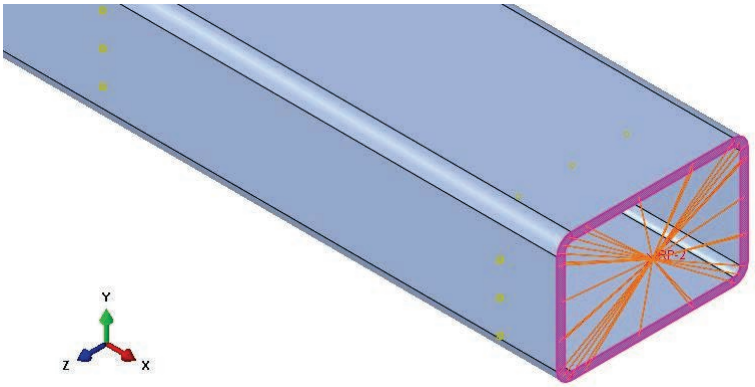

(f)

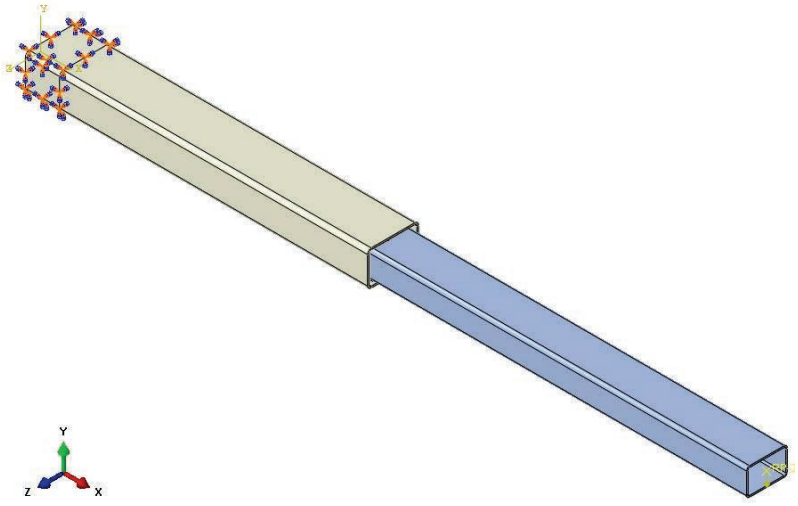

(g)

Figure 6-1 (a) Beam sections in solid (b) Beam section in 3D planar (c) Telescopic assembly in global coordinate system (d) example of Tie pairs (e) example of Contact pairs (f) Coupling pairs (g) Loading point and Boundary Condition region

Table 6-1 General simulation set up condition in Abaqus

Step	Description	Illustration
Parts	• First set of beam sections are created out of solid. • Second set of beam are created out of 3D planar geometry. • The rest of the components are all created out of 3D solid geometry.	Figure 6-1 (a) Figure 6-1 (b) Figure 6-1 (a) & (b)
Mesh and element	Subject to investigation in this section	
Material Property	Steel: E= 210000MPa ρ=7.85e-9 tonnes/ mm3 ν=0.33 Nylon: E= 4000MPa ρ= 1.85e-9 tonnes/mm3 ν=0.33	
Step (alternative)	General static followed by second General static General static followed by linear perturbation frequency Buckling procedure	
Assembly	• The assembly placed in a coordinate system where x is along the length of the telescope, y is the height direction, and z is in the width direction. • Components are added to the assembly as required	Figure 6-1(c)
Interactions	• Tie interactions in places where no relative motions or sliding is predicted e.g. wear pads glue to beam sections. • Contact interaction where the components are free to slide or detach e.g. sliding surfaces between sections and beam. Coefficient of friction is set as 0.1 • Coupling interaction to connect the load application point to the structure.	Figure 6-1(d) Figure 6-1(e) Figure 6-1(f)
Loads and BCs	• A 100 mm at the fixed end of the assembly is encastered. • Gravity applied in the first general static step. • The pay load is applied as a concentrated force at the tip end in the second general static step in a fixed incremental fashion.	Figure 6-1(g) Figure 6-1(g)
Job	Jobs are created and submitted as required	

6.2 Stress behaviour at vicinity of contact area

This section aims to assess the stress behaviour in contact vicinity due to variation of independent parameters. Stress behaviour is explored in accordance with study 1 of Table 5-2. The required analysis of 1, 2, 3, 4-8 from Table 5-3 satisfies this objective by producing results for corresponding MPCs. The first and second instant of realities as outlined in Table 5-4 are conducted in order to verify and validate the simulation for the stress-displacement analysis.

6.2.1 Element variation

The analyses conditions, taken from analyses 1 and 2 of Table 5-3, are elaborated in Table 6-2. The mission of this study is to quantify the impact of the element variation on the stress at vicinity of contact, with the corresponding MPCs.

Table 6-2 Stress study condition, dependency on the choice of element

Stakeholders' requirement	MPCs	Fixed Parameter	Variable Parameter
Stress behaviour near contact area	Von Mises stress Stress tensor Strain tensor Analysis running time	Overlap = 500 mm Load type: symmetric Load magnitude= 50kg	Element type: Shell, Solid

6.2.2 Element performance and verification

The independent FE models are created to accommodate the use of shell and solid elements. Under these two classes of elements a number of variations are examined as listed in Table 6-3.

Table 6-3 Choice of elements for the telescopic cantilever study (Dassault Systèmes, 2007, b)

Class	Name	Description
Solid	C3D8	linear 8 node, fully integrated
	C3D8I	Linear 8 node, incompatible
	C3D20	Quadratic 20 node fully integrated
Shell	S4	Linear fully integrated
	S4R	Linear reduced

A set of 9 nominated reading points equally distanced by 100 mm, are chosen on the centreline of the top surface of the outer section as shown in Figure 6-2.

Table 6-4 shows the Von mises results for each node in comparison with bending stress calculation. The engineer's theory of bending (Rees, 2000) is employed to conduct the verification on the non-contact zone:

Eq. 6-1

$$\sigma = \frac{yM}{I}$$

Plotting the Von Mises results on the diagram shows a minor difference between shell and solid performance. Among the solid options however fully integrated elements (C3D8) show slight over-stiffness near the contact vicinity, Figure 6-3.

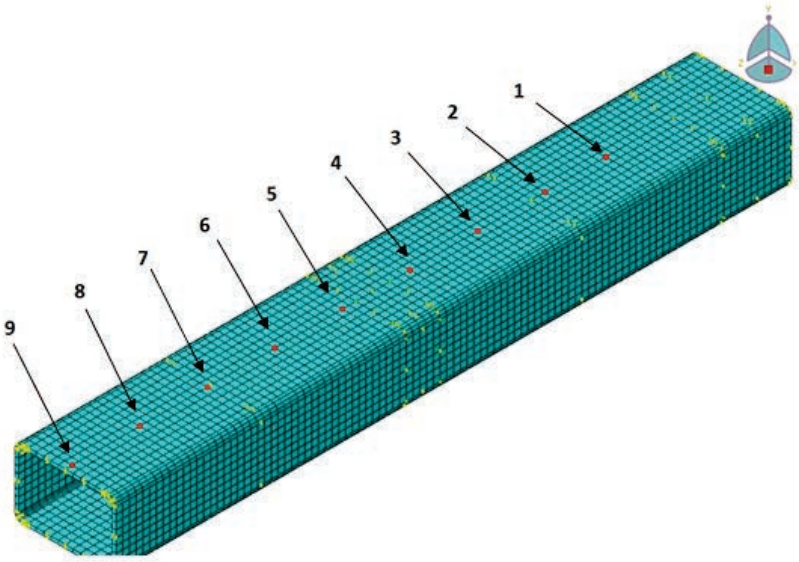

Figure 6-2 Nominated reading points on the centreline of the outer section

Table 6-4 Von Mises stress results and analysis running time with variation of elements

Element	Reading point				Von Mises Total	Von Mises Self weight	Von Mises Payload	Running time
	ID	x	y	z	MPa	MPa	MPa	Hr:min:sec
C3D8I	1	200	50.85	0	14.77	3.46	11.31	00:06:14
	2	300	50.85	0	14.03	3.15	10.88	
	3	400	50.85	0	12.56	2.69	9.87	
	4	500	50.85	0	10.77	2.19	8.57	
	5	600	50.85	0	10.88	1.79	9.09	
	6	700	50.85	0	6.85	1.32	5.53	
	7	800	50.85	0	4.83	0.88	3.96	
	8	900	50.85	0	2.54	0.46	2.08	
	9	1000	50.85	0	0.54	0.16	0.38	
C3D8	1	200	50.85	0	14.69	3.45	11.24	00:05:20
	2	300	50.85	0	14.01	3.14	10.86	
	3	400	50.85	0	12.58	2.68	9.90	
	4	500	50.85	0	11.17	2.20	8.97	
	5	600	50.85	0	11.10	1.80	9.30	
	6	700	50.85	0	6.93	1.34	5.59	
	7	800	50.85	0	4.93	0.89	4.04	
	8	900	50.85	0	2.48	0.45	2.03	
	9	1000	50.85	0	0.80	0.16	0.63	
C3D20	1	200	50.85	0	14.71	3.45	11.26	00:31:07
	2	300	50.85	0	13.98	3.15	10.84	
	3	400	50.85	0	12.51	2.68	9.83	
	4	500	50.85	0	10.68	2.18	8.49	
	5	600	50.85	0	10.83	1.79	9.04	
	6	700	50.85	0	6.81	1.32	5.49	
	7	800	50.85	0	4.80	0.87	3.93	
	8	900	50.85	0	2.51	0.45	2.06	
	9	1000	50.85	0	0.50	0.16	0.34	
S4	1	200	50.85	0	14.41	3.47	10.94	00:06:44
	2	300	50.85	0	13.62	3.16	10.47	
	3	400	50.85	0	12.09	2.67	9.41	
	4	500	50.85	0	10.42	2.19	8.23	
	5	600	50.85	0	10.76	1.80	8.96	
	6	700	50.85	0	6.50	1.31	5.19	
	7	800	50.85	0	4.65	0.87	3.77	
	8	900	50.85	0	2.46	0.46	2.00	
	9	1000	50.85	0	0.52	0.16	0.36	
S4R	1	200	50.85	0	14.44	3.48	10.96	00:05:14
	2	300	50.85	0	13.64	3.16	10.48	
	3	400	50.85	0	12.11	2.68	9.43	
	4	500	50.85	0	10.41	2.19	8.22	
	5	600	50.85	0	10.77	1.80	8.97	
	6	700	50.85	0	6.52	1.31	5.21	
	7	800	50.85	0	4.66	0.88	3.78	
	8	900	50.85	0	2.47	0.46	2.01	
	9	1000	50.85	0	0.53	0.16	0.37	
	ID	x	y	z	Bending moment	Ixx	Von Mises Payload	
Hand calculations	1	200	50.85	0	928516.5	4140589	11.40	
	2	300	50.85	0	879466.5	4140589	10.80	
	3	400	50.85	0	830416.5	4140589	10.20	
	4	500	50.85	0	781366.5	4140589	9.60	
	5	600	50.85	0	732316.5	4140589	8.99	
	6	700	50.85	0	683266.5	4140589	8.39	
	7	800	50.85	0	634216.5	4140589	7.79	
	8	900	50.85	0	585166.5	4140589	7.19	
	9	1000	50.85	0	536116.5	4140589	6.58	

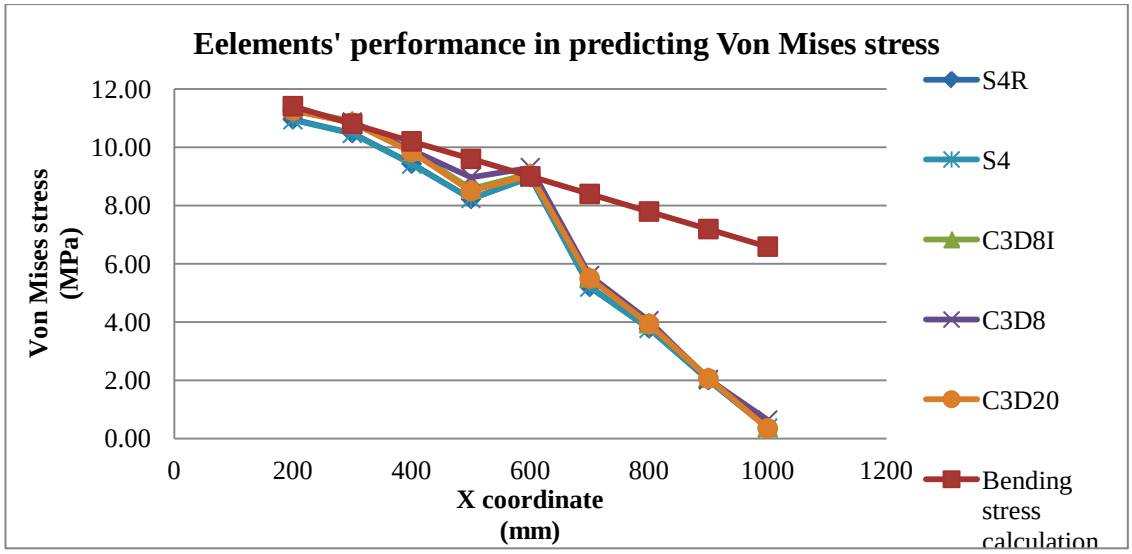

Figure 6-3 Von Mises stress along the centreline for element variation

The largest stress component on the centreline axis appears in the bending direction that is calculated by the bending stress relationship. The stress pattern in overlap area diverges from linear bending due to influence of the wear pads contact. This behaviour is not influenced by the choice of element as both classes show close approximations.

The analysis problem size is compared with the application of the different elements in Table 6-5 and detailed in Appendix XIII. The elements performance in terms of problem size against running time is plotted in Figure 6-4. The number of elements are all kept consistent to make a correct comparison between the problem size. It is observed that C3D8I element perform an efficient analysis with respect to the available degrees of freedom. Figure 6-4 shows the graphical comparison for the time efficiency of the elements. Due to the time efficient performance, two choices of S4R and C3D8I are shortlisted for more detailed comparison between stress components. The stress tensor notations are selected with respect to the global coordination system as detailed in Figure 6-5.

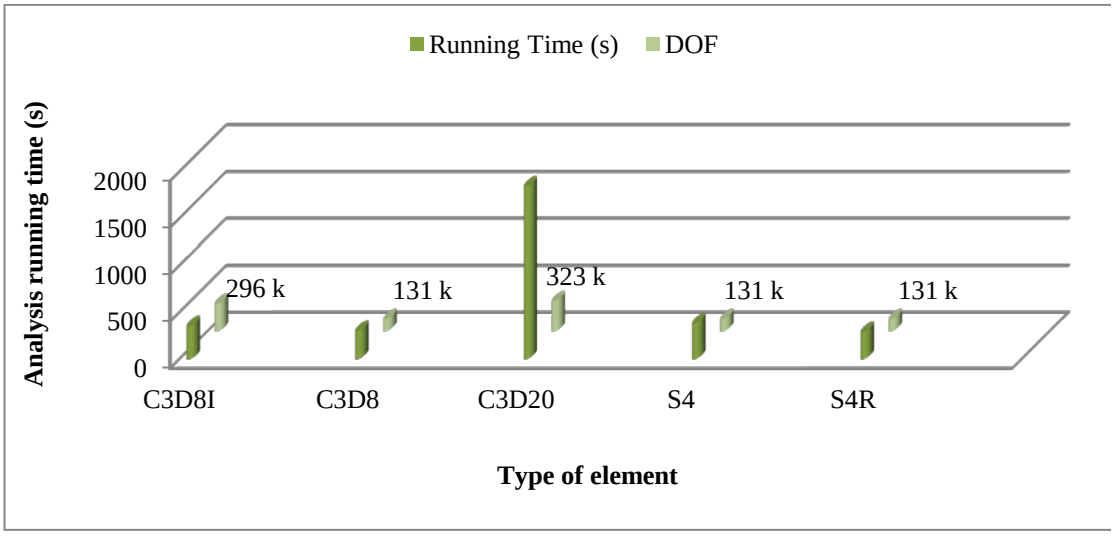

Figure 6-4 Element performance vs. Analysis running time

Table 6-5 FEA problem size using different elements

Class of Element	Type of Element	Degrees of Freedom	Number of Elements	Wallclock time (s)
Solid Element	C3D8	130524	18945	306
	C3D8I	296300	18945	358
	C3D20	322740	18945	1846
Structural Element	S4	130524	18945	386
	S4R	130524	18945	295

Reduction in dimensionality caused by choice of shell element eliminates the stress components in the thickness direction, S22, S12 and S23 (Dassault Systèmes, 2010). Table 6-6 shows this compromise does not result in significant loss on the existing stress components. The complete stress tensor produced by solid element shows a very small stress magnitude in the reduced components. Both types of elements also agree on the non-existence of the in plane shear component on the axis of symmetry, S13. Only slight variation in the stress magnitude is observed in the other two perpendicular directions.

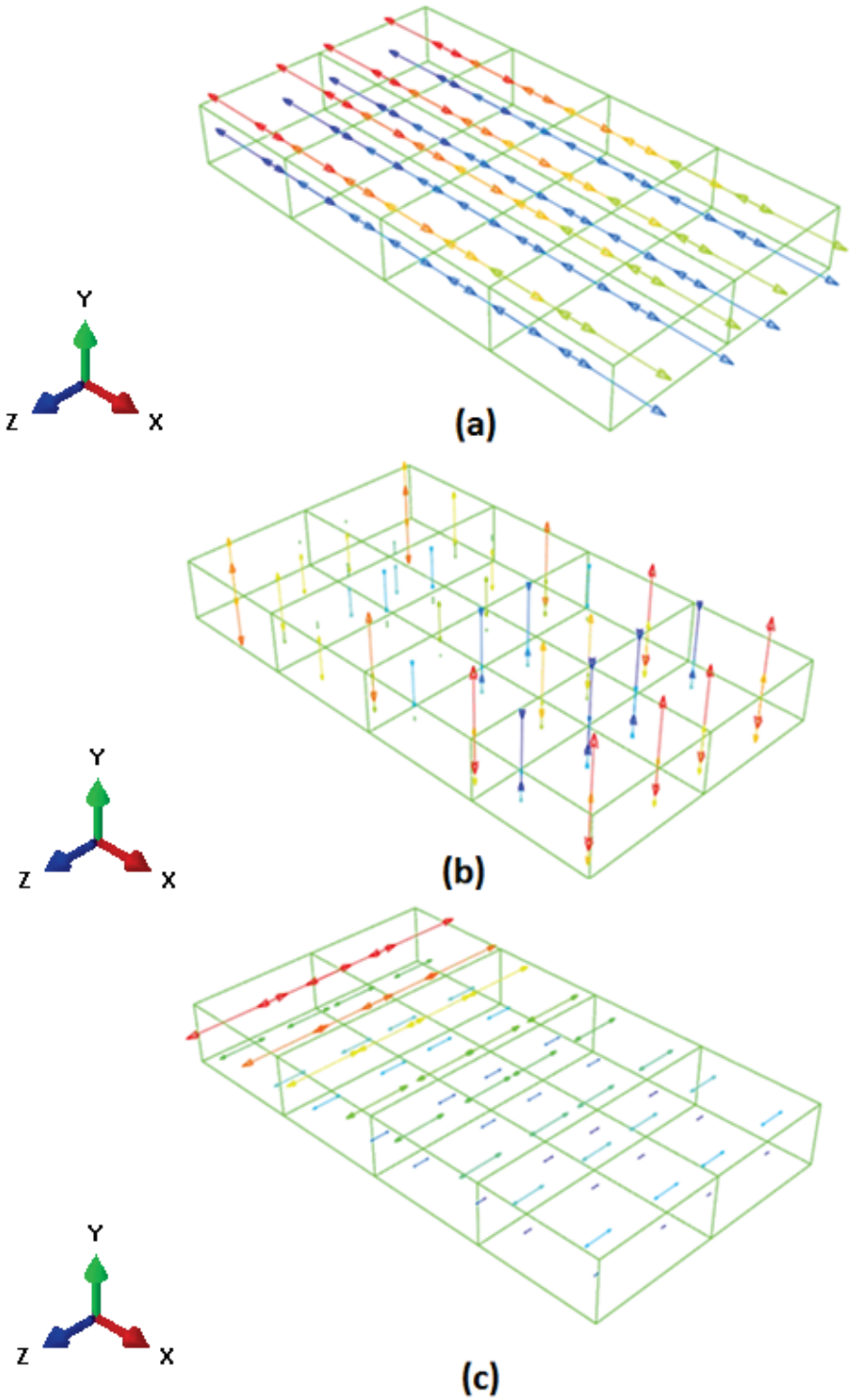

Figure 6-5 Stress components directions with respect to the global coordinates system (a) S11 in x direction along the length of the beam, (b) S22 in y direction in the thickness direction (c) S33 in z direction across the width of the cross section (Dassault Systèmes, 2009, a)

Table 6-6 Stress tensor comparison between shell and solid elements

Element	Reading point				Stress tensor					
	ID	X	Y	Z	S_{11}	S_{22}	S_{33}	S_{12}	S_{13}	S_{23}
C3D8I	1	200	50.85	0	15.26	-0.01	1.05	-0.02	0.00	0.00
	2	300	50.85	0	13.95	0.00	-0.16	0.00	0.00	0.00
	3	400	50.85	0	12.61	0.00	0.10	0.00	0.00	0.00
	4	500	50.85	0	12.18	-0.03	4.06	0.07	0.00	0.00
	5	600	50.85	0	12.51	-0.02	5.51	-0.11	0.00	0.00
	6	700	50.85	0	7.05	0.01	0.43	-0.01	0.00	0.00
	7	800	50.85	0	4.85	0.00	0.06	0.00	0.00	0.00
	8	900	50.85	0	2.66	0.00	0.28	0.00	0.00	0.00
	9	1000	50.85	0	0.28	0.00	-0.32	0.00	0.00	0.00
S4R	1	200	50.85	0	14.73		0.62		0.00	
	2	300	50.85	0	13.56		-0.17		0.00	
	3	400	50.85	0	12.18		0.13		0.00	
	4	500	50.85	0	11.87		4.38		0.00	
	5	600	50.85	0	12.44		5.88		0.00	
	6	700	50.85	0	6.75		0.50		0.00	
	7	800	50.85	0	4.68		0.06		0.00	
	8	900	50.85	0	2.58		0.27		0.00	
	9	1000	50.85	0	0.26		-0.33		0.00	

6.2.3 Element validation

The elements' performances are related to the physical performance of the test rig. The first instant of reality from Table 5-4 is constructed in this study. In order to avoid discrepancies at the fixed end, the validation study contains the complete test rig assembly, as appears in Figure 6-6,

Four nominated reading points, shown in Figure 6-6, are selected as:

- a neutral point without including the effect of contact, Point 1
- the contact vicinity, Point 2
- the direct contact zone on the symmetrical point of the structure , Point 3 and 4

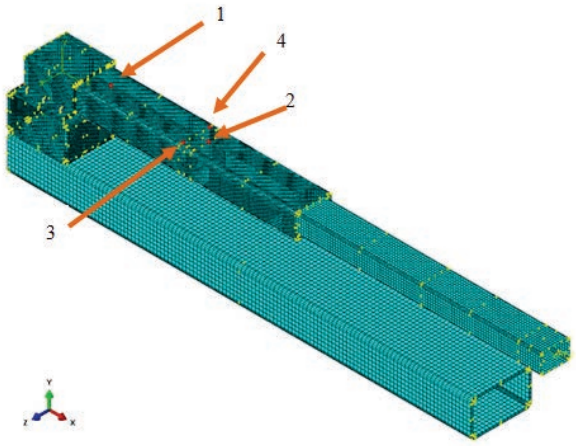

Figure 6-6 Assembly simulation and validation measurement points

Four Rosette strain gauges are mounted in the selected locations as shown in Figure 6-7 and Figure 6-8. The strain gauge instrumentations layout are schematically shown in Figure 6-9, and specifications are detailed in Appendices IX, X and XI (NI, 2008, a,b,c).

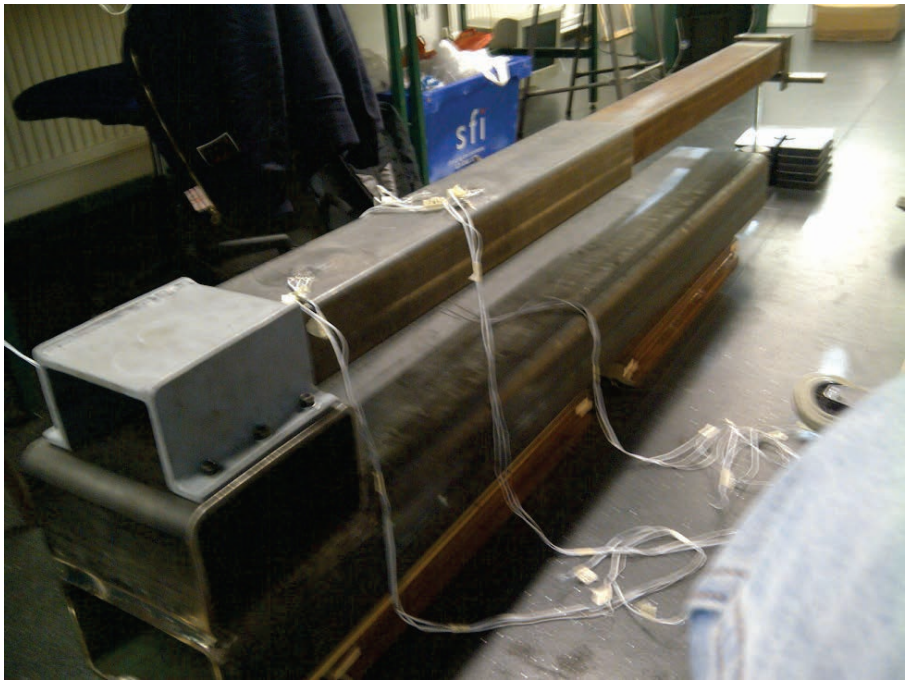

Figure 6-7 Test rig assembly

Figure 6-8 Strain gauges arrangement

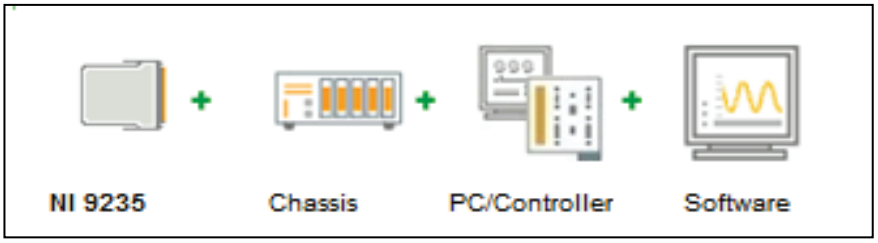

Figure 6-9 Strain measurement instruments lay out (NI, 2012)

During the experimental measurement the impact of gravity is eliminated by calibrating strain gauges under the self-weight. The analysis results also adapted to reflect the same, by deducting the values under the self-weight from the total values.

The direct relationship between simulation and experimental measurement can only be established between strain tensors (NI, 2008, a). Table 6-7 reports the collected values under the maximum payload of 50 Kg.

The strain comparison near to the fixed end, Point 1, shows a close comparison between tensor components. The strain components show a large tensile component in the length direction and a relatively smaller compression in the width direction which completely agrees with the simulation findings.

However the comparison in the direct contact region, points 3 and 4, shows a variation in strain components. The strain components suggest that while one side of the assembly is taking the larger proportion of the reaction load, and showing tensile strain in two perpendicular directions, the response from the opposite side is negligible. The smaller tensile strain component in the length direction and a compressive component in the width direction confirm that one side barely reacts to the applied load.

The effect of this behaviour is also observed in reading point 2 where the feedback of contact is expected. Strain components in point 2 are influenced by an asymmetric feature in the test rig and show a shear strain component where according to verification test it is not expected to be presented in the centreline.

The strain tensor is converted to the stress tensor using the strain-stress relationships outlined in Chapter 2. Comparison between out of contact readings, point 1 and 2 with simulation show a very small variation caused by asymmetric feature of the test rig assembly. This can be observed by the existence of the minimal shear in the axis of symmetry. However in the contact regions the observation of strain behaviour is repeated in the stress tensor components.

Table 6-7 Element validation and quantitative comparison

	Reading points				Strain tensor						Stress tensor						Von Mises	Von Mises	Von Mises
	Point ID	x	y	z	E11	E22	E33	E12	E13	E23	S11	S22	S33	S12	S13	S23	Self-weight	Pay-load	Total
					μs						MPa						MPa	MPa	MPa
C3D8I	1	200	50.85	0	54	-20	-14	0	0	0	11.70	-0.01	0.82	-0.01	0.00	0.00	3.46	11.31	14.77
	2	600	50.85	0	42	-25	8	-1	0	0	10.54	-0.02	5.06	-0.10	0.00	0.00	1.79	9.09	10.88
	3	550	50.85	-54.75	58	-28	-4	0	0	0	13.05	-0.41	3.23	-0.01	-2.14	1.34	2.74	13.77	16.51
	4	550	50.85	54.75	58	-28	-4	0	0	0	13.05	-0.41	3.23	-0.01	2.14	-1.34	2.74	13.77	16.51
S4R	1	200	50.85	0	53		-15		0		11.19		0.49		0.00		3.48	10.96	14.44
	2	600	50.85	0	41		9		0		10.44		6.39		0.00		1.80	8.97	10.77
	3	550	50.85	-54.75	57		-1		21		13.34		5.46		1.63		2.75	13.23	15.98
	4	550	50.85	54.75	57		-1		-21		13.34		5.46		-1.63		2.75	13.23	15.98
Strain Gauge	1	200	50.85	0	57		-21		1		11.55		-0.51		0.08			12.09	
	2	600	50.85	0	47		8		-19		11.46		5.43		-1.50			10.51	
	3	550	50.85	-54.75	86		66		34		24.87		21.78		2.68			24.41	
	4	550	50.85	54.75	47		-21		12		9.25		-1.27		0.95			10.75	

The stress due to contact, manifested by two perpendicular tensile stresses, is not observed in the light side of the test rig. Also different shear behaviour on two sides confirms a different behaviour of two contact regions in the prototype.

The Von Mises resultant on the neutral regions of point 1 and 2 show an insignificant impact of the above phenomena and produce a comparable results with simulation. The Von Mises stress at the contact region is heavily influenced by the asymmetry of the structure and the significant difference can be observed in stress resultants.

6.2.4 Load magnitude variation

The outlines of this study, extracted from Table 5-3, are detailed in Table 6-8. The integrated analysis plan suggests that the required MPCs for this parameter variation can be obtained from the results of the previous analysis. Table 5-4 also indicates the commonality between the instant of realities for verification and validation.

Table 6-8 Stress study condition, dependency to the load magnitude

Stakeholders' requirement	MPCs	Fixed Parameter	Variable Parameter
Stress behaviour near contact area	Von Mises stress Stress tensor Strain tensor	Overlap = 500 mm Load type: symmetric Element type, S4R	Pay load: n_1=10kg n_2=20kg n_3=30kg n_4=40kg n_5=50kg

Table 6-9 and Figure 6-10 (a), (b) and (c) report the Von Mises stress propagation due to the applied load in equal increments as suggested in study condition, Table 6-8. This study also discounts the effect of the gravity in order to establish the consistency between simulation and experiment. In order to achieve repeatability in the experimental measurement the cycle of loading and unloading is obtained.

This comparison also shows a very similar pattern for the Von Mises stress propagation pattern, to the one has been discussed in section 6.2. A close agreement in the non-contact area along with violated results in the contact region demonstrates an inherited asymmetric feature in the test rig. The linear gradient shows the recorded results are within the elastic limit of the material.

Table 6-9 Von Mises stress results for incremental loading

Payload	Reading points				S4R	Strain Guage
	Point ID	x	y	z	Von Mises	Von Mises
(KG)		(mm)	(mm)	(mm)	(MPa)	(MPa)
10					2.76	2.38
20					5.53	4.77
30					8.31	7.12
40					11.09	9.49
50	1	200	50.85	0	13.87	11.93
40					11.09	9.47
30					8.31	7.11
20					5.53	4.74
10					2.76	2.35
10					3.94	2.35
20					6.00	4.6
30					8.06	6.79
40					10.12	8.46
50	2	600	50.85	0	12.17	10.33
40					10.12	8.68
30					8.06	7.08
20					6.00	5.29
10					3.94	2.95
10					3.08	4.48
20					6.16	10.9
30					9.23	16.9
40					12.29	20.61
50	3	550	50.85	-54.75	15.34	24.13
40					12.29	21.42
30					9.23	18.69
20					6.16	15
10					3.08	8.58
10					3.08	2.09
20					6.16	4.26
30					9.23	6.46
40					12.29	8.22
50	4	550	50.85	54.75	15.34	10.56
40					12.29	8.13
30					9.23	6.40
20					6.16	5.00
10					3.08	2.92

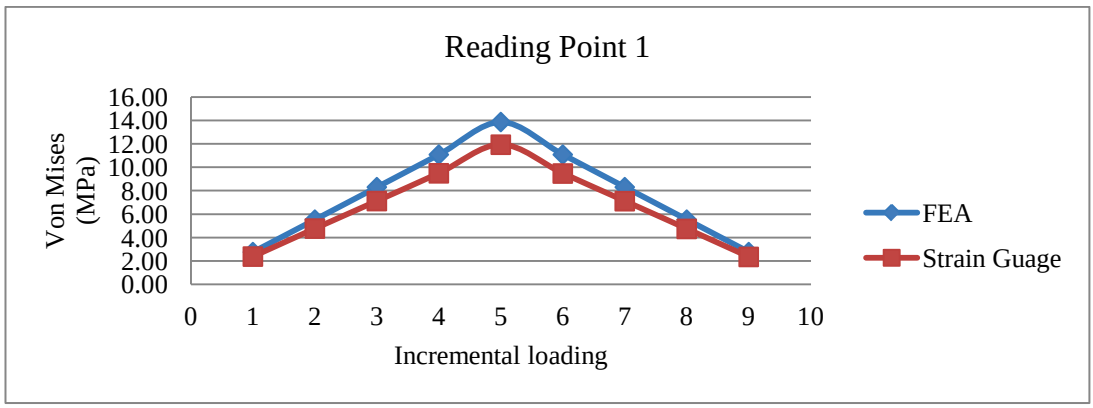

(a)

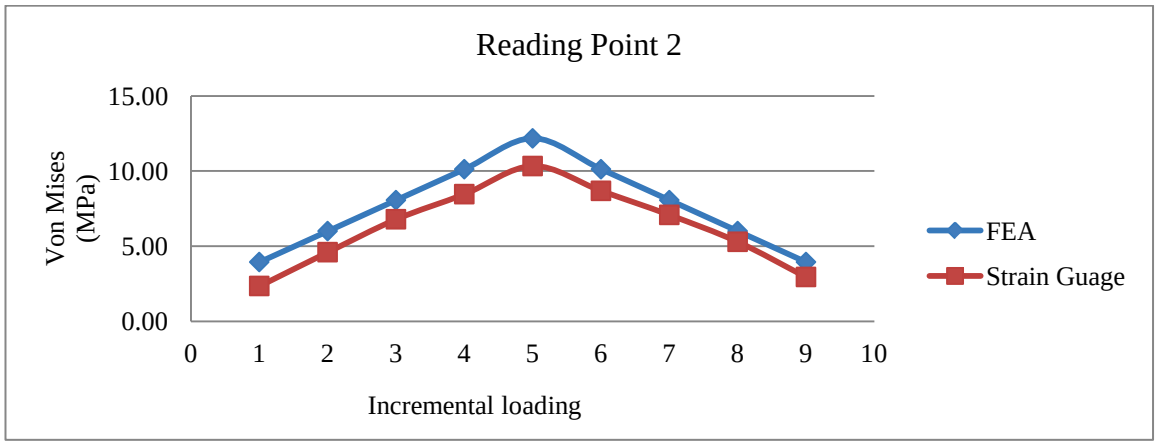

(b)

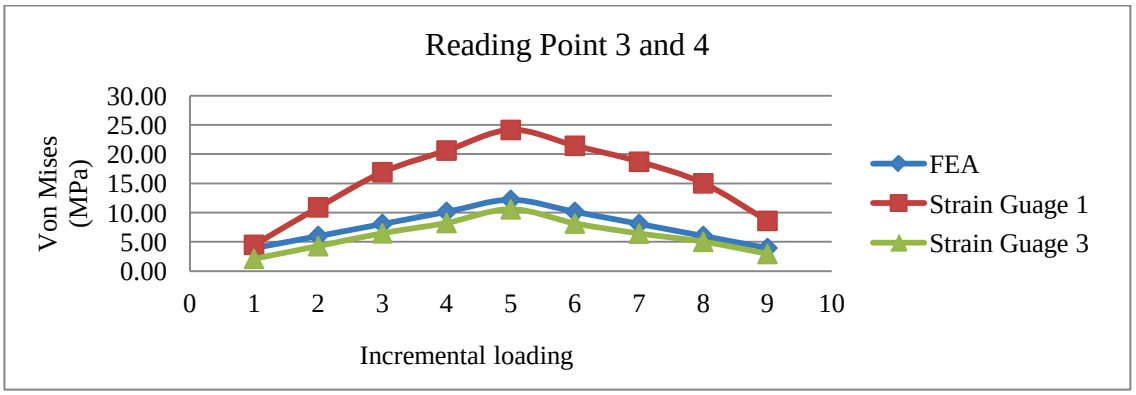

(c)

Figure 6-10 Von Mises stress propagation due to incremental loading

In order to quantify the stress distribution at the contact vicinity further investigation of Von Mises stress is conducted on five equidistance locations as shown in Figure 6-11. 12 selected nodes cover 50mm of the length of the outer section from the centreline to

the side wall. Figure 6-12 (a) to (e) shows the progress of Von Mises stress along these lines under the 5 load increments up to the maximum payload of 50kg.

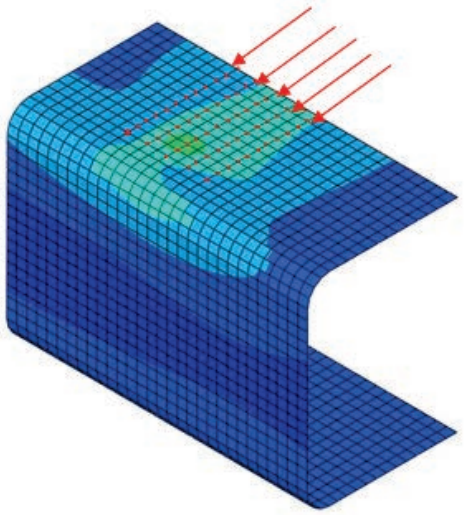

Figure 6-11 Axis of reading on contact area in one side of the structure

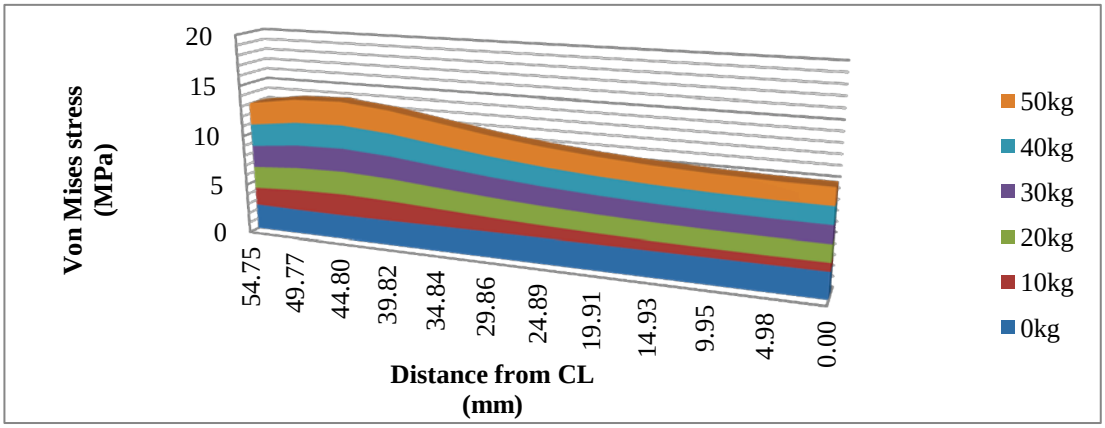

(a) Axis 1

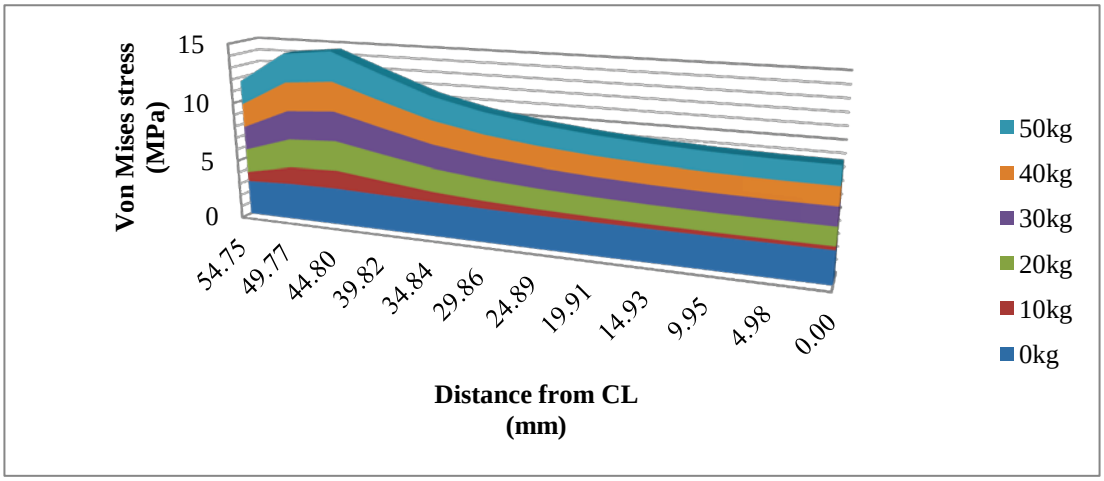

(b) Axis 2

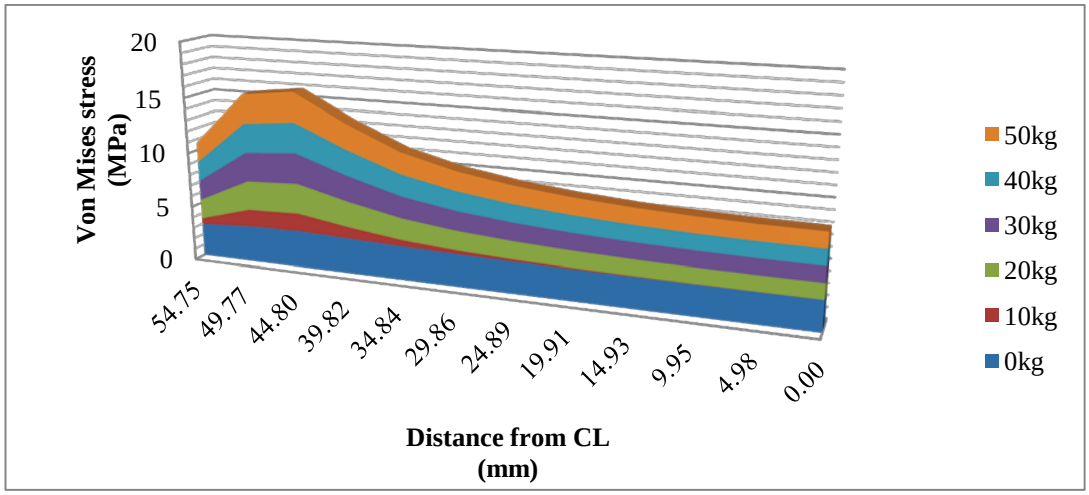

(c) Axis 3

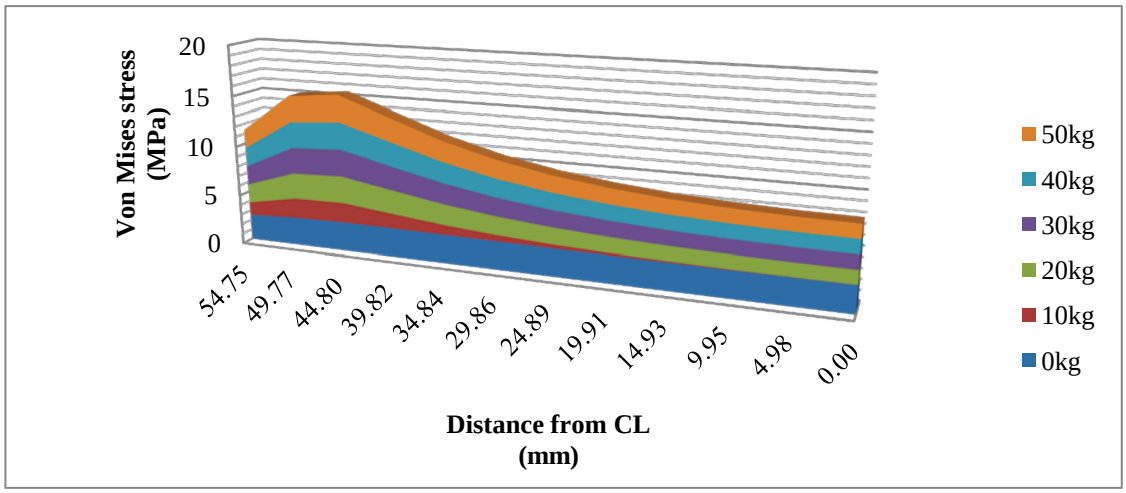

(d) Axis 4

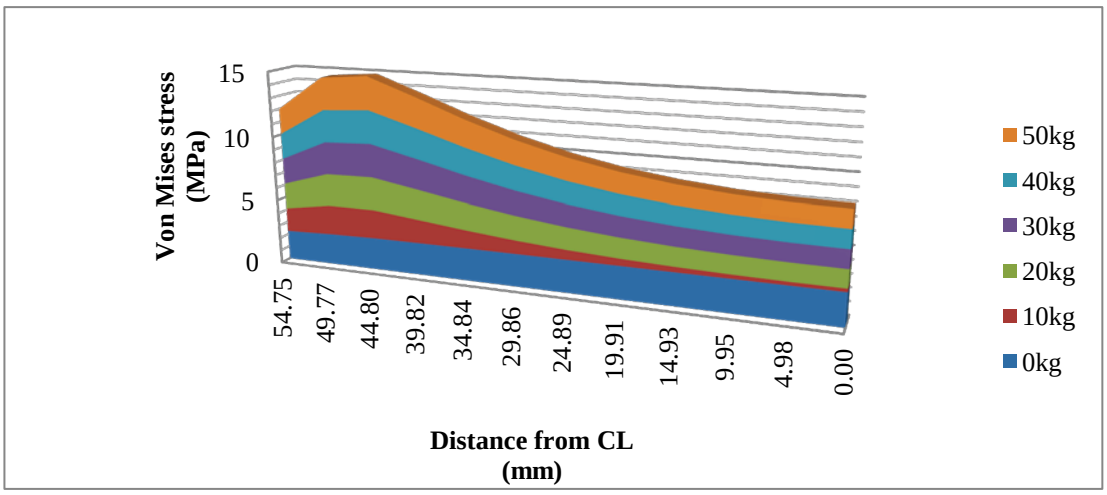

(e) Axis 5

Figure 6-12 Stress increase due to load magnitude variation on the contact region

Table 6-10 Strain and stress tensor propagation in incremental loading

Incremental Load	Reading points				S4R						Strain Gauge					
					Strain tensor			Stress tensor			Strain tensor			Stress tensor		
	Point ID	x	y	z	E11	E33	E13	S11	S33	S13	E11	E33	E13	S11	S33	S13
(kg)					(μs)			(MPa)			(μs)			(MPa)		
10	1	200	50.85	0	12	-8	0	2.13	-0.99	0.00	11	-4	-7	2.29	-0.07	-0.58
20					12	-16	0	4.26	-1.99	0.00	23	-8	4	4.66	-0.02	0.34
30					35	-24	0	6.40	-3.00	0.00	34	-12	5	6.89	-0.14	0.37
40					47	-32	0	8.53	-4.01	0.00	45	-16	5	9.12	-0.32	0.40
50					59	-41	0	10.66	-5.02	0.00	57	-20	-2	11.53	-0.28	-0.17
40					47	-32	0	8.53	-4.01	0.00	45	-16	-2	9.13	-0.24	-0.18
30					35	-24	0	6.40	-3.00	0.00	34	-12	1	6.83	-0.25	0.12
20					12	-16	0	4.26	-1.99	0.00	22	-8	2	4.53	-0.17	0.13
10					12	-8	0	2.13	-0.99	0.00	11	-4	2	2.18	-0.14	0.14
10	2	600	50.85	0	9	3	0	2.38	1.38	0.00	10	1	-6	2.49	1.11	-0.47
20					18	6	0	4.77	2.75	0.00	20	3	-12	4.86	2.25	-0.94
30					28	8	0	7.15	4.12	0.00	30	5	-16	7.24	3.46	-1.29
40					37	11	0	9.52	5.47	0.00	37	7	-17	9.18	4.49	-1.36
50					46	14	0	11.88	6.82	0.00	46	8	-18	11.32	5.39	-1.45
40					37	11	0	9.52	5.47	0.00	38	8	-18	9.41	4.70	-1.42
30					28	8	0	7.15	4.12	0.00	31	7	-16	7.59	3.95	-1.29
20					18	6	0	4.77	2.75	0.00	22	6	-14	5.55	2.97	-1.14
10					9	3	0	2.38	1.38	0.00	12	3	-9	3.05	1.55	-0.69

Table 6-9 continued

Incremental Load	Reading points				S4R						Strain Gauge					
					Strain tensor			Stress tensor			Strain tensor			Stress tensor		
	Point ID	x	y	z	E11	E33	E13	S11	S33	S13	E11	E33	E13	S11	S33	S13
(kg)					(μs)			(Mpa)			(μs)			(Mpa)		
10					27	5	-8	3.42	1.91	-0.37	16	12	5	4.62	3.98	0.36
20					40	8	-13	6.81	3.79	-0.73	36	32	14	10.85	10.15	1.08
30					53	12	-17	10.20	5.66	-1.09	56	50	24	16.66	15.75	1.92
40					67	16	-22	13.57	7.53	-1.45	71	58	29	20.73	18.72	2.29
50	3	550	50.85	-54.75	80	19	-26	16.94	9.38	-1.81	85	65	34	24.59	21.48	2.65
40					67	16	-22	13.57	7.53	-1.45	72	61	31	21.32	19.67	2.48
30					53	12	-17	10.20	5.66	-1.09	60	57	29	18.10	17.68	2.25
20					40	8	-13	6.81	3.79	-0.73	45	49	22	14.09	14.66	1.74
10					27	5	-8	3.42	1.91	-0.37	24	29	15	7.81	8.46	1.18
10					13	4	5	3.42	1.91	0.37	7	-8	0	0.89	-1.44	0.02
20					26	7	9	6.81	3.79	0.73	13	-18	2	1.62	-3.08	0.15
30					40	11	14	10.20	5.66	1.09	19	-27	4	2.43	-4.66	0.30
40					53	15	18	13.57	7.53	1.45	31	-27	7	5.17	-3.79	0.57
50	4	550	50.85	54.75	66	18	23	16.94	9.38	1.81	46	-22	12	9.06	-1.45	0.92
40					53	15	18	13.57	7.53	1.45	33	-23	8	5.87	-2.81	0.63
30					40	11	14	10.20	5.66	1.09	21	-25	4	3.04	-4.04	0.35
20					26	7	9	6.81	3.79	0.73	10	-23	0	0.57	-4.59	0.03
10					13	4	5	3.42	1.91	0.37	4	-14	-1	-0.15	-2.90	-0.11

The direct comparison of strains and stress components are detailed in Table 6-10. Ther state of the strain in the prependicular direction to the overall bending, E33, determine the state of contact at the region (Aalami and Williams, 1975). Comparison of the E33 at the reading point 3 and 4 are plotted against FEA prediction in Figure 6-13.This shows the light side of the test rig start reacting to the load nearly at the last load increment. The negative progress of the strain value in the width direction is similar to the behaviour of non-contact areas, e.g. point 1 Figure 6-14.

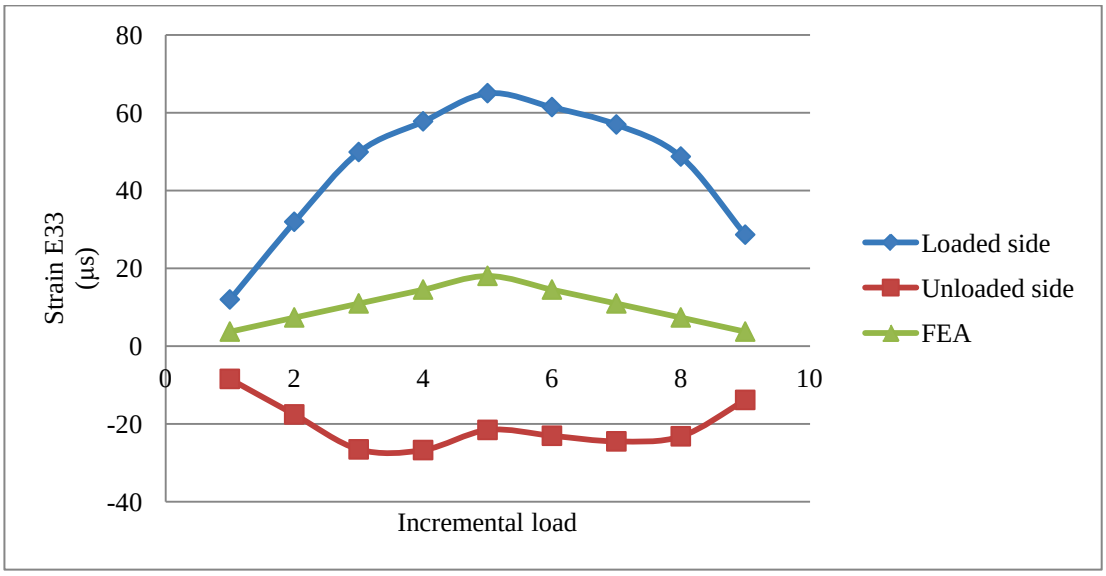

Figure 6-13 E33 comparison in contact area

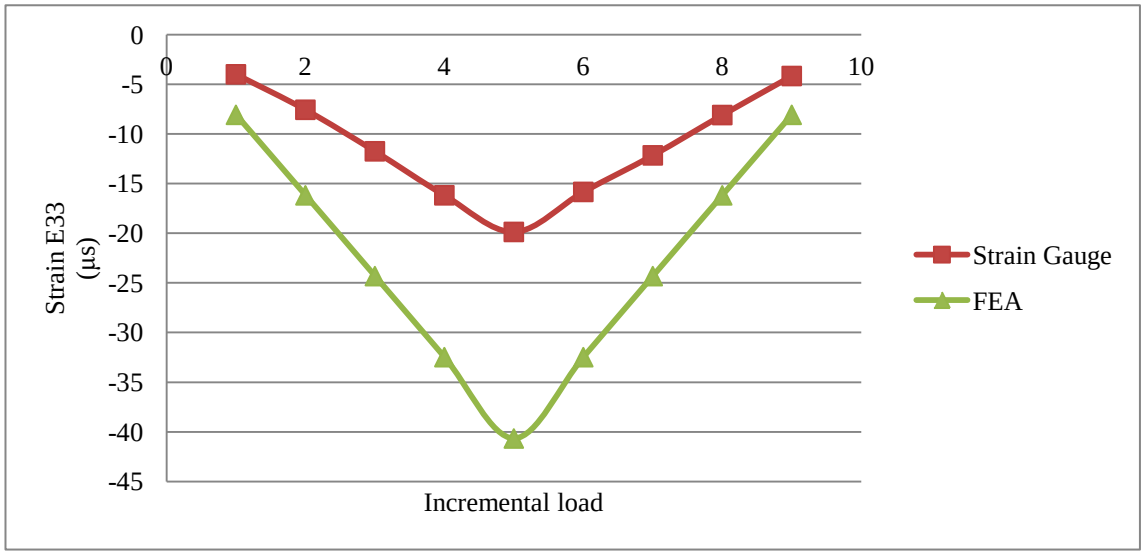

Figure 6-14 E33 comparison near to the fixed end

6.2.5 Load type variation and validation

The analysis condition, taken from Table 5-3 is elaborated in Table 6-11. This study aims to quantify the impact of variation of the load type on the stress behaviour due to contact. Plan for integrated analysis suggested that the required MPCs for the symmetric load case can be obtained from the previous analysis. Therefore an additional analysis to apply a moment component to the concentrated force, in the x direction, Figure 6-15, is conducted to complete this section. The second instant of reality as proposed by Table 5-4 is also constructed for validation.

Table 6-11 Stress study condition, dependency to the type of load

Stakeholders' requirement	MPCs	Fixed Parameter	Variable Parameter
Influence of the type of load on the Stress behaviour near contact area	Von Mises stress Stress tensor Strain tensor	Overlap = 500 mm Pay load= 50kg Element type: S4R	Type of load: 50 in CL 50kg at 300mm offset from CL

Figure 6-15 Asymmetric load application, 300mm offset from centreline

The Von Mises stress results for two types of applied loads are extracted from simulation and experiment and presented in Table 6-12. Despite the significant difference in two contact regions the effect of moment on non-contact regions, point 1 and 2 is negligible. The inherited asymmetry in the test rig is magnified under the asymmetric payload by generating larger stress.

Comparing the stress and strain components shows the difference mostly caused by two normal stress components rather than the shear component Table 6-13. FEA results shows the strain component of E22 in the perpendicular direction to the overall bending, significantly varies between load cases. The unloaded side of the structure shows slight compression whereas the heavy side is going through a significant tension, the pattern that is visible in experimental measurement. Despite the agreements in the pattern, experimental results show a different magnitude due to an inherited asymmetry in the overall assembly. Figure 6-16 demonstrates the Von Mises stress magnitudes for two loading case.

Table 6-12 Von Mises stress validation under the impact of asymmetric loading

Loading condition	**Reading points**				**Von Mises Stress (MPa)**	
	ID	x	y	z	FEA (S4R)	Experimental measurement Strain Gauge
Symmetric	1	200	50.85	0	10.96	12.09
	2	600	50.85	0	8.97	10.51
	3	550	50.85	-54.75	13.23	24.41
	4	550	50.85	54.75	13.23	10.75
Asymmetric	1	200	50.85	0	15.19	12.70
	2	600	50.85	0	11.02	9.64
	3	550	50.85	-54.75	23.85	34.67
	4	550	50.85	54.75	10.56	10.18

Table 6-13 Strain and stress tensor validation for asymmetric loading

Loading condition	Reading points				Simulation S4R						Experimental study					
					Strain tensor			Stress tensor			Strain tensor			Stress tensor		
	ID	x	y	z	E11	E33	E13	S11	S33	S13	E11	E22	E12	S11	S22	S12
					(μs)	(μs)	(μs)	MPa	MPa	MPa	(μs)	(μs)	(μs)	MPa	MPa	MPa
Symmetric	1	200	50.85	0	59	-41	0	10.66	-5.02	0.00	57	-21	1	11.55	-0.51	0.08
	2	600	50.85	0	46	14	0	11.88	6.82	0.00	47	8	-19	11.46	5.43	-1.50
	3	550	50.85	-54.75	66	18	23	16.94	9.38	1.81	86	66	34	24.87	21.78	2.68
	4	550	50.85	54.75	66	18	-23	16.94	9.38	-1.81	47	-21	12	9.25	-1.27	0.95
Asymmetric	1	200	50.85	0	59	-41	-20	10.66	-5.07	-1.61	57	-20	15	11.63	-0.27	1.14
	2	600	50.85	0	49	14	3	12.62	7.09	0.20	44	8	6	10.76	5.20	0.47
	3	550	50.85	-54.75	82	65	29	24.47	21.73	2.29	103	106	42	31.84	32.31	3.28
	4	550	50.85	54.75	41	-35	-25	7.01	-5.13	-1.96	37	-31	15	6.18	-4.34	1.18

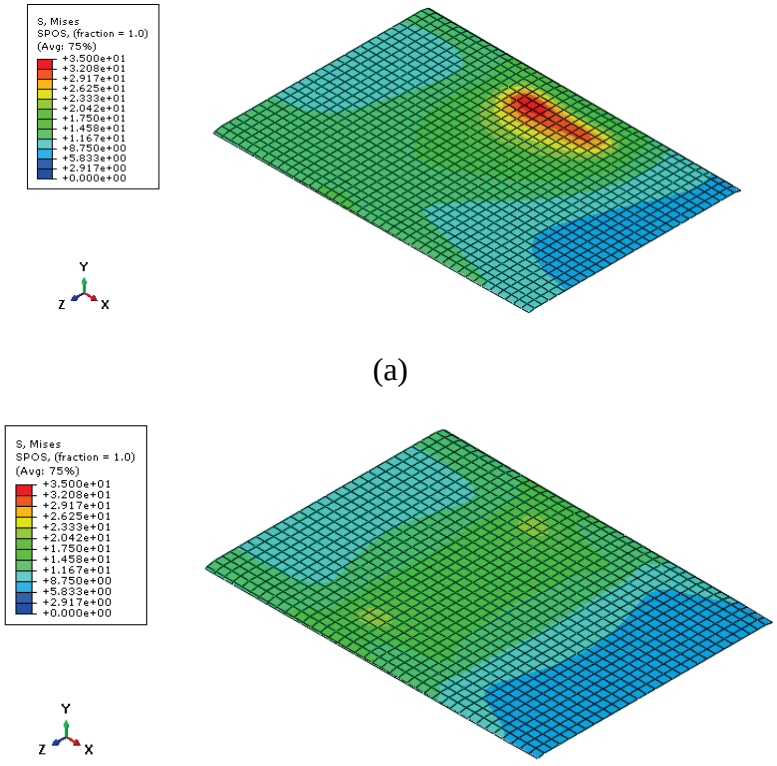

Figure 6-16 Qualitative comparison of Von Mises stress plot for load type variation, (a) Symmetric load (b) Asymmetric load

6.2.6 Effect of the overlap length

The analysis condition, taken from studies 4-8 of Table 5-3, is elaborated in Table 6-14. This study aims to clarify the impact of the overlap variation on the stress behaviour at the contact region. Since the task of stress-displacement verification and validation is achieved in the previous stages, the observations of this section are concluded based on the simulation results.

The general conditions of the analysis are as described in Table 6-1. The measurement points are selected in the same fashion as described in section 6.2.1, shown in Figure 6-11. Due to the symmetry only half of the model is chosen for this study. Since the contact location varies with overlap change, the reading points are offset equal to the overlap increment to locate in the identical position respective to the contact zone.

The Von Mises stress comparison for similar reading points are presented in Figure 6-17(a)-(e). A sudden increase in the stress values is observed by reducing the overlap length.

Table 6-14 Stress behaviour study, dependency to the overlap length

Stakeholders' requirement	MPCs	Fixed Parameter	Variable Parameter
Stress behaviour near contact area	Von Mises stress	Element type S4R Pay load= 50kg Load type: Symmetric	Overlap n_1=500 mm n_2=400 mm n_3=300 mm n_4=200 mm n_5=100 mm

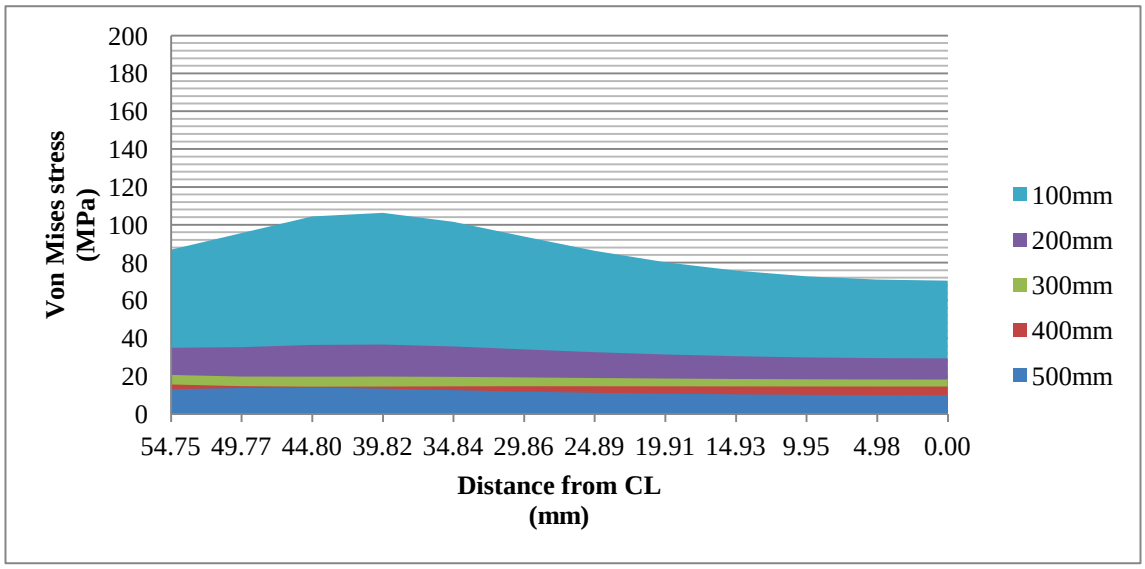

(a)

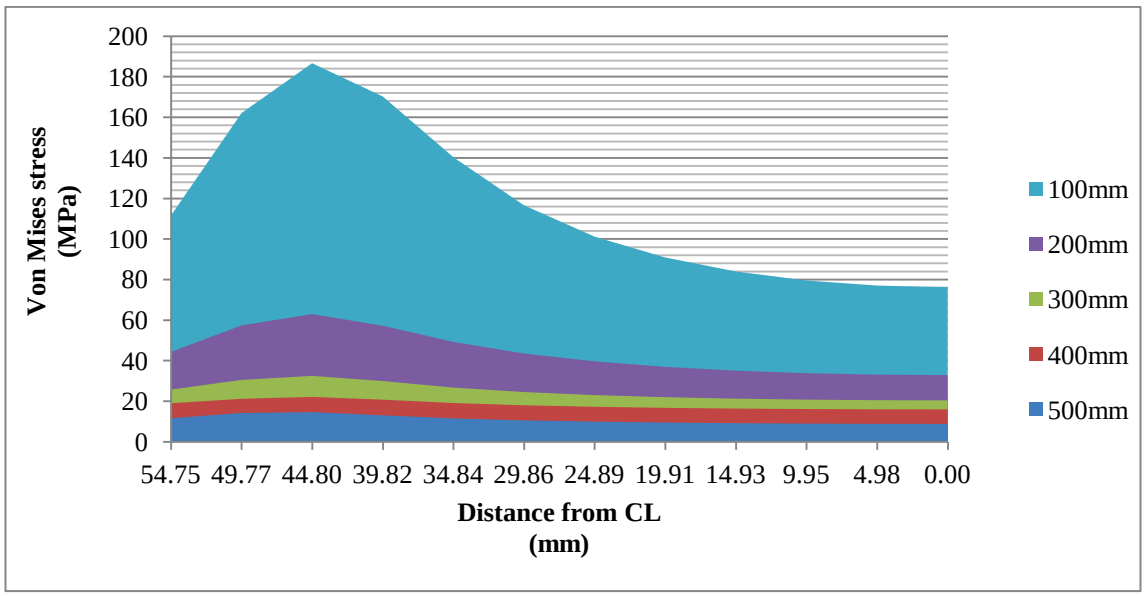

(b)

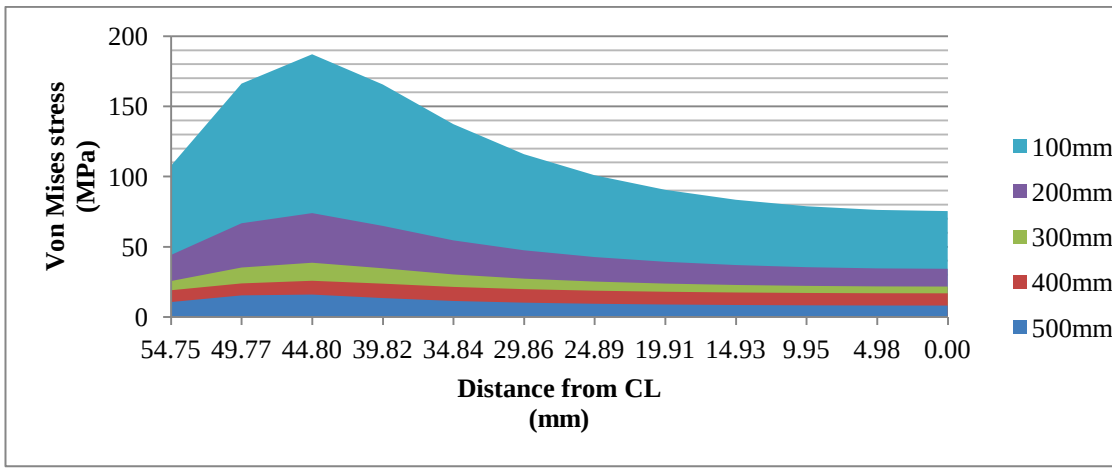

(c)

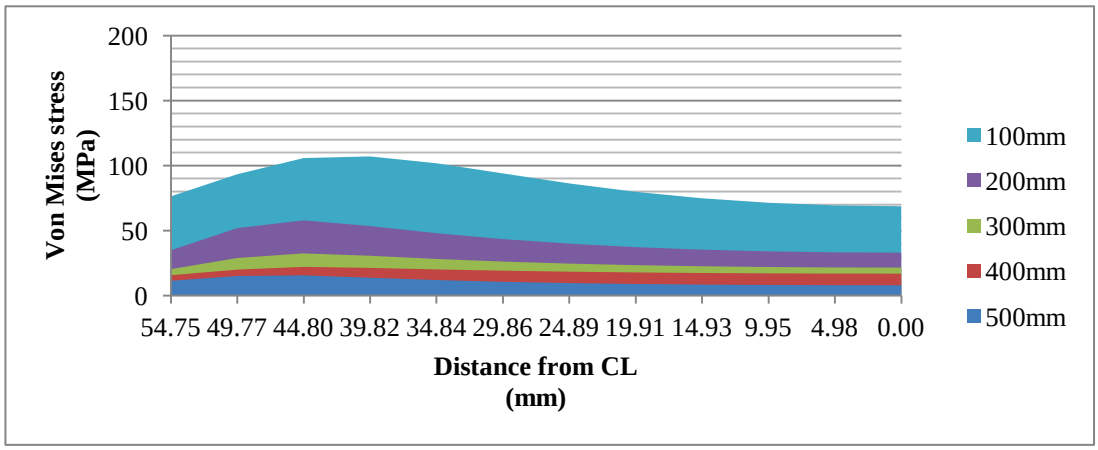

(d)

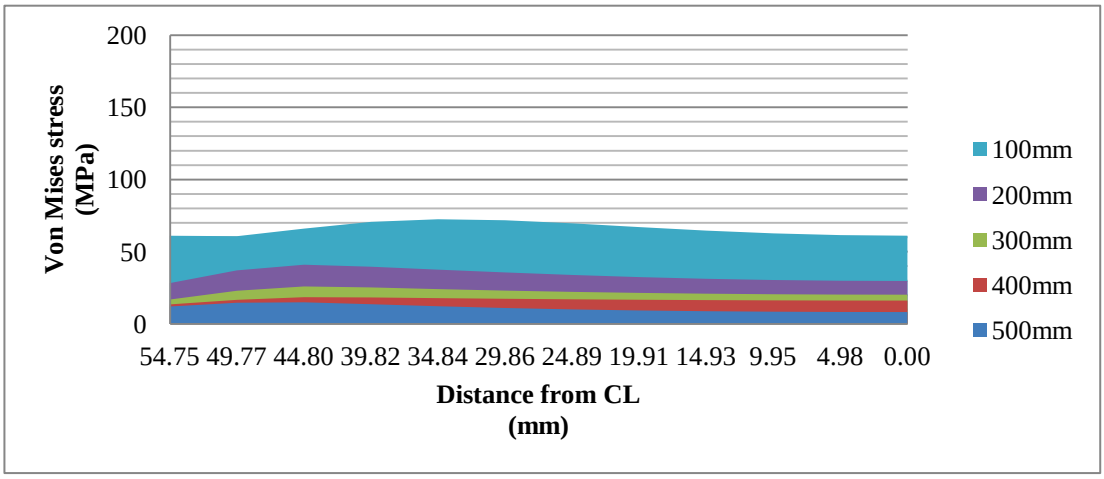

(e)

Figure 6-17 Von Mises stress plot with overlap variation across half of the width of the outer section (a) reading axis 1(b) reading axis 2 (c) reading axis 3 (d) reading axis 4 (e) reading axis 5

6.2.7 Conclusion on stress behaviour due to contact

The contact stress behaviour of the telescopic cantilever boom is characterised for the variation of specified parameters. The instants of realities determined in Chapter 5 assists to verify and validate the FEA outcomes.

On the subject of element variation, the response variation for the use of shell and solid elements is investigated. It is found that the loss of dimensionality due to the use of shell elements does not significantly distract the stress performance. However there is a slight advantage for the shell elements in terms of analysis running time which makes it preferable for the more detailed structure.

The instant of reality is used to verify and validate the FEA results. The verification process is conducted in the less complex areas where the theoretical calculation leads to an accurate answer.

In the validation stage, the performances of the elements are compared against the measurements from physical test rig. The quantitative comparison leads to identification of inaccuracy in the test rig assembly that affects the strain and stress components in the vicinity of contact. The lack of correlation in stress and strain responses is predominately caused by asymmetric feature in the test rig at the wear-pads interaction region. More detail investigation into the strain tensors correlation suggests the asymmetric feature presents in a form that cause a delay between two wear-pads to react to the applied load equally and uniformly. The findings of the study in conceptual level, indicates noticeable design sensitivity for the stress at the vicinity of contact, and the risk of repetition in the design of the full-scale product. Therefore this analysis prescribes a multi-parametric sensitivity analysis with the aim of contact optimisation.

The contact stress and strain propagation with load magnitude is investigated and compared against experimental measurement. The findings of the element selection stage are reconfirmed in this practice. Also the detail behaviour of asymmetry in the structure and unequal reaction of the wear pads to the applied load is identified by comparing the contributing strain components.

The effect of load type variation is analysed and compared against through identified MPCs. This study shows the contributing stress and strain components in the event of asymmetric loading that characterise the contact variation.

The impact of the overlap variation on the contact stress is quantified. The non-linear ascending of the Von Mises stress at the contact area specifies the importance of the optimised overlap length in the full-scale design.

6.3 Displacement behaviour

The displacement performance of the telescopic boom is discussed in this section. The corresponding MPCs are collected from the analyses 1,2 and 4-8 of Table 5-3, and validated through the first instant of reality of Table 5-4.

6.3.1 Effect of the element variation

The effect of elements variation on tip displacement and deflection along the length of the assembly in y direction, U2, is studies as outlines in Table 6-15. The required analysis and V&V case are in common with the contact stress behaviour study as discussed in Table 5-3 and Table 5-4.

Table 6-15 element variation study on displacement behaviour

Stakeholders' requirement	MPCs	Fixed Parameter	Variable Parameter
Displacement behaviour	Total tip displacement Deflection along the length	Overlap = 500 mm Load type: symmetric Payload= 50 kg	Element type: Shell, Solid

The vertical deflection of the structure along the length of the beam for the studied elements of Table 6-3, are collected at a equal distance Table 6-16 and plotted Figure 6-18.

The vertical tip displacement is also measured and plotted for the variable pay load in Table 6-17 and Figure 6-19. The close incline gradient in the tip displacement and radius of curvature in the length deflection confirms the minimal loss due to element variation and in particular shell assumptions.

Table 6-16 Telescope vertical deflection under the maximum payload on the centreline along the length

Reading points			Reading parameter				
			U2 (mm)				
x	y	z	C3D8	C3D8I	C3D20	S4	S4R
200	50.85	0	0.0042	0.0049	0.0049	0.0056	0.0056
300	50.85	0	0.0246	0.0250	0.0250	0.0240	0.0240
400	50.85	0	0.0560	0.0554	0.0553	0.0530	0.0531
500	50.85	0	0.0881	0.0874	0.0873	0.0823	0.0825
600	50.85	0	0.1387	0.1378	0.1375	0.1304	0.1306
700	50.85	0	0.2199	0.2190	0.2185	0.2108	0.2112
800	50.85	0	0.2937	0.2937	0.2930	0.2832	0.2837
900	50.85	0	0.3702	0.3699	0.3691	0.3569	0.3576
1000	50.85	0	0.4497	0.4497	0.4485	0.4340	0.4348
1100	40	0	0.5953	0.5986	0.5987	0.5838	0.5850
1200	40	0	0.7250	0.7292	0.7293	0.7115	0.7129
1300	40	0	0.8666	0.8714	0.8716	0.8504	0.8522
1400	40	0	1.0185	1.0241	1.0242	0.9992	1.0013
1500	40	0	1.1793	1.1856	1.1856	1.1565	1.1590
1600	40	0	1.3474	1.3544	1.3543	1.3207	1.3237
1700	40	0	1.5213	1.5290	1.5288	1.4906	1.4939
1800	40	0	1.6996	1.7081	1.7077	1.6646	1.6684
1900	40	0	1.8805	1.8902	1.8897	1.8415	1.8457
2000	40	0	2.1172	2.1329	2.1324	2.0747	2.0796

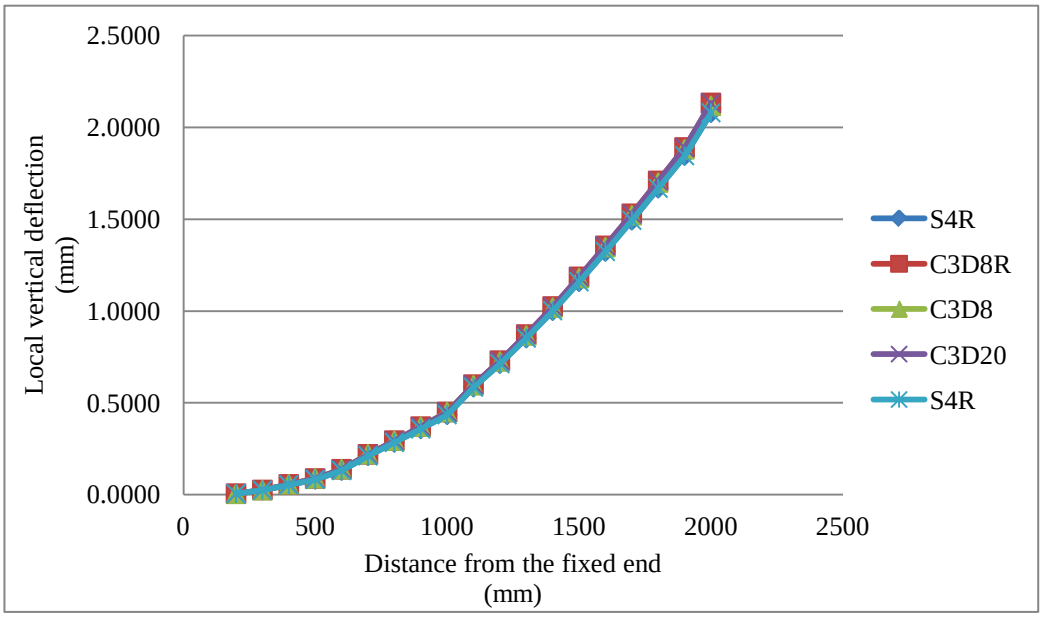

Figure 6-18 Telescope vertical deflection on the centreline along the length

Table 6-17 Telescopic cantilever tip displacement variation with incremental symmetric load

	C3D8	C3D8I	C3D20	S4	S4R	Verification
Load	Displacement					
(KG)	(mm)	(mm)	(mm)	(mm)	(mm)	(mm)
0	0.35	0.36	0.36	0.36	0.36	0.34
10	0.71	0.71	0.71	0.70	0.70	0.67
20	1.06	1.07	1.07	1.05	1.05	1.01
30	1.41	1.42	1.42	1.39	1.39	1.33
40	1.77	1.78	1.78	1.73	1.74	1.67
50	2.12	2.13	2.13	2.08	2.08	2.01

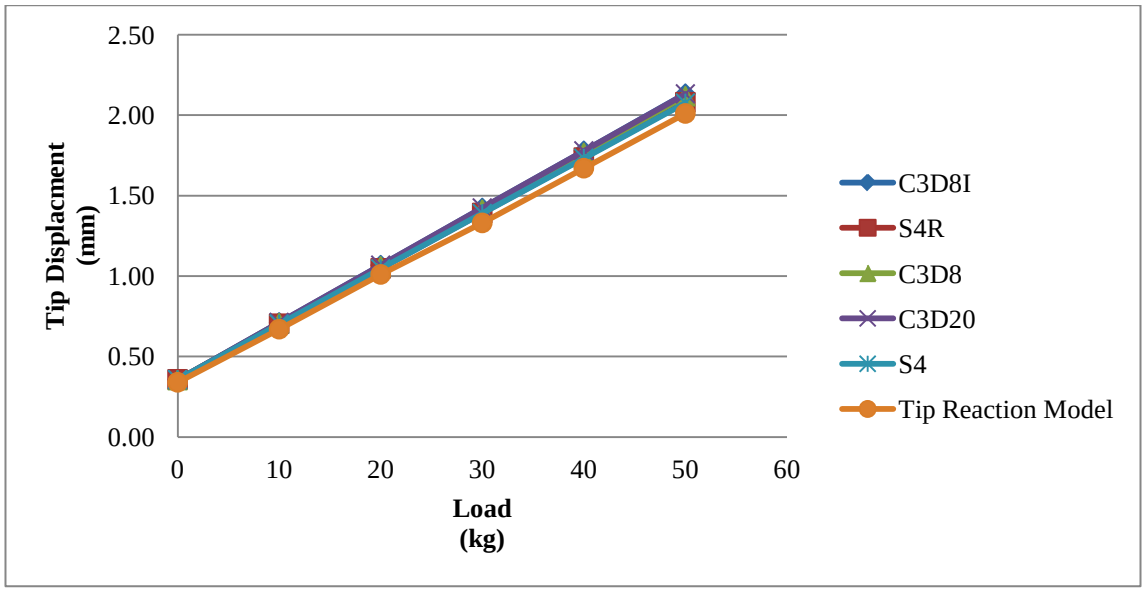

Figure 6-19 Structure's tip displacement VS. incremental symmetric load

6.3.2 Displacement verification

Abraham and Sivaloganathan formulised the telescopic cantilever tip end displacement by proposing the Tip reaction Model (2011). This theory that employs direct integration method was verified true a three staged telescopic cantilever case-study and developed to a C programme. This C programme flowchart is available in Appendix XIII . This programme has been used for the purpose of analysis verification in this study. The verification study is considered for the displacement response of the two nested sections in isolation, to avoid the discrepancy that may cause by structures translation due to the test rig components deformation. The results comparison are shown in Table 6-17 and Figure 6-19.

6.3.3 Displacement behaviour validation

The complete assembly nodal displacement is measured on the assembly, completed by test rig components, using a dial gauge as shown in Figure 6-20. This ensures both the displacement measurements by both analysis and the experiment, will consider the structure's translation due to the test rig deformation.

The tip displacement comparison between FEA and experiments under the payload is established for the shell elements due to its advantageous convergence rate. The numerical and graphical results are presented in Table 6-18 and Figure 6-21 respectively. Comparison shows a close approximation by the analysis in this respect.

The similar comparison is made for the beam displacement under the same condition, along the length of the beam as presented in Table 6-19 and Figure 6-22.

This study confirms a minimal impact of the test rig asymmetric feature, found in the previous section, on the displacement behaviour.

Figure 6-20 Tip displacement experimental measurement with dial gauge

Table 6-18 Tip displacement validation along the length of the beam under the maximum payload

	Simulation	Experiment
Load	S4R	Dial Gauge
(KG)	(mm)	(mm)
0	0.00	0.00
10	1.28	1.00
20	2.57	2.15
30	3.85	3.36
40	5.14	4.64
50	6.43	6.07

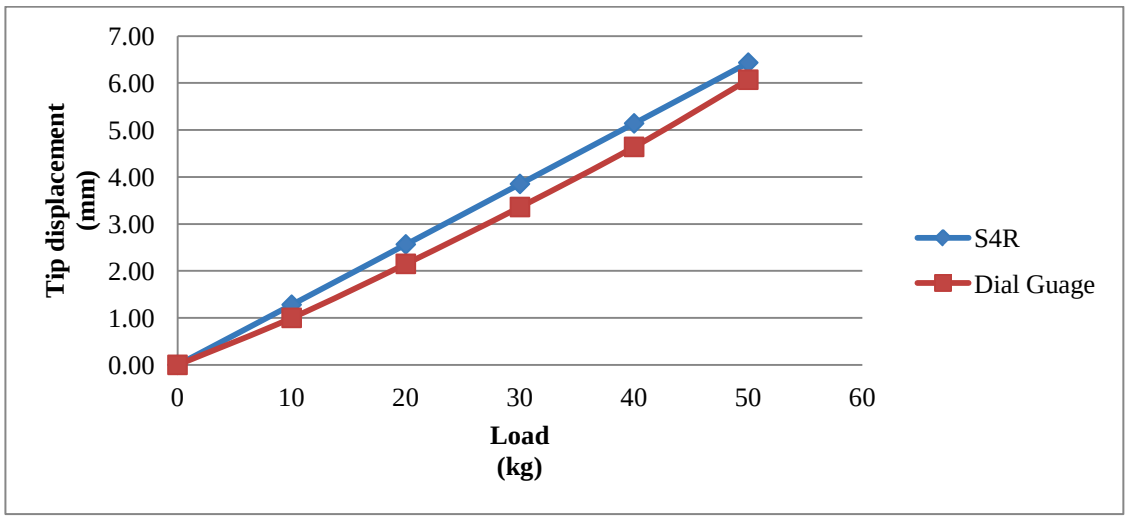

Figure 6-21 Tip displacement validation between simulation with shell and experimental measurement

Table 6-19 Vertical deflection validation along the length of the beam under the maximum payload

Reading point			Vertical displacement	
			U2	
x	y	z	S4R	Dial gauge
			(mm)	(mm)
200	50.85	0	0.31	0.42
400	50.85	0	0.80	0.76
600	50.85	0	1.34	1.25
800	50.85	0	1.95	1.85
1000	50.85	0	2.55	2.38
1200	40	0	3.27	3.3
1400	40	0	4.00	4.04
1600	40	0	4.76	4.23
1800	40	0	5.54	5.1
2000	40	0	6.43	6.24

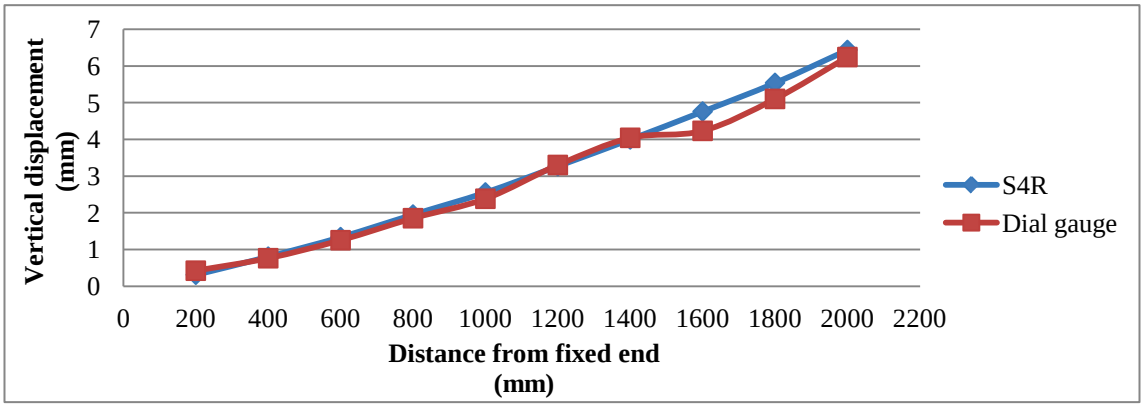

Figure 6-22 Vertical displacement validation across the length of the beam under the maximum payload

6.3.4 Effect of the load magnitude

Abraham, Sivaloganathan and Rees (2011) have established that a telescopic cantilever beam exhibits Hookean behaviour within the elastic limits. This means that when a telescopic cantilever is loaded at the tip, within its elastic limit, the tip deflection will be proportional to the applied tip load applied. The force-displacement graph is a straight line and the slope of the graph will be a multiple of the beam equivalent rigidity.

Choosing the fixed load increments in the previous study the propagation of the displacement with load is demonstrated in Figure 6-21. However the measured values of this graph cannot be used for the structure's rigidity calculation since they contain the effect of structure's translation. The structure's rigidity value is calculated for the displacement of the structure in isolation in Table 6-20.

6.3.5 Effect of the overlap length

In order to avoid disruption on the force-displacement plot by the deflection of the fixing components of the test rig, test rig base and clamping assembly are replaced with encastered boundary conditions, applied at the fixed end. This will ensure the measured quantity at the tip end is due to the actual structure deflection and not the rigid body translation caused by the deformation of the clamping components.

The force-displacement plot for variation of the overlap length is shown in Figure 6-23. The structures rigidity can be calculated from the graph gradients as listed in Table 6-20. The rigidity values are plotted against overlap variation in Figure 6-24 that shows a linear gradient with the increase in overlap length. This graph makes the designer able to approximate the required overlap for the target displacement at the tip end in the conceptual design phase.

Table 6-20 Tip displacement results for variable overlaps

Applied Force		Overlap length				
		500mm	400mm	300mm	200mm	100mm
		Tip displacement				
(kg)	(N)	(mm)	(mm)	(mm)	(mm)	(mm)
0	0	0	0	0	0	0
10	98	0.34	0.43	0.56	0.84	2.82
20	196	0.69	0.86	1.11	1.69	5.64
30	294	1.03	1.29	1.67	2.54	8.45
40	392	1.37	1.72	2.23	3.39	11.25
50	491	1.72	2.15	2.78	4.24	14.04
Slope (N/m)		285690	228520	176310	115460	34931

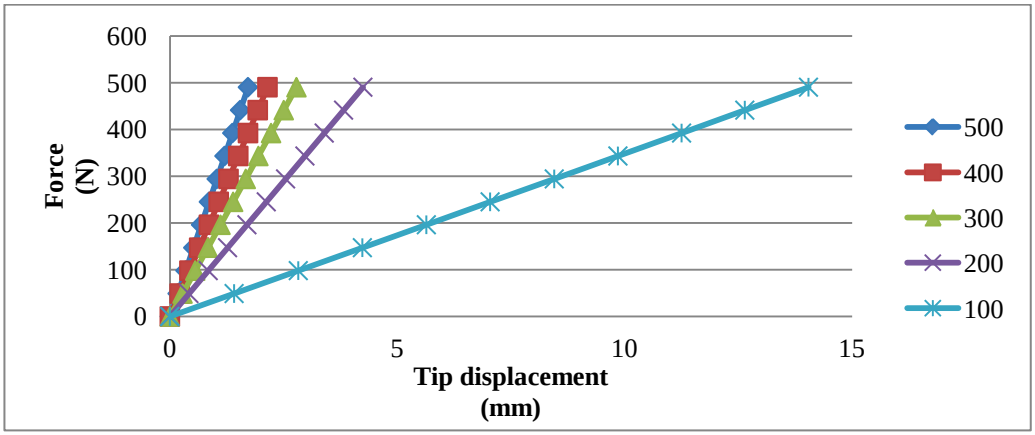

Figure 6-23 Tip displacement plot against variable overlap

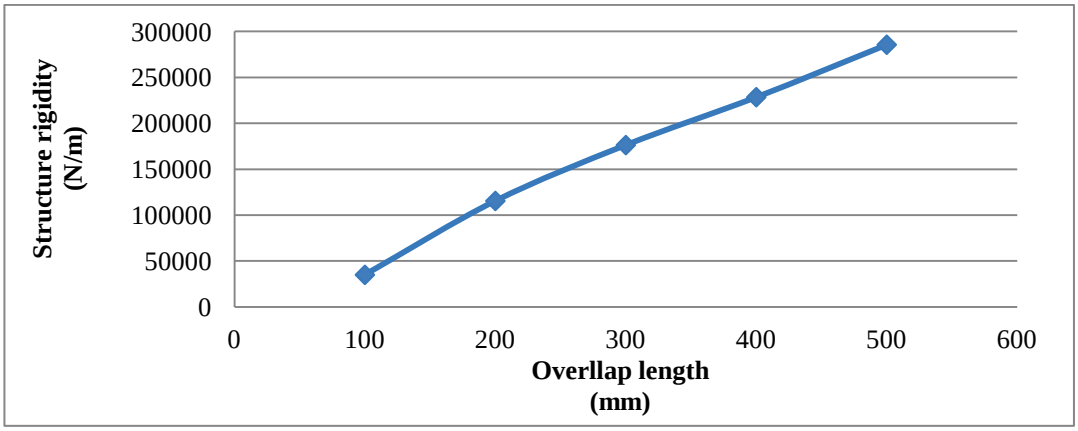

Figure 6-24 Structure's rigidity variation with overlap length

6.3.6 Conclusion

The displacement behaviour of the telescopic cantilever boom is characterised for the variation of specified parameters. The MPCs are collected from the previous analysis for the contact stress behaviour, and validated with the same instant of reality.

The element variation response is assessed as insignificant on both local deflection and tip end displacement. The validation results shows also the previously found discrepancy on the test rig that affect the contact stress behaviour, is not visible on the displacement response.

The load magnitude variation is analysed and the response on the tip end displacement is used to quantify the structure's rigidity.

The effect of overlap variation on the tip end displacement is studied. Using the load-displacement graph the variation in rigidity of the structure is calculated. The graphical representation shows a linear relationship between overlap and structure's rigidity.

6.4 Vibration behaviour

This section is dedicated to characterisation of the structure's vibration behaviour with variation of input parameters. The analysis 9-13 and 14-18 of Table 5-3 along with the third and fourth V&V case of Table 5-4 are collecting the corresponding MPCs and verify and validate them. The analysis procedure is also different from the stress-displacement analysis. This sections starts with the general analysis set up for linear perturbation analysis as it is required to obtain natural frequency. Also the verification method that is used to confirm the FEA outcomes is discussed in this section.

6.4.1 General linear perturbation analysis set up

The required analysis in this section is specified as the general static to obtain the deformed structure under the payload, followed by linear perturbation to obtain the natural frequency response. The procedure, detailed in Figure 6-25 defines the set up for a natural frequency analysis of a pre-loaded structure (Dassault Systèmes, 2009, b).

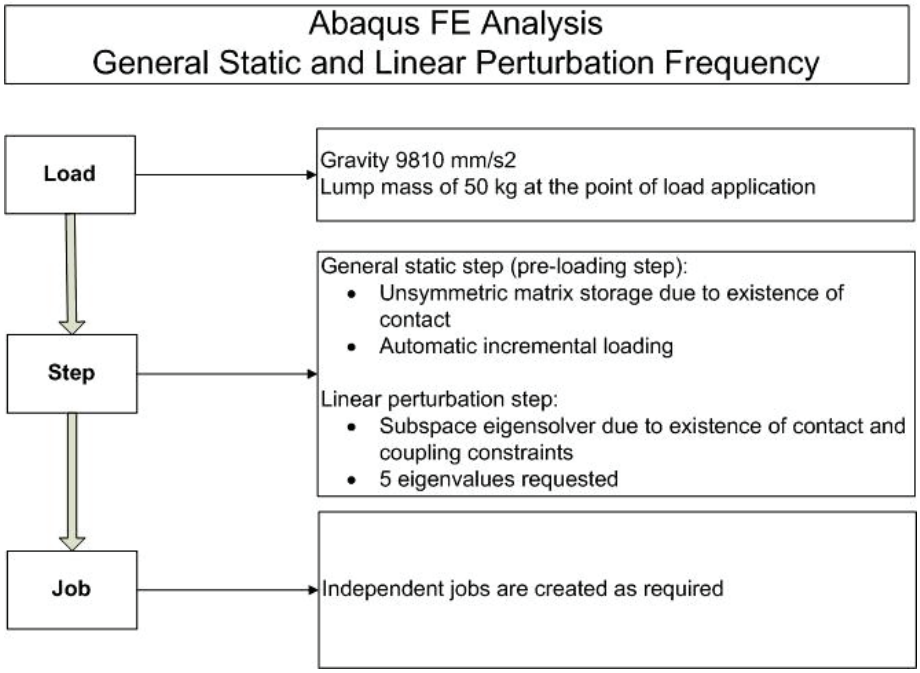

Figure 6-25 Natural frequency analysis general set up

6.4.2 Verification method

The verification is conducted using Dunkerly method as established by Salazar et al. (2011) as an approximation method to predict structure's natural frequency. The application of this theory on cantilever structures, holding a tip mass, has been verified in a comparative study via Lagrange's multipliers method (Gurgoze et al. 1984). To explain Dunkerley's method consider a system with several masses (n) as shown in Figure 6-26 (Green, 1962). Each mass when considered alone has its amplitude and frequency as shown in Figure 6-26. If f_{n1} denotes the vibration of mass m_1 with amplitude of x_1 and similarly f_{n2} denotes the vibration of mass m_2 with amplitude of x_2, according to Dunkerley's method the first natural frequency of the overall system, f_n, is:

Eq. 6-2

$$\frac{1}{f_n^2} = \frac{1}{f_{n1}^2} + \frac{1}{f_{n2}^2} + \ \ldots + \frac{1}{f_{ni}^2}$$

Green suggests that the natural frequency behaviour of a cantilever contains self-weight and tip mass can be obtained using the Superposition Theorem (Green, 1962):

Eq. 6-3

$$\frac{1}{f_n^2} = \frac{1}{f_{n1}^2} + \frac{1}{f_{n2}^2}$$

where f_n indicates natural frequency of the overall system, f_{n1} is natural frequency of the beam under its self-weight and f_{n2} is the tip mass. The required parameter for the Eq. 6-3 is the natural frequency of the weightless beam carrying tip load that can be obtained by (Salazar et all, 2011):

Eq. 6-4

$$f_n = \frac{1}{2\pi}\sqrt{\frac{Slope}{M}}$$

and the natural frequency of the compound beam under the self-weight that is (Salazar et all, 2011):

Eq. 6-5

$$f_n = \frac{1}{2\pi} 1.875^2 \sqrt{\frac{Slope}{3M}}$$

Where M is the mass of the system and slope refers to the structures rigidity value as described in section 6.3.

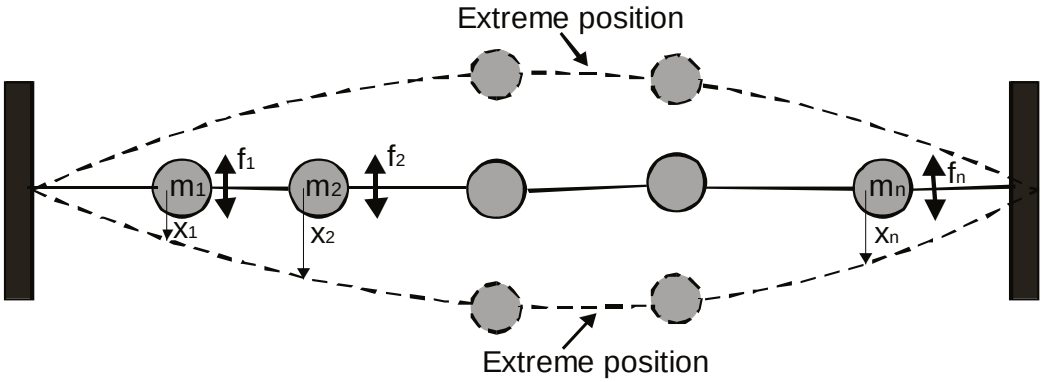

Figure 6-26 A System with Several Masses

6.4.3 The variation of load magnitude

The effect of the load magnitude variation on the natural frequency response is studied analysed as suggested by analysis 9-13 of Table 5-3, detailed in Table 6-21. Table 6-22 shows the quantitative comparison for the verification practice. Figure 6-27 plot the natural frequency values against the variable payloads in each overlap increment. The plots show the close agreement between formulation and simulation results. The results show a larger difference on the lower ranges of the payload.

Table 6-21 Natural frequency study, dependency to the load magnitude

Stakeholders' requirement	MPCs	Fixed Parameter	Variable Parameter
Natural frequency behaviour of the structure	Natural frequency	Element type: S4R Load type: Symmetric Overlap= 500 mm	Overlap n_1=500 mm n_2=400 mm n_3=300 mm n_4=200 mm n_5=100 mm

Table 6-22 Natural frequency verification results

Dunkerley method calculation for natural frequency							**FEA**
Section mass	Overlap	Slope	Fn1	Payload	F_{n2}	F_n	F_n
(kg)	(mm)	(N/m)	(Hz)	(kg)	(Hz)	(Hz)	(Hz)
37	500	285690	28.39	50	12.03	11.08	11.61
				40	13.45	12.15	12.82
				30	15.53	13.63	14.51
				20	19.02	15.80	17.10
				10	26.90	19.53	21.87

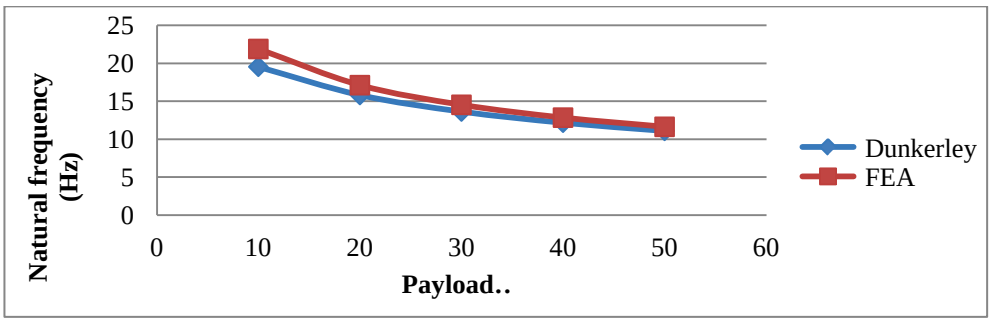

Figure 6-27 Natural frequency verification for payload variation

The validation process is conducted on the third instant of reality of Table 5-4.

The validation results comparison with the verification result for structure in isolation shows, a significant interference from the test rig assembly in the natural frequency of the system. This suggests that analysis on the isolated telescopic structure does not represent the physical practice. The presence of the load hanger part can also affect the accuracy of the simulation not only by its additional mass but also slight variation in the payload application point. Table 6-23 shows the quantitative comparison between FEA and experimental results for the variation of payload. The results are plotted in Figure 6-28.

Table 6-23 Validation of natural frequency, quantitative comparison

Load (kg)	**Natural frequency (Hz)**	
	FEA	Experiment
0	19.98	17.4
10	12.03	10.25
20	9.48	8.20
30	8.42	7.20
40	7.80	7.20
50	7.23	6.20

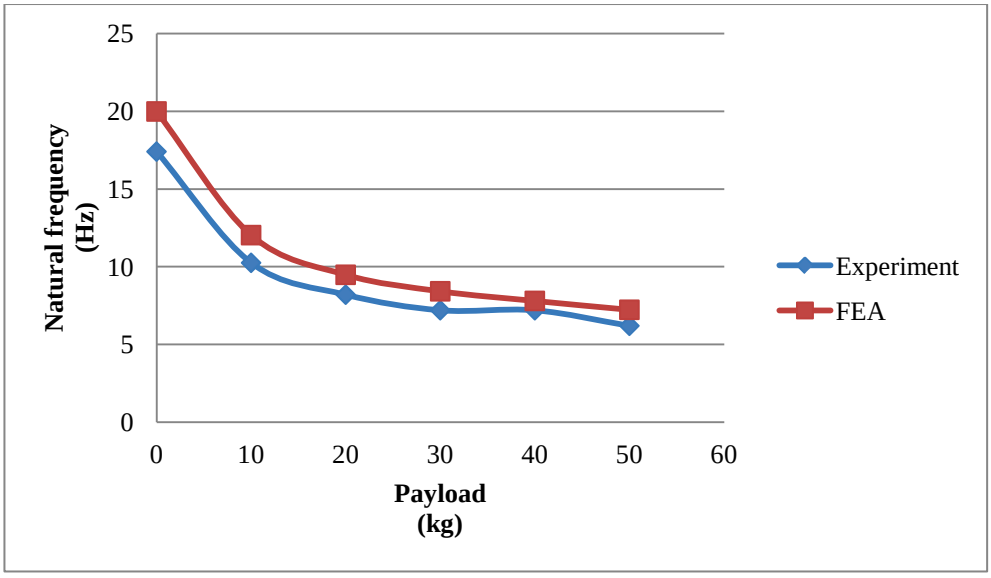

Figure 6-28 Natural frequency verification for payload validation

6.4.4 The effect of the overlap length

The effect of overlap variation on natural frequency response is analysed using studies 14-18 of Table 5-3, detailed in Table 6-24.

The verification comparison is reported in Table 6-25. Graphical comparison in Figure 6-29 shows that the formulation may not be sufficient on the lower ranges of the overlap length.

Table 6-24 Natural frequency study, dependency to the overlap length

Stakeholders' requirement	MPCs	Fixed Parameter	Variable Parameter
Natural frequency behaviour of the structure	Natural frequency	Element type: S4R Load type: Symmetric Payload= 50 kg	Overlap n_1=500 mm n_2=400 mm n_3=300 mm n_4=200 mm

Table 6-25 Natural frequency verification results

Dunkerley method calculation for natural frequency							FEA
Section mass (kg)	Overlap (mm)	Slope (N/m)	Fn1 (Hz)	Payload (kg)	Fn2 (Hz)	Fn (Hz)	NF (Hz)
37	500	285690	28.39	50	12.03	11.08	11.61
37	400	228520	25.39	50	10.76	9.91	10.51
37	300	176310	22.30	50	9.45	8.70	9.52
37	200	115460	18.05	50	7.65	7.04	8.54
37	100	34931	9.93	50	4.21	3.87	7.12

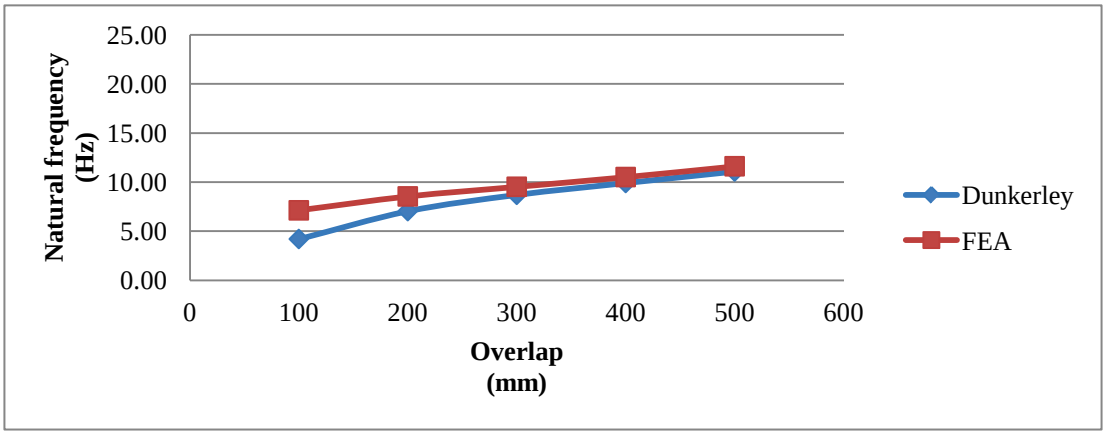

Figure 6-29 Verification of natural frequency response to overlap variation

The quantitative comparison between experimental results and FEA on the overall assembly is reported in Table 6-26 and demonstrated graphically in Figure 6-30. The forth instant of reality of Table 5-4 is used for this purpose.

Table 6-26 Validation of natural frequency response to overlap variation

Overlap length (mm)	Natural frequency (Hz)	
	FEA	Experiment
500	7.23	6.20
400	6.75	6.15
300	6.3	5.15
200	5.84	5.15

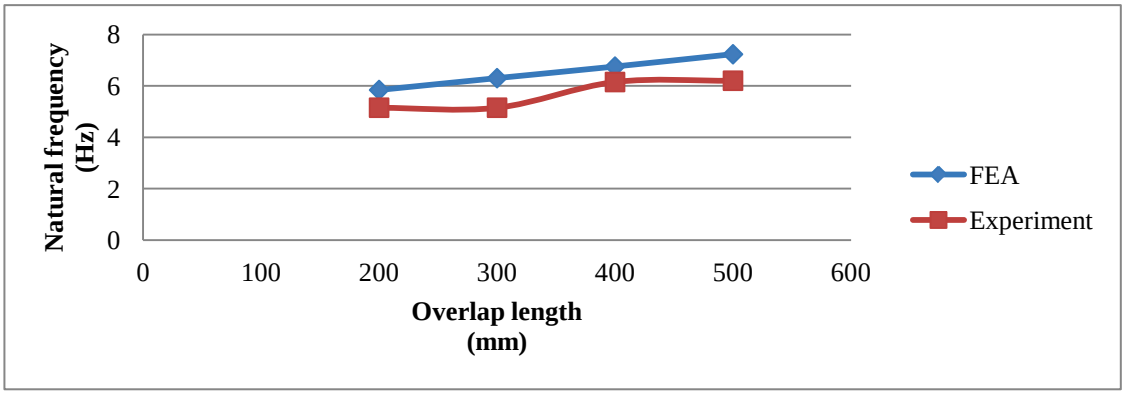

Figure 6-30 Validation of natural frequency response to overlap variation

6.4.5 Conclusion on natural frequency behaviour

The structure's vibration behaviour, translated to the natural frequency, is studied in this section. The impact of the load magnitude variation and overlap length variation is analysed verified and validated independently.

The proposed formulation to calculate the natural frequency of the compound beam is established based on the Dunkerley method and the theory of equivalent beam and the range of its application is discussed in this stage.

The validation of the results is conducted using the instant of realities. It is understood that the input from the ancillary supportive parts can significantly change the magnitude of the measured values. This input must be considered for the future development of the full-scale structure. The behavioural pattern of the natural frequency is plotted as a monogram for further design considration.

6.5 Buckling performance

This section studies the buckling performance of the telescopic cantilever with input parameters variation. The required analyses of 19, 20 and 21-24 as outlined in Table 5-3, are conducted in his section to obtain corresponding MPCs as Buckling Critical Load and buckling mode. The required analysis procedure to obtain the MPCs is detailed in this section.

As it is discussed in Chapter 2 the buckling failure is the effect of compressive stress and from the previous studies it has been emerged that the variation of load type and overlap length vary the structure's stress response that in turn varies Buckling Critical Load.

6.5.1 General buckling analysis procedure

The required procedure for buckling analysis is outlined in Figure 6-31. The analysis starts with an Eigenvalue analysis. The purpose of this analysis is to investigate singularities in a linear perturbation of the structure's stiffness matrix. This estimation is useful in design only if the linear perturbation is a realistic reflection of the structure's response before it buckles. Eigenvalue buckling is useful for "stiff" structures that exhibit only small, elastic deformations prior to buckling. The objective of an Eigenvalue buckling analysis is to find the load level at which the equilibrium becomes unstable or estimate the maximum load level which the structure can sustain.

The stiffness of the structure in the base state K_0 , is defined by application of pre-load in the form of "dead" load, P_0 (Dassault Systèmes, 2011). Presuming that the response of the structure is stiff and linear elastic, the stress and the structural stiffness will change proportionally by addition of the "live" load , $\lambda\Delta P$, where λ is the magnitude ΔP is the pattern of the live load as $K_0 + \lambda\Delta K$.

Where ΔK is made up of two parts: the internal stress and the applied load, due to incremental loading pattern:

Eq. 6-6

$$\Delta K = K_{\Delta\sigma} + K_{\Delta P}$$

A loss of stability occurs when the total stiffness matrix is singular:

Eq. 6-7

$$(K_0 + \lambda \Delta K)V = 0$$

Values λ_{cr} which provide nontrivial solutions to this Eigen-problem, define the critical buckling load as $P_0 + \lambda_{cr}\Delta P$.

Buckling mode shapes, V, are normalized vectors and do not represent actual magnitudes of deformation at the critical load.

Eigenvalue, λ_{cr} and corresponding mode V, are often the most useful outcomes of the Eigenvalue analysis since they predict the likely failure mode of the structure. The closer approximation can be achieved with a higher preload condition that is generated by a higher dead-load at the general static step obtained from the Buckling load calculation. (Falzon, Hitchings, 2006).

The Eigenvalue buckling is not producing a reliable response if the elasticity of the structure is violated during the loading. Also if by applying the buckling critical load it is expected that a part of the structure exceeds the yield point then the predicted value can be incorrect.

In this occasion the buckling analysis workflow continues with regular static procedure. In this step two techniques are available as:

- Load control: Loading applied via applied load (e.g. concentrated force, distributed pressure).
- Displacement control: Loading applied by enforcing non-zero boundary conditions. In some simple cases displacement control can provide a solution, even when the reaction force decreases as the displacement increases.

In the load control approach the structure is loaded up to or slightly above calculated Buckling Critical Load from the previous stage in a single static step. If the Eigenvalue estimation is valid general static step reaches the vicinity of the predicted buckling mode.

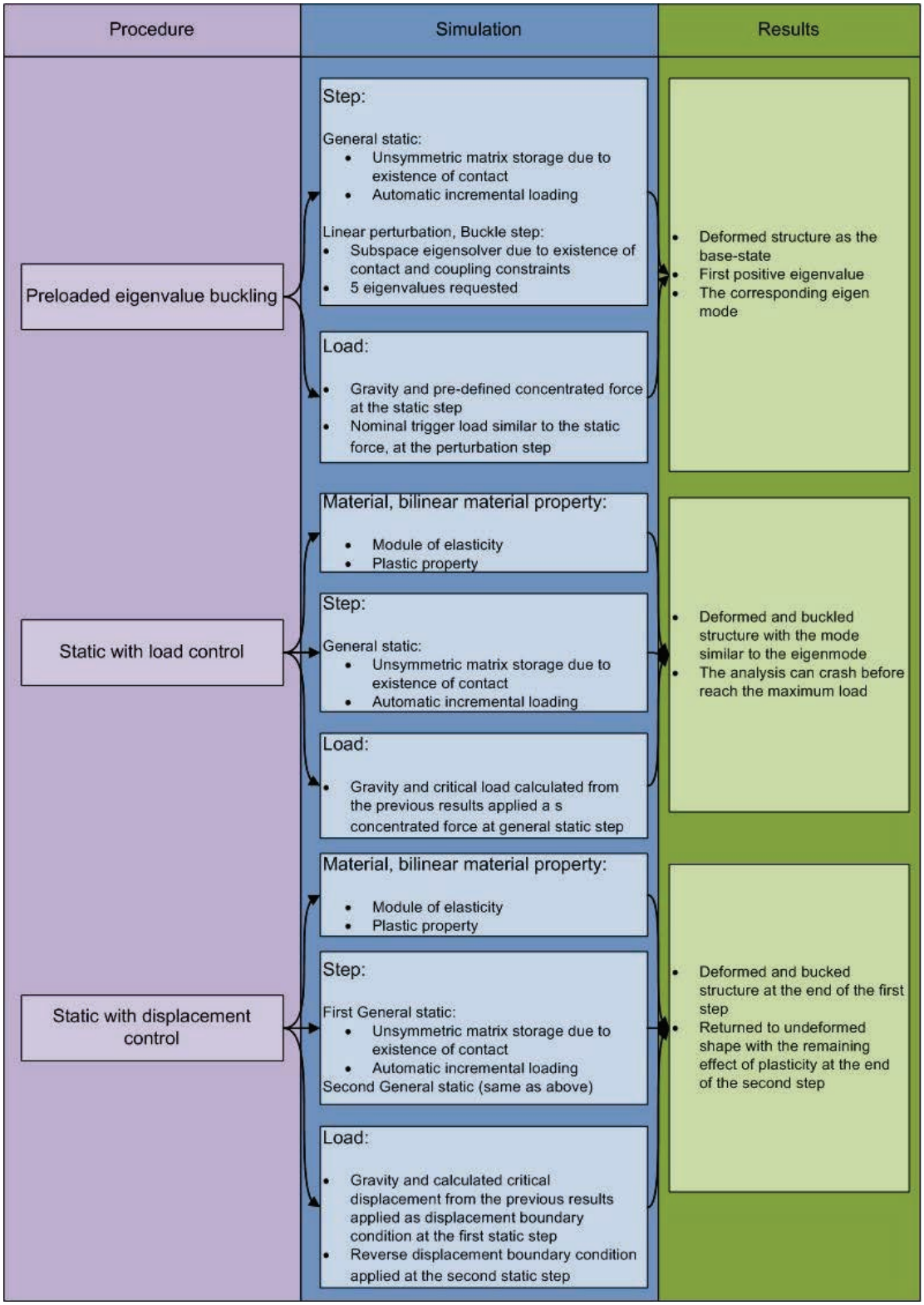

Figure 6-31 Buckling analysis procedure in Abaqus

The general static analysis in Abaqus/Standard uses an incremental-iterative solution technique based on the Newton-Raphson method for solving the nonlinear equilibrium equations. The method can be understood in one dimension from a load-displacement

diagram as demonstrated in Figure 6-32 (Dassault Systèmes, 2011). The analysis follows the below path to converge into a solution:

1. Apply an increment of load or time.

2. Iterate until the sum of all forces acting on each node is small (statics) or is equal to the inertia force (dynamics).

3. Update the state once equilibrium has been satisfied.

4. Go back to Step 1, and apply the next increment.

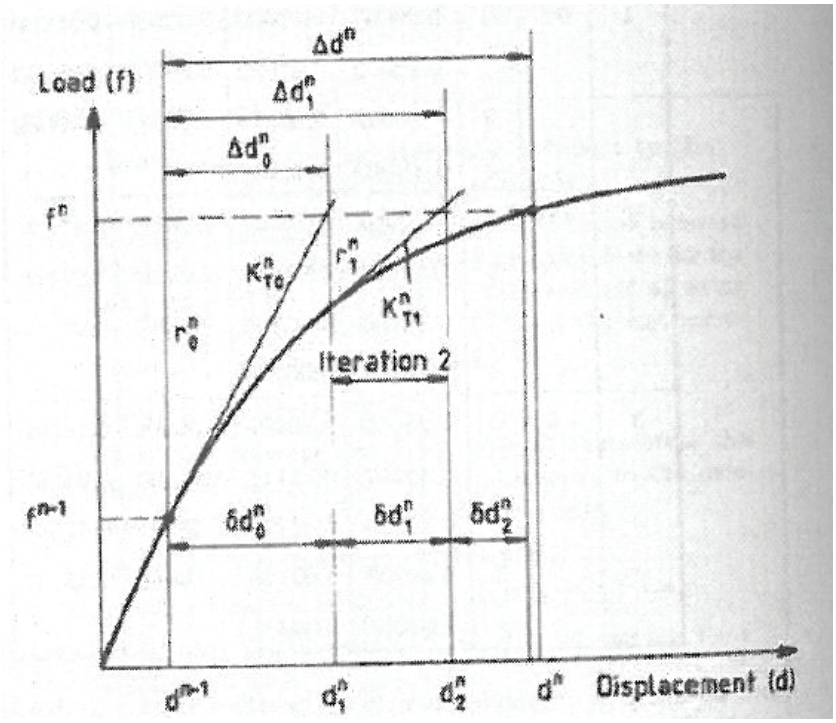

Figure 6-32 Newton-Raphson solution convergence (Hinton, 1992).

Despite the great convergence ratio this method is less likely to converge to an unstable equilibrium configuration. The Newton-Raphson method breaks down completely when a critical load is reached as a solution does not exist or is far removed from the starting point, as shown in Figure 6-33.

This method can also incorporate the effect of material non-linearity in the form of plastic deformation. In order to increase the accuracy of deformation prediction when parts of the structure are expected to exceed the yield point the material model needs to represent the post-yield stiffness by the shape strain-stress. (Chillery, 2010, a). The two gradient curves shown in Figure 6-34 creates a sufficient fit to the actual post-yield stress-strain curve of a typical engineering steel.

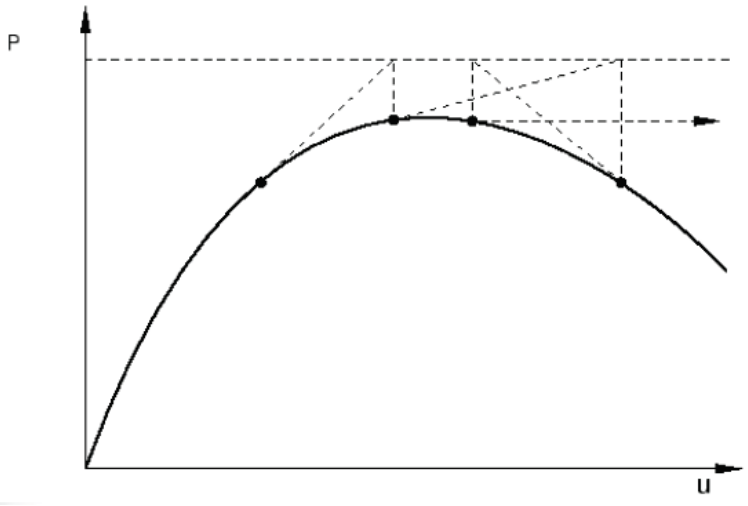

Figure 6-33 Newton-Raphson limitation near the load maximum (Dassault Systèmes, 2011).

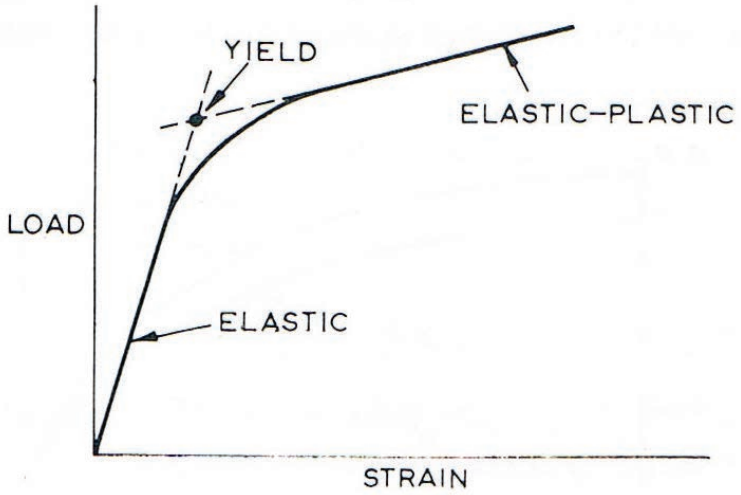

Figure 6-34 Bilinear material model for post-yield behaviour (Johnson and Mellor, 1973).

Therefore while the method can predict the buckling mode and required load more accurately than Eigenvalue estimation, it will not be able to produce any information about post-buckling behaviour of the structure in certain circumstances.

If the state of buckling reached the next step is displacement control method to achieve an initial indication for the post-buckling behaviour. Critical displacement can be obtained from the load-displacement graph from the Load control analysis. In the case of cantilever beam displacement can be estimated by the structure's rigidity graph, discussed in section 6.3. The applied displacement in the form of non-zero boundary condition can deform the structure up to the critical point (Smolira, 1980).

As discussed earlier in this section the buckling phenomenon is always accompanied with lose of stiffness locally or globally to the structure. This phenomenon can be best characterised by the force-displacement diagram, and will be used to assess the buckling behaviour in the forthcoming analysis.

6.5.2 Load type variation

The effect of load type variation on the buckling response is studied in this section. The details of the analysis condition is extracted from analysis 19 and 20 of Table 5-4 and presented in Table 6-27.

Table 6-27 Buckling behaviour study, dependency to load type variation

Stakeholders' requirement	MPCs	Fixed Parameter	Variable Parameter
Buckling behaviour of the structure	Buckling load factor Buckling mode	Element type: S4R Pay load= 50 kg Overlap= 500mm	Type of load: Symmetric:50 in CL Asymmetric: 50kg at 300mm offset from CL

Following the procedural practice suggested in Figure 6-31, the analysis is started with Eigenvalue study. Table 6-28 suggests the required BCL in addition to the self-weight. The corresponding buckling mode suggests that the structure will lose its stiffness near to the fixed end, as it is shown in Figure 6-35 (a) and (b). There is no significant variation observed in the MPCs due to load type variation. The compressive stress on the bottom surface of the section, illustrated in Figure 6-35 (c) and (d) shows the buckled surfaces experience very similar compressive stress magnitude in both type of loads.

Table 6-28 Eigenvalue buckling study results for load type variation

	Loading					Results	
	Gravity	Dead-load		Live-load		EV	BCL
		Concentrated Force (F_y)	Concentrated Moment (M_x)	Concentrated Force (F_y)	Concentrated moment (M_x)		
	(mm/s^2)	(N)	(N.mm)	(N)	(N.mm)		(N)
Symmetric load	9810	-490	------	-100	------	663.10	66800
Asymmetric load	9810	-490	147150	-100	30000	658.62	66352

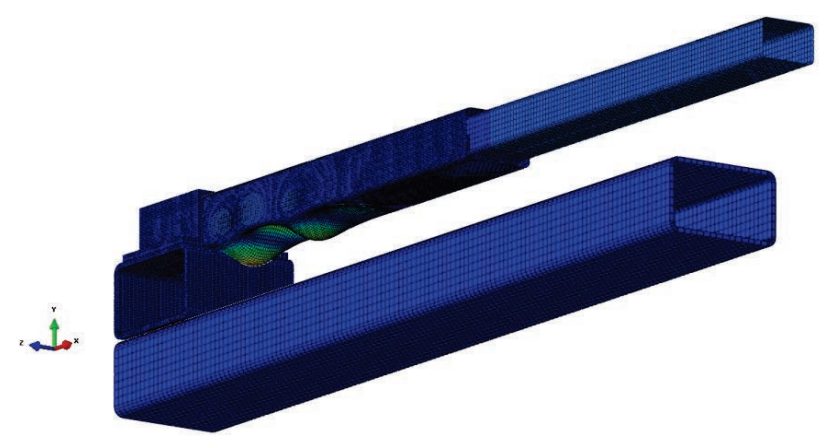

(a)

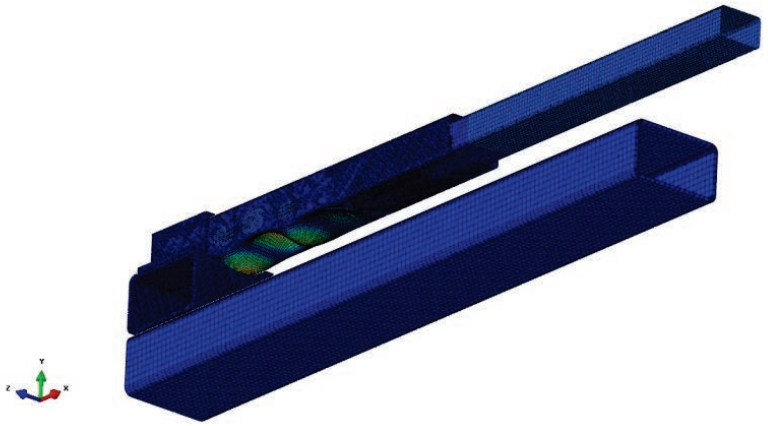

(b)

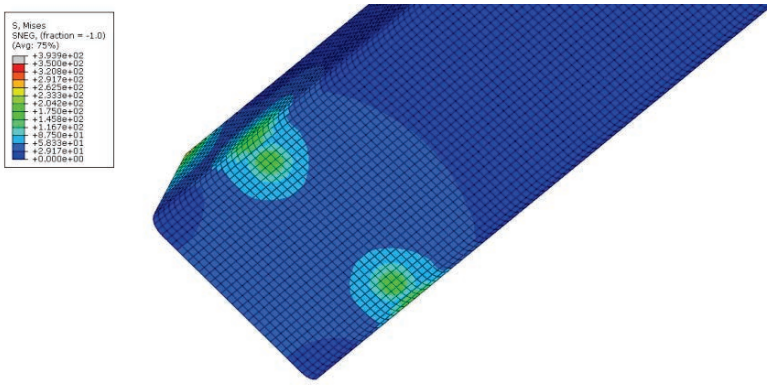

(c)

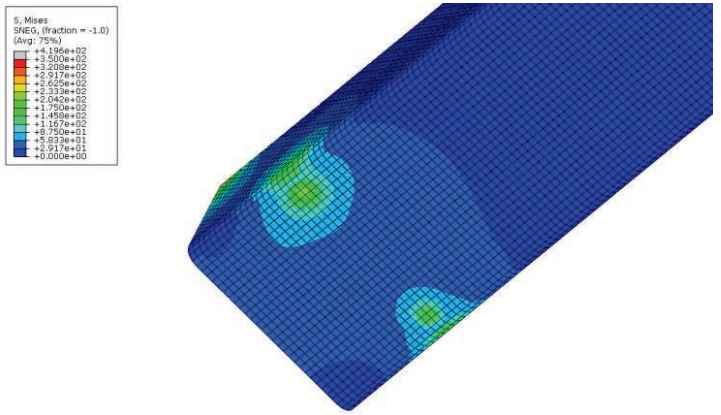

(d)

Figure 6-35 Qualitative comparison for load type variation (a) Symmetric load case (b) Asymmetric load case (c) Stress plot at the buckling vicinity under symmetric load (d) Stress plot at the buckling vicinity under asymmetric load

The magnitude of predicted BCL is significantly higher than the applied load. The comparison shows almost an additional 6800 kg is required to observe the first probable buckling mode. Comparing this with the current state of stress recommends that the structure will certainly exceed the yield point. Although inelastic instability is assessed unlikely with the Eigenvalue analysis, the risk of buckling after the elastic limit remains unknown.

To characterise the behaviour of the structure after the yield limit, the load control analysis is conducted for both load types scenarios. The effect of bilinear material is also incorporated to determine the structure's deflection path beyond yield point. The analysis is set up in two static steps to segregate the impact of gravity and applied load. The applied load is chosen higher than the predicted BCL to allow for the solution to approach the closest possible to the buckling mode. The asymmetric load case would be under the same load at 300mm offset from the z direction.

The results of both variations of the load type shows the structure deformed to the plastic phase and start penetrating into the test rig base until the analysis break down due to excessive deformation, Figure 6-36. The deformation plots for both load cases, Figure 6-37, do not show any similarity to the buckling modes Figure 6-35.

The load-displacement diagram in both cases, Figure 6-38, do not show any indication of loss of stiffness or bifurcation. The non-linear deformation after application of force, Figure 6-39 suggests the deformation is completely plastic until the analysis crash. This would discount the necessity of conducting the displacement control analysis to visualise post-buckling behaviour.

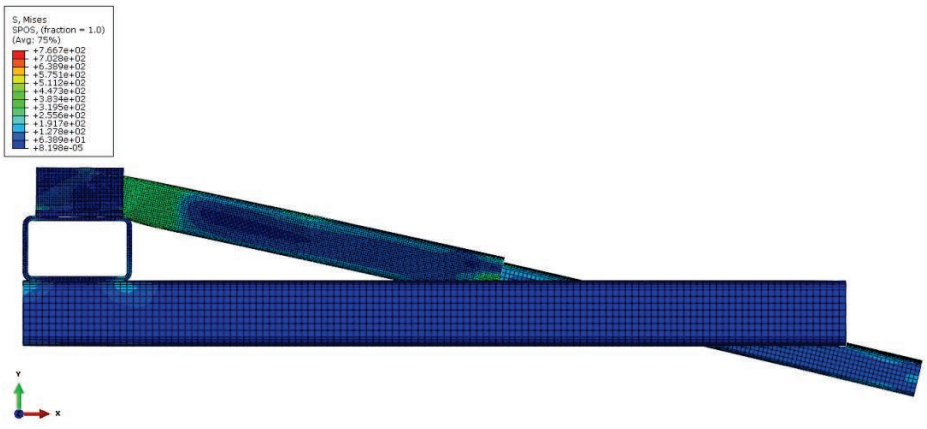

Figure 6-36 Structure deformation due to application of BCL

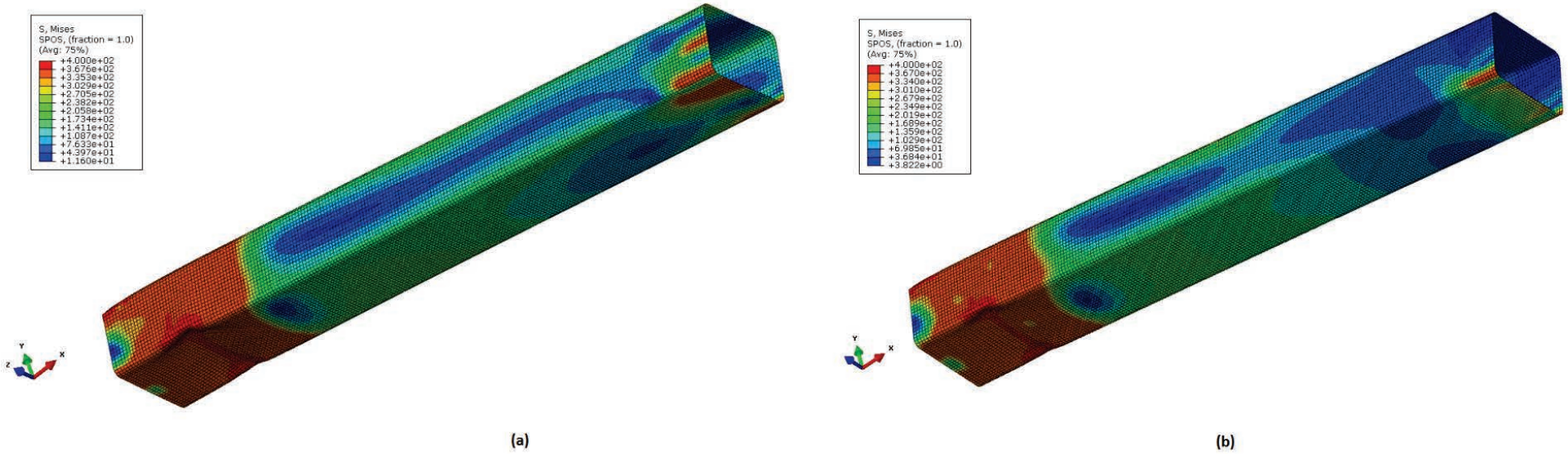

Figure 6-37 Stress plot (a) Asymmetric load case (b) Symmetric load case

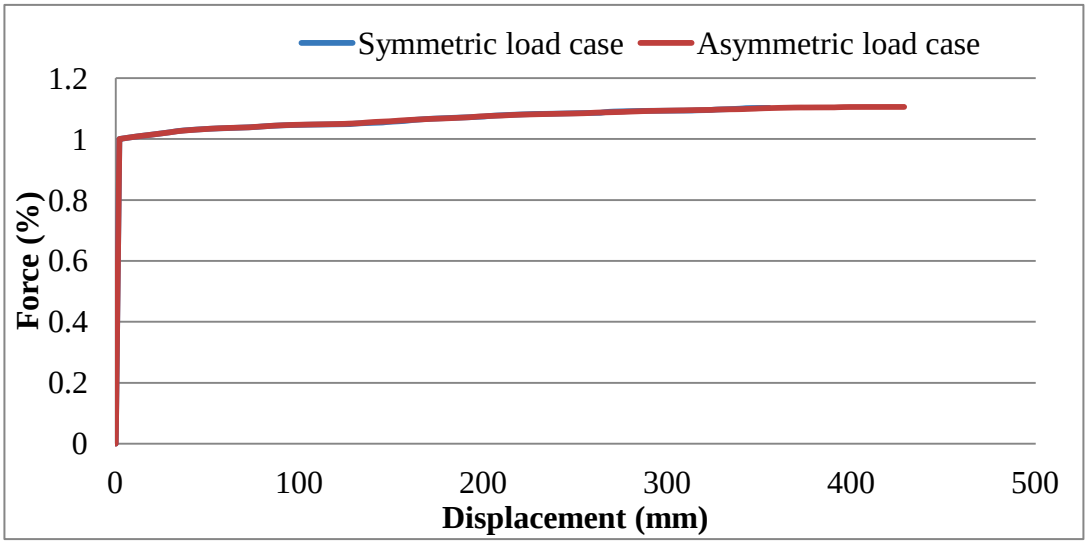

Figure 6-38 Load-displacement diagram, for the two loading steps

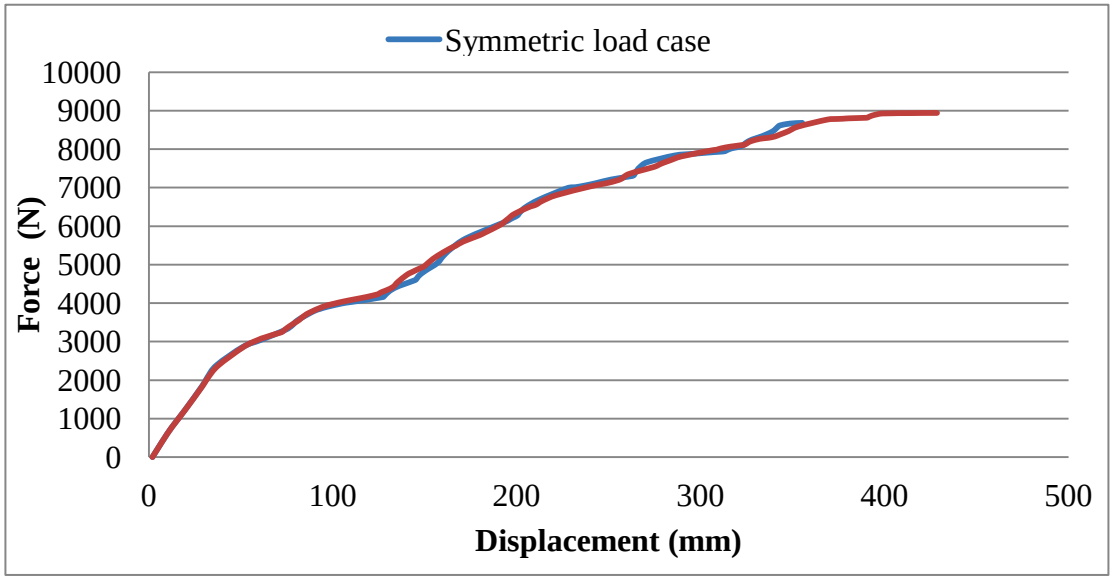

Figure 6-39 Load-displacement diagram for payload application step

Table 6-29 Results for the load control study up to the maximum feasible tip displacement (up to material interference occurrence)

Analysis condition	Applied load			Analysis completion	Feasible Payload	Feasible Tip displacement
	Gravity	Concentrated Force (F_y)	Concentrated Moment (M_x)			
	(mm/s^2)	(N)	(N.mm)	(%)	(N)	(mm)
Symmetric load	9810	-85000	----------	6.6852	5682	172.5
Asymmetric load	9810	-85000	25500000	6.7863	5768	181.7

6.5.3 Effect of the overlap length

This section address the effect of overlap variation in the buckling response as suggested in Table 6-27. The analyses of 21-24 from Table 5-3 are conducted for the required MPCs.

Similar to the previous study the procedural process starts with Eigenvalue study. As it has been already observed that the BCL is far above the structures load capacity this study does not proceed further beyond. The result of these analyses, summarised in

Table 6-31, confirms that the risk of plastic failure is more imminent than buckling in this structure. The ratio between BCL to designated payload quantifies the safety level of the structure. Figure 6-40 plot the input variable against the calculated safety ratio.

Table 6-30 Buckling behaviour study, dependency to overlap length variation

Stakeholders' requirement	MPCs	Fixed Parameter	Variable Parameter
Buckling behaviour of the structure	Buckling load factor	Element type: S4R	Overlap
		Pay load= 50 kg	n_1=500 mm
		Load type: Symmetric	n_2=400 mm
	Buckling mode		n_3=300 mm
			n_4=200 mm
			n_5=100 mm

Table 6-31 Buckling results for the Eigenvalue buckling study with load type variation

Overlap length	**Loading**			**Results**		
	Gravity	Dead-load	Live-load	EV	BCL	Safety ratio
		Concentrated Force (F_y)	Concentrated Force (F_y)			
(mm)	(mm/s^2)	(N)	(N)		(N)	
500	9810	-490	-100	663.10	66800	136
400	9810	-490	-100	626.35	63125	129
300	9810	-490	-100	593.18	59808	122
200	9810	-490	-100	563.28	56818	116
100	9810	-490	-100	536.21	54111	110

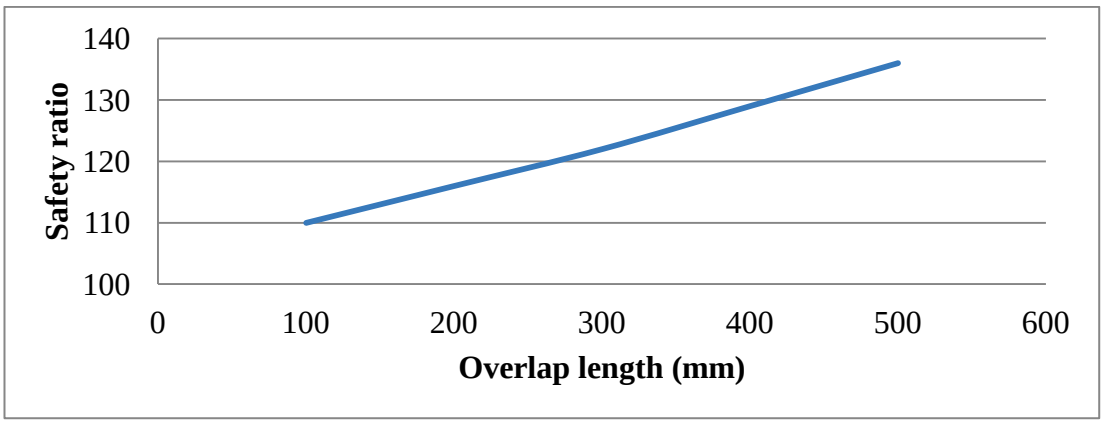

Figure 6-40 Safety index variation with overlap length change

6.5.4 Conclusion on buckling behaviour

The procedural steps to obtain the buckling response are illustrated in this section.

The buckling behaviour of the nominated structure is characterised only analytically through FE simulation for the variation of load type and overlap length. Different numerical techniques are incorporated to verify the analysis outcomes by cross-checking.

The effect of load type variation assessed not significantly influential on the buckling performance; consistent local buckling is predicted at the bottom surface of the outer section near to the clamped end. The structure shows more considerable response to overlap length variation, although conducted analysis does not indicate any feasible buckling mode. An index of safety as the ratio between BCL to the maximum service load is introduced. The progression of this index with overlap length in this study is observed as linear.

The proposed salient benchmark is assessed as far too stiff to be used for the buckling validation purpose.

6.6 Chapter summary

The list of required analyses along with the instants of reality for the verification and validation practice that are produced in Chapter 5, are put into practice in this chapter to obtain the corresponding the required MPCs to each stakeholder's requirement.

The required analyses for each section are proven to be adequate to collect the required MPCs and create a sufficient account to be considered in the next level of design iteration. Each of stakeholder's requirements are investigated independently and the

conclusive remarks for each sections are provided at the end of each study. Furthermore, the verified and validate analytical methods create a reliable analytical procedure for future use in the more detailed and complicated design level.

Following the successful application of the design integrated structural analysis methodology on the nominated structure, the proposal is assessed as functional, and adequate for the designated purpose. The findings of this section create a credible platform for the next iteration in the structural design and analysis of the telescopic cantilever boom.

7 Discussions and Conclusions

7.1 Summary

Structural analysis has a critical role in the design and development of mechanical products. Many key decisions about size, shape, and material are directly taken based on the structural performance. Commercial entrepreneurs invest in software, hardware, and human resources to simulate mechanical systems. These components are necessary but not sufficient to incorporate structural analysis in its full capacity as a design tool and do not lead to the maximum benefit from the investment. This research addressed the above issue by enhancing the position of structural analysis in the design process by proposing a QFD-Based Design Integrated Structural Analysis Methodology.

The structural analysis process was conventionally conducted by theoretical calculations that are, in a more pragmatic environment, accompanied by experimental measurements. In modern applications, the use of Computer Aided Engineering and simulation has been significantly improved by the advent of computers in engineering leads to yet the most exact prediction of stress and strain distribution in the components

The first step to achieve this aim, identified as a common ground between Design and Analysis disciplines, has been established by introducing the analysis aim and objectives. Furthermore, the structural analysis quest has been identified with its quantifiable parameters. This knowledge is fundamental for two involved disciplines to communicate effectively and contribute to the product development process. As the mean of achieving the objectives, analysis methods and tools are discussed in this study.

In the second step the design perspective, its procedure and requirements are introduced. This perspective is established based on the accepted mainstreams in the field that are regarding the design process as a systematic procedural practice. The state-of-the-art practices to organise the structural analysis workflow is assessed critically. Despite the efficiency and productivity of the available practices lack of total design and product multi-functionality view are identified as prohibitive factor for design integration.

In the third step a creative adaptation of the QFD method has been proposed as the key element to create a descriptive form of reality of interest. The combination of the QFD with benchmark, and V&V boost the impact of the proposed methodology to reliably integrate with design process from the early stages.

The validity of the proposed methodology has been investigated through an application on an industrial structure. The telescopic cantilever boom as it appears in the crane and access platforms has been the subject of this study. The structural multi-functional aspect of the product as well as variety in the design input parameters make it an ideal candidate to explore the functionality of the proposed methodology.

The structural multi-functional aspect, translated into the measurable performance characteristics has been quantified, verified and validated through the most effective number of analyses and experimentations. The basic presentations of the results demonstrate the capability of the methodology to characterise performance behaviours of the structure with respect to design parameter variation. The integrity of the process with the product design from early stages reduces the chance of error propagation in the finalised product. The limitations of existing structural analysis approaches have been discussed. The following section defines the contribution of this research to knowledge.

7.2 Contribution to knowledge

The key contribution of this work to knowledge are summarised below:

- A creative adaptation of Quality Function Deployment (QFD) that leads to a generic Design Integrated Structural analysis Methodology.
- Application of a technique from one field to overcome a shortcoming in another field that assists analysts to tackle unfamiliar problems in a systematic way
- The effectiveness of the methodology is examined in an industrial case-study.

Furthermore the impacts of this research in industry are:

- to develop a tool to capture all design requirements and eliminate wasteful rework and encourage value-adding iterative structural analysis
- higher return on investment.

7.3 Recommendation for future developments

This research has shown benefits in using a new approach to structural analysis. The following areas of interest could offer opportunities for further development:

- Design of the salient benchmark that covers product multi-functional structural aspects is not always possible. The minimum instant of realities for verification and validation can be identified from the proposed methodology, however this

outcomes might need further considerations and developments on special cases e.g. when the test associated with the risk of structure to failure.

- The iterative route is suggested as a possibility and initial test does not indicate any amendments. However this route needs further validation by implementation to an iterative design process.
- The methodology has a potential to contribute to Knowledge-base creation. In a commercial application this option can convert the findings into the commercial solution for structural analysis to be reused in similar product development projects.
- The opportunity to propose alternative methodologies using different design tools and combinations can be further explored and assessed against the QFD bases methodology for improvements and optimisation

7.4 Conclusion

This research enhances the mutual understanding between two fields of design and structural analysis and improve the extent and the quality of contribution of structural analysis process for design of the mechanical product. Therefore this research investigates the question of:

> *"How is it possible to increase the effectiveness of structural analysis by its interactive and systematic integration within the product design process?"*

The significance of this question can only be understood knowing the conventional structural analysis practice in industry:

- In a typical commercial design environment the process of the structural analysis is started near to the finalised state of the structure, when many aspects such as fabrication, drive mechanism, packaging etc. have already been decided. This type of structural analysis, termed as Design Verification, and follows the Design-Commitment-Validation approach as discussed in Table 3-1. All the downside effects of the DCV approach as outlined in Chapter 3, including the risk of error propagation, and the cost and inefficiency of error hunting in the finalised design, are applicable to this practice.
- Assuming the design environment is committed to the application of V&V, the correlation process starts following the outcomes of experimental measurements. It is very common that the correlation exercise shows a discrepancy that in turn

follows by error quantification process. This practice can be cumbersome, inefficient and frustrating, and in many occasions unachievable with the product in its finalised stage ready for the market delivery.

- The finalised product leaves the structural analysis with only limited options to optimise the required function. The limitation leads to random change of either design Variable Input Parameters or product specification until the practice converges to the acceptable level of safety. This practice leads to an exhausting process with no clear tractability, which in many occasions reaches the conclusion only due to the market pressure.
- Moreover the structural analysis process in this stage normally targets the most significant or common aspect of the structural failure and optimise the structure towards an ideal performance. In the situations that more than one failure modes is expected, the response of the Variable Input Parameters and their interdependencies require more comprehensive process.

These malfunctions and complications in the conventional process usually abort the structural analysis pre-maturely without a definitive answerer, considering the market pressure for the ready-to-commission design.

The QFD-Based Design Integrated Structural Analysis Methodology aims to enhance the capability of the structural analysis for the product design application by finding a solution to the above outstanding issues. The functionality of the proposed methodology, proven via an industrial case-study shows its potential for expansion in the range of commercial application.

Despite the proposed methodology main effect is in productivity of the structural analysis in design it also contributes to the time efficiency of the process. This methodology was practised during the design and development of the company partner of the project, new Access Platform product HR28. The design and development of this product is conducted for the period of 3 years, in comparison with smaller product in the family HR21 that took over 5 years with company’s conventional practice.

Appendix I – Stress invariants

The concept is better described in an infinitesimal tetrahedron with a known stress on the reference planes, as shown in the figure. Inclined face of ABC can be considered as principle plane if the principal stress σ be in the normal direction to this plane $\bar{n}$, having direction cosines $a_{nx}, a_{ny}, and\ a_{nz}$. In the absence of body and inertia force the Newton's second law of motion in Z-direction can be applied as:

$$\sigma.ABC.a_{nz} - \sigma_z.AOB - \tau_{yz}.AOC - \tau_{xz}.BOC = 0$$

Dividing by the area ABC and similarly for other directions of X and Y:

$$(\sigma_x - \sigma).a_{nx} + \tau_{xy}.a_{ny} + \tau_{xz}.a_{nz} = 0$$

$$\tau_{xy}.a_{nx} + (\sigma_y - \sigma).a_{ny} + \tau_{yz}.a_{nz} = 0$$

$$\tau_{xz}.a_{nx} + \tau_{yz}.a_{ny} + (\sigma_z - \sigma).a_{nz} = 0$$

Therefore three simultaneous homogeneous equations can be written in a matrix format as:

$$\begin{bmatrix} \sigma_x - \sigma & \tau_{xy} & \tau_{xz} \\ \tau_{xy} & \sigma_y - \sigma & \tau_{yz} \\ \tau_{xz} & \tau_{yz} & \sigma_z - \sigma \end{bmatrix} \begin{bmatrix} a_{nx} \\ a_{ny} \\ a_{nz} \end{bmatrix} = \begin{bmatrix} 0 \\ 0 \\ 0 \end{bmatrix}$$

By using Cramer's rule:

$$a_{nx} = \frac{\begin{bmatrix} 0 & \tau_{xy} & \tau_{xz} \\ 0 & \sigma_y - \sigma & \tau_{yz} \\ 0 & \tau_{yz} & \sigma_z - \sigma \end{bmatrix}}{\begin{bmatrix} \sigma_x - \sigma & \tau_{xy} & \tau_{xz} \\ \tau_{xy} & \sigma_y - \sigma & \tau_{yz} \\ \tau_{xz} & \tau_{yz} & \sigma_z - \sigma \end{bmatrix}}$$

a_{nx} will be zero unless the denominator in the preceding equation is zero so as to permit an indeterminate result. But all the other direction cosines can not be zero, because:

$$a_{nx}^2 + a_{ny}^2 + a_{nz}^2 = 1$$

Expanding the determinant of the denominator matrix produces a cubic equation:

$$\sigma^3 - I_1\sigma^2 + I_2\sigma - I_3 = 0$$

where:

$$\sigma_x + \sigma_y + \sigma_z = I_1 = First\ Invariants\ of\ stress$$

$$\sigma_x\sigma_y + \sigma_y\sigma_z + \sigma_x\sigma_z - \tau_{xy}^2 - \tau_{yz}^2 - \tau_{xz}^2 = I_2 = Second\ Invariant\ of\ stress$$

$$\sigma_x\sigma_y\sigma_z - \sigma_x\tau_{yz}^2 - \sigma_y\tau_{xz}^2 - \sigma_z\tau_{xy}^2 + 2\tau_{xy}\tau_{yz}\tau_{xz} = I_3 = Third\ Invariant\ of\ stress$$

The cubic equation can be solved by Newton-Raphson approximation method. If the approximated root for the above equation chosen as σ_i , then the better approximates can be estimated by:

$$\sigma_{i+1} = \sigma_i - \frac{f(\sigma_i)}{f'(\sigma_i)}\ , \qquad i = 0,1,2, \ldots$$

The iteration process may be continued until the between the two successive roots is not appreciable as demanded by the accuracy. Thus the three principal stresses, σ_1, σ_2, σ_3 can be determined.

Three direction cosines can be computed by substituting back. Then the non-trivial solution for σ_1 is:

$$a_{nx1} = \frac{A}{\sqrt{A^2 + B^2 + C^2}}\ , \qquad a_{ny1} = \frac{B}{\sqrt{A^2 + B^2 + C^2}}\ , \qquad a_{nz1} = \frac{C}{\sqrt{A^2 + B^2 + C^2}}$$

where

$$A = \begin{vmatrix} \sigma_y - \sigma_1 & \tau_{yz} \\ \tau_{yz} & \sigma_2 - \sigma_1 \end{vmatrix} = cofactor\ of\ first\ term\ of\ determined\ D$$

$$B = -\begin{vmatrix} \tau_{xy} & \tau_{yz} \\ \tau_{xy} & \sigma_2 - \sigma_1 \end{vmatrix} = cofactor\ of\ second\ term\ of\ determined\ D$$

$$C = \begin{vmatrix} \tau_{xy} & \sigma_y - \sigma_1 \\ \tau_{xz} & \tau_{yz} \end{vmatrix} = cofactor\ of\ third\ term\ of\ determined\ D$$

The direction cosine for other principal stresses can be determined similarly.

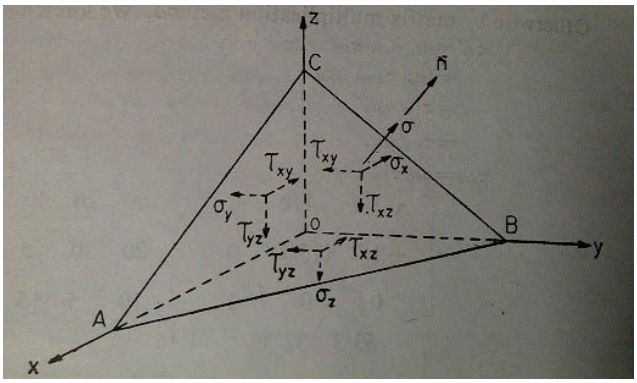

Appendix II – Maximum shearing stress

maximum shearing stress can be specified by choosing the axis of coordinates 0 xyz in the direction of the normal, $\bar{n}$, along the principal stresses in an arbitrary area whose direction cosines are $a_{nx}, a_{ny}\ and\ a_{nz}$. The normal stress in this area is:

$$\sigma_n = \sigma_1 a_{nx}^2 + \sigma_2 a_{ny}^2 + \sigma_3 a_{nz}^2$$

The resultant stress is:

$$\sigma_R^2 = \sigma_n^2 + \tau_{ns}^2$$

$$\therefore \tau_{ns}^2 = \sigma_R^2 - \sigma_n^2$$

Knowing the above equation and having:

$$\sigma_R^2 = \sigma_1^2 a_{nx}^2 + \sigma_2^2 a_{ny}^2 + \sigma_3^2 a_{nz}^2$$

$$\therefore \tau_{ns}^2 = \left(\sigma_1^2 a_{nx}^2 + \sigma_2^2 a_{ny}^2 + \sigma_3^2 a_{nz}^2\right) - \left(\sigma_1 a_{nx}^2 + \sigma_2 a_{ny}^2 - \sigma_3 a_{nz}^2\right)$$

For the shear stress, τ_{ns} , to be maximum or minimum:

$$\frac{\partial \tau_{ns}^2}{\partial a_{nx}} = \frac{2\tau_{ns}\,\partial \tau_{ns}}{\partial a_{nx}} = 0$$

$$\frac{\partial \tau_{ns}^2}{\partial a_{ny}} = \frac{2\tau_{ns}\,\partial \tau_{ns}}{\partial a_{ny}} = 0$$

∴ Either:

$$\tau_{ns} = 0\ , \qquad \frac{\partial \tau_{ns}}{\partial a_{nx}} = 0\ , \qquad \frac{\partial \tau_{ns}}{\partial a_{ny}} = 0$$

The first term of above equation happens at principal area whereas the second and third terms, with the condition of $\sigma_1 \neq \sigma_2 \neq \sigma_3$ lead to:

$$\left\{\sigma_1 - \sigma_3 - 2\left[(\sigma_1 - \sigma_3)a_{nx}^2 + (\sigma_2 - \sigma_3)a_{ny}^2\right]\right\}a_{nx} = 0$$

$$\left\{\sigma_2 - \sigma_3 - 2\left[(\sigma_1 - \sigma_3)a_{nx}^2 + (\sigma_2 - \sigma_3)a_{ny}^2\right]\right\}a_{ny} = 0$$

Therefore $a_{nx} = a_{ny} = 0\ and\ a_{nz} = 1$ must be dropped since it gives a principal area lying in the plane oxy. Three feasible cases are:

$$a_{nx} \neq 0, a_{ny} = 0, \quad a_{nx} = 0, a_{ny} \neq 0, \quad a_{nx} \neq 0, a_{ny} \neq 0$$

The first and second case gives:

$$a_{nx} = \pm\frac{1}{\sqrt{2}}\ , a_{ny} = 0\ , a_{nz} = \pm\frac{1}{\sqrt{2}}$$

$$a_{ny} = \pm\frac{1}{\sqrt{2}}\ , a_{nx} = 0\ , a_{nz} = \pm\frac{1}{\sqrt{2}}$$

The third condition is impossible since cancelling $a_{nx} and\ a_{ny}$ and subtracting the resulting equations from each other get $\sigma_1 = \sigma_2$ which contrary to the assumption$\sigma_1 \neq \sigma_2 \neq \sigma_3$. Repeating the analysis for a_{ny} instead of a_{nz} gives:

$$a_{nx} = \pm\frac{1}{\sqrt{2}}\ , a_{ny} = \pm\frac{1}{\sqrt{2}}\ , a_{nz} = 0$$

Each of these two solutions determines the area passing through one of the coordinate axes and inclined to the other at angles of 45° and 135°. Substituting back:

$$\tau_{ns}^2 = \frac{\sigma_1^2 - \sigma_3^2}{2} - \left(\frac{\sigma_1 + \sigma_3}{2}\right)^2 = \left(\frac{\sigma_1 - \sigma_3}{2}\right)^2$$

Eq. 2-9 along with the remaining two solutions give:

$$\tau_{ns}(\max) = \pm\left(\frac{\sigma_1-\sigma_3}{2}\right),\ \tau_{ns}(\max) = \pm\left(\frac{\sigma_1-\sigma_2}{2}\right),\ \tau_{ns}(\max) = \pm\left(\frac{\sigma_2-\sigma_3}{2}\right)$$

Therefore the direction cosines for planes of $\tau_{ns}(\max)$ and $\tau_{ns}(\min)$ are given in the table and plane of maximum shear stress are shown in the figure.

	$\tau_{ns}(\max)$			$\tau_{ns}(\min)$		
a_{nx}	$\pm\frac{1}{\sqrt{2}}$	0	$\pm\frac{1}{\sqrt{2}}$	0	0	±1
a_{ny}	$\pm\frac{1}{\sqrt{2}}$	$\pm\frac{1}{\sqrt{2}}$	0	0	±1	0
a_{nz}	0	$\pm\frac{1}{\sqrt{2}}$	$\pm\frac{1}{\sqrt{2}}$	±1	0	0

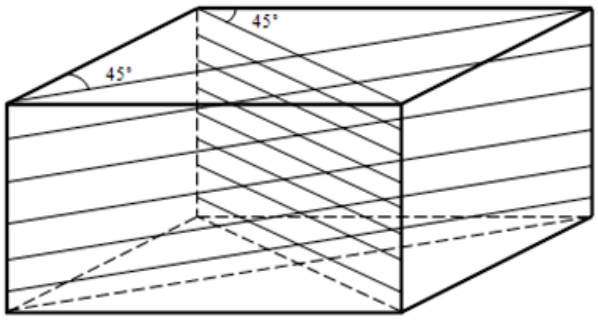

Appendix III – Principal strains

The problem of computing the extreme value of the strain components reduces to the determination of the initial directions $(a_{x\prime x}, a_{x\prime y}, a_{x\prime z})$ for which $\epsilon_{x\prime x\prime}$ under the restriction:

$$a_{x\prime x}{}^2 + a_{x\prime y}{}^2 + a_{x\prime z}{}^2 = 1$$

The extreme values of $\epsilon_{x\prime x\prime}$ are called the principal strains and the initial directions along which $\epsilon_{x\prime x\prime}$ attains stationary values are called the principal directions of strain.

Using $\frac{\partial \epsilon_{x\prime x\prime}}{\partial a_{x\prime x}} = \frac{\partial \epsilon_{x\prime x\prime}}{\partial a_{x\prime y}} = \frac{\partial \epsilon_{x\prime x\prime}}{\partial a_{x\prime z}} = 0$ gives:

$$2\epsilon_x \mathrm{a_{x\prime x}} + \gamma_{\mathrm{xy}}\, \mathrm{a_{x\prime y}} + \gamma_{\mathrm{xz}} \mathrm{a_{x\prime z}} = 0$$

$$\gamma_{\mathrm{xy}}\, \mathrm{a_{x\prime x}} + 2\epsilon_y \mathrm{a_{x\prime y}} + \gamma_{\mathrm{yz}} \mathrm{a_{x\prime z}} = 0$$

$$\gamma_{\mathrm{xz}} \mathrm{a_{x\prime x}} + \gamma_{\mathrm{yz}}\, \mathrm{a_{x\prime y}} + 2\epsilon_z \mathrm{a_{x\prime z}} = 0$$

Which may be written:

$$\begin{bmatrix} \epsilon_x & \frac{\gamma_{\mathrm{xy}}}{2} & \frac{\gamma_{\mathrm{xz}}}{2} \\ \frac{\gamma_{\mathrm{xy}}}{2} & \epsilon_y & \frac{\gamma_{\mathrm{yz}}}{2} \\ \frac{\gamma_{\mathrm{xz}}}{2} & \frac{\gamma_{\mathrm{yz}}}{2} & \epsilon_z \end{bmatrix} \begin{Bmatrix} \mathrm{a_{x\prime x}} \\ \mathrm{a_{x\prime y}} \\ \mathrm{a_{x\prime z}} \end{Bmatrix} = \begin{Bmatrix} 0 \\ 0 \\ 0 \end{Bmatrix}$$

The non-trivial solution may be obtained by determining the eigen-value of the strain matrix if $\epsilon_i, i = 1, 2, 3$ be the eigen values of the strain matrix ϵ_{ij} then the characteristic equation of the eigen-value of the determinant would be $\left|\epsilon_{ij} - \epsilon_i \mathrm{I}\right| = 0$, where I is the unit matrix.

$$\begin{vmatrix} \epsilon_x - \epsilon_i & \frac{\gamma_{\mathrm{xy}}}{2} & \frac{\gamma_{\mathrm{xz}}}{2} \\ \frac{\gamma_{\mathrm{xy}}}{2} & \epsilon_y - \epsilon_i & \frac{\gamma_{\mathrm{yz}}}{2} \\ \frac{\gamma_{\mathrm{xz}}}{2} & \frac{\gamma_{\mathrm{yz}}}{2} & \epsilon_z - \epsilon_i \end{vmatrix} = 0$$

Solving the determinant gives:

$$\epsilon_i{}^3 - J_1 \epsilon_i{}^2 + J_2 \epsilon_i - J_3 = 0$$

Where:

$$J_1 = \epsilon_x + \epsilon_y + \epsilon_z = first\ invariant\ of\ strain$$

$$J_2 = \epsilon_x\epsilon_y + \epsilon_y\epsilon_z + \epsilon_z\epsilon_x - \frac{\gamma_{xy}{}^2}{4} - \frac{\gamma_{yz}{}^2}{4} - \frac{\gamma_{xz}{}^2}{4} = second\ invariant\ of\ strain$$

$$J_3 = \begin{vmatrix} \epsilon_x & \frac{\gamma_{xy}}{2} & \frac{\gamma_{xz}}{2} \\ \frac{\gamma_{xy}}{2} & \epsilon_y & \frac{\gamma_{yz}}{2} \\ \frac{\gamma_{xz}}{2} & \frac{\gamma_{yz}}{2} & \epsilon_z \end{vmatrix} = third\ invariant\ of\ strain$$

To change the sense of the angle requires only reversing the sign of Eq. 2-48. Thus:

Eq. 7-1

$$\varphi_{P,Q} = -\theta = \frac{1}{2}\tan^{-1}\left(\frac{2\varepsilon_2 - \varepsilon_1 - \varepsilon_3}{\varepsilon_1 - \varepsilon_3}\right)$$

Appendix IV - List of failure modes

1. Force and/or temperature induced elastic deformation
2. Yielding
3. Brinnelling
4. Ductile Rupture
5. Brittle Fracture
6. Fatigue
    a. High-cycle fatigue
    b. Low-cycle fatigue
    c. Thermal fatigue
    d. Surface fatigue
    e. Impact fatigue
    f. Corrosion fatigue
    g. Fretting fatigue
7. Corrosion
    a. Direct chemical attack
    b. Galvanic corrosion
    c. Crevice corrosion
    d. Pitting corrosion
    e. Intergranular corrosion
    f. Selective corrosion
    g. Erosion corrosion
    h. Cavitation corrosion
    i. Hydrogen damage
    j. Biological corrosion
    k. Stress corrosion
    a. Fretting fatigue
    b. Fretting wear
    c. Fretting corrosion
8. Wear
    a. Adhesive wear
    b. Abrasive wear
    c. Corrosive wear
    d. Surface fatigue wear
    e. Deformation wear
    f. Impact wear
    g. Fretting wear
9. Impact
    a. Impact fracture
    b. Impact deformation
    c. Impact wear
    d. Impact fretting
    e. Impact fatigue
10. Fretting
11. Creep
12. Thermal relaxation
13. Stress rupture
14. Thermal shock
15. Galling and seizure
16. Spalling
17. Radiation
18. Buckling
19. Creep buckling
20. Stress corrosion
21. Corrosion wear
22. Combined creep fatigue

Appendix V - Nodal degrees of freedom convention

Degrees of freedom Except for axisymmetric elements, the degrees of freedom are always referred to as follows:

1) x-displacement
2) y-displacement
3) z-displacement
4) Rotation about the x-axis, in radians
5) Rotation about the y-axis, in radians
6) Rotation about the z-axis, in radians
7) Warping amplitude (for open-section beam elements)
8) Pore pressure, hydrostatic fluid pressure, or acoustic pressure
9) Electric potential
10) Connector material flow (units of length)
11) Temperature (or normalized concentration in mass diffusion analysis)
12) Second temperature (for shells or beams)
13) Third temperature (for shells or beams)
14) Etc.

Here the x-, y-, and z-directions coincide with the global X-, Y-, and Z-directions, respectively; however, if a local transformation is defined at a node they coincide with the local directions defined by the transformation. A maximum of 20 temperature values (degrees of freedom 11 through 30) can be defined for shell or beam elements in Abaqus/Standard. The displacement and rotation degrees of freedom in axisymmetric elements are referred to as follows:

1) r-displacement
2) z-displacement

5) Rotation about the z-axis (for axisymmetric elements with twist), in radians

6) Rotation in the r–z plane (for axisymmetric shells), in radians

Here the r- and z-directions coincide with the global X- and Y-directions, respectively; however, if a local transformation is defined at a node, they coincide with the local directions defined by the transformation.

Appendix VI – Principal strain angle in rosette

The physical direction of the acute angle given by either Eq. 2-48 or Eq. 7-1 is always anticlockwise if positive, and clockwise if negative. The only difference is that θ is measured from the principal axis to Grid 1, while φ is measured from Grid 1 to the principal axis. Since $\tan 2\varphi \equiv \tan 2(\varphi + 90)$, the calculated angle can refer to either principal axis. This ambiguity can readily be resolved (for the rectangular rosette) by application of the following simple rules:

- if $\varepsilon_1 > \varepsilon_3$, then $\varphi_{P,Q} = \varphi_P$
- if $\varepsilon_1 < \varepsilon_3$, then $\varphi_{P,Q} = \varphi_Q$
- if $\varepsilon_1 = \varepsilon_3$ and $\varepsilon_2 < \varepsilon_1$, then $\varphi_{P,Q} = \varphi_P = -45^\circ$
- if $\varepsilon_1 = \varepsilon_3$ and $\varepsilon_2 > \varepsilon_1$, then $\varphi_{P,Q} = \varphi_P = 45^\circ$
- if $\varepsilon_1 = \varepsilon_2 = \varepsilon_3$, then $\varphi_{P,Q}$ is indeterminate (equal biaxial strain).

Appendix VII – Benchmark parts drawings

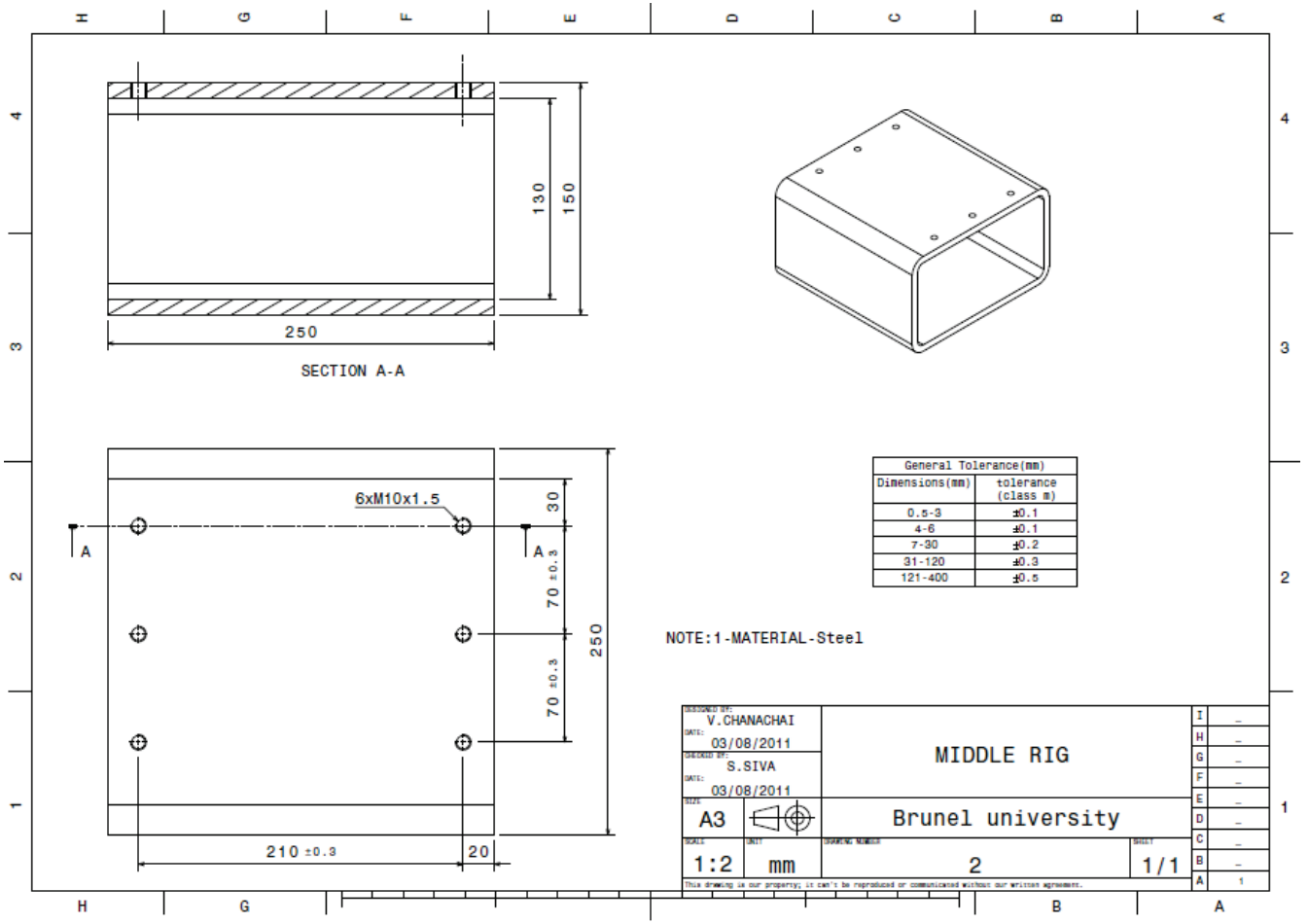

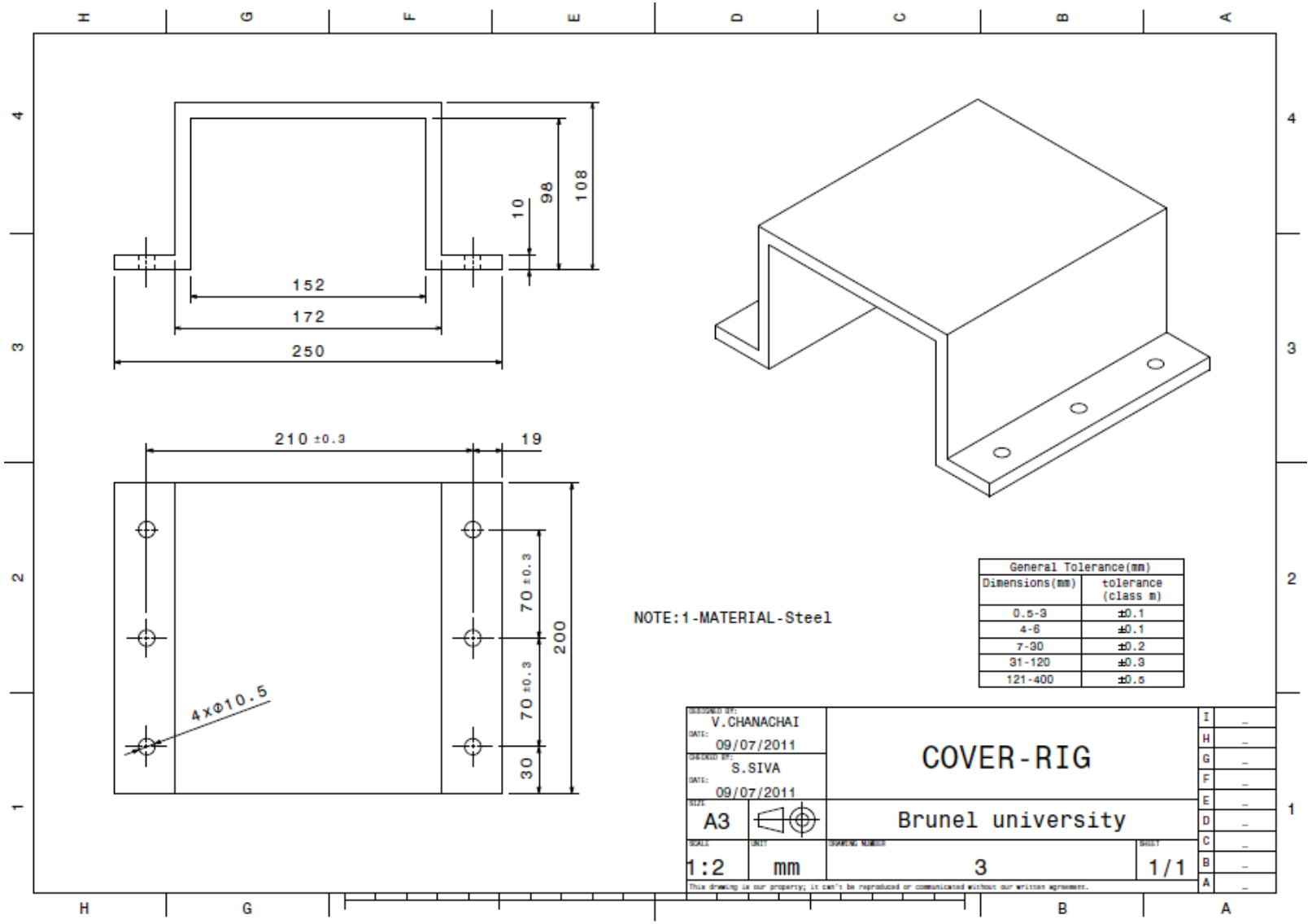
H
G
F
E
D
C
B
A
4
3
2
1
10
98
108
152
172
250
210 ±0.3
19
70 ±0.3
70 ±0.3
200
30
4XΦ10.5
NOTE:1-MATERIAL-Steel
General Tolerance(mm)
Dimensions(mm)
tolerance (class m)
0.5-3
±0.1
4-6
±0.1
7-30
±0.2
31-120
±0.3
121-400
±0.5
DESIGNED BY: V.CHANACHAI
DATE: 09/07/2011
CHECKED BY: S.SIVA
DATE: 09/07/2011
SIZE A3
SCALE 1:2
UNIT mm
DRAWING NUMBER 3
SHEET 1/1
COVER-RIG
Brunel university
This drawing is our property; it can't be reproduced or communicated without our written agreement.
I
H
G
F
E
D
C
B
A

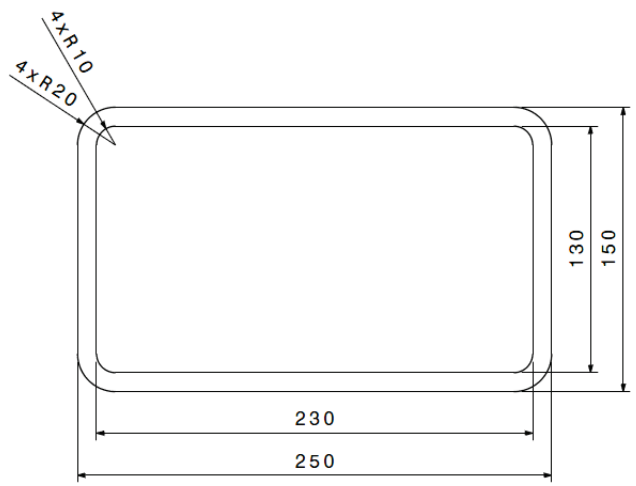

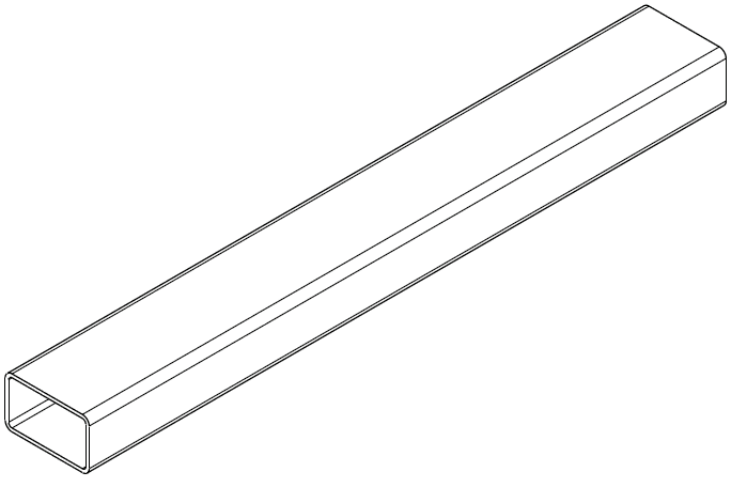

NOTE:1-MATERIAL-Steel
2-Lenght= 1900mm.

General Tolerance(mm)	
Dimensions(mm)	tolerance (class m)
0.5-3	±0.1
4-6	±0.1
7-30	±0.2
31-120	±0.3
121-400	±0.5

DESIGNED BY: V.CHANACHAI DATE: 09/07/2011	LOWER STAND		
CHECKED BY: S.SIVA DATE: 09/07/2011			
SIZE A3	Brunel university		
SCALE 1:2	UNIT mm	DRAWING NUMBER 3	SHEET 1/1

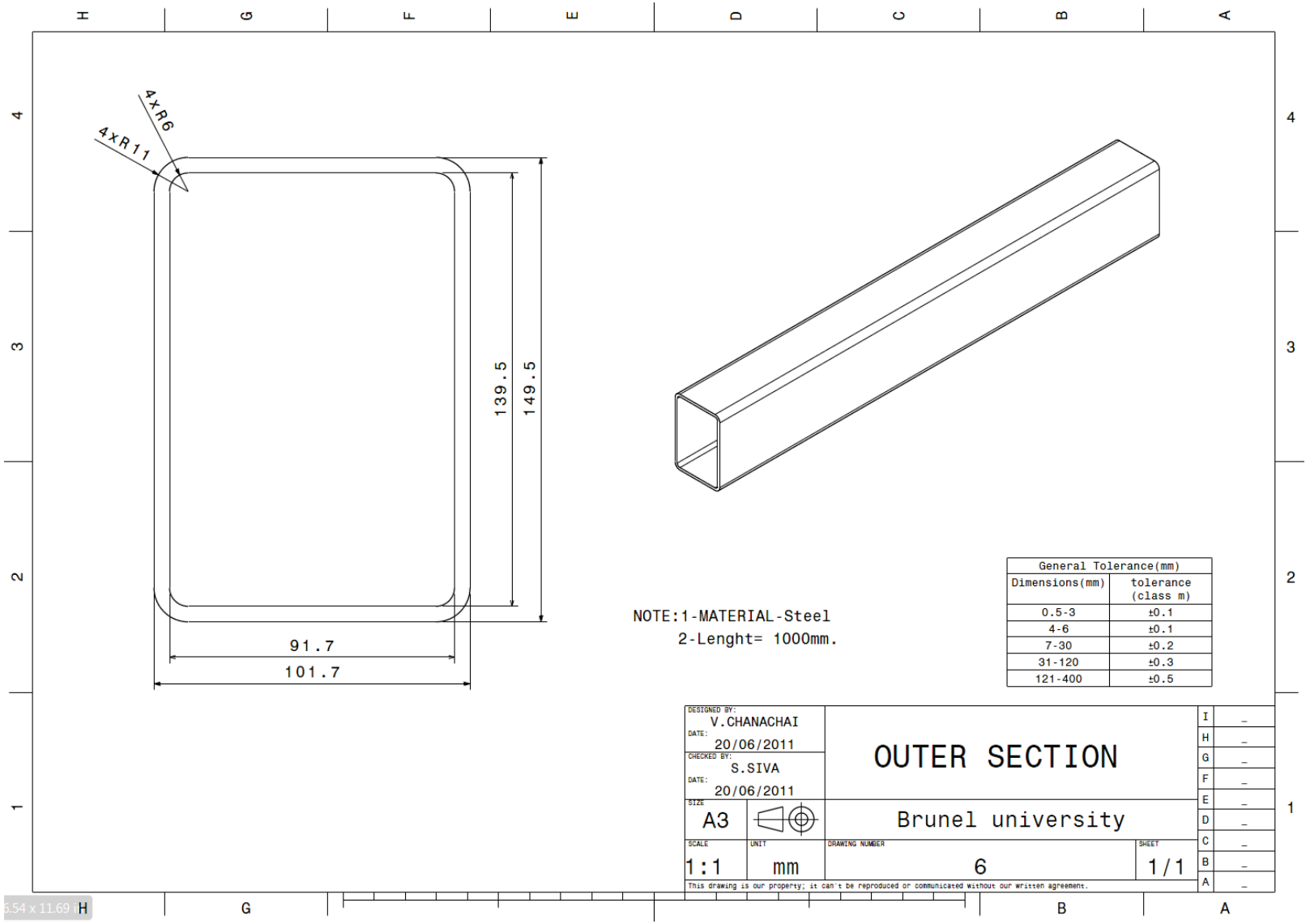

NOTE:1-MATERIAL-Steel
2-Lenght= 1000mm.

General Tolerance(mm)	
Dimensions(mm)	tolerance (class m)
0.5-3	±0.1
4-6	±0.1
7-30	±0.2
31-120	±0.3
121-400	±0.5

DESIGNED BY: V.CHANACHAI		OUTER SECTION	
DATE: 20/06/2011			
CHECKED BY: S.SIVA			
DATE: 20/06/2011			
SIZE A3		Brunel university	
SCALE 1:1	UNIT mm	DRAWING NUMBER 6	SHEET 1/1

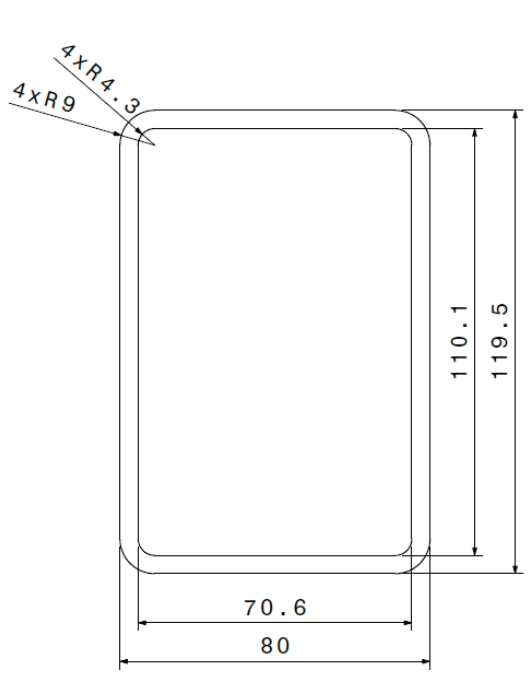

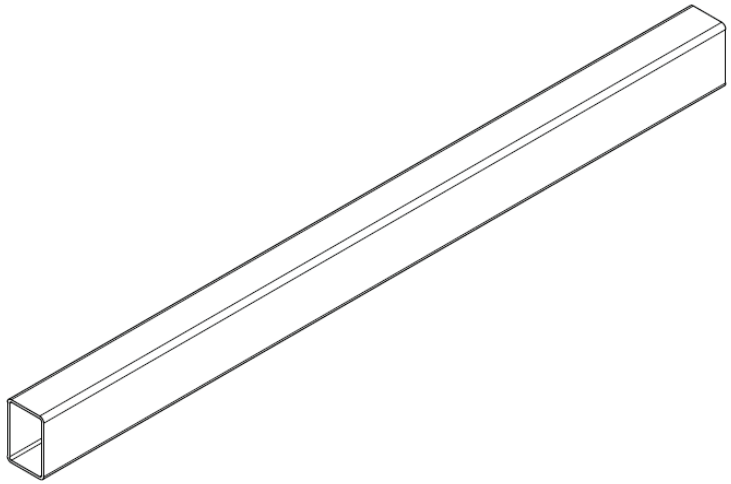

NOTE:1-MATERIAL-Steel
2-Lenght= 1493mm.

General Tolerance(mm)	
Dimensions(mm)	tolerance (class m)
0.5-3	±0.1
4-6	±0.1
7-30	±0.2
31-120	±0.3
121-400	±0.5

DESIGNED BY: V.CHANACHAI DATE: 20/06/2011	SMALL SECTION		
CHECKED BY: S.SIVA DATE: 20/06/2011			
SIZE A3	Brunel university		
SCALE 1:1	UNIT mm	DRAWING NUMBER 5	SHEET 1/1

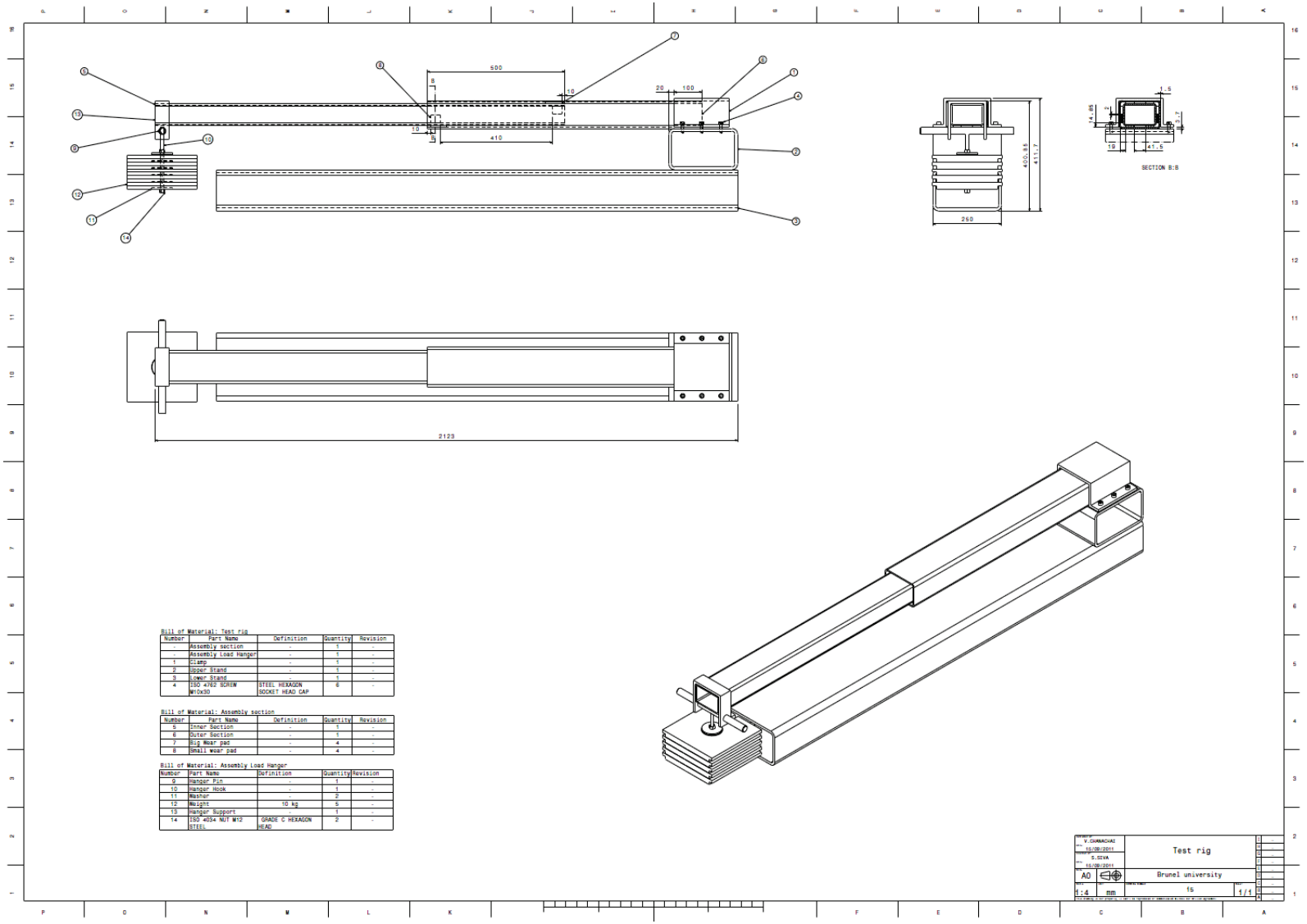

Bill of Material: Test rig

Number	Part Name	Definition	Quantity	Revision
-	Assembly section	-	1	-
-	Assembly Load Hanger	-	1	-
1	Clamp	-	1	-
2	Upper Stand	-	1	-
3	Lower Stand	-	1	-
4	ISO 4762 SCREW M10x30	STEEL HEXAGON SOCKET HEAD CAP	6	-

Bill of Material: Assembly section

Number	Part Name	Definition	Quantity	Revision
5	Inner Section	-	1	-
6	Outer Section	-	1	-
7	Big Wear pad	-	4	-
8	Small Wear pad	-	4	-

Bill of Material: Assembly Load Hanger

Number	Part Name	Definition	Quantity	Revision
9	Hanger Pin	-	1	-
10	Hanger Hook	-	1	-
11	Washer	-	2	-
12	Weight	10 kg	5	-
13	Hanger Support	-	1	-
14	ISO 4034 NUT M12 STEEL	GRADE C HEXAGON HEAD	2	-

V.CHANACHAI 15/09/2011	Test rig	
S.SEVA 15/09/2011		
A0	Brunel university	
1:4 mm	15	1/1

Appendix VIII - Size of the FEA Problem with Different Elements

```
Abaqus 6.10-EF1                                    Date 16-Dec-2011
Time 10:15:31
   For use at BRUNEL UNIVERSITY under license from Dassault Systemes
or its subsidiary.

C3D8 50 kg, 500 mm overlap

P R O B L E M   S I Z E

NUMBER OF ELEMENTS IS                                    18945   NUMBER
OF ELEMENTS DEFINED BY THE USER AND *TIE       15057
NUMBER OF INTERNAL ELEMENTS GENERATED FOR CONTACT      3888
NUMBER OF NODES IS                                    48930
NUMBER OF NODES DEFINED BY THE USER                   29633
NUMBER OF INTERNAL NODES GENERATED BY THE PROGRAM     19297
TOTAL NUMBER OF VARIABLES IN THE MODEL               130524
(DEGREES OF FREEDOM PLUS MAX NO. OF ANY LAGRANGE MULTIPLIER
VARIABLES. INCLUDE *PRINT,SOLVE=YES TO GET THE ACTUAL NUMBER.)

       JOB TIME SUMMARY
       USER TIME (SEC)      =   291.30
       SYSTEM TIME (SEC)    =   3.5000
       TOTAL CPU TIME (SEC) =   294.80
       WALLCLOCK TIME (SEC) =        306

---------------------------------------------------------------------

Abaqus 6.10-EF1                                    Date 15-Dec-2011
Time 16:07:06
   For use at BRUNEL UNIVERSITY under license from Dassault Systemes
or its subsidiary.

C3D8I 50 kg, 500 mm overlap

P R O B L E M   S I Z E

NUMBER OF ELEMENTS IS                                    18945
NUMBER OF ELEMENTS DEFINED BY THE USER AND *TIE       15057
NUMBER OF INTERNAL ELEMENTS GENERATED FOR CONTACT      3888
NUMBER OF NODES IS                                   112690
NUMBER OF NODES DEFINED BY THE USER                   29633
NUMBER OF INTERNAL NODES GENERATED BY THE PROGRAM     83057
TOTAL NUMBER OF VARIABLES IN THE MODEL               296300
(DEGREES OF FREEDOM PLUS MAX NO. OF ANY LAGRANGE MULTIPLIER
VARIABLES. INCLUDE *PRINT,SOLVE=YES TO GET THE ACTUAL NUMBER.)

       JOB TIME SUMMARY
       USER TIME (SEC)      =   341.80
       SYSTEM TIME (SEC)    =   3.6000
       TOTAL CPU TIME (SEC) =   345.40
       WALLCLOCK TIME (SEC) =        358




Abaqus 6.10-EF1                                    Date 16-Dec-2011
Time 11:14:26
```

For use at BRUNEL UNIVERSITY under license from Dassault Systemes or its subsidiary.

C3D20 50 kg, 500 mm overlap

P R O B L E M S I Z E

NUMBER OF ELEMENTS IS	18945
NUMBER OF ELEMENTS DEFINED BY THE USER AND *TIE	15057
NUMBER OF INTERNAL ELEMENTS GENERATED FOR CONTACT	3888
NUMBER OF NODES IS	113002
NUMBER OF NODES DEFINED BY THE USER	93705
NUMBER OF INTERNAL NODES GENERATED BY THE PROGRAM	19297
TOTAL NUMBER OF VARIABLES IN THE MODEL	322740

(DEGREES OF FREEDOM PLUS MAX NO. OF ANY LAGRANGE MULTIPLIER VARIABLES. INCLUDE *PRINT,SOLVE=YES TO GET THE ACTUAL NUMBER.)

JOB TIME SUMMARY
USER TIME (SEC) = 1818.9
SYSTEM TIME (SEC) = 11.700
TOTAL CPU TIME (SEC) = 1830.6
WALLCLOCK TIME (SEC) = 1846

Abaqus 6.10-EF1 Date 15-Dec-2011 Time 16:18:20

For use at BRUNEL UNIVERSITY under license from Dassault Systemes or its subsidiary.

shell S4R 50 kg, 500 mm overlap

P R O B L E M S I Z E

NUMBER OF ELEMENTS IS	18945
NUMBER OF ELEMENTS DEFINED BY THE USER AND *TIE	15057
NUMBER OF INTERNAL ELEMENTS GENERATED FOR CONTACT	3888
NUMBER OF NODES IS	36074
NUMBER OF NODES DEFINED BY THE USER	16777
NUMBER OF INTERNAL NODES GENERATED BY THE PROGRAM	19297
TOTAL NUMBER OF VARIABLES IN THE MODEL	130524

(DEGREES OF FREEDOM PLUS MAX NO. OF ANY LAGRANGE MULTIPLIER VARIABLES. INCLUDE *PRINT,SOLVE=YES TO GET THE ACTUAL NUMBER.)

JOB TIME SUMMARY
USER TIME (SEC) = 282.20
SYSTEM TIME (SEC) = 2.5000
TOTAL CPU TIME (SEC) = 284.70
WALLCLOCK TIME (SEC) = 295

Shell S4 50 kg, 500 mm overlap

P R O B L E M S I Z E

NUMBER OF ELEMENTS IS	18945
NUMBER OF ELEMENTS DEFINED BY THE USER AND *TIE	15057
NUMBER OF INTERNAL ELEMENTS GENERATED FOR CONTACT	3888
NUMBER OF NODES IS	36074
NUMBER OF NODES DEFINED BY THE USER	16777
NUMBER OF INTERNAL NODES GENERATED BY THE PROGRAM	19297
TOTAL NUMBER OF VARIABLES IN THE MODEL	130524

(DEGREES OF FREEDOM PLUS MAX NO. OF ANY LAGRANGE MULTIPLIER VARIABLES. INCLUDE *PRINT,SOLVE=YES TO GET THE ACTUAL NUMBER.)

JOB TIME SUMMARY

USER TIME (SEC)	=	342.40
SYSTEM TIME (SEC)	=	3.3000
TOTAL CPU TIME (SEC)	=	345.70
WALLCLOCK TIME (SEC)	=	386

Appendix IX- Strain gauge specification

Manufacturer: Tokyo Sokki Kenkyujo co. Ltd.

	Type	Gauge size (mm)		Backing (mm)	Resistance Ω	Gauge Factor		
		Length	Width	φ		1	2	3
 FRA-3	FRA-3-350-11	3	2	11	350	2.10	2.10	2.10

Appendix X- Specification NI cDAQ-9172

These specifications are for the NI cDAQ-9172 chassis only. These specifications are typical at 25 °C unless otherwise noted. For the C Series I/O module specifications, refer to the documentation for the C Series I/O modules you are using.

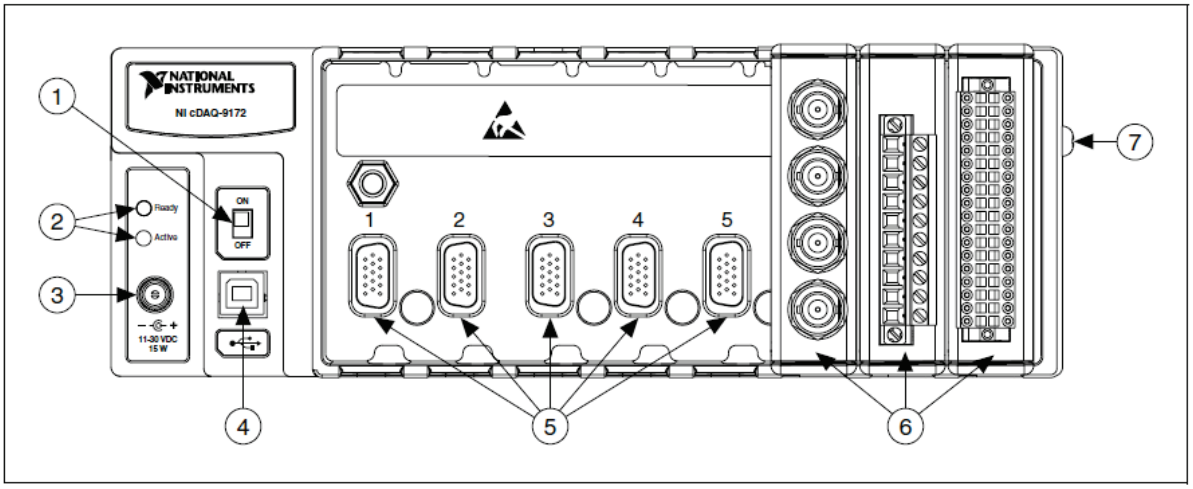

1	Power Switch	5	Empty Module Slots
2	Ready/Active LEDs	6	Installed C Series I/O Modules
3	Power Connector	7	Screw for Ground Connection
4	USB Connector		

Analogue Input

Input FIFO size ..... 2,047 samples

Sample rate1

Maximum..... 3.2 MS/s (multi-channel, aggregate)

Minimum ..... 0 S/s

Timing accuracy ..... 50 ppm of sample rate

Timing resolution ..... 50 ns

Number of channels supported .....Determined by the C Series I/O modules

Analogue Output

Numbers of channels supported

In hardware-timed task 16

In non-hardware-timed task .....Determined by the C Series I/O modules

Maximum update rate ..... 1.6 MS/s (multi-channel, aggregate)

Timing accuracy..... 50 ppm of sample rate

Timing resolution ..... 50 ns

Output FIFO size..... 8,191 samples shared among channels used

AO waveform modes.....Non-periodic waveform,

periodic waveform regeneration mode from onboard

memory, periodic waveform regeneration from host

buffer including dynamic update

Power Requirements

You must use a National Electric Code (NEC) Class 2 power source with the NI cDAQ-9172 chassis.

Note: Some I/O modules have additional power requirements. For more information about

C Series I/O module(s) power requirements refer to documentation included with the C Series I/O module(s).

Note: Sleep mode for C Series I/O modules is not supported in the NI cDAQ-9172.

Input voltage range..... 11 V to 30 V

Maximum required input power ..... 15 W

Power input connector .....DC input jack with locking, threaded ring 0.8

in. (2 mm) center pin

Power input mating connector ..... Switchcraft S760K

Appendix XI - Specification NI 9236

8-Channel, 24-Bit Quarter-Bridge Analogue Input Module

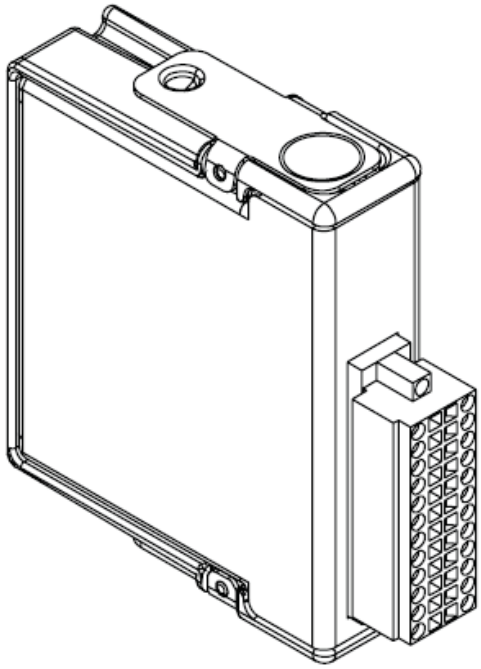

The following specifications are typical for the range –40 to 70 °C unless otherwise noted.

Input Characteristics

Number of channels.....8 analogue input channels

Quarter-bridge completion ..... 350 Ω, 10 ppm/°C max

ADC resolution..... 24 bits

Type of ADC.....Delta-Sigma (with analogue pre-filtering)

Sampling mode .....Simultaneous

Internal master time-base (*fM*)

Frequency .....12.8 MHz

Accuracy.....±100 ppm max

Accuracy

Measurement condition	% of Reading* (Gain Error)	% of range (Offset Error)	
		30 days after cal. (±5° C)	**1 year after cal. (±5° C)**
Calibrated typ (25°C ± 5°C)	0.02%	0.08%	0.14%
Calibrated max(-40 to 70° C)	0.07%	0.16%	0.39%
Uncalibrated typ (25° C ± 5° C)	0.15%	0.79%	
Uncalibrated max (-40 to 70° C)	0.53%	01.67%	

*Exclusive of lead wire desensitisation error.
† Range equals 29.4 mV/V
‡Calibrated errors represent offset stability following unstrained measurement. Errors include the effect of completion resistors tolerance and drift.

Shunt Calibration Characteristics

Accuracy

Measurement condition	% of Reading (Gain Error)
Typical (25° C, ±5°C)	0.07 %
Maximum (-40 to 70° C)	0.2%

Resistance ..... 100 kΩ

Output value .....–873.47 µV/V

Temperature drift ..... 15 ppm/°C

Method.....Shunt across completion resistor

Excitation Characteristics

Excitation type.....Constant voltage

Excitation value .....3.3 V ± 1%

Maximum output current .....46 mA

Power Requirements

Power consumption from chassis

Active mode .....675 mW max

Sleep mode.....25 µW max

Thermal dissipation (at 70 °C)

Active mode .....675 mW max

Sleep mode.....25 µW max

Appendix XII- Specification NI 9234

4-Channel, ±5 V, 24-Bit Software-Selectable IEPE and AC/DC Analog Input Module

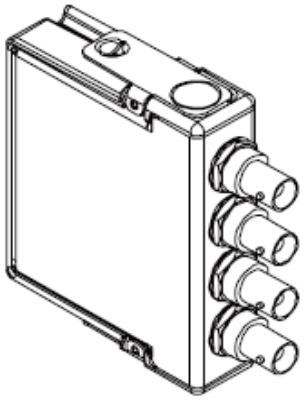

The following specifications are typical for the range –40 to 70 °C unless otherwise noted.

Input Characteristics:

Number of channels.....4 analog input channels

ADC resolution..... 24 bits

Type of ADC.....Delta-Sigma (with analog prefiltering)

Sampling mode .....Simultaneous

Type of TEDS supported ..... IEEE 1451.4 TEDS Class I

Internal master timebase (f_M)

Frequency .....13.1072 MHz

Accuracy.....±50 ppm max

Data rate range (*fs*) using internal master timebase

Minimum.....1.652 kS/s

Maximum..... 51.2 kS/s

Data rate range (*fs*) using external master timebase

Minimum.....0.391 kS/s

Maximum..... 52.734 kS/s

Accuracy

Measurement condition	% of Reading (Gain Error)	% of range * (Offset Error)
Calibrated max(-40 to 70° C)	0.34%, ± 0.03 dB	±0.14%, 7.1 mV
Calibrated typ (25°C ± 5°C)	0.05%, ± 0.005 dB	±0.006%, 0.3 mV
Uncalibrated max (-40 to 70° C)	1.9%, ±0.16 dB	± 0.27%, 13.9 mV
Uncalibrated typ (25° C ± 5° C)	0.48%, ± 0.04 dB	±0.04%, 2.3 mV
*Range = 5.1 V_{pk}		

Idle channel noise and noise density

Idle Channel	51.2 kS/s	25.6 kS/s	2.048 kS/s
Noise	97 dBFS	99 dBFS	103 dBFS
	50 μV_{rms}	40 μV_{rms}	25 μV_{rms}
Noise density	310 nV/√Hz	350 nV/√Hz	780 nV/√Hz

Input impedance

Differential ..... 305 kΩ

AI– (shield) to chassis ground.... 50 Ω

Total harmonic distortion (THD)

Input Amplitude	1 kHz	8 kHz
-1 dBFS	-95 dB	-87 dB
-20 dBFS	-95 dB	-80 dB

Power Requirements

Power consumption from chassis

Active mode .....900 mW max

Sleep mode .....25 µW max

Thermal dissipation (at 70 °C)

Active mode .....930 mW max

Sleep mode .....25 µW max

Appendix XIII- Tip Displacement Calculation Flowchart

(Abraham and Sivaloganathan, 2011)

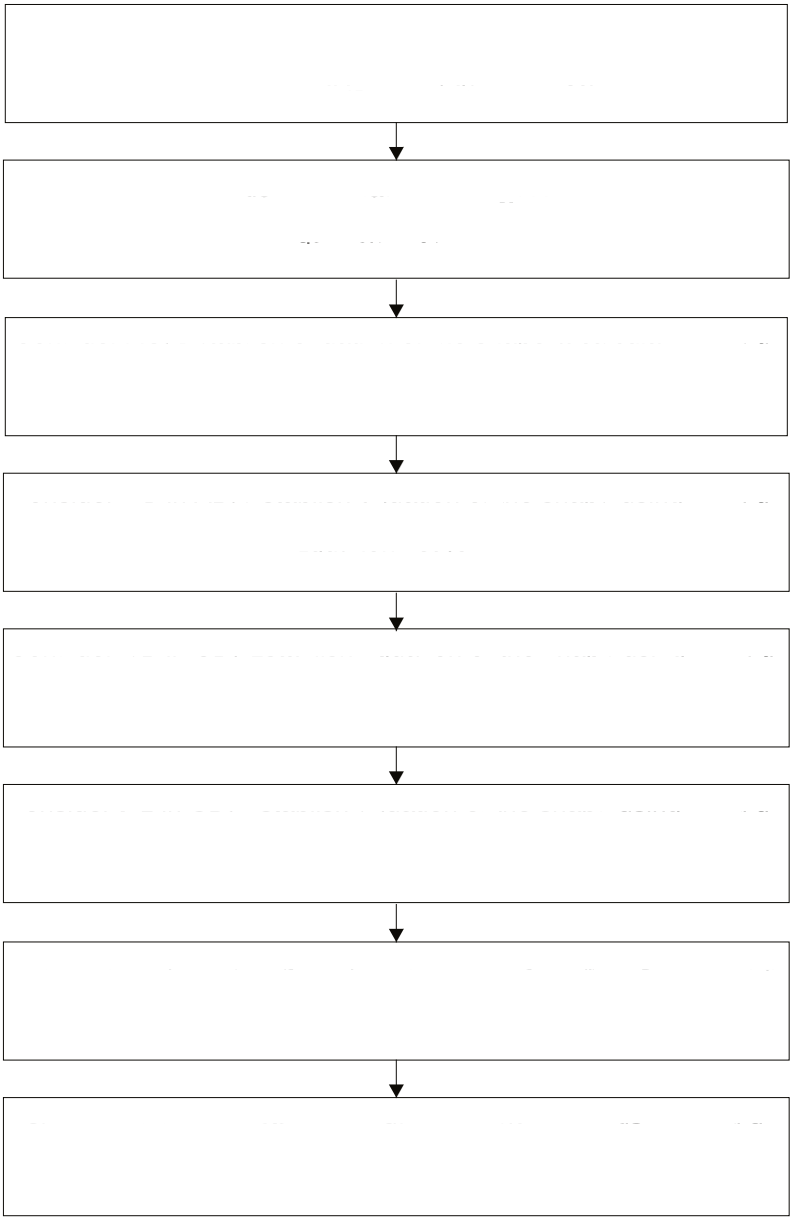

References:

1. Aalami, B. and Williams, D.G. (1975) *Thin plate design for transverse loading,* London: Crosby Lockwood Staples.
2. Abbod, M.F., Talamantes-Silva, J., Linkens, D.A. and Howard, I. (2004) 'Modelling of plane strain compression (PSC) test for aluminium alloys using finite elements and fuzzy logic', *Engineering Applications of Artificial Intelligence,* 17(5), pp. 447-456.
3. Abd El-Ghany, K.M. and Farag, M.M. (2000) 'Expert system to automate the finite element analysis for non-destructive testing', *NDT & E International,* 33(6), pp. 409-415.
4. Abraham, J., Sivaloganathan, S., and Rees, D.A. (2011), 'The Telescopic Cantilever Beam, Part 1: Deflection Analysis', *Engineering Integrity*. 30, pp 6-15.
5. Adams, R.S. and Atman, C.J. (1999), 'Cognitive Processes in Iterative Design Behavior', *Proceedings of the 29th ASEE/IEEE Frontiers in Education Conference*, San Juan de Puerto Rico, pp 10-13.
6. Adams, V. (2006), *How To Manage Finite Element Analysis in the Design Process*, Glasgow: NAFEMS Ltd.
7. Adams, V. (2008), *A designer's guide to simulation with finite element analysis,* Glasgow: NAFEMS Ltd.
8. Akao, Y. (1990), *Quality function deployment: integrating customer requirements into product design,* Oregon: Productivity Press.
9. Andreassen, M.M. (1998), 'Conceptual Design Capture, Keynote Address', *Proceedings of the Engineering Design Conference 98,* Professional Engineering Publications, pp 21-30.
10. ASME (2006), *Guide for Verification and Validation in Computational Solid Mechanics*, New York: American Society of Mechanical Engineers.
11. Bathe, K. (1996), *Finite element procedures*, Englewood Cliffs: Prentice Hall.
12. Beerel, A.C. (1987), *Expert systems: strategic implications and applications,* Chichester: Ellis Horwood.
13. Bellenger, E., Benhafid, Y. and Troussier, N. (2008), 'Framework for controlled cost and quality of assumptions in finite element analysis', *Finite Elements in Analysis and Design,* 45(1), pp. 25-36.

14. British Standards Institution (2001), BS EN 280:2001 Mobile elevating work platforms — Design calculations — Stability criteria — Construction —Safety — Examinations and tests. London: BSI.
15. Carino, C. (2006), 'Structural layout assessment by orthogonal array based simulation', *Mechanics Research Communications,* 33(3), pp. 292-301.
16. Carnevalli, J.A. and Miguel, P.C. (2008), 'Review, analysis and classification of the literature on QFD—Types of research, difficulties and benefits', *International Journal of Production Economics,* 114(2), pp. 737-754.
17. Carpinteri, A. (1997), *Structural mechanics: a unified approach,* London: E & FN Spon.
18. Chan, L. and Wu, M. (2005), 'A systematic approach to quality function deployment with a full illustrative example', *Omega,* 33(2), pp. 119-139.
19. Chandrupatla, T.R. and Belegundu, A.D. (2002), *Introduction to finite elements in engineering,* 3rd edn, Englewood Cliffs: Prentice-Hall.
20. Chillery, M. (2010), 'Nominal and Non-linear Stresses' in *Knowledge base don't forget the basics,* Quinn D. (ed.), Glasgow: NAFEMS (a), pp. 14-15.
21. Chillery, M. (2010), 'The Importance of Mesh Convergence' in *Knowledge base don't forget the basics*, Quinn D. (ed.), Glasgow: NAFEMS (b), pp. 5-6.
22. Chou, P. C. and Pagano, N. J. (1967), Elasticity, Tensor, Dyadic and Engineering Approaches, Canada: Van Nostrand Company Inc.
23. Cohen, L. (1995), *Quality Function Deployment: How to Make, QFD Work for You*, Massachusetts: Addison-Wesley.
24. Collins, J.A. (1993), *Failure of Materials in Mechanical Design,* 2nd edn, New York: John Wiley & Sons, Inc.
25. Cooper, R.G. and Kleinschmidt, E.J. (1987), 'New products: What separates winners from losers?', *Journal of Product Innovation Management,* 4(3), pp. 169-184.
26. Costa, R. and Sobek, D.K. (2003), 'Iteration in Engineering Design: Inherent and Unavoidable or Product of Choices Made?', *International conference on design theory and methodology,* Chicago, IL.
27. Craig, A. and Hart, S. (2003), Dimensions of success in new product development. In: Baker M. J. (ed.) *Perspectives on Marketing Management*. (3), London: John M. Wiley & Sons. Ltd.

28. Cross, M. and Sivaloganathan, S. (2004), 'A methodology for developing company-specific design process models', *Proc. IMechE, Part B: J. Engineering Manufacture,* 219, pp. 265-282.
29. Culbert, C., Riley, G. and Savery, R.T. (1989), 'An expert system development methodology that supports verification and validation', *ISA transactions,* 28 (1), pp. 15-18.
30. Dar, F.H., Meakin, J.R. and Aspden, R.M. (2002), 'Statistical methods in finite element analysis', *Journal of Biomechanics,* 35(9), pp. 1155-1161.
31. Dassault Systèmes (2007), *Abaqus 6.7 Analysis User's ManualVolume II: Analysis Procedures, Solution and Control,* Dassault Systèmes (a), USA.
32. Dassault Systèmes (2007), *Abaqus 6.7 Analysis User's Manual Volume IV: Elements,* Dassault Systemes (b), USA.
33. Dassault Systèmes (2009), *Introduction to Abaqus 6.9,* Dassault Systemes (a), USA.
34. Dassault Systèmes (2009), *Linear Dynamic with Abaqus 6.9,* Dassault Systemes (b), USA.
35. Dassault Systèmes (2009), *Modelling Contact with Abaqus 6.9,* Dassault Systemes (c), USA.
36. Dassault Systèmes (2010), *Element Selection in Abaqus 6.10,* Dassault Systems, USA.
37. Dassault Systèmes (2011), *Essentials of Modeling Buckling and Postbuckling with Abaqus 6.11,* Dassault Systèmes, USA.
38. Dolsak, B. (2002), 'Finite element mesh design expert system', *Knowledge-Based Systems,* 15(5-6), pp. 315-322.
39. Dolšak, B. and Novak, M. (2011), 'Intelligent decision support for structural design analysis', *Advanced Engineering Informatics,* vol. 25, no. 2, pp. 330-340.
40. Kang, K.H. (1995), 'Intelligent Finite Element Mesh Generation', *Engineering with Computers,* 11, pp. 70-82.
41. Falzon, B.G. and Hitchings, D. (2006), *An Introduction to Modelling Buckling and Collapse,* Glasgow: NAFEMS.
42. Forsyth, R. (1989), *Expert systems: principles and case studies,* 2nd edn, London: Chapman and Hall.

43. Gerstle, K.H. (1974), *Basic structural analysis,* Prentice-Hall, Englewood Cliffs: London.
44. Green, W.G. (1962), *Theory of Machines*, London & Glasgow: Blackie and Son Ltd.
45. Griffin, A. and Page, A.L. (1993), 'An interim report on measuring product development success and failure', *Journal of Product Innovation Management,* 10 (4), pp. 291-308.
46. Gürgöze, M. (1986), 'On the approximate determination of the fundamental frequency of a restrained cantilever beam carrying a tip heavy body', *Journal of Sound and Vibration*,105 (3) , pp 443-449
47. Hinton, E. (1992), 'Incremental-Iterative Solution', in Hinton, E. (ed.) *Introduction to Nonlinear Finite Element Analysis*, Reprint Glasgow: NAFEMS (2010).
48. Huebner, K.H., Dewhirst, D.L., Smith, D.E. and Byrom, T.G. (2001), *The finite element method for engineers,* 4th edn, New York: Wiley.
49. Jeang, A., Chung, C., Chen, C. and Li, H. (2009), 'Optimizing process parameters of hot-bar soldering process through quality function deployment and Taguchi method', *Journal of Materials Processing Technology,* 209 (6), pp. 2967-2977.
50. Jonson, W., Mellor, P.B. (1973), *Engineering Plasticity,* Berkshire: Van Nostrand Reinhold Company Ltd.
51. *Computational Methods in Design and Manufacturing*, [CD-ROM], Department of Mechanical Engineering, Madras: Indian Institute of Technology Madras.
52. Kurowski, P.M. (2004), *Finite element analysis for design engineers*, Warrendale, PA : SAE International.
53. Labrie, R., Thilloy, C., Tanguy, P.A. and Moll, G.H. (1994), 'An expert assistant to monitor finite element simulations', *Mathematics and Computers in Simulation,* 36 (4-6), pp. 413-422.
54. Li, B., Reis, L. and de Freitas, M. (2006), 'Simulation of cyclic stress/strain evolutions for multiaxial fatigue life prediction', *International Journal of Fatigue,* 28 (5-6), pp. 451-458.

55. Lin, Y. and Lo, S. (2005), 'Modeling of chemical mechanical polishing process using FEM and abductive network', *Engineering Applications of Artificial Intelligence,*18 (3), pp. 373-381.
56. Lo, C., Tseng, K.C. and Chu, C. (2010), 'One-Step QFD based 3D morphological charts for concept generation of product variant design', *Expert Systems with Applications,* 37 (11), pp. 7351-7363.
57. MacLeod, I.A. (2005), *Modern structural analysis: Modelling process and guidance*, London: Thomas Telford.
58. Mair (1984), *Guidelines to finite element practice,* Dept. of Trade and Industry, National Engineering Laboratory, Glasgow: NAFEMS.
59. Maropoulos, P.G. and Ceglarek, D. (2010), 'Design verification and validation in product lifecycle', *CIRP Annals - Manufacturing Technology,* 59 (2), pp. 740-759.
60. Martin, J. (1988), *Building Expert Systems,* Cliffs: Prentice-Hall.
61. Mottram, J.T. and Shaw, C.T. (1996), *Using finite elements in mechanical design,* London: McGraw Hill.
62. National Agency for Finite Element Methods and Standards and National Engineering Laboratory (2006), *What is Verification and Validation?* National Agency of Finite Element Methods and Standards, Glasgow.
63. National Agency for Finite Element Methods and Standards and National Engineering Laboratory (1987), *A finite element primer* , National Engineering Laboratory : National Agency for Finite Element Methods and Standards, Glasgow.
64. NI (2008), *operating instructions and specifications NI 9235/9236,* National Instruments Corp.
65. NI (2008), *operating instructions and specifications NI 9234,* National Instruments Corp.
66. NI (2008), *user guide and specifications NI cDAQ-9172,* National Instruments Corporation.
67. Niftylift Ltd (2010), *Access Platform Catalogue*, Niftylift Ltd, Milton Keynes, UK.
68. Novak, M. and Dolšak, B. (2008), 'Intelligent FEA-based design improvement', *Engineering Applications of Artificial Intelligence,* 21 (8), pp. 1239-1254.

69. Oberkampf, W.L. and Barone, M.F. (2006), ‘Measures of agreement between computation and experiment: Validation metrics’, *Journal of Computational Physics,* 217 (1), pp. 5-36.
70. Oberkampf, W.L. and Trucano, T.G. (2008), ‘Verification and validation benchmarks’, *Nuclear Engineering and Design,* 238 (3), pp. 716-743.
71. Oberkampf, W.L., Trucano, T.G. and Hirsch, C. (2004), ‘Verification, validation, and predictive capability in computational engineering and physics’, *Applied Mechanics Reviews,* 57 (1-6), pp. 345-384.
72. Ostrofsky, B. (1977), *Design, planning and development methodology,* London : Prentice-Hall.
73. Pahl, G. and Wallace, K. (2006), *Engineering design: a systematic approach,* 3rd edn, London: Springer.
74. Parameswaran, M.A. (2004), *An introduction to design engineering,* Harrow: Alpha Science International,.
75. Peterson, R.E. (1974), *Stress concentration factor,* John Wiley and Sons, USA
76. Pilkey, W.D. (1994), *Formulas for stress, strain, and structural matrices,* Wiley, New York ; Chichester.
77. Pinfold, M. and Chapman, C. (2001), ‘The application of KBE techniques to the FE model creation of an automotive body structure’, *Computers in Industry,* 44 (1) , pp. 1-10.
78. Potma, T. (1967), *Strain Gauges Theory and Application,* Netherlands: Philips
79. Prasad, B. (1998), ‘Review of QFD and related deployment techniques’, *Journal of Manufacturing Systems,* 17 (3), pp. 221-234.
80. Pugh, S. (1991), *Total design: integrated methods for successful product engineering,* Pearson Education Ltd., Harlow.
81. Ratchev, S., Phuah, K. and Liu, S. (2007), ‘FEA-based methodology for the prediction of part–fixture behaviour and its applications’, *Journal of Materials Processing Technology,* 191 (1-3), pp. 260-264.
82. Ray, M.S. (1985), *Elements of engineering design: an integrated approach,* New York: Prentice-Hall.
83. Reddy, J.N. (1984), *An introduction to the finite element method,* New York: McGraw-Hill.
84. Rees, D. (1997), *Basic solid mechanics,* London: Macmillan.

85. Rees, D. (2000), *The mechanics of solids and structures,* London: Imperial College Press.
86. Ross, P.J. (1996), *Taguchi techniques for quality engineering: loss function, orthogonal experiments, parameter and tolerance design,* 2nd edn, New York: McGraw-Hill.
87. Roy, C.J. and Oberkampf, W.L. (2011), 'A comprehensive framework for verification, validation, and uncertainty quantification in scientific computing', *Computer Methods in Applied Mechanics and Engineering,* 200 (25-28), pp. 2131-2144.
88. Sack, R.L. (1984), *Structural analysis,* London: McGraw-Hill.
89. Sadd, M.H. and Rolph III, W.D. (1987), 'On training programs for design engineers in the use of finite element analysis', *Computers & Structures,* 26 (1-2), pp. 411-414.
90. Salazar, J.R., Mobasseri, S.O. and Sivaloganathan, S. (2012), 'Equivalent Rigidity Method for Estimating the Natural Frequency of Telescopic Cantilever Beams', *International Journal of Computer Application Technology*, 44 (6).
91. Samuel, A.E. and Weir, J. (2005), *Introduction to engineering design*, Elsevier Butterworth-Heinemann, Oxford.
92. Shephard, M.S. and Wentorf, R. (1994), 'Toward the implementation of automated analysis idealization control', *Applied Numerical Mathematics,* 14 (1-3), pp. 105-124.
93. Singh, S. (1979), *Applied stress analysis,* First edn, Delhi: KHANA Publishers.
94. Sivaloganathan, S., Evbuomwan, N.F.O., Jebb, A. and Wynn, H.P. (1995) 'Design function deployment — a design system for the future', *Design Studies,* 16 (4), pp. 447-470.
95. Smolira, M. (1980), *Analysis of Structure by the Force-Displacement Method,* London: Applies Scince Publishers.
96. Spreng, R.A., MacKenzie, S.C., Olshavsky, R.W. (1996), 'A re-examination of the determinants of consumer satisfaction', *Journal of Marketing*, 60: pp 15-32.
97. Timoshenko, S.P. and Young, D.H. (1965), *Theory of structures,* 2nd edn, London: McGraw-Hill.
98. Timoshenko, S. P. and Goodier, J. N. (1951), *Theory of Elasticity*, 2nd ed., USA: McGrow Hill.

99. Trahair, N.S. (1993), *Flexural-torsional buckling of structures,* London: Spon.

100. Turkiyyah, G.M. and Fenves, S.J. (1996), 'Knowledge-based assistance for finite-element modeling', *IEEE Expert,* 11 (3), pp. 23-32.

101. Ugural, A.C. (1999), *Stresses in plates and shells,* 2nd edn, London : McGraw-Hill.

102. Vinson, J.R. (1989), *The behavior of thin walled structures : beams, plates, and shells,* Dordrecht: Kluwer Academic Publishers.

103. Vishay (2010), *Strain Gauge Rosettes- Selection, Application and Data Reduction,* Vishay Micro-Measurements (a).

104. Vishay (2010), *Strain Guage selection: Criteria, Procedures, Recommendations,* Vishay Micro-Measurements (b).

105. Vishay (2011), *Surface Preparation for Strain Gage Bonding,* Vishay Micro-Measurements.

106. Wang, C. T., (1953), *Applied Elasticity*, USA: McGrow Hill

107. Wu, D.H., Tsai, Y.J. and Yen, Y.T. (2003), 'Robust design of quartz crystal microbalance using finite element and Taguchi method', *Sensors and Actuators B: Chemical,* 92 (3), pp. 337-344.